

Alma Mater Studiorum – Università di Bologna

DOTTORATO DI RICERCA IN

CHIMICA

Ciclo XXX

Settore Concorsuale: 03/A2

Settore Scientifico Disciplinare: CHIM/02

Conformational Equilibria, Non-Covalent Interactions and Large Amplitude Motions
in Molecules and Small Molecular Clusters Revealed by Rotational Spectroscopy

Presentata da: Weixing Li

Coordinatore Dottorato

Aldo Roda

Supervisore

Sonia Melandri

Co-supervisore

Walther Caminati

Esame finale anno 2018

Preface

We start our journey to know the world when we open the eyes, but you cannot rely on the eyes if you want to “see” what constitute the world. Nowadays, we already know that the basic world is formed by atoms and molecules, thanks to their interactions with electromagnetic radiation. In the microworld, the physical properties, such as the momentum, are quantized rather than consequent. So, the change of the physical quantities will absorb or emit a characteristic energy in the form of electromagnetic radiation. We can realize the physical properties and “see” the microworld by detecting the electromagnetic radiation. Different frequency regions of the electromagnetic spectrum can reflect different kinds of information of the atoms and molecules. Rotational spectroscopy is concerned with the transitions between quantized rotational states of molecules in the gas phase. For most molecules and molecular systems, the rotational spectra commonly lie in the microwave region designated as extending from wavelengths of approximately 30 cm to those of 0.3 mm, or from frequencies of approximately 1 GHz to those of 1000 GHz. As an excellent method traditionally associated with molecular structure determination, today’s microwave spectroscopy has been developed to address a wide variety of basic and key information and properties of molecules and molecular systems, such as conformational and tautomeric conversion, chemical bonding, charge transfer, hyperfine structures, internal dynamics, and large-amplitude motions. The scope of microwave spectroscopy has been widened from intramolecular observations to intermolecular interactions. The investigation extends from van de Waals complexes, hydrogen-bonded complexes, and electron donor-acceptor complexes to chiral recognition, molecular aggregation, quantum solvation. The study targets include molecules of organic interest, molecules of biological interest, atmospheric species, interstellar compounds, metal, semiconductor, ions and radicals.

Microwave spectroscopy has progressed rapidly in the past decades.^[1-10] One of the major experimental advances was the development of the pulsed jet (molecular beam) Fourier transform

microwave (PJ-FTMW) spectroscopy which uses a Fabry-Pérot interferometer, invented by Balle and Flygare in 1979.^[8] This spectrometer measures time-domain spectroscopy by detecting the rotational free induction decay (FID) following polarization by a short microwave pulse. Then the spectrum can be transferred from time-domain to frequency-domain via Fourier transformation of the signal. The spectroscopy resolution and detected sensitivity was highly improved by PJ-FTMW and without the power broadening found in Stark modulation spectrometer. The rapid cooling of the molecules in the seeded molecular beam makes it possible to study the variety of molecular conformations, large molecules, and the weakly bound molecular clusters. It greatly expands the range of the molecular systems that can be analyzed by rotational spectroscopy. Another technique expanding the range of analyzed targets was the combination of the pulsed molecular beam with the laser ablation. The laser ablation could “softly” vaporize the solid samples and seed the molecules in the carrier gas. In 2006, Brooks H. Pate and co-workers invented the broadband chirped pulse Fourier transform microwave (CP-FTMW) spectrometer.^[9] This spectrometer reduced significantly the spectrum acquisition time and implemented the spectra acquisition of all the possible molecules in the molecular beam at the same time. Besides that, it brought the possibility of analytical chemistry application on mixtures with unknown species. In addition, this spectrometer could also study the excited vibrational state of molecules prepared by laser excitation with tunable laser.

In this dissertation, the introduction of the basic knowledge of microwave spectroscopy including the fundamental theory of the rotational spectroscopy and the spectrometer techniques has been reviewed firstly. Then the work that I have performed during my PhD career was discussed. The PJ-FTMW spectroscopy has been used to study the different conformers of monomers, and bimolecular clusters formed with hydrogen bond (HB) or weakly non-covalent bonds. Difluoromethane and water oligomers have been studied by CP-FTMW spectrometer.

I started my PhD thesis works with the rotational study of the indan monomer and its dimer with trifluoromethane, which was performed by PJ-FTMW spectroscopy at the University of Bologna (UNIBO). From the rotational spectrum of indan, I found the tunneling splitting due to the five-member ring puckering motion. The rotational spectrum of its complex with trifluoromethane showed a cage structure connected by a $\text{CH}\cdots\pi$ interaction and four cooperative $\text{CH}\cdots\text{F}$ interactions. The CHF_3 moiety was linked by the cooperative interactions in this kind of cage structure, and no evidence of internal rotation detected, differently from what was found for the CHF_3 -Benzene complex, where a free rotation around the single $\text{CH}\cdots\pi$ bond was found.

The main investigations I performed during the first two years were the rotational studies of formic acid (FA) interacting with several systems. All of them were performed with the PJ-FTMW spectrometer at UNIBO. One of the most interesting results was the observation of the competition

between reactivity and the pre-reactivity in the mixtures of carboxylic acids and alcohols, which is a basic phenomenon in organic synthesis. I spent more than one year on this project, and more than ten molecular systems were investigated. Formic acid and alcohols were seeded in the carrier gas helium, just ahead of the supersonic expansion. The experimental results of the primary and secondary alcohol mixing with carboxylic acid has shown that an esterification occurs, whereas just spectra of adducts could be identified by mixing the tertiary alcohol and formic acid. Besides the study of FA with alcohols, I also studied the configuration and the interaction between the acid with isopropyl formate, β -propiolactone, cyclobutanone, dimethyl ether. The successful experiments are as listed here: 1) FA-isopropanol, 2) FA-cyclobutanone, 3) FA-beta-propiolactone, 4) FA-dimethyl ether, 5) FA-tert-butyl alcohol, 6) FA-isopropyl formate, 7) 2-methyl-2-butanol, 8) 1-methylcyclohexanol, 9) 1-methyl-cyclopropanol, 10) FA-1-methyl-cyclopropanol, 11) cyclohexanol, 12) FA-cyclohexanol, 13) methyl trifluoroacetate.

Another interesting work is the pure rotational spectrum of the “non-polar” dimer of formic acid. I have assigned the rotational spectra of DCOOH-HCOOH, DCOOD-HCOOH and DCOOH-HCOOD. From the fit of the spectra, the structural information can be obtained as well as the binding energy is determined to be ~ 57 kJ/mol. More interesting, the barrier of the double-proton transfer can be estimated from the tunneling splitting.

At the beginning of the third year, I spent three months in Dr. Emilio J. Cocinero’s laboratory at the Universidad del País Vasco (Spain). With the CP-FTMW spectrometer present in the laboratory, I assigned the spectra of the clusters of difluoromethane (DFM) with deuterated water with ratios 1:2, 2:1, and 2:2. By mixing normal and deuterated water we could produce the liquid where the molecules H_2O , D_2O , and DOH exist simultaneously. Seeding this sample into the cavity I have measured the rotational transitions of the clusters with single, double, triple deuterated water molecules, respectively. Combining with the spectra of DFM with normal water from Prof. Brooks H. Pate’s group, the substituted structures of the clusters have been confirmed.

After coming back to Italy, the first successful experiment was the rotational study of 3,5-heptanedione. Its two tautomers have been discriminated unambiguously by FTMW spectroscopy. The spectra of the ^{13}C and deuterium substituted species have been successfully assigned for the most stable conformer. That shows us a substituted structure which indicates the detailed structure information. The adduct of 3,5-heptanedione with one water molecule has already been studied by FTMW spectroscopy. Two conformers were assigned from the rotational spectrum. 3,5-heptanedione adopts different conformers in the water adducts comparing the structures we identified for the monomer.

Some results of my PhD work have been published on scientific journals, the rotational

transition frequencies and structure information are available in the corresponding papers. Most of them have not been published, but you will see them online in the near future. I will report the detailed information of parts of the work in the dissertation.

Abstract

In this dissertation, the introduction of the basic knowledge of microwave spectroscopy including the fundamental theory of the rotational spectroscopy and the experimental techniques was reviewed firstly. Then the work that I have performed during my PhD career is discussed. Pulsed-jet Fourier transform microwave (PJ-FTMW) spectroscopy has been used to study the monomers, and the bimolecular clusters formed with hydrogen bond or weakly non-covalent bonds. Difluoromethane and water oligomers have been studied by Chirped-Pulse Fourier transform microwave (CP-FTMW) spectroscopy.

The spectroscopic work in this dissertation includes three parts:

1) Isolated molecules with large amplitude motions. Three subjects are involved in this part, which are the rotational studies of indan, 1,2-dimethoxyethane, and 1-methylcyclohexanol. The transitions were split due to ring puckering motion, the internal rotations of methyl groups, and the rotation of the hydroxyl group, respectively.

2) Clusters formed by the cooperation of different classes of HBs. Four subjects are involved in this chapter. Firstly, formic acid clustering with dimethyl ether and cyclobutanone, respectively, indicate that both complexes are formed with one typical O-H \cdots O HB and two C-H \cdots O weak hydrogen bonds (WHBs). Secondly, the investigation of the complex of indan with trifluoromethane showed a cage structure based on the cooperative effects of C-H $\cdots\pi$ and C-H \cdots F WHB interactions. Lastly, The study of oligomer of (CH₂F₂)_m-W_n, (m,n = 1,2) has broaden our knowledge of the cooperation of different HBs in a cluster. The trimer (CH₂F₂)-W₂ displayed a cyclic structure linked with O-H \cdots O, C-H \cdots O, and O-H \cdots F bonds. The trimer (CH₂F₂)₂-W showed a geometry connected with O-H \cdots F, C-H \cdots O, and C-F \cdots H-C bonds. In the tetramer (CH₂F₂)₂-W₂, the cluster is bound by 7 non-covalent bonds including O-H \cdots O, O-H \cdots F, C-H \cdots O, C-F \cdots H-C bonds.

3) Another interesting result is the observation of the competition between reactivity and the pre-reactivity in the mixtures of carboxylic acids and alcohols, which is a basic phenomenon in organic synthesis. The experimental results on the primary and secondary alcohols mixed with carboxylic acids have shown that the esterification reaction occurs, whereas only the spectra of the adducts could be identified by mixing the tertiary alcohols and formic acid.

Catalogs

Preface.....	I
Abstract.....	IV
Chapter I. Theory of Rotational Spectroscopy.....	1
1.1. Classical rotational energy and classes of molecules.....	1
1.2. Quantumechanical rigid rotors	3
1.2.1. Spherical tops	4
1.2.2. Linear molecules.....	4
1.2.3. Symmetric-top molecules	5
1.2.4. Asymmetric-top molecules.....	5
1.3 Non-rigid rotor	7
1.3.1. Classic description of centrifugal and Coriolis forces	8
1.3.2. Centrifugal distortion and effects of vibrational excitation on the B value in linear molecules	8
1.3.3. Centrifugal distortion in symmetric-top molecules	9
1.4 Nuclear quadrupole coupling	9
1.5 Internal motions	11
1.5.1. Internal rotation	11
1.5.2. Inversion motion	15
1.6. Molecular structure evaluation	16
1.6.1. r_e : the equilibrium structure for the hypothetical vibrationless state.	17
1.6.2. r_0 : the effective structure for the ground vibrational state.....	17
1.6.3. r_s : the substitution structure.....	18
Chapter II. Experimental techniques in rotational spectroscopy	20
2.1. Free-Jet Millimeter-Wave Stark Modulated Absorption (FJ-MMWA) Spectrometer.....	20
2.2. Pulsed jet Fourier transform microwave (PJ-FTMW) spectroscopy	23
2.2.1. Pulsed supersonic jet expansion	24
2.2.2. Time domain technique	25
2.2.3. PJ-FTMW spectrometer at UNIBO	26
2.3. Chirped pulse Fourier transform microwave (CP-FTMW) spectrometer	28
Chapter III. Isolated molecules with large amplitude motions	31
3.1. Ring Puckering Splittings in Indan	32
3.2. 1,2-Dimethoxyethane with CH ₃ Internal Rotation	39
3.3. 1-Methylcyclohexanol with OH rotation	48
Chapter IV Clusters formed by the cooperation of different classes of HBs.....	55
4.1. Formic acid cluster with Dimethyl ether.....	57
4.2. The cluster of Formic acid with Cyclobutanone	63
4.3. The dimer of Indan-CHF ₃	70
4.4. [CH ₂ F ₂] _n ···[H ₂ O] _m trimers and tetramers.....	77
Chapter V. Pre-reactivity and reactivity between gaseous carboxylic acids and alcohols	86
Appendices.....	91

Appendix I.....	91
Appendix II.	95
Appendix III.	103
Appendix IV.....	113
Appendix V.	116
Appendix VI.....	121
Appendix VII.....	125
Appendix VIII.	149
References.....	159
Acknowledgement	167

Chapter I

Theory of Rotational Spectroscopy

The transition of electrons in atoms and molecules are known to produce characteristically spectra from optical to ultraviolet region. The vibrational motions of the atoms in molecules are primarily responsible for the infrared spectra. The slower end-over-end rotation of molecules has characteristic frequencies in the microwave range. A molecule interacts appreciably with a microwave electromagnetic field only if it has a permanent electric or magnetic dipole moment, usually electric dipole moment. Thus, the molecule is a rotating dipole which acts as a small antenna in radiating or receiving electromagnetic waves which have frequencies coinciding with the frequencies of the rotating dipole.

Discussion of the interpretation of microwave spectroscopy in this chapter will begin with symmetric-top and asymmetric-top molecules. Then quadrupole hyperfine structures and the effects of hindered motions of molecules on the rotational spectra will be considered. The characterization of the molecule structure from rotational spectra will be discussed after the broader outline of rotational spectra have been treated.

The comprehensive and detailed knowledge of rotational spectroscopy is available in several monographs.^[1-3]

1.1. Classical rotational energy and classes of molecules

To derive the information of the molecular structure from the observed rotational constants requires the knowledge of classical moments of inertia.

In the classical angular momentum formula of a rigid system

$$\mathbf{P} = \mathbf{I} \cdot \boldsymbol{\omega} \quad (1.1)$$

$\boldsymbol{\omega}$ is the angular velocity and \mathbf{I} is the moment of inertia tensor, written as

$$\begin{aligned} \mathbf{I} = & I_{xx}\mathbf{i}\mathbf{i} + I_{xy}\mathbf{i}\mathbf{j} + I_{xz}\mathbf{i}\mathbf{k} \\ & + I_{yx}\mathbf{j}\mathbf{i} + I_{yy}\mathbf{j}\mathbf{j} + I_{yz}\mathbf{j}\mathbf{k} \\ & + I_{zx}\mathbf{k}\mathbf{i} + I_{zy}\mathbf{k}\mathbf{j} + I_{zz}\mathbf{k}\mathbf{k} \end{aligned} \quad (1.2)$$

where:

$$\begin{aligned}
I_{xx} &= \sum m(y^2 + z^2) \\
I_{yy} &= \sum m(z^2 + x^2) \\
I_{zz} &= \sum m(x^2 + y^2) \\
I_{xy} &= I_{yx} = -\sum mxy \\
I_{yz} &= I_{zy} = -\sum myz \\
I_{zx} &= I_{xz} = -\sum mxz
\end{aligned} \tag{1.3}$$

where m is the mass of a particle and x, y, z are its coordinates relative to a rectangular coordinate system fixed on the rotor. Generally the origin of the coordinate system is chosen at the center of mass of the rotor. In this way, the total kinetic energy can be treated as the sum of the translational motion of the mass center and rotational motion with respect to the mass center. The elements in the moment of inertia tensor can vanish except the three diagonal elements by the diagonalization of the tensor. The three diagonal elements are called principal moments of inertia. Or we can obtain them by resolving equation

$$\mathbf{I}\xi = I\xi \tag{1.4}$$

where \mathbf{I} is the inertia matrix in any reference frames, ξ is the eigenvector of the matrix, and I is the eigenvalue relative to ξ . The eigenvalues I are the values that will appear in the diagonalized form of inertia matrix \mathbf{I} . So by finding the eigenvalues we have diagonalized the matrix. By resolving the cubic equation

$$\begin{vmatrix}
I_{xx} - I & I_{xy} & I_{xz} \\
I_{yx} & I_{yy} - I & I_{yz} \\
I_{zx} & I_{zy} & I_{zz} - I
\end{vmatrix} = 0 \tag{1.5}$$

we can obtain three roots which are the eigenvalues, notated as I_x, I_y, I_z , respectively. They are the principal moments of inertia of the rigid body rotating along x, y, z . The notations x, y, z represent the principal axes system, which are the roots of the eigenvector ξ in the equation (1.4) with respect to I_x, I_y, I_z , respectively. In the principal axes system, the products of inertia vanish, so the rotational kinetic energy can be written easily

$$E_r = \frac{P_x^2}{2I_x} + \frac{P_y^2}{2I_y} + \frac{P_z^2}{2I_z} \tag{1.6}$$

The moments of inertia of a molecule can be represented by an ellipsoid whose orientations are fixed in the molecule and whose center coincides with mass center of the molecule. The relative magnitude of the molecular moment of inertia along any axis is just equal the distance between the mass center and the intersection of the axis and the ellipsoid. If we choose the coordinate system along the principal axes of the ellipsoid, then the equation of the ellipsoid of inertia can be

formulated as:

$$\frac{x^2}{I_x^2} + \frac{y^2}{I_y^2} + \frac{z^2}{I_z^2} = 1 \quad (1.7)$$

where I_x , I_y , and I_z are the moments of inertia along the principal axes.

For convenience, the moments of inertia will be substituted by rotational constants in the rotational energy calculation.

$$A = \frac{\hbar}{4\pi I_x}; \quad B = \frac{\hbar}{4\pi I_y}; \quad C = \frac{\hbar}{4\pi I_z} \quad (1.8)$$

Rotational constants are generally expressed in MHz; moments of inertia are in amu \AA^2 . In the general convention, the increasing orders are normally defined as:

$$I_x \leq I_y \leq I_z; \quad A \geq B \geq C \quad (1.9)$$

Based on the symmetry of the molecular structures, they can be classified into four classes:

- 1) Spherical tops ($A = B = C$). All three principal moments of inertia are equal to each other. However, the spherical top molecules generally cannot interest microwave spectroscopists, since the high degree symmetry does not allow the molecular dipole moment to be present.
- 2) Linear molecules ($I_x \ll I_y = I_z$). which belong to the class with a zero moment of inertia about one of the molecular axes, and with other two principal moments of inertia equal in value. For most purpose, I_x can be taken to be 0.
- 3) Symmetric tops. A symmetric top is a molecule in which two moments of inertia are same. It is characterized by a threefold or higher symmetry axis. For the symmetric-top molecules, if x or a axis lie on the symmetry axis ($A \geq B = C$), they are called prolate-tops; if z or c axis lie on the figure axis ($A = B \geq C$), the molecules are called oblate-tops.
- 4) Asymmetric tops. The general rotor where all the three principal moments of inertia are different is called asymmetric rotor or asymmetric top. The asymmetry of a molecule can be described in terms of an asymmetry parameter κ , as below,

$$\kappa = \frac{2B - A - C}{A - C} \quad (1.10)$$

It is obvious that κ varies from -1 (prolate symmetric-top) to +1 (oblate symmetric-top).

1.2. Quantumechanical rigid rotors

The microwave spectral frequencies are relative to the transitions between two characteristic energy levels, which are the eigenvalues of the Hamiltonian operator for molecular rotation. In the free field, the rotational kinetic Hamiltonian operator of rigid rotor can be expressed in terms of

angular momentum principal axes as stated in equation 1.6 replaced by the conjugate operators (in bold). So in the body fixed principal axes system, the operator is

$$\mathbf{H}_r = \frac{\mathbf{P}_x^2}{2I_x} + \frac{\mathbf{P}_y^2}{2I_y} + \frac{\mathbf{P}_z^2}{2I_z} \quad (1.11)$$

where

$$\begin{aligned} \mathbf{P}_x &= -i\hbar(y \frac{\partial}{\partial z} - z \frac{\partial}{\partial y}) \\ \mathbf{P}_y &= -i\hbar(z \frac{\partial}{\partial x} - x \frac{\partial}{\partial z}) \\ \mathbf{P}_z &= -i\hbar(x \frac{\partial}{\partial y} - y \frac{\partial}{\partial x}) \end{aligned} \quad (1.12)$$

The operators which commute have a common set of eigenfunctions. Thus, for the operators \mathbf{P}^2 , \mathbf{P}_z , and \mathbf{P}_Z , the eigenvalues can be obtained with the same eigenfunction's set, as shown below,

$$\begin{aligned} \mathbf{P}^2 \psi_{JKM} &= \hbar^2 J(J+1) \psi_{JKM} \\ \mathbf{P}_z \psi_{JKM} &= \hbar K \psi_{JKM} \\ \mathbf{P}_Z \psi_{JKM} &= \hbar M \psi_{JKM} \end{aligned} \quad (1.13)$$

where Z is from XYZ axes system in terms of the space fixed reference, and z is from the body fixed principal axes system xyz . J , K , and M are the quantum numbers of \mathbf{P} , \mathbf{P}_z , and \mathbf{P}_Z respectively, and integers with $|K| \leq J$, and $|M| \leq J$. It is worth noting that the quantum number K appears only for symmetric tops and corresponds to the projection of the angular momentum along the symmetry axis.

1.2.1. Spherical tops.

Since the three principal moments of inertia are equal each other ($I_x = I_y = I_z = I$). The Hamiltonian operator can be expressed as:

$$\mathbf{H}_r = \frac{1}{2I} (\mathbf{P}_x^2 + \mathbf{P}_y^2 + \mathbf{P}_z^2) = \frac{\mathbf{P}^2}{2I} \quad (1.14)$$

The eigenvalues of \mathbf{H}_r are simply as:

$$E_J = \langle J, K | \mathbf{H}_r | J, K \rangle = \frac{\hbar^2 J(J+1)}{2I} = hBJ(J+1) \quad (1.15)$$

1.2.2. linear molecules

When we take the condition as $I_y = I_z = I$, $I_x = 0$, and $\mathbf{P}_x = 0$. The Hamiltonian operator can be expressed as:

$$\mathbf{H}_r = \frac{1}{2I} (\mathbf{P}_y^2 + \mathbf{P}_z^2) = \frac{\mathbf{P}^2}{2I} \quad (1.16)$$

The energy levels in the free field can be obtained as:

$$E = \frac{\hbar^2}{2I_y} J(J+1) = hBJ(J+1) \quad (1.17)$$

Considering only the interaction of the electric component of the electromagnetic radiation with the electric dipole moment, the selection rules for rotational transition of the linear molecules are

$$\Delta J = \pm 1; \Delta M = 0, \pm 1 \quad (1.18)$$

Applying this selection rules to the energy levels, one can get the rigid rotational frequencies:

$$\nu = 2B(J+1) \quad (1.19)$$

1.2.3. Symmetric-top molecules

For the prolate-tops ($I_x \leq I_y = I_z$), the Hamiltonian can be expressed as:

$$\mathbf{H}_r = \frac{\mathbf{P}^2}{2I_y} + \left(\frac{1}{2I_x} - \frac{1}{2I_y} \right) \mathbf{P}_x^2 \quad (1.20)$$

The energy for prolate-top is

$$E = hBJ(J+1) + h(A-B)K^2 \quad (1.21)$$

For the oblate-tops ($I_x = I_y \leq I_z$), the Hamiltonian can be expressed as:

$$\mathbf{H}_r = \frac{\mathbf{P}^2}{2I_y} + \left(\frac{1}{2I_z} - \frac{1}{2I_y} \right) \mathbf{P}_z^2 \quad (1.22)$$

The energy for oblate-top is

$$E = hBJ(J+1) + h(C-B)K^2 \quad (1.23)$$

From the equations, one can see that all levels for $K > 0$ are doubly degenerate. Since K is the projection of J on the molecular symmetry axis, $J \geq K$, for any given K , the lowest energy level is when $J = K$. With a given J , for the prolate-top the energy levels are increased with K while for the oblate-top the energy levels decrease with K .

The selection rules for rotational transition in the symmetric molecules are

$$\Delta J = \pm 1; \Delta K = 0; \Delta M = 0, \pm 1 \quad (1.24)$$

Applying this selection rules to the energy levels, one can get the rigid rotational frequencies:

$$\nu = 2B(J+1) \quad (1.25)$$

1.2.4. Asymmetric-top molecules

When it comes to asymmetric-top rotor, $I_x \neq I_y \neq I_z$, The projection of the angular momentum

is not constant along any axis fixed on the molecular body. Thus, K is no longer a good quantum number. Thus, \mathbf{H}_r is not diagonal in the J, K representation. The matrix elements of \mathbf{H}_r are both diagonal and off-diagonal, but they do not represent the eigenvalues of \mathbf{H}_r . In the coordinates of the principal axes of inertia, the non-vanishing diagonal matrix elements of \mathbf{H}_r are expressed as

$$\langle J, K | \mathbf{H}_r | J, K \rangle = \frac{\hbar^2}{4} \left[J(J+1) \left(\frac{1}{I_x} + \frac{1}{I_y} \right) + \left(\frac{2}{I_z} - \frac{1}{I_x} - \frac{1}{I_y} \right) K^2 \right] = \frac{h}{2} [(A+B)J(J+1) + (2C-A-B)K^2] \quad (1.26)$$

and the non-vanishing non-diagonal elements are

$$\begin{aligned} \langle J, K | \mathbf{H}_r | J, K \pm 2 \rangle &= \frac{\hbar^2}{8} [J(J+1) - K(K \pm 1)]^{1/2} [J(J+1) - (K \pm 1)(K \pm 2)]^{1/2} \left(\frac{1}{I_y} - \frac{1}{I_x} \right) \\ &= \frac{h}{4} (B-A) [J(J+1) - K(K \pm 1)]^{1/2} [J(J+1) - (K \pm 1)(K \pm 2)]^{1/2} \end{aligned} \quad (1.27)$$

Although K is no longer the good quantum number, the parameter K can be kept labelling the rotational energy level. K_{-1} (or K_a) represents the value of K for the limiting case of prolate top while the K_1 (or K_c) is K for the limit of oblate top. So the rotational energy level is labeled as notation $J_{K_{-1}K_1}$. In another way the energy level can be also labeled with a simply subscript τ , written as J_τ . τ has no any physical meaning only serves as the label of the different rotational energy level. The relationship between them is $\tau = K_{-1} - K_1$.

Following Ray's proposal, let A, B, C be substituted by $\sigma A + \rho, \sigma B + \rho, \sigma C + \rho$, respectively, where

$$\sigma = 2/(A-C), \rho = -(A+C)/(A-C) \quad (1.28)$$

So

$$\begin{aligned} \sigma A + \rho &= 1 \\ \sigma B + \rho &= (2B-A-C)/A-C = \kappa \text{ (asymmetry parameter)} \\ \sigma C + \rho &= -1 \end{aligned} \quad (1.29)$$

Then

$$E(\sigma A + \rho, \sigma B + \rho, \sigma C + \rho) = [(\sigma A + \rho)Pa^2 + (\sigma B + \rho)Pb^2 + (\sigma C + \rho)Pc^2]/\hbar^2 = \sigma E(A, B, C)/h + \rho J(J+1) \quad (1.30)$$

The rotational energy can be expressed in terms of reduced energy $E(1, \kappa, -1)$ or $E(\kappa)$:

$$E(A, B, C) = h \left[\frac{A+C}{2} J(J+1) + \frac{A-C}{2} E(\kappa) \right] \quad (1.31)$$

The reduced energy $E(\kappa)$ has been well tabulated, thus the rotational energy can be conveniently obtained from the equation (4.11). Additionally, the reduced energy tabulation has the equality:

$$E_\tau^J(\kappa) = -E_{-\tau}^J(-\kappa) \quad (1.32).$$

Figure 1.1. shows the energy levels diagram as a function of the asymmetry parameter κ .

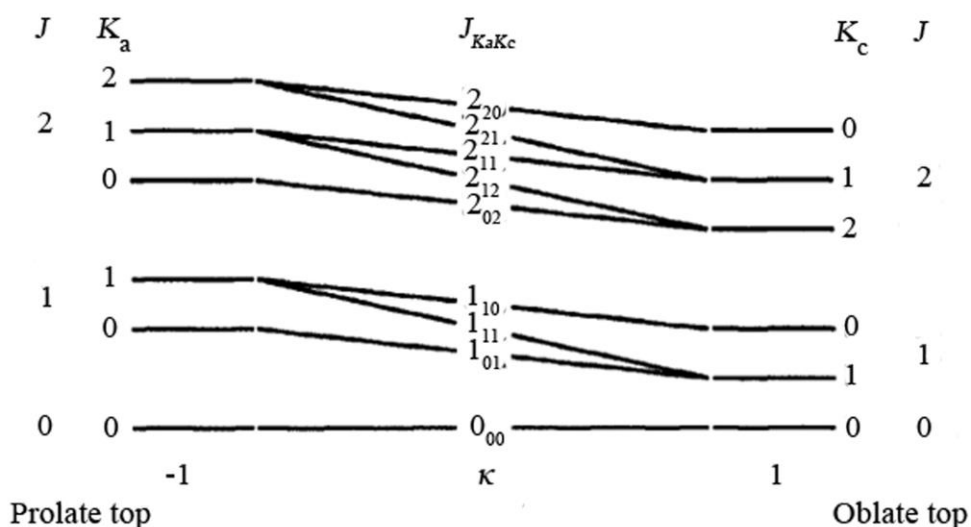


Figure 1.1. energy levels diagram as a function of the asymmetry parameter κ . the limit values of κ are shown for prolate-top (-1) and oblate-top (1).

Three types of rotational transitions can occur for a rigid asymmetric top with respect to J . The selection rule for J is $\Delta J = 0, \pm 1$. $\Delta J = 0$ specifies the Q branch when $\Delta J = -1$ and 1 represent P and R branches, respectively. By considering electric dipole moments, the selection rules for rotational transition in the asymmetric molecules can be expressed in terms of K_a and K_c , as shown in the table below,

Table 1.1. The selection rule in terms of ΔK of rigid asymmetric top.

	ΔK_a	ΔK_c
μ_a	$0, \pm 2, \pm 4, \dots$	$\pm 1, \pm 3, \pm 5, \dots$
μ_b	$\pm 1, \pm 3, \pm 5, \dots$	$\pm 1, \pm 3, \pm 5, \dots$
μ_c	$\pm 1, \pm 3, \pm 5, \dots$	$0, \pm 2, \pm 4, \dots$

Depending on the components of the dipole moment, the transition can be classified as three types of transitions which are a -type, b -type and c -type. All the transitions can be expected if the corresponding components of dipole moment are present. Generally, the transitions with smaller ΔK_a or ΔK_c will dominate the spectra.

1.3 Non-rigid rotor

As expected, the rigid rotor theory is not sufficient to describe the observed high resolution rotational spectra. The rotational energy levels are influenced by the perturbation resulting from the

vibration-rotation interaction, centrifugal distortion, and other effects. The rotational frequencies can deviate from the rigid-rotor theoretical predictions from a few to hundreds of MHz, especially for high J transitions and for non-covalent binding cluster system.

1.3.1. Classic description of centrifugal and Coriolis forces.

As we know in a non-inertial reference frame, the inertial force on the target object should be considered, while in a rotational reference frame another Coriolis effect should be added on the moving object. Thus when a vibrational-rotational molecule is considered with respect to the axis system fixed on the rotor, these two kinds of forces are present which perturb the pure rigid rotational energy levels. They are centrifugal and Coriolis forces, respectively. They can be expressed in classical theory respectively as:

$$\begin{aligned} F_c &= m\omega^2 \mathbf{r} \\ F_\zeta &= 2m\mathbf{v} \times \boldsymbol{\omega} \end{aligned} \quad (1.33)$$

Where $\boldsymbol{\omega}$ is the angular velocity of the body-fixed axis system with respect to the space-fixed axis system, \mathbf{v} is the linear velocity of the atoms with respect to the body-fixed axis system, \mathbf{r} is the distance of a mass m from the rotational axis. From the formula one can see that the centrifugal force is only related with the rotation, while the Coriolis effect is a vibration-rotation interaction. As the molecule rotates, the centrifugal distortion is exerted on the atoms to produce linear motion. The inter-atomic distance increases with the velocity of rotation and is function of the rotational states. The Coriolis force can produce velocity components perpendicular to the normal velocity vectors, which makes the coupling between different vibrational modes.

1.3.2 Centrifugal distortion and effects of vibrational excitation on the B value in linear molecules

According to the rigid rotor theory mentioned above, the transitions of a rigid rotor should be spaced by $2B$, where B is the rotational constant. However, the experimental transitions appear at lower frequencies, with discrepancies increasing with J . This effect is responsible by the centrifugal distortion, which can slightly increase the bond length. In the Schrödinger equation, this effect generally is treated as a perturbation on the rigid rotor. The resulting energy expression is

$$E = hBJ(J + 1) - hDJ^2(J + 1)^2 \dots \quad (1.34)$$

where D is the distortion constant, and B is the effective rotational constant including the vibrational terms instead of the equilibrium one as described in the rigid rotor. Thus, B can be expressed as below included the distortion contribution,

$$B_v = B_e - \sum_i \alpha_i \left(v_i + \frac{d_i}{2} \right) - D_v J(J+1) \quad (1.35)$$

where v and d_i are the vibrational quantum number and degeneracy of the i -th vibration. B_e is the equilibrium rotational constant, α_i is the vibration-rotation constant for the i -th vibration. For the ground state of the molecular system the rotational constant should be

$$B_0 = B_e - \sum_i \frac{\alpha_i d_i}{2} - DJ(J+1) \quad (1.36)$$

From this formula one can see that the rotational constant of the ground state is not equal to the equilibrium value. The frequency transition from J to $J+1$ state takes the form:

$$\nu = 2B_v(J+1) - 4D_v(J+1)^3 \quad (1.37)$$

D is always positive, and this is why the observed spectrum tends to converge with increasing J . The distortion constant is related to the force constant of the vibrational mode, for example for the diatomic molecule it can be evaluated as

$$D = 4B_e^3 / \omega^2 \quad (1.38)$$

1.3.3. Centrifugal distortion in symmetric-top molecules

Similarly, as linear molecules, centrifugal distortion also influences the rotational spectra of symmetric-top molecules. The effect generally forces the atoms away from the rotational axes. With the consideration of this effect, the rotational energy levels for a prolate top should be expressed as:

$$E = hBJ(J+1) + h(A-B)K^2 - hD_J J^2(J+1)^2 - hD_{JK} J(J+1)K^2 - hD_K K^4 \quad (1.39)$$

The measured transition frequencies from J to $J+1$ state should be fitted in the equation:

$$\nu = 2B(J+1) - 2D_{JK}(J+1)K^2 - 4D_J(J+1)^3 + H_{JJJ}(J+1)^3 \times [(J+2)^3 - J^3] + 4H_{JJK}(J+1)^3 K^2 + 2H_{JKK}(J+1)K^4 \quad (1.40)$$

The last three terms are the second order distortion corrections, which are needed for the fit of high J transitions. From the equation it is worth to note that the transition frequency also depends on the value of K which does not appear in the rigid top expression.

In addition, for the asymmetric-top molecules the quantum number K , the angular momentum along figure axis, is not a good quantum number any more. However by introducing a Hamilton term $H^{(1)}$ representing centrifugal distortion to the rigid Schrödinger equation, the similar energy expression has been obtained, as we discuss here for linear and symmetric-top.

1.4. Nuclear quadrupole coupling

In brief, this effect is originated from the coupling between the nuclear spin angular momentum I and the molecular rotational angular momentum J , through the interaction between the

quadrupole moment Q of the nuclei and the electric field gradient raised by the electrons and the other nucleus of the molecule at the position of the nuclei. The interaction generates a twisting torque on the nuclei and tends to align the spin momentum along the direction of the field gradient. As a result, the spin momentum will precess around the direction of the field gradient, arousing a added precessional frequency and splitting the energy levels. Such a quadrupole interaction needs a non-spherical charge distribution in the nuclei which is satisfied in the nuclei with $I > 1/2$. I is the quantum number of I with a value of half-integer or integer which depend on the composition of the nuclei. 1) I equal zero if both the number of the neutrons and the protons in the nuclei are even; 2) I is a half integer number ($1/2, 3/2, 5/2 \dots$) if the sum of the neutrons and protons is odd; 3) I is an integer ($1, 2, 3 \dots$) if both the number of the neutrons and the protons are odd. The quadrupole moment Q is positive if the nuclei has a prolate charge distribution when it is negative if the charge distribution as a oblate shape. The coupling of spin angular momentum I and the rotational angular momentum J can produce a total angular momentum F as shown in schematic diagram Figure 1.2.

$$\mathbf{F} = \mathbf{J} + \mathbf{I} \quad (1.41)$$

So, the quantum number F is quantized and can take the following values:

$$F = J + I, J + I - 1, \dots, |J - I| \quad (1.42)$$

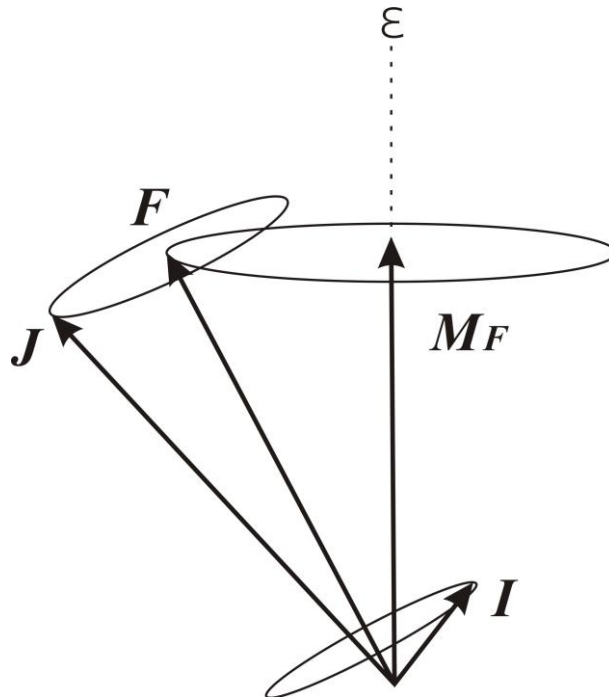


Figure 1.2. The vector model of F formed by J and I . M_F is the projection of F along the external field ϵ .

The selection rule of the transitions between different energy level are:

$$\Delta J = 0, \pm 1; \Delta F = 0, \pm 1 \quad (1.43)$$

As we know the electrical energy of the nuclei in the extra-nuclear field is:

$$E = \int \rho_n V d\tau_n \quad (1.44)$$

where ρ_n represent the density of the charge of the nuclei in elemental volume $d\tau_n = dXdYdZ$, where XYZ is the space-fixed reference, and V is the potential arising from other charge in the molecule. When the potential is expressed in the Taylor's expansion, one can obtain the first order term (the usual monopole interaction), the vanished second order term, and the third order term, which is the quadrupole interaction E_Q . In the rotating molecule, the interaction of a single coupling nuclei is written as:

$$E_Q = -\frac{1}{6} \mathbf{Q} \cdot \nabla \mathbf{E} = \frac{2}{(J+1)(2J+3)} \sum_{g=a,b,c} \chi_{gg} \langle J, i | J_g^2 | J, i \rangle \left[\frac{\frac{3}{4} C(C+1) - (J+1)I(I+1)}{2J(2J-1)I(2I-1)} \right] \quad (1.45)$$

where $g = a, b, c$ are the principal inertia axes, i is one of the axes of the space-fixed reference, and

$$C = F(F+1) - J(J+1) - I(I+1) \quad (1.46)$$

and by convention, the coupling constants are designated as:

$$\chi_{gg'} = eQq_{gg'} \quad (1.47)$$

where

$$q_{gg'} = \frac{\partial^2 V}{\partial g g'} \quad (1.48)$$

Hold by Laplace's equation,

$$\chi_{aa} + \chi_{bb} + \chi_{cc} = 0 \quad (1.49)$$

By customary, they are expressed in terms of one coupling constant with the most nearly symmetric axis, such as χ_{cc} , and an asymmetric parameter η :

$$\eta = \frac{\chi_{aa} - \chi_{bb}}{\chi_{cc}} \quad (1.50)$$

1.5. Internal motions

As of considerable interest for physicists and chemists, large amplitude internal motions such as internal rotation and ring puckering, have been studied for a long time by MW spectroscopy. The study the potential functions and barrier heights can provide the essential information to test and improve the theoretically predictive methods, and help us understand the origin and of the potential barrier and the forces in charge of the conformational performance.

1.5.1. Internal rotation

The internal rotation in a molecule can be described as a function of a torsional angle α with respect to the two rotating groups of the molecule. Apparently, the potential energy is a periodic function of α with the period $2\pi/N$, where N represents the degree of the symmetry of the rotor. With the setting potential $V=0$ at $\alpha=0$, the potential function can be expressed as a Fourier expansion as:

$$V(\alpha) = \frac{V_N}{2}(1 - \cos N\alpha) + \frac{V_{2N}}{2}(1 - \cos 2N\alpha) + \dots \quad (1.51)$$

As an example, we consider here only the threefold barrier such as the internal rotation of the CH_3 group in many organic molecules. In this way the potential function (omitting the higher orders V_6 term which is generally less than 3% of V_3) can be expressed as:

$$V(\alpha) = \frac{V_3}{2}(1 - \cos 3\alpha) \quad (1.52)$$

The function can be depicted as Fig 1-3.

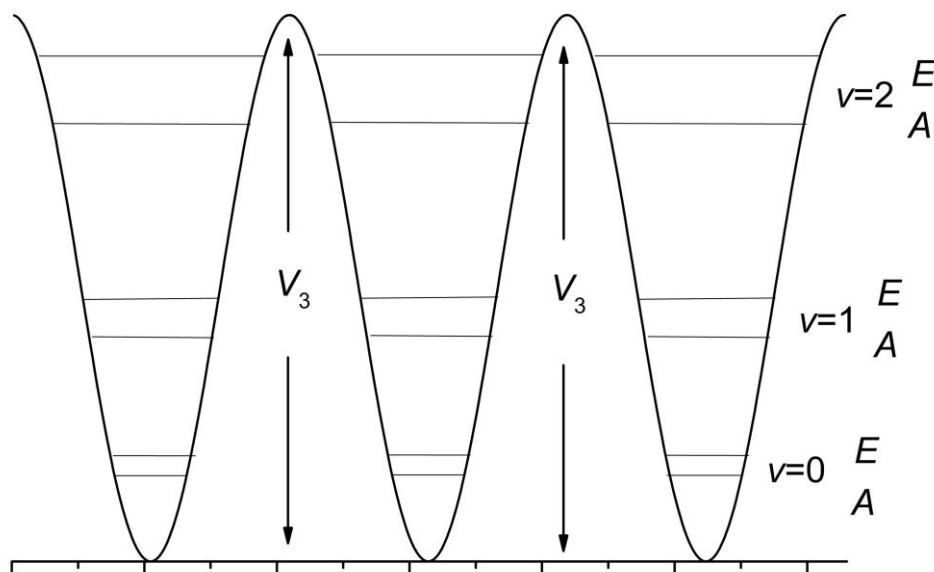


Figure 1.3. The potential curve and the torsional energy levels as the function of α . v is the torsional quantum number and A and E are their symbols related to their symmetry.

Substituting the potential function into the wave equation for internal rotation, it is:

$$-F \frac{d^2 U(\alpha)}{d\alpha^2} + \left[\frac{V_3}{2}(1 - \cos 3\alpha) - E \right] U(\alpha) = 0 \quad (1.53)$$

where:

$$F = \frac{\hbar^2}{2I_r} \quad (1.54)$$

I_r is the reduced moment of inertia of the two parts (α , β) rotated with respect to each other in the molecule, calculated as:

$$I_r = \frac{I_\alpha I_\beta}{I_\alpha + I_\beta} \quad (1.55)$$

In order to understand the the spacing between the energy levels in the case of a finite t barrier, it is helpful to consider two extreme cases, which are the free rotor limit ($V_3 \rightarrow 0$) and the three-fold harmonic oscillator limit ($V_3 \rightarrow \infty$). For a general case with a finite barrier, the torsional energy level can be represented as the schematic diagram as below,

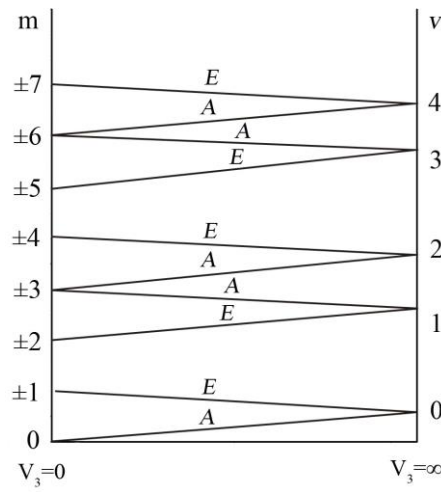


Figure 1.4. The torsional energy level between the energy levels of free internal rotation labeled by quantum number m , and three-fold harmonic torsional oscillation labeled by quantum number v . The levels labeled by A are nondegenerate while the E levels are doubly degenerate.

For the two extremes, the eigenfunctions and eigenvalues can be obtained easily from equation (1.53). For the free rotor limit, they are

$$U_{v\sigma}(\alpha) = \frac{1}{\sqrt{2\pi}} e^{i(3k+\sigma)\alpha} \quad (1.56)$$

$$E_{v\sigma} = F(3k + \sigma)^2 \quad (1.57)$$

where $k = 0, \pm 1, \pm 2, \dots$, and the indexes $\sigma = 0, \pm 1$ represent A and E states, respectively. For the infinite barrier limit, they are

$$U_{v0}(\alpha) = \frac{1}{\sqrt{3}} [H_v^{(1)} + H_v^{(2)} + H_v^{(3)}]$$

$$U_{vI}(\alpha) = \frac{1}{\sqrt{3}} [H_v^{(1)} + \epsilon H_v^{(2)} + \epsilon^2 H_v^{(3)}]$$

$$U_{v,l}(\alpha) = \frac{1}{\sqrt{3}} [H_v^{(1)} + \varepsilon^2 H_v^{(2)} + \varepsilon H_v^{(3)}] \quad (1.58)$$

$$E_v = 3(V_3 F)^{1/2} (v + 1/2) \quad (1.59)$$

where $\varepsilon = \exp(i2\pi/3)$, and $H_v^{(1)}$, $H_v^{(2)}$, $H_v^{(3)}$ are the harmonic oscillator functions with the centers at 0, $2\pi/3$, and $4\pi/3$, respectively.

The splitting of the rotational spectra can be interpreted by the interaction between the overall and internal rotations. In the classical theory, the kinetic energy of a molecule with an internal rotation top can be written as:

$$T = \frac{1}{2} \sum_g I_g \omega_g^2 + \frac{1}{2} I_\alpha \dot{\alpha}^2 + I_\alpha \dot{\alpha} \sum_g \lambda_g \omega_g \quad (1.60)$$

$g = x, y, z$

I_g are the principal moments of inertia of the whole molecule, I_α is the moment of inertia of the rotating top around its symmetry axis, ω_g are the angular velocity components of the molecule, α' is the angular velocity of the top relative to the framework, and λ_g are the cosines between the rotating top and the principal axes of the molecule. By substituting the following equations

$$P_g = \frac{\partial T}{\partial \omega_g} = I_g \omega_g + \lambda_g I_\alpha \dot{\alpha} \quad (1.61)$$

$$p = \frac{\partial T}{\partial \dot{\alpha}} = I_\alpha \dot{\alpha} + I_\alpha \sum_g \lambda_g \omega_g$$

into (7.10), then it can be written as

$$T = \frac{1}{2} \sum_g \frac{P_g^2}{I_g} + \frac{1}{2} r I_\alpha \dot{\alpha}^2 \quad (1.62)$$

and

$$r = 1 - \sum_g \frac{\lambda_g^2 I_\alpha}{I_g} \quad (1.63)$$

So, the Hamiltonian operator involving overall and internal rotations can be expressed as

$$H = H_r + F(r I_\alpha \dot{\alpha})^2 + V(\alpha) \quad (1.64)$$

Applying the Van Vleck transformation, the Hamiltonian can be expressed as

$$H_{v\sigma} = H_r + F[W_{v\sigma}^{(0)} + W_{v\sigma}^{(1)}(p - r I_\alpha \dot{\alpha}) + W_{v\sigma}^{(2)}(p - r I_\alpha \dot{\alpha})] \quad (1.65)$$

with

$$H_r = A_{v\sigma} P_x^2 + B_{v\sigma} P_y^2 + C_{v\sigma} P_z^2 \quad (1.66)$$

where

$$\begin{aligned}
A_{v\sigma} &= A_x + W_{v\sigma}^{(2)} F \rho_x^2 \\
B_{v\sigma} &= B_y + W_{v\sigma}^{(2)} F \rho_y^2 \\
C_{v\sigma} &= C_z + W_{v\sigma}^{(2)} F \rho_z^2
\end{aligned}
\tag{1.67}$$

and

$$\rho_g = \frac{\lambda_g I_\alpha}{I_g}
\tag{1.68}$$

The W coefficients are dependent on the reduced barrier, V_3/F . It is worth noting that in the Hamiltonian, the rotational constants A_x , B_y , C_z have been replaced by $A_{v\sigma}$, $B_{v\sigma}$, $C_{v\sigma}$.

1.5.2. Inversion motion

Another hindered internal motion which can split the rotational spectra is the inversion motion. This interaction generally exists when a molecule possesses two energetically equivalent configurations, for example NH_3 , *gauche*-Ethanol, indan. The two equivalent configurations are separated by a potential barrier, as shown in Figure 1.5.

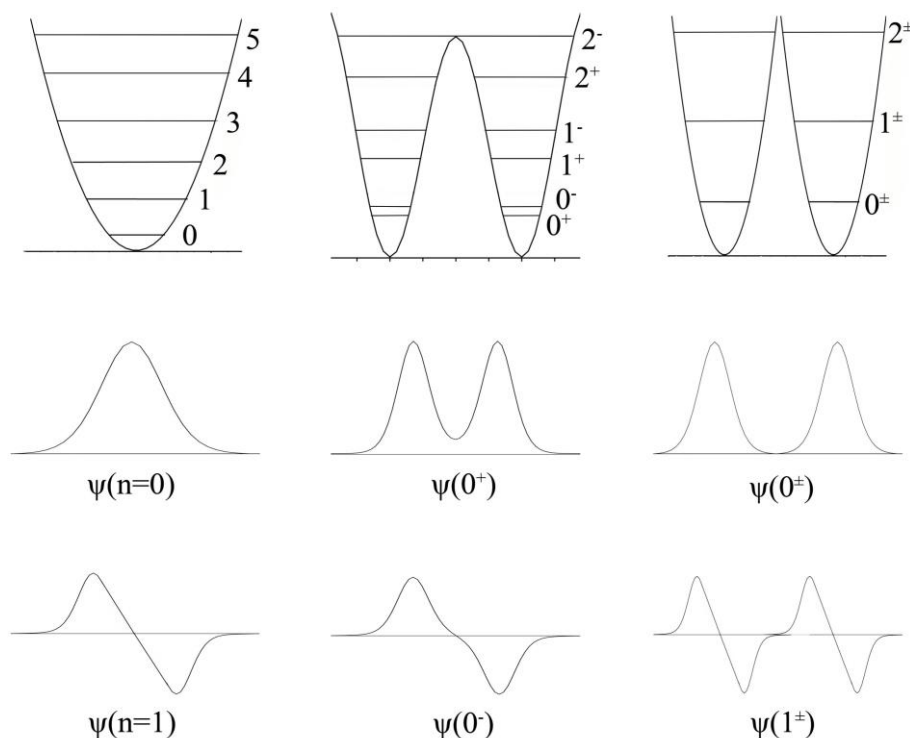


Figure 1.5. Potential functions and partial wave functions of harmonic oscillator (left), finite inversion barrier (middle), and infinite inversion barrier (right).

On the left, one can see that when the absence of the inversion barrier, the vibrational energy levels are evenly spaced in the harmonic potential well. When an infinite barrier separates the wells, the molecule will be trapped in one of the two wells with double degenerate vibrational states. In the finite barrier case, the quantum mechanism allows the states lying below the barrier to tunnel

through the barrier at a rate which is a function of barrier height and width. The coupling of the two equivalent states through tunneling can lift the degeneracy and produce a pair of vibrational states (+, -). The signs (+, -) represent the symmetric and antisymmetric wave functions respectively. In the case of inversion tunneling, two kinds of rotational transitions can occur. The first group are the intrastate transitions which occurs between the levels with same symmetry. The other is the interstate transitions between levels with different symmetry. As shown in Figure 1.6, a schematic diagram illustrates these two kinds transitions.

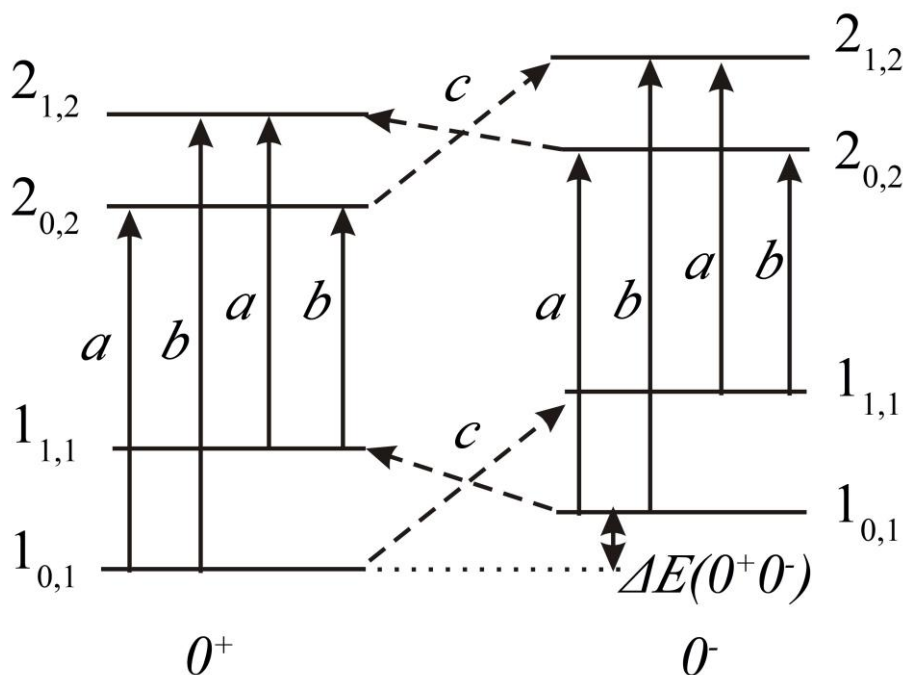


Figure 1.6. The intra- and inter- state transitions. As an example, here the *a* and *b* types transitions are intrastate transitions while *c*-type transition occur between different astates

From Figure 1.6, we can see that the tunneling splitting $\Delta E(0^+0^-)$ can be directly obtained from the interstate transitions. In this dissertation, there is a good example to illustrate this situation, which is the study of the rotational spectroscopy of indan.

1.6. Molecular structure evaluation

Microwave spectroscopy provides a very accurate method to determine the rotational constants and moments of inertia. However, this is not the ultimate aim for the spectroscopist unless some methods were available for converting these data into molecular structure information. In this process, not only the uncertainties of the Planck's constant but also the vibrational effect has been proved to be the difficult problems to overcome in evaluating the structural parameters with a satisfying accuracy, especially for the second one even in the ground vibrational state. Different procedures have been introduced into the correction of the various degrees for vibrational effect. In

general, three types structures are used in the spectroscopic study and defined as r_e , r_0 , and r_s .

1.6.1 r_e : the equilibrium structure for the hypothetical vibrationless state.

It corresponds to the minimum of the potential surface. It can be evaluated by correction for the effects of vibration including zero-point vibration.

The relationship between the equilibrium and the effective moments of inertia can be expressed as:

$$I_\alpha^v = I_e^v + \sum_s \left(v_s + \frac{d_s}{2} \right) \varepsilon_s^\alpha; \quad \alpha = a, b, c \quad (1.69)$$

where the rotation-vibration parameters are:

$$\varepsilon_s^\alpha = \left(\frac{8\pi^2}{h} \right) (I_\alpha^e)^2 \alpha_s^\alpha \quad (1.70)$$

$$\alpha_s^\alpha = - \left(\frac{6B_e^2}{\omega_e} \right) (1 + a_1) \quad (1.71)$$

In addition, I_α^v and I_α^e are the effective and equilibrium moments of inertia, respectively. v_s is the s -th vibration, d_s is its degeneracy, ω_e is the classical harmonic vibrational frequency, a_1 is the cubic anharmonic constant.

The equilibrium structure might be the most meaningful one in physics, however it is not usually feasible to acquire enough experimental data to obtain its value. Plenty of knowledge on the potential constants is required, except for simple molecules in which the anharmonic constants are available.

1.6.2. r_0 : the effective structure for the ground vibrational state.

The most obvious method to obtain the molecular structure is directly derived from the experimental rotational constants B_0 . The relations between them are:

$$B_0 = \frac{h}{8\pi^2 I_b^0} \quad (1.72)$$

$$I_b^0 = \frac{1}{<1/\sum_i m_i r_i^2>} = \sum_i m_i r_{0i}^2 \quad (1.73)$$

From the equation, one can see that

$$r_0 = <\frac{1}{r^2}>^{-\frac{1}{2}} \neq r_e \neq <r> \neq <r^2>^{\frac{1}{2}} \quad (1.74)$$

The r_0 differ slightly for each isotopic species. By assuming r_0 to be identical for each isotopic species, a set of equations can be solved to give the r_0 structure. This procedure, least-

squares fitting techniques, is based on the linearization of the equations set:

$$I_i^0 = I_i^* + \sum_j \left(\frac{\partial I_i}{\partial p_j} \right)_0 \Delta p_j \quad (1.75)$$

where I_i^0 is the i -th experimental moment of inertia, p_j is the i -th structural parameter, I_i^* is the i -th moment of inertia of the initially assumed structure, $\partial I_i / \partial p_j$ represents the change of I_i^* with a small change in p_j when fixing all other parameters. This procedure will be repeated until the discrepancies between calculated and measured values are acceptable, and then a satisfying parameter correction Δp_j from the initial structure can be obtained.

1.6.3. r_s : the substitution structure.

It is derived from the rotational constants of isotopic substitutions. In principle, the r_s distance lies between the r_e and r_0 distances and hence closer to the equilibrium value. However sometimes it is not accurate, for example when the substituted atom is closed to principal axes. By assuming that the position of each atom does not change upon isotopic substitution, the substituted coordinates e can be derived by resolving Kraitchmann's equations. We will discuss here the non-planar asymmetric-top as a general case. It is convenient to use the planar moments of inertia \mathbf{P} to obtain the r_s . The principal moments of the parent and substituted species can be obtained from the experimental rotational constants and the relationship between them with the principal moments of inertia are:

$$\begin{aligned} P_x &= \frac{1}{2}(-I_x + I_y + I_z) \\ P_y &= \frac{1}{2}(-I_y + I_z + I_x) \\ P_z &= \frac{1}{2}(-I_z + I_x + I_y) \end{aligned} \quad (1.76)$$

The matrix of the planar moments of inertia \mathbf{P} of the parent molecule in its principal axis system can be expressed as:

$$\mathbf{P} = \begin{vmatrix} \sum m_i x_i^2 & 0 & 0 \\ 0 & \sum m_i y_i^2 & 0 \\ 0 & 0 & \sum m_i z_i^2 \end{vmatrix} \quad (1.77)$$

For the isotopically substituted molecule with respect to the same axes system, the elements of \mathbf{P}' are:

$$\begin{aligned}
P_{xx}' &= P_x + \mu x^2 \\
P_{yy}' &= P_y + \mu y^2 \\
P_{zz}' &= P_z + \mu z^2 \\
P_{xy}' &= \mu xy \\
P_{xz}' &= \mu xz \\
P_{yz}' &= \mu yz
\end{aligned} \tag{1.78}$$

The reduced mass for the substituted species is defined as

$$\mu = \frac{M\Delta m}{M + \Delta m} \tag{1.79}$$

with M is the total mass of the parent molecule, Δm is the mass difference of the isotopically substituted atoms.

The secular equation for the substituted molecule is hence:

$$\begin{vmatrix}
P_x + \mu x^2 - P' & \mu xy & \mu xz \\
\mu xy & P_y + \mu y^2 - P' & \mu yz \\
\mu xz & \mu yz & P_z + \mu z^2 - P'
\end{vmatrix} = 0 \tag{1.80}$$

by resolving the equation, the coordinates of the substituted atom can be given as

$$\begin{aligned}
|x| &= \left[\frac{\Delta P_x}{\mu} \left(1 + \frac{\Delta P_y}{P_y - P_x} \right) \left(1 + \frac{\Delta P_z}{P_z - P_x} \right) \right]^{1/2} \\
|y| &= \left[\frac{\Delta P_y}{\mu} \left(1 + \frac{\Delta P_z}{P_z - P_y} \right) \left(1 + \frac{\Delta P_x}{P_x - P_y} \right) \right]^{1/2} \\
|z| &= \left[\frac{\Delta P_z}{\mu} \left(1 + \frac{\Delta P_x}{P_x - P_z} \right) \left(1 + \frac{\Delta P_y}{P_y - P_z} \right) \right]^{1/2}
\end{aligned} \tag{1.81}$$

where

$$\begin{aligned}
\Delta P_x &= \frac{1}{2} (-\Delta I_x + \Delta I_y + \Delta I_z) \\
\Delta P_y &= \frac{1}{2} (-\Delta I_y + \Delta I_z + \Delta I_x) \\
\Delta P_z &= \frac{1}{2} (-\Delta I_z + \Delta I_x + \Delta I_y)
\end{aligned} \tag{1.82}$$

Chapter II

Experimental techniques in rotational spectroscopy

As a powerful tool in molecular science, rotational spectroscopy has been progressing impressively.^[4,5] Since the first study of the microwave spectrum on a molecule (NH_3) in 1934,^[6] this technique has experienced more than 80 years. People working in this field never stop developing this technique and just recently still impressive advancements have been achieved. The rotational spectrometer was developed from the microwave Stark spectrometer by Hughes and Wilson^[7], then the Fabry-Pérot Fourier transform microwave spectrometer by Balle and Flygare was introduced in 1981^[8], then the broadband chirped pulse Fourier transform microwave spectrometer by B. H. Pate was developed^[9], and just recently the three-wave mixing technique is utilized to discriminate enantiomers in chiral samples^[10].

The application of the time-domain detection of the rotational free induction decay (FID) made it possible to achieve high frequency resolution without the power broadening found in Stark modulation. The pulsed molecular beam source used in MW spectrometer has greatly expanded the research range of molecular systems and made it possible to characterize larger molecules and non-covalent bonded clusters. Different designs of sample sources, for example a great advance was achieved with the introduction of supersonic jet sources coupled to microwave spectrometers and also with the fast mixing nozzle and laser ablation techniques, giving us the chance to investigate more systems such as pre-reactive adducts and solid samples.

2.1. Free-Jet Millimeter-Wave Stark Modulated Absorption (FJ-MMWA) Spectrometer (Frequency-Domain)

In the free-jet-microwave laboratory at the University Bologna, the first free-jet spectrometer was built by Prof. P. Favero, Prof. W. Caminati and Prof. S. Melandri in 1993^[11] and it was, similar to the one already present at Monash University.^[12] In brief, a monochromatic radiation passes through a cylindrical vacuum chamber and crosses vertically with a molecular beam. The radiation intensity can be modified by the molecular absorption. The transmission recorded as the function of the radiation frequency yields the spectrum.

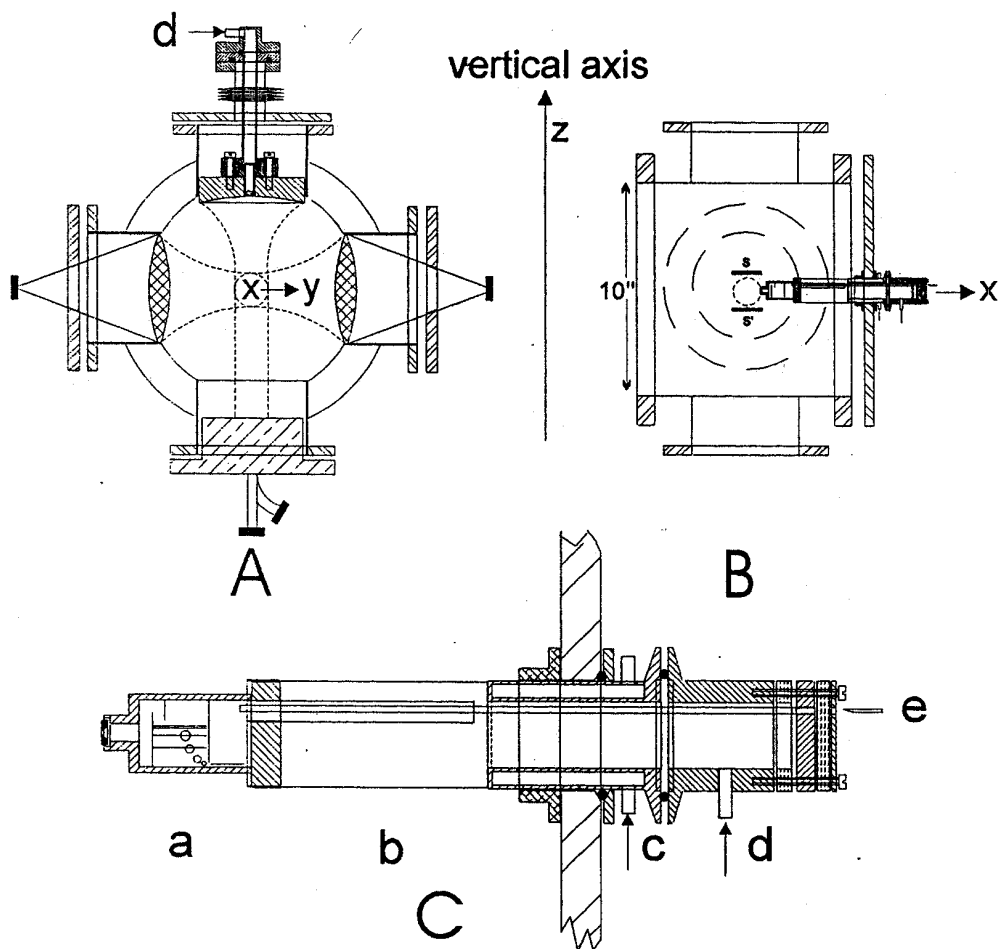


Figure 2.1. Schematic absorption cell (A and B) and the molecular beam system (C).

As shown in Figure 2.1, the molecular beam is expanded along the axis (x) of a cylindrical vacuum chamber with diameter of 25 cm and length of 25 cm. The chamber is evacuated with a diffusion pump yielding a throughput of around 4000L/s and the background pressure is kept in the region of 10^{-5} Pa. At the end of the chamber, a chevron baffle cooled with liquid nitrogen is settled to protect the vacuum system from the pollution of the non-volatile components in the molecular beam. The nozzles with diameters ranging from 0.03 to 0.05cm are used and generally Argon is used as the carrier gas with a stagnation pressures 10-100kPa. The molecular beam can achieve an estimated rotational temperature of about 10 K. Lines separated by more than 300 kHz are resolvable and the estimated accuracy of the frequency measurements is better than 50 kHz. There are four parts in the absorption cell (see Figure 2.1(A)) where the microwave radiation interacts with the molecular jet plume (dotted circle). The molecular beam system (Figs. 2-1(B) and (C)) is movable along the x -axis to obtain the best conditions. The lens system along the y -axis can concentrate the radiation into the plume region with a waist of about 2cm. Along the z -axis, S and S' are two plates spaced by 5 cm which provide the Stark modulation. The unearthed plates are

guarded and a voltage of up to 3 kV with a frequency of 33 kHz are applied to the plates. Along the z -axis there is a Fabry-Pérot semiconfocal interferometer which can produce a radiation with concentration similar with that of the lens system. The spherical mirror is movable under vacuum controlled by an automatic electro-mechanical control (the driving system is not shown) so that the interferometer can be kept resonant at the operating microwave frequency. Figure 2.1(C) is the detailed diagram of a heated nozzle system: section *a* is the nozzle saturation chamber where the sample is electrically heated, and the temperature can be controlled up to 400°C; section *b* is the preheating chamber for the carrier gas; section *c* is the water-cooled system; section *d* are the entrances of the carrier gas and substance, where the liquid or powdered solid substance can be filled into the saturation chamber under vacuum operation.

Recently the MW source of radiation system was updated as described below.^[13] In addition to the 2013 design, a new radio-frequency source has been used and a box diagram of the microwave circuit and modulating scheme used in the experiment is reported in Figure 2.2. It is based on an X-Band synthesizer followed by a x4 multiplier chain composed of two multipliers (doubblers). The first doubler is active and the second one is passive, and they are separated by an isolator and a low pass filter. The presence of the isolator improves the coupling between adjacent elements of the chain, and the filter helps to eliminate unwanted harmonic signals that could be present. In fact, the frequency multiplication process is not an ideal one because it can give rise to some disturbances (unwanted harmonic frequencies, phase noise, and even spurious signals) in the output signal, but if a high-frequency generator is not available, the introduction of filters placed downstream of the generator and each multiplier improves the performances of this kind of multiplication system. Depending on the section of the chain, both a band-pass filter and a filtering effect due to waveguide cutoff have been used. Power amplifiers as well as variable attenuators have been placed to drive correctly the multipliers and the FJAMMW. The transmitted power is detected by Schottky diodes (Millitech DXW10, Millitech 47324H-1211) and a lock-in amplifier. The lens system had been designed for the 48-72GHz frequency range, however it can work up to 78 GHz without any apparent degradation of the factory specifications. The spectrometer has a resolving power of about 300 kHz and an estimated accuracy of about 50 kHz.

The schematic diagram and the introduction of the entire spectrometer is shown in Figure 2.2, and the photo of the FJ-AMMW laboratory at UNIBO is shown in Fig 2.3., as below.

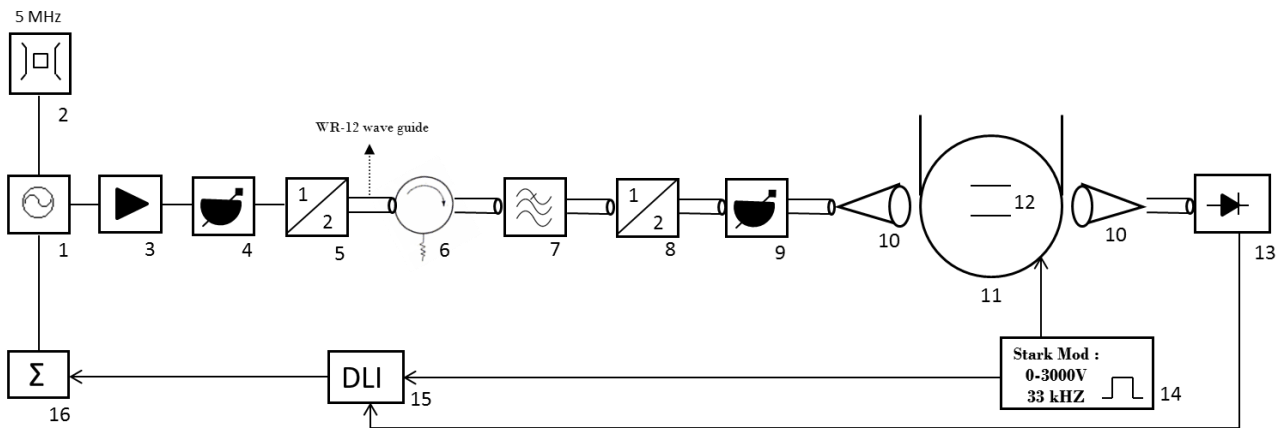


Figure 2.2. Block diagram of the Free-jet absorption millimeter wave spectrometer (FJAMMW): 1. Microwave synthesizer HP8672A (2–18 GHz). 2. Reference signal, Rb oscillator (5 MHz), Ball-Efraton FRK-LLN. 3. Hittite Amplifier MW (5–20 GHz) Gain: +20 dB. 4. Variable attenuator, NARDA (10 dB). 5. Frequency doubler Spacek-laboratories (26.5–40 GHz). Output power: +17 dBm Waveguide WR28. 6. Dorado Isolator (26.5–40 GHz, 41 GHz). 7. Low pass filter Spacek-laboratories, $f_{\max} = 41$ GHz. 8. Frequency doubler Spacek-laboratories (53–80 GHz). Output power: –3 dBm to 0 dBm, Waveguide WR12. 9. Variable attenuator (0–35 dB). 10. Horn-dielectric lens system (Montech-Clayton, Australia). 11. Supersonic-jet expansion chamber. 12. Stark plates. 13. Schottky-diode detector: Millitech DXW10 for frequencies above 60 GHz or a Millitech 4731 4H-1111 for frequencies below 60 GHz. 14. High-voltage square-wave modulation: electric field up to $750 \text{ V} \cdot \text{cm}^{-1}$ at a frequency of 33 kHz. 15. Digital lock-in amplifier. 16. Experimental control and data acquisition.

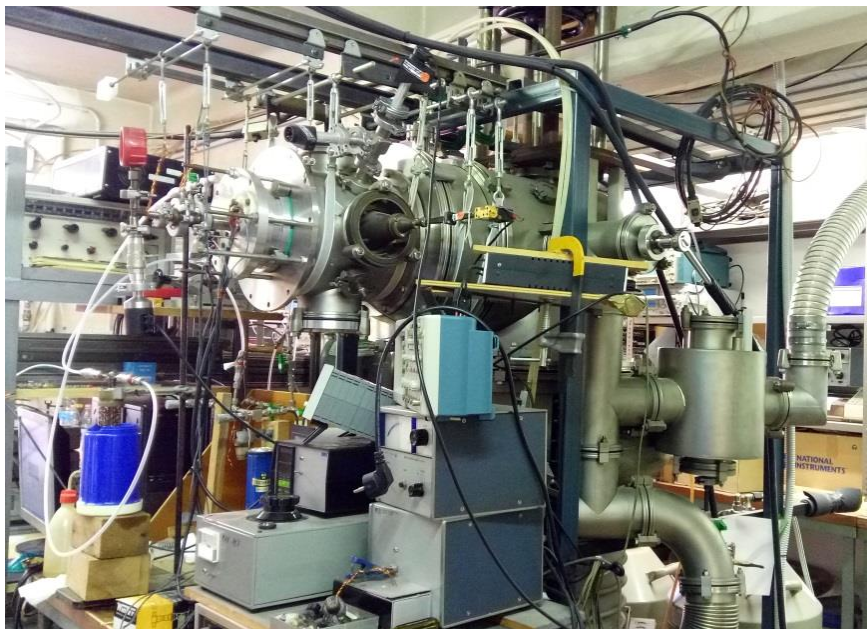


Figure 2.3. the picture of the FJAMMW spectrometer in UNIBO.

2.2. Pulsed jet Fourier transform microwave (PJ-FTMW) spectroscopy

2.2.1. Pulsed supersonic jet expansion

The use of the pulsed jet valve can ideally combine with the pulsed exciting radiation and lighten the load of the vacuum system. In our PJ-FTMW spectrometer,^[14] the molecular beam is coaxially propelled into the Fabry-Pérot resonator. This arrangement can increase both the resolution and the sensitivity than in the case where the jet valve is perpendicular with the symmetry axis of the resonator.

When the gas species expands into the evacuated chamber a supersonic jet, as a result of the adiabatic expansion, the effective vibration and rotation temperature of the sample is dramatically decreased, and the molecular beam travels without collision along the direction of propagation of the radiation. Before the expansion the gas species abide by the Maxwell-Boltzmann distribution and the molecular velocities v_0 are determined by the equilibrium temperature T_0 . Then during the initial stage of the adiabatic expansion, the binary collisions can lead to the conversion of the random motions of the molecules into a directional transition along the chamber axis. The internal energy of the molecular species is also transformed into kinetic energy. The velocity distribution of the seeded molecules become narrow and shifted toward the terminal value:

$$v_{\infty} = \sqrt{(2k_B T_0 / m \times \gamma / (\gamma - 1))}; \gamma = c_p / c_v \quad (2.1)$$

where c_p and c_v represent the mean heat capacities at constant pressure and volume, respectively. m is the mean mass of all species and k_B is the Boltzmann constant. The terminal velocity v_{∞} corresponds to the one at the extreme when all the internal energy is converted to the kinetic energy with temperature $T_0 \gg T_t \approx 0$. In an ideal situation, the properties of the expansion are dependent only on the carrier gas, thus the m and γ values are set to the carrier gas, and the translational temperature is calculated below 1 K.

All the molecules in the molecular beam travel with the same velocity v_{∞} along the radial direction. At the time t , distance r from the nozzle, and angle θ with respect to the radial axis, the molecular number density can be expressed as:

$$N(r, t) = \frac{(b+1)N}{2\pi v_{\infty} T_M} \times \frac{\cos^b(\theta)}{r^2} \quad (2.2)$$

where T_M is the supersonic pulse duration, b value varies from 1 to 3 corresponding to ideal effusive and supersonic expansion, respectively.

In our laboratory at UNIBO, the solenoid valve (General valve, series 9, nozzle diameter 0.5 mm) is applied to generate supersonic molecular beam, and it is located in the center of the fixed mirror of Fabry-Pérot resonator. The MW antennae pointing to the radial axis is located on the same mirror and below the nozzle (coaxially oriented beam resonator arrangement, COBRA), with

shape and location optimized for the operation in our frequency range. The diagram as shown in the Figure 2.4.

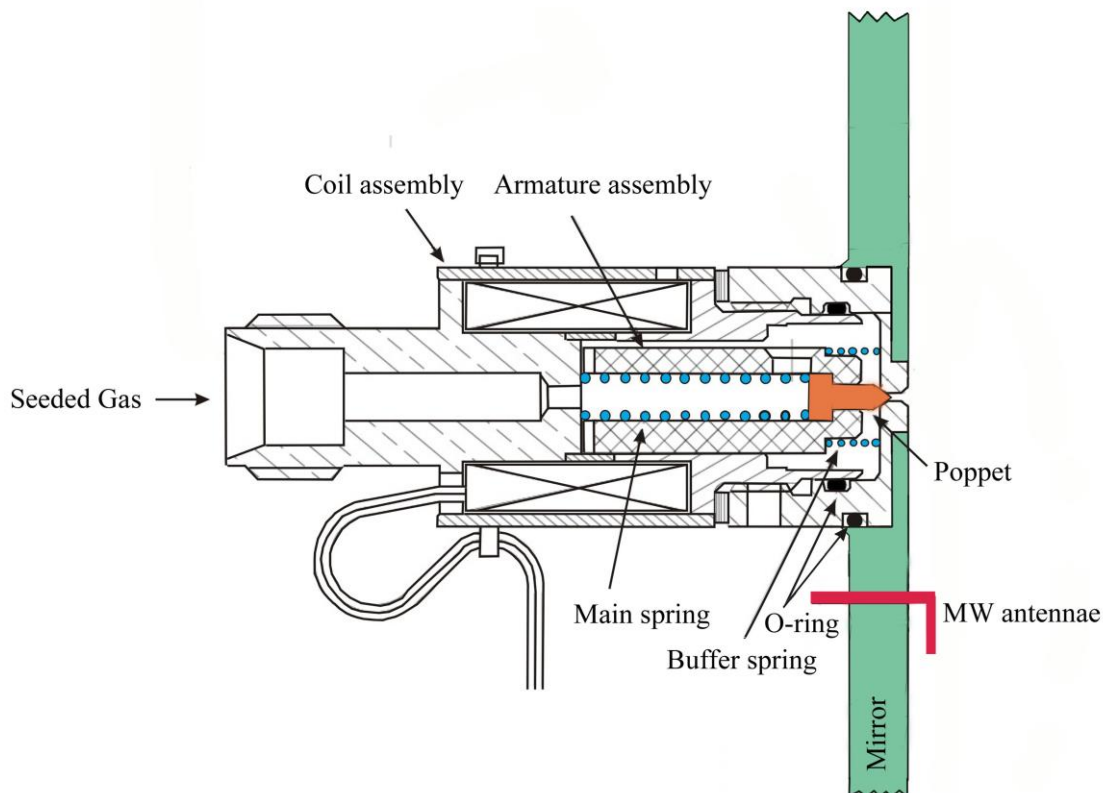


Figure 2.4. Supersonic-jet expansion source.

For the works in this dissertation, ~1% samples in rare gas at a stagnation pressure 0.1~0.6 MPa are expanded into the evacuated chamber ($\sim 10^{-5}$ mbar) different condition will be discusses separately.

2.2.2. Time domain technique

Instead of the previous technique to detect the transmitted signal as a function of frequency by passing a monochromatic radiation through a sample cell, the contemporary MW spectrometer records the radiative response signal as a function of time by passing a short period radiation through the molecular beam in a vacuum cavity. Then the time-domain signal is subjected to Fourier transformation to get a frequency-domain signal.

The rotational transitions can be measured in the time domain due to the time-dependent behavior of absorption and emission of two level quantum mechanical systems, even if the relaxation time in the gas phase rotational system is very short. Because of the detection of the response signal takes place in the absence of any power from the microwave oscillator and

modulation, the signal-to-noise (S/N) ratio is unaffected by any source noise and the resolution is increased considerably.

The molecular rotational resonant transient has two main processes: 1) *transient absorption* (or transient nutation, TN). During this process molecular systems absorb energy from the radiation field increasing their energy. The two-level quantum system is driven, in a shorter time than relaxation, from stationary conditions characterized by the equilibrium population difference ΔN_{ab}^0 and negligible polarization to a new state that features a macroscopic polarization \mathbf{P} at a non-equilibrium population difference ΔN_{ab} ; 2) *transient emission* (or free-induction delay, FID). During this process the energy stored in the molecules is subsequently released as a spontaneous coherent emission. The molecular system is taken from a condition of interaction with the radiation, where the system is polarized and in the thermal non-equilibrium, to the condition, where the external radiation is removed from the interaction with the system.

The amplitude of the molecular signal at the receiving antenna is proportional to the square root of the power flow $P_{ab}^{1/2}$, and can be expressed as

$$|S_{ab}| \propto \sqrt{\frac{\pi \omega_0^2 \omega_{ab}}{4 \omega_0 \delta}} \frac{\kappa_p \Delta N_{ab} \mu_{ab}}{v_\infty^2 T_M T_E} \sin(x T_p) \times \cos(k v_\infty t) |\exp(i(\omega_{ab} t + \theta_{ab}))| \quad (2.3)$$

Where $\omega = 2\pi\nu$ is the angular frequency, $\kappa_p = (b+1)/2$, ΔN_{ab} is the two-level population difference in the molecular beam, μ_{ab} is the dipole matrix element for the transition from state a to b , T_p is the radiation pulse length, T_E represents the expansion period from the closing of the valve to the onset of the observation of the transition emission, and $k = \omega/c$ is the wave number of the radiation.

The coaxial molecular beam and resonator axis result in:

$$S_{ab}(t) \propto s' \exp(i(\omega_{ab} - k v_\infty)t + \theta'_{ab}) + s'' \exp(i(\omega_{ab} + k v_\infty)t + \theta''_{ab}) \quad (2.4)$$

Thus, a Doppler doublet can be observed in the frequency domain consisting of frequency components at $\nu_{ab}(1-v_\infty/c)$ and $\nu_{ab}(1+v_\infty/c)$, respectively. Then the molecular resonance frequency is recovered as the arithmetic mean of the two components separated by $\Delta \nu_{ab} = 2\nu_{ab}v_\infty/c$. The line width of each component is around 1.5 kHz.

In our laboratory at UNIBO, the spectral line position was determined after Fourier transformation of the 8k data point time domain signal, recorded at intervals of 100 ns. Each rotational transition is split by Doppler effect and the estimated accuracy of frequency measurements is better than 3 kHz and lines separated by more than 7 kHz are resolvable.

2.2.3. PJ-FTMW spectrometer at UNIBO

The first Fabry–Pérot cavity PJ-FTMW spectrometer of the Balle–Flygare type in our lab was built by Prof. W. Caminati and his colleagues in 2004.^[14] The spectrometer was designed under the

guide of Prof. Grabow and Prof. Alonso since most of the details were taken from the spectrometer at the University of Valladolid. The frequency region covers 6–18 GHz. The mirrors are made from aluminum with diameter of 35 cm and curvature radius of 60 cm. The vacuum chamber was built by HVP (Parma, Italy) and it is a stainless steel cylinder with a diameter of 40 cm and length of 85 cm. The chamber is evacuated with a 8000 L/s diffusion pump operated by a block of two Leybold mechanical pumps (D65B and Ruvac WAU 251, rotary and booster pumps, respectively). The photo of this spectrometer is shown in Figure 2.5 and the block diagram includes the vacuum chamber and electric part is shown in Figure 2.6, as below.

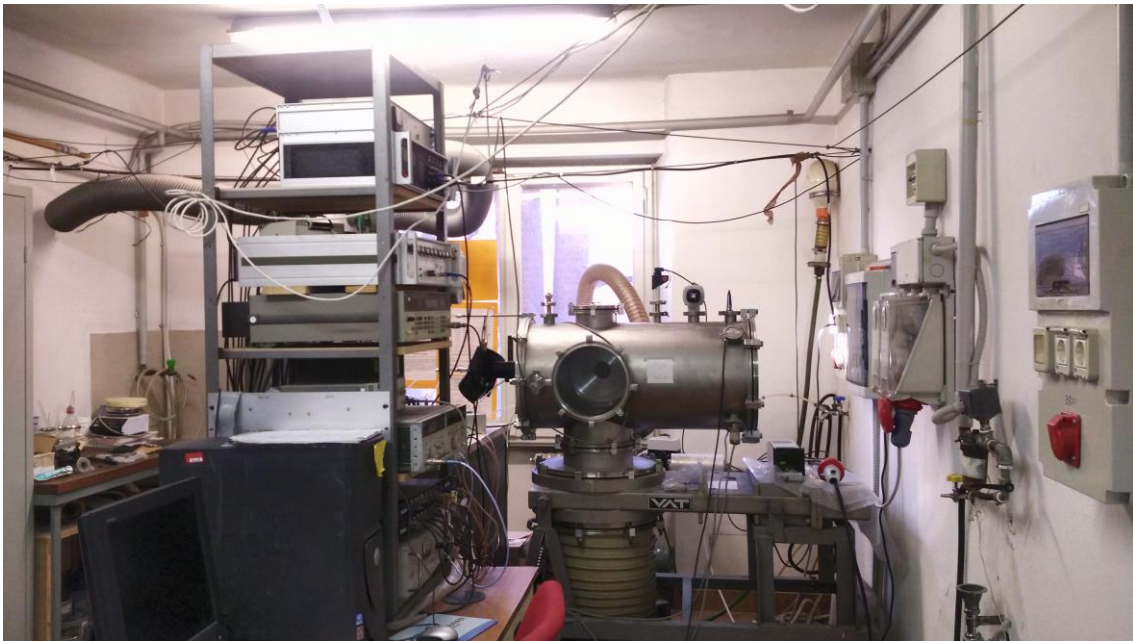


Figure 2.5. the PJ-FTMW spectrometer at Unibo.

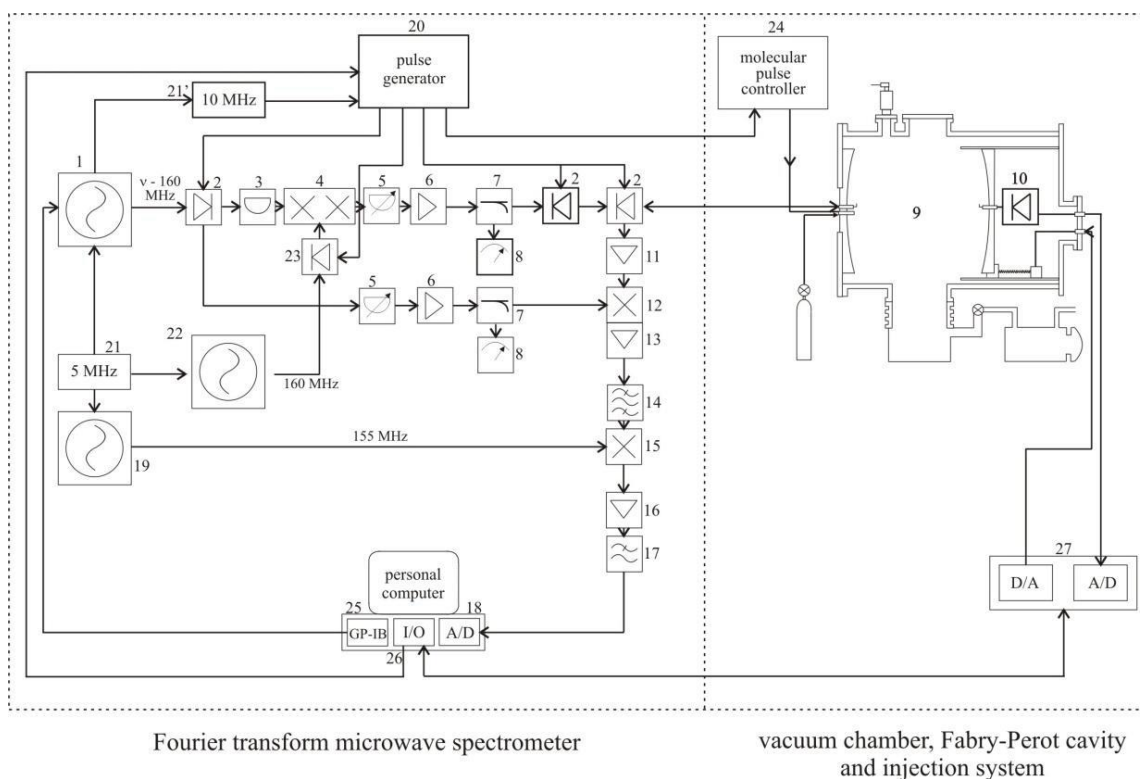


Figure 2.6. Block diagram of the PJ-FTMW spectrometer. MW = Microwave; RF = Radio Frequency; P = output power, IF = intermediate frequency, IL = insertion losses, G = gain, NF = noise figure, IS = isolation, IR = image rejection: 1. MW synthesizer, HP 8672 A. 2. MW switch SPDT, SMT SFD0526-001S. 3. Fixed attenuator MCL BW-S3W2. 4. Single side band modulator, MITEQ MN0226LC1C. 5. Variable attenuator, NARDA 4798. 6. MW amplifier ALC Microwave ALS0618-30-20. 7. Directional coupler NARDA 4203-16. 8. Power meter, HP 435 B + Power sensor 8485A. 9. Fabry-Pérot resonator, see text. 10. MW crystal detector HP8470B. 11. MW low noise amplifier, MITEQ JSD4-0600-1800-16-8P. 12. Image rejection mixer, MITEQ IR0226LC1C. 13. 160 MHz RF amplifier, MITEQ AU-1466-140. 14. BAndpass filter, TTE KC6-160M-20M. 17. RF mixer, HP 10514A. 16. RF amplifier, MCL MAN 1LN. 17. Lowpass Filter, TTE LC5-25M-50-7135. 18. Transient recorder, SPECTRUM PAD 82A, modified following the design of the Kiel University. 19. RF synthesizer, PTS 160-M7020. 20. Pulse Sequencer TTL, made at the University of Valladolid, based on a PCB card from the University of Kiel. 21. Reference signal, Rb oscillator 5 MHz, Ball-Efraton FRK-LLN. 22. RF synthesizer, MARCONI 2019A. 23. RF switch MCL 7MSW-1111. 24. Pulse controller General Valve IOTA ONE. 25. IEEE 488 interface, NI GP-IB-488 PCII. 26. I/O card, NI PC-DIO-96. 27. A/D and D/A converter for Stepper motor control made in Valladolid.

2.3. Chirped pulse Fourier transform microwave (CP-FTMW) spectrometer

Since 2006, the invention of CP-FTMW spectrometer by Prof. Brooks H. Pate has transformed the field of microwave spectroscopy.^[10] This design overcomes the problem of the narrow bandwidth of conventional FTMW spectrometers and reduces significantly the spectral acquisition time and sample consumption. The technique enables the collection of more than 10

GHz bandwidth spectrum in a single shot of the spectrometer. In principle, the spectrometer consists of three main components: 1) chirped pulse microwave generation, 2) molecular beam chamber, and 3) free induction decay detection. The schematic diagram of this technique is shown in Figure 2.7., which is taken as an example from the one built in Pate's group.

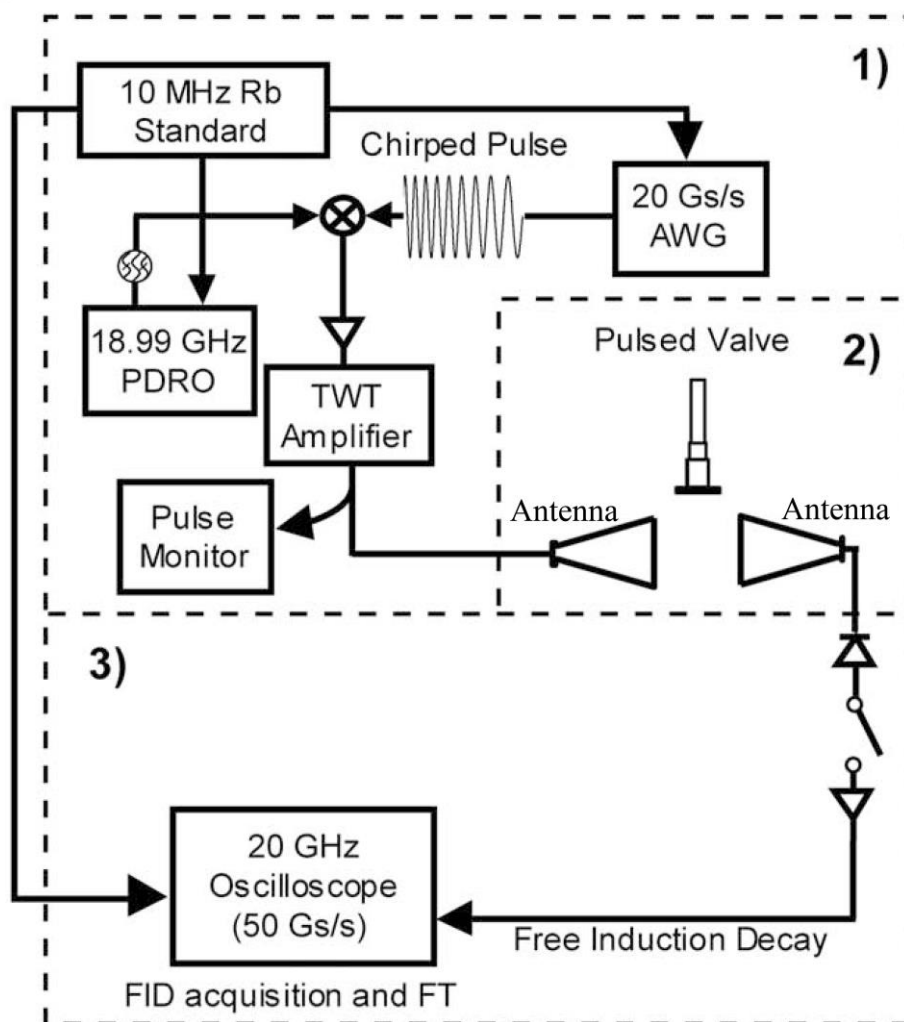


Figure 2.7. Schematic diagram for CP-FTMW spectrometer. The chirped pulse is generated by a AWG and mixed with a phase-locked dielectric resonator oscillator (PDRO) in a broadband mixer. After up-conversion, the pulse is amplified by a amplifier and sent into the chamber. The FID is amplified and directly digitized by a digital oscilloscope.

I worked with CP-FTMW spectrometer for three months in the spectroscopy group at the University of the Basque Country (UPV/EHU) led by Emilio J. Cocinero. The spectrometer was built based on the original design of B.H. Pate and can measure the rotational spectra over the entire span of 6-18 GHz in a single acquisition. The schematic diagram of this spectrometer is shown below:^[15]

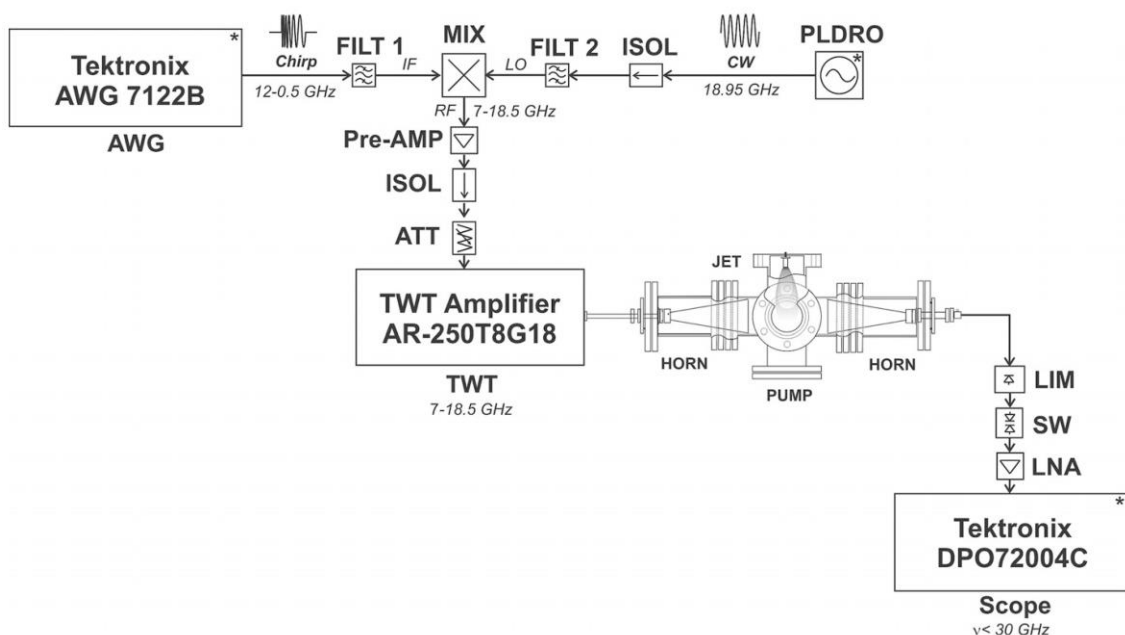


Figure 2.8. The CP-FTMW at the UPV/EHU. A chirped-pulse created by an arbitrary waveform generator (AWG) covering a base band of 12 GHz is filtered (FILT 1) and upconverted to the operating region 7–18.5 GHz with a broadband mixer (MIX). The local radiation originates from a stabilized oscillator (PLDRO, 18.95 GHz), followed by an isolator (ISOL) and a filter (FILT 2). The polarizing radiation is preamplified (Pre-AMP), leveled (ATT) and power amplified with a travelling-wave-tube (TWT), to be finally radiated through a horn antenna (HORN). The jet propagates perpendicular to the exciting emission. The molecular free-induced-decay (FID) captured by a second horn passes a power limiter (LIM) and a protection switch (SW), and is amplified (LNA) and digitized in the time domain. The components marked with an asterisk are frequency-referenced to a 10 MHz Rb standard.

Chapter III

Isolated molecules with large amplitude motions

From the microwave spectra, not only the information of the molecular structures can be obtained, but also that on large amplitude motions within the molecules. Since the first measurements of the rotational spectrum of ammonia with the inversion motion tunneling splitting, large amplitude motions have attracted more and more the attention of spectroscopists and many molecular systems with large amplitude motions have been characterized by MW spectroscopy. Typically, this kind of motions are present as: i) internal rotation of symmetric groups (*i.e.* methyl); ii) inversion of amino or imino hydrogen atoms; iii) internal rotation of light asymmetric groups (*i.e.* OH, SH, NH₂); iv) ring puckering of four (saturated) or five (near saturated) members rings; v) pseudorotation. In this chapter I will introduce three isolated molecules which show three different motions. In the first work the rotational study of indan with a ring puckering motion is involved, where the energy splitting is directly deduced by the position of μ_c type transition. As a second example, I will discuss the rotational spectra for two conformers of 1,2-dimethoxyethane, the spectra of both of which were split by the internal rotations of two methyl groups. The splittings of equivalent and in-equivalent internal rotors allow the precise determination of the values of their barriers to internal rotation. Last one in this chapter will be the rotational investigation of the 1-methylcyclohexanol. For this molecular system, four conformers have been seen in the spectrum relative to the different directions of hydroxyl group and relative positions between hydroxyl group and chair shape saturated six-members carbon ring. As aforementioned both *gauche* conformers displayed a spectral split concerted to OH rotation.

Even large group or whole molecule motions can produce tunneling splitting in molecular clusters. Some examples concerted to this kind motions will be considered in the next chapters, and in this chapter, I only limit the work on the isolated monomers

3.1. Ring Puckering Splittings in Indan

3.1.1. Introduction

This molecule consists of a six-membered aromatic ring and a five-membered ring (see Figure 3.1.1) and has interested spectroscopists since this kind molecule can be characterized by three large amplitude motions of the five membered ring: ring puckering, flapping and ring twisting^[16-35]. Indan is the prototype model for this kind of molecular systems. The experimental methods (involving FIR^[16], vibronic^[17], MW^[18], one-color, resonance enhanced two-photon ionization spectra (R2PI) and dispersed fluorescence (DF)^[19], and two-color resonantly enhanced multiphoton ionization and zero-kinetic-energy photoelectron spectroscopy^[20]) have been used to investigate this molecule. However, due to the weak value and the inversion of the μ_c dipole moment component, it was too difficult and failed to measure the interstate μ_c -type transitions^[18], which is significant to directly supply the value of the vibrational tunnelling splitting. Nowadays, it is feasible to measure even quite weak transitions with PJ-FTMW spectroscopy. For this reason, we decided to measure the μ_c -type transitions of the most abundant isotopic species (normal) of indan. The strong intensity of the signal has also allowed us to measure the rotational spectra of its ^{13}C -mono substituted isotopologues in natural abundance. The molecular shape of indan, including the principal axes and of the atom labels used through the text, is shown in Figure 3.1.1.

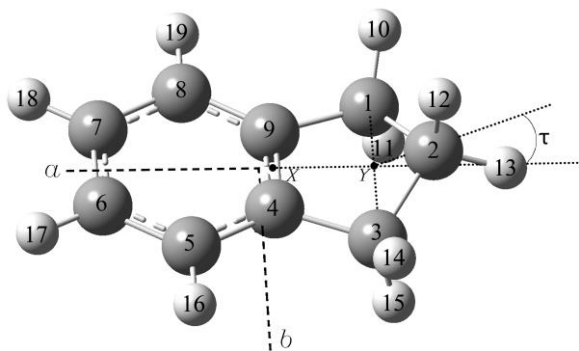


Figure 3.1.1. Molecular shape, principal axes and atom numbering of indan.

3.1.2. Experimental methods

A commercial sample of indan 98% (Aldrich) was used without further purification. The spectra of the mono-substituted ^{13}C isotopologues were measured in natural abundance. The rotational spectra have been measured with PJ-FTMW spectroscopy^[36]. Helium, as carrier gas, was

passed over indan at 60° C temperature, at a backing pressure of about 0.2·MPa, and expanded into the Fabry-Perot cavity.^[37]

3.1.3. Rotational spectra

Based on the results of the rotational constants determined in the previous room temperature absorption MW spectroscopy study, the μ_a -type transition spectrum of the normal species has been easily identified with PJ-FTMW spectroscopy^[18]. Even if the μ_a -type spectra are intra-state transitions, they displayed small splittings due to the difference of the rotational constants of the two tunneling sub-states originated by the above-mentioned ring puckering motion. In order to detect the much weaker inter-state μ_c -type lines we increased the MW pulse power of the spectrometer up to the maximum, and in order to increase its concentration in the molecular beam the sample was heated up to 60 °C ahead of the supersonic expansion. All these interstate transitions were split into two evenly separated component lines. This splitting is ca 44.7 MHz which is the double of the ring puckering splitting. We have measured 67 a-type and 14 c-type transitions, which have been fitted together with the rotational frequency reported in Ref. [18]. All transitions have been fitted simultaneously with a coupled Hamiltonian using Pickett's suite of programs^[38]. The following expression was used:

$$\mathbf{H} = \sum_i \mathbf{H}_i^R + \mathbf{H}^{CD} + \Delta E_{01}, \text{ with } i = 0, 1 \quad (3.1.1)$$

where \mathbf{H}_i^R represents the rotational Hamiltonian of the state i , \mathbf{H}^{CD} is the centrifugal distortion corrections, corresponding to the I' -representation of Watson's "S" reduced Hamiltonian^[39], assumed to be the same for both states. ΔE_{01} is the energy difference between the $\nu = 0$ and $\nu = 1$ tunneling states. The fitted spectroscopic parameters are reported in Table 3.1.1.

Table 3.1.1. Spectroscopic parameters of the parent species of indan.

	0	1
A/MHz	3531.0444(7) ^a	
B/MHz	1498.3739(1)	1498.3750(1)
C/MHz	1082.8714(1)	1082.8724(1)
D_J/Hz	32.2(7)	
D_{JK}/Hz	52(4)	
D_K/kHz	0.6(1)	
d_1/Hz	-7.1(4)	
d_2/kHz	-2.9(3)	
$\Delta E_{01}/\text{MHz}$	22.364(1)	
$\sigma/\sigma_{\text{exp}}^b$	1.3	
N^c	242	

^aError in parentheses in units of the last digit. ^bRoot-mean-square deviation of the fit, referred to an estimated measure errors of 3 kHz and of 50 kHz for the transition frequencies of this investigation and for those of Ref. [18], respectively. ^cNumber of lines in the fit (81 from the present work and 161 from Ref. [18]).

An improved accuracy of the experimental parameters has been achieved, compared with previous work^[3]. In addition, the energy splitting ΔE_{01} ($= 22.3652(6)$ MHz) has been precisely determined from the fit, the rotational constants have been obtained separately for the two tunneling states accompanied with all quartic centrifugal distortion constants.

The intensity of the spectrum was high enough to allow the measurement of ^{13}C -monosubstituted isotopologues, which are as $\sim 1\%$ population with respect to parent species in natural abundance. Five sets spectra of ^{13}C species have been observed and analysed Four of them have an abundance of ca. 2% of that of the parent species, since each spectrum is contributed by two equivalent carbons due to the symmetry of the molecule ($^{13}\text{C1}$ and $^{13}\text{C3}$, $^{13}\text{C4}$ and $^{13}\text{C9}$, $^{13}\text{C5}$ and $^{13}\text{C8}$, $^{13}\text{C6}$ and $^{13}\text{C7}$). The fifth isotopologue's population ($^{13}\text{C2}$) is only 1%. A portion of the spectrum displaying the $3_{12} \leftarrow 2_{11}$ transitions of the parent and ^{13}C isotopologues in natural abundance is shown in Figure 3.1.2 All rotational transitions are also reported in the appendix I. They have been fitted in the same way as the normal species, supplying the spectroscopic constants of Table 3.1.2. Since the abundance of ^{13}C species do not support the detection of many transitions, the centrifugal distortion parameters have been fixed to the values of the normal species.

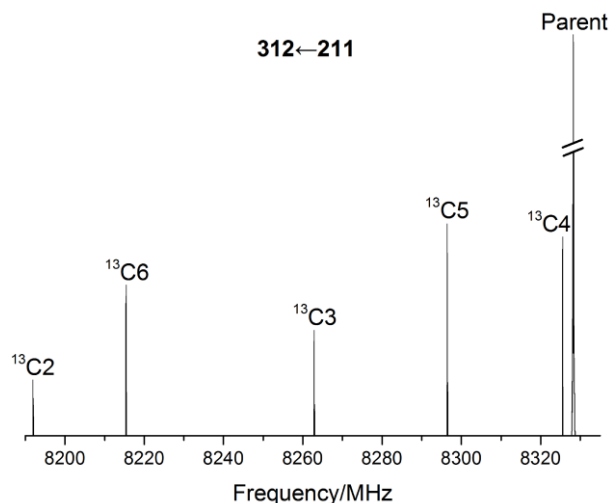


Figure 3.1.2. Portion of the spectrum with the $3_{12} \leftarrow 2_{11}$ transitions of the parent and ^{13}C isotopologues in natural abundance.

Table 3.1.2: Experimental spectroscopic parameters of the ^{13}C isotopologues of indan. Centrifugal distortion constants and the tunneling splitting have been fixed to the values of the parent species.

	A/MHz	B/MHz	C/MHz	σ^b/kHz	N^c
$^{13}\text{C1}$ (or $^{13}\text{C3}$)	3494.71(1) ^a	1486.9640(3)	1073.5820(2)	0.9	9

¹³ C2	3529.16(1)	1472.0361(3)	1069.2427(2)	0.6	9
¹³ C4 (or ¹³ C9)	3519.11(1)	1498.2566(3)	1081.7008(2)	0.6	9
¹³ C5 (or ¹³ C8)	3483.37(1)	1493.8816(3)	1076.0163(2)	0.8	9
¹³ C6 (or ¹³ C7)	3519.39(1)	1476.9880(3)	1070.5935(2)	0.9	9

^aStandard error in parentheses in units of the last digit. ^bStandard deviation of the fit. ^cNumber of fitted transitions.

Table 3.1.3. Substitution coordinates (r_s) of the carbon atoms in the principal axes system of parent indan.

	$a/\text{\AA}$		$b/\text{\AA}$		$c/\text{\AA}$	
	r_s	r_e	r_s	r_e	r_s	r_e
C2	$\pm 2.4460(6)^a$	2.4366	0.0*	0.0	$\pm 0.288(5)$	-0.3136
C1(3) ^b	$\pm 1.6008(9)$	1.6112	$\pm 1.223(1)$	1.2204	$\pm 0.14(1)$	0.1483
C4(9)	$\pm 0.15(1)$	0.1925	$\pm 0.696(2)$	0.7026	$\pm 0.06(3)$	0.0634
C5(8)	$\pm 1.005(2)$	-1.0100	$\pm 1.407(1)$	1.4128	$\pm 0.01(13)^*$	0.0072
C6(7)	$\pm 2.2123(7)$	-2.2169	$\pm 0.697(2)$	0.7016	$\pm 0.05(3)$	-0.0578

^aErrors in parenthesis are expressed in units of the last digit. ^bThe sign for the b value is opposite by symmetry for the species in parenthesis.

3.1.4. Structure information

From the rotational constants of these isotopologues, the substitution Cartesian coordinates of the carbon atoms have been obtained by applying Kraitchmann's method^[40] and using Costain's uncertainties^[41]. The results are shown in Table 3.1.3 comparing the *ab initio* Cartesian coordinates of the C atoms in the principal axes. The r_s structural parameters of the framework derived from the substituted coordinates are shown in Figure 3.1.3 and Table 3.1.4. The equilibrium geometry and the parameters of indan, calculated at the MP2/6-311++G(d,p) level^[42], are reported together with the experimental results as a comparison. The puckering angle (180° - XYZ2) is shown in Figure 3.1.1, where X and Y represent the intermediate points of the C4-C9 and C1-C3 carbon bonds. The predictions of rotational and first order centrifugal distortion constants, as well as the values of the a and c components of the electric dipole moment (b is zero by symmetry) are listed in Table 3.1.5. They are in agreement with the experimental observations. In addition, the experimental rotational constants could be achieved with the initial geometry of *ab initio* calculation by the least squares fitting. The result indicates to increase the value of τ from 33.2° (r_e) to 35° (r_0). This is reverse with our expectation which was $r_e > r_0$, because for the vibrational ground state wavefunction a considerable density should exist in the region between the two minima. However, the value of r_s is 30° , which is smaller than r_e .

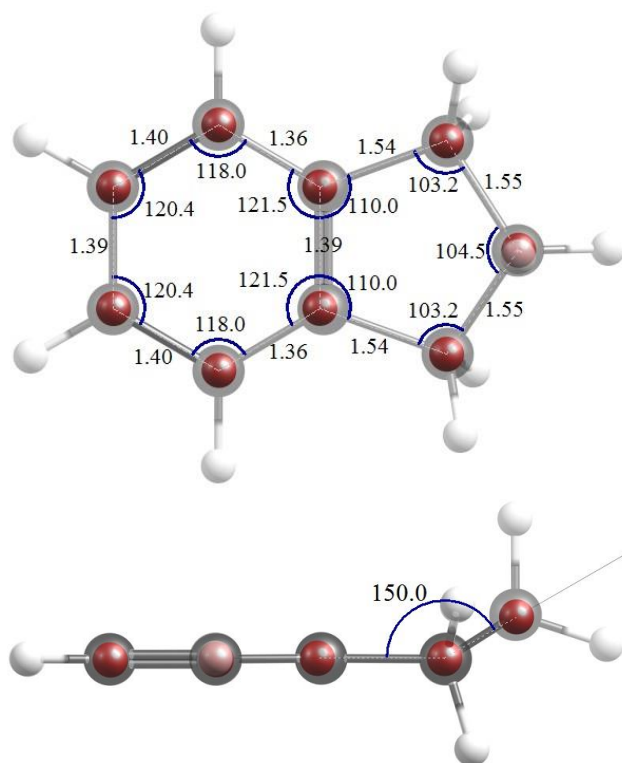


Figure 3.1.3. The r_s structure parameters. The full molecule geometry is from *ab initio* at MP2/6-311++G** level, when the smaller red spheres indicate experimental r_s positions of the C atoms from isotopic substitution. The parameters shown here are derived from the r_s framework.

Table 3.1.4. The theoretical (r_e , MP2/6-311++G(d,p)), and the heavy atoms r_s geometries of indan.

Bond lengths/Å		Valence angles/°	
	r_e/r_s		r_e/r_s
C1-C2	1.5440/1.547(7)	C1C2C3	104.4/104.5(3)
C1-C9	1.5126/1.543(9)	C2C3C4	102.4/103.2(8)
C4-C5	1.3978/1.359(9)	C3C4C9	110.0/110.0(7)
C4-C9	1.4051/1.392(3)	C4C5C6	119.0/118(1)
C5-C6	1.4024/1.402(5)	C5C6C7	120.5/120.4(5)
C6-C7	1.4032/1.394(3)	C8C9C4	120.5/121.5(9)
C1-H10	1.0947	H10C1C9	113.2
C1-H11	1.0991	H11C1C9	110.0
C2-H12	1.0959	H12C2Y	131.6
C2-H13	1.0941	H13C2Y	141.5
C5-H16	1.0881	H16C5C4	120.7
C6-H17	1.0870	H17C6C5	119.8
Significant dihedral angles/° ^a			
$\tau = 32.3/30(3)$ H10C1-C9C4 = -141.8 H11C1-C9C4 = 97.6			

^a All dihedral angles of the aromatic part very close to 0 or 180°

Table 3.1.5. MP2/6-311++G** spectroscopic parameters of indan.

A/MHz	3519	D_J /Hz	33.1
B/MHz	1496	D_{JK} /Hz	42.2

C/MHz	1082	D_K/Hz	234
μ_a/D	-0.6	d_1/Hz	8.5
μ_c/D	0.036	d_2/Hz	1.4

3.1.5. Barrier to ring puckering

Ab initio calculations also provided the energy of the transition state with a planar conformation of the main frame of indan. The energy difference with respect to the global minimum energy corresponds to the barrier to ring puckering. The value $B_2 = 733 \text{ cm}^{-1}$ has been deduced at MP2/6-311++G(d,p) level and 670 cm^{-1} at MP2/6-31++G(d,p) level^[19]. Laser-induced fluorescence experiments indicated that $B_2 = 488 \text{ cm}^{-1}$ ^[18]. However, all the values are higher than the experimental values ($B_2 = 434 \text{ cm}^{-1}$) obtained in our work^[18], which is derived from the value E_{01} (22.364(1) MHz) directly concerning with *c*-type transition by using Meyer's flexible model^[43]. Some experimental and theoretical values of the potential energy function are summarized in Table 3.1.6, while a graphical comparison of the MW and of the MP2/6-311++G(d,p) potential energy surfaces is given in Figure 3.1.4.

Table 3.1.6. Experimental and theoretical values of the potential energy function of the ring puckering motion in indan.

Experiments			Theory	
	MW	LIF ^{ref.18}	MP2/6-31++G** ^{ref.19}	MP2/6-311++G**
$B_2 (\text{cm}^{-1})$	434	488	670	733
$\tau (^{\circ})$	34.0	8.5 ^a	30.8	32.3

^aDeduced from the value $x_1 = 0.14 \text{ \AA}$ at the energy minima

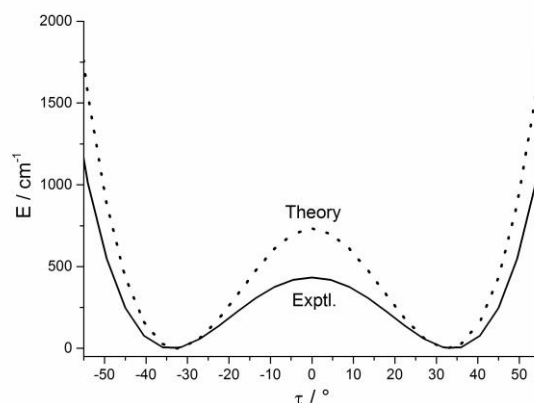


Figure 3.1.4. MP2/6-311++G** and experimental shapes of the puckering B_2 barrier.

3.1.6. Conclusions

With FTMW spectroscopy we successfully assigned the μ_c type transition of indan which can directly indicate the energy splitting in the ground vibrational state. Moreover, we also assigned the rotational spectra of the five possible ^{13}C mono-substituted isotopologues. From the rotational constants we have obtained the r_s geometrical parameters. With the present investigation we precisely measured the ΔE_{01} splitting, 22.364(1) MHz, related to the puckering of the methylenic apex of the five-membered ring of indan. It is interesting to outline that the theoretical methods can not satisfyingly model the puckering motion and the B_2 barrier is overestimated by about 60%.

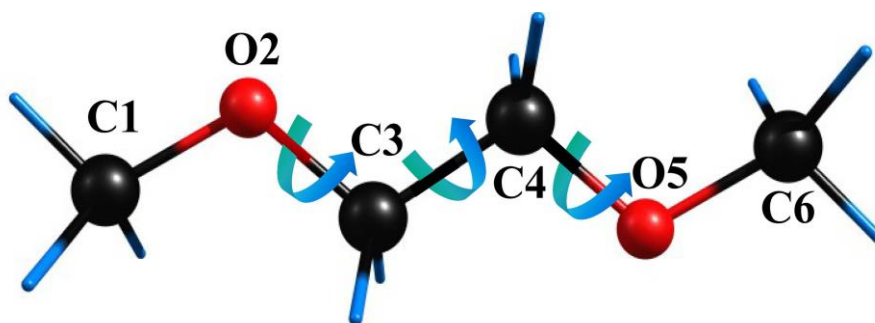
3.2. 1,2-Dimethoxyethane with CH₃ Internal Rotation

3.2.1. Introduction

1,2-Dimethoxyethane (DME) is an important aprotic solvent and the molecule has a high flexible chain. The studies of its conformations has attracted a lot attentions over the last years.^[44-48] In order to find the preferred conformer and understand the “*gauche* effect” around its C-C bond and the “*trans* preference” around the C-O bond in gas and condensed phases several literatures have been reported by using NMR and vibrational spectroscopy^[44-48]. An agreement has been achieved that in gas phase the *TTT* conformer (considering the O-C-C-O chain, see Sketch 3.2.1) is the most stable as predicted by *ab initio* calculations. Moreover, the *TGT* and *TGG'* conformers should be also highly populated based on the theoretical calculation.^[49] Regarding to the liquid phase, a different conclusion was obtained where the population of the *gauche* conformer is preferred due to the influence of polar solvents such as water.^[49,50] In this case the *TGT* conformer is the most populated form rather than the *TTT* one. In this work, I have unraveled the conformational preferences of DME in the gas phase using rotational spectroscopy.

3.2.2. Experimental section

The rotational spectrum was measured with PJ-FTMW spectrometer and FJ-MMWA spectrometer, respectively.^[12,15,37,51,52] Helium with stagnation pressure of ca. 0.22 MPa and argon with stagnation pressure 0.2 MPa at room temperature were used as carrier gas of DME (supplied by Sigma–Aldrich and used without further purification).



Sketch 3.2.1. The mainframe of DME with the atom labels, and the dihedral angles variation along the arrow can generate various isomers.

3.2.3. Theoretical calculations

Before scanning the rotational spectra, all the possible conformers and their relative energies

have been optimized and the spectroscopic constants of each expected conformer have been calculated. The mainframe structure of the DME is controlled by three dihedral angles (see Sketch 3.2.1). The combination of the three dihedral angles with three values for each one can result in 3^3 plausible configurations and display 10 non-equivalent conformers. As previously reported,^[44,49] the complete conformational space of DME has been explored at different levels of computations and taking into account also the effect of intramolecular basis set superposition error.^[45] In this work we have performed new calculations at the MP2/6-311++G** level on the structures of all the ten plausible conformers using the Gaussian 09 program package^[42]. The optimized results show that 9 of them exist on the potential surface and three of them, TTT, *TGT* and *TGG'*, are much more stable than the other ones. All 9 conformers are reported in Figure 3.2.1 and the three most stable ones have conformation degeneracy 1, 2, 4, respectively. The configuration transforming pathways have also been calculated with the transition states calculation at the same level as listed in Figure 3.2.2.

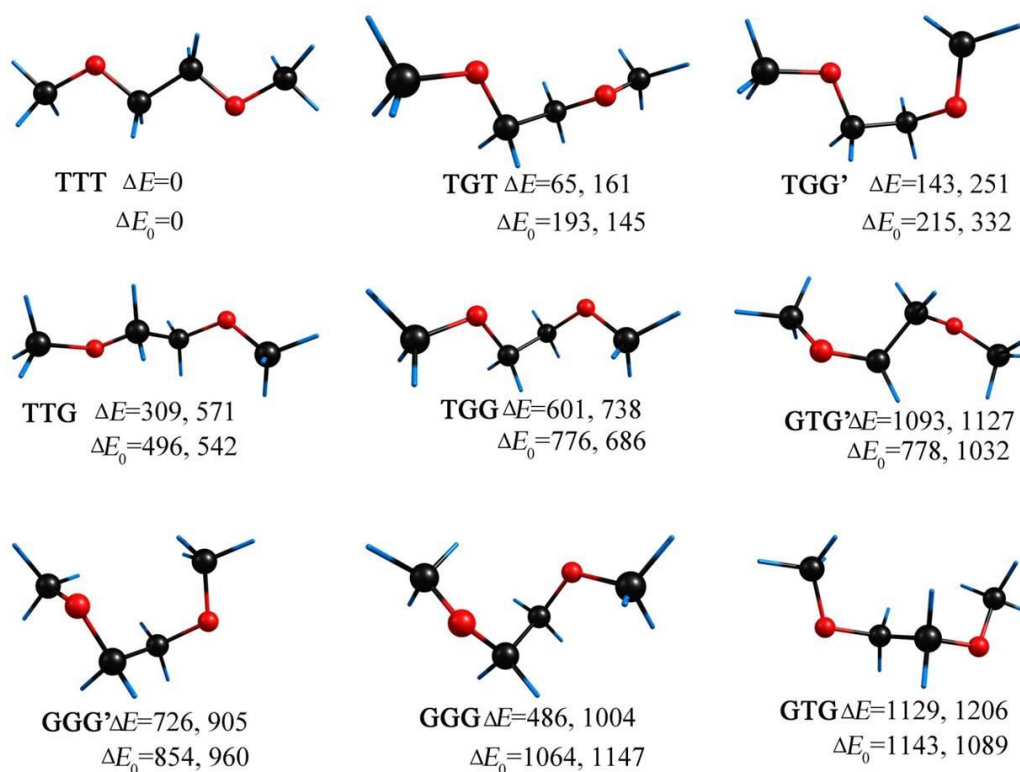


Figure 3.2.1. All the energy and frequency preferred conformers on the potential surface. The relative energies (cm^{-1}) were optimized and calculated at MP2/6-311++G** and B3LYP/6-311++G** levels, respectively. The left values are from MP2 calculation when the right is from DFT calculation, and the upper and lower values are calculated with and without zero-point energy, respectively.

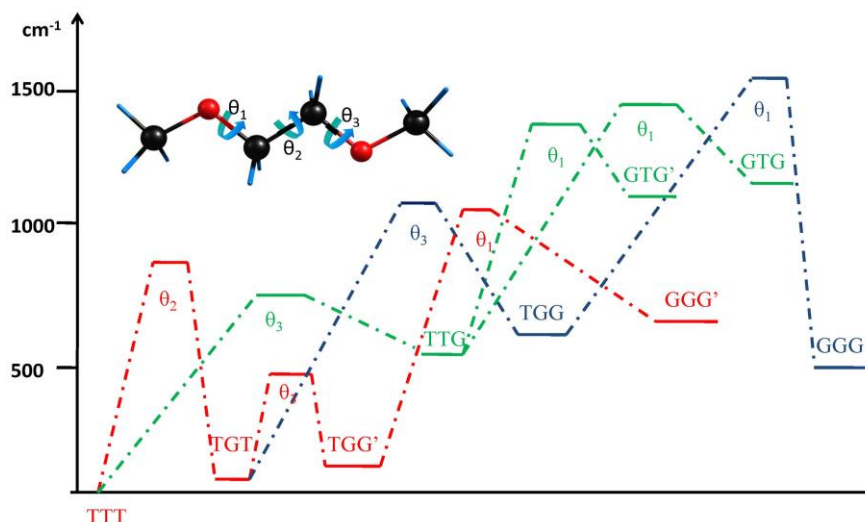


Figure 3.2.2. The pathways of the conformers variations calculated at MP2/6-311++G** level. The barriers between the stable conformers were performed with the transition state optimization, where only one imaginary frequency is allowed for the frequency check.

The rotational constants, electric dipole moments components, relative energies and zero-point energies of the most stable conformers are reported in Table 3.2.1. The computational results indicate that the global minimum (*TTT* conformer) has no dipole moment due to its symmetry, and for this reason it cannot be observed by pure rotational spectroscopy. However, the small relative energy difference the other conformers relative to the global minimum appears promising for the rotational spectral observation. In order to predict the possible internal rotation splittings, the potential energy curve for the internal rotations of the two methyl groups have been also calculated. The *ab initio* scans varying the dihedral angle (HC-OC) were carried out with 5° per step over the full range. The dihedral angle was kept fixed at each step while all the other structural parameters were optimized at each point along the path. The corresponding values of the V_3 energy barriers are also reported in Table 3.2.1.

Table 3.2.1. MP2/6-311++G(d,p) calculated spectroscopic parameters of DME.

	<i>TTT</i>	<i>TGT</i>	<i>TGG'</i>
A / MHz	18731	10965	6869
B / MHz	1298	1547	2036
C / MHz	1253	1461	1705
D_J, D_{JK}, D_K / kHz	0.044, 9.95, 0.001	0.44, 2.88, 87.66	0.67, 0.08, 0.036
d_1, d_2 / kHz	0.004, -0.0008	-0.06, 0.006	-0.178, -0.023
$ \mu_a $ / D	0	0	1.7
$ \mu_b $ / D	0	1.5	0.3

$ \mu_c / \text{D}$	0	0	0.3
$V_{3_C1} / \text{kJ mol}^{-1a}$	9.87	10.02	9.71
$V_{3_C6} / \text{kJ mol}^{-1a}$	9.87	10.02	6.90
$\Delta E_e / \text{cm}^{-1}$	0 ^b	65	143
$\Delta E_0 / \text{cm}^{-1}$	0 ^c	193	215

^aOnly the B3LYP/6-311++G(d,p) values are reported; ^bAbsolute energy is -308.954892 E_h; ^cAbsolute energy is -308.811452 E_h.

3.2.4. Rotational spectra

As mentioned above, the most stable one, *TTT* conformer, cannot be observed with our technique due to the lack of a permanent dipole moment. For this reason, we focused on the search of the other “polar” conformers. The initial survey scan targeted the *TGT* form. The first attempt was performed on the FJ-MMWA spectrometer because it allows a fast scan within its frequency range. A μ_b -type spectrum was expected due to the relatively stronger dipole moment and in fact a recognizable pattern of transitions was displayed on the spectrum. From the prediction, we first assigned the strongest calculated transitions, belonging to the *R*-type families $(J+1)_{1,J+1} \leftarrow J_{0,J}$ and $(J+1)_{0,J+1} \leftarrow J_{1,J}$, with J ranging from 4 to 6. Each transition was split into four component lines, as expected for a molecule with two equivalently rotating methyl groups. Some other transitions displayed a pattern of six component lines due to the presence of the “dipole forbidden transitions”. By exploiting this initial assignment, we moved to the PJ-FTMW spectrometer, where we could assign many more *R*-type rotational transitions and finally also some *Q*-branch lines. No lines due to μ_a and μ_c dipole moment components have been observed, which is in agreement with the expected C_2 symmetry of this conformer. The experimental measurements of the *TGT* conformer were later extended to the ¹³C mono-substituted species in natural abundance. This species as a reduced symmetry and as a consequence, the rotational transitions appeared split into five components.

Besides the assignment of conformer *TGT*, we could observe other quite strong transitions which were assigned to the *TGG'* conformer. In the second assignment, each rotational transition was split into five components due to the fact that the internal rotors are not equivalent anymore. The intensity of the spectrum is lower than that of *TGT*, even if in this case we were also able to observe the single mono-substituted ¹³C in natural abundance. No transitions belonging to other conformers have been observed in the analyzed microwave spectrum. The missing of experimental signals for *TGG'* conformer in FJ-MMWA spectrometer can be explained with different reasons. But to the best of my knowledge, the first reason is probably due to a conformational relaxation effects upon supersonic expansions. This is often observed when the barriers connecting different

minima are of the order of $2kT$,^[53] especially when argon is used instead of helium as carrier gas. Moreover, the higher relative energy of the *TGG'* conformer implies its lower concentration and signal intensity. The 59.6-74.4 GHz frequency range of FJ-MMWA, in principle, is just responsible for the high $J \mu_a$ -type transition which is not well modulated by the Stark effect. All the experimental frequencies are listed in the appendix II and in Figure 3.2.3 we reported examples of the measured transitions for the *TGT* and *TGG* conformers. Since the conformers are near prolate asymmetric tops, the *S*-reduction and *F*-representation have been chosen to fit the rotational transitions.^[39] Several programs can be used to fit rotational transitions using the Watson's semi-rigid Hamiltonian^[38,54-56] and comparison among the various methods have already been reported.^[57-60] In this work, we fitted all the transitions components using the XIAM (based on the combined axis method, CAM)^[54] and ERHAM (which fits an effective rotational Hamiltonian)^[55] programs. The derived spectroscopic constants obtained by both methods are reported in Table 3.2.2. As reported in others articles, XIAM provides parameters with a clear physical meaning while ERHAM needs a more deep expertise in choosing the best set of parameters to be fitted. This is mainly due to the fact that the internal rotation is treated by a Fourier expansion and the values are not easily interpretable. However, ERHAM reproduces high frequency rotational spectra with high accuracy along with other periodic motions not fitted by XIAM. Interestingly, both program supply the angles ($\angle(a,i)$ $\angle(b,i)$ $\angle(c,i)$) that are formed by the internal rotation axis *i* of the methyl groups with the principal axis of inertia (*a*, *b* and *c*), respectively. These values from two programs are in good agreement for both the conformers of DME. XIAM also directly provides the experimental values of the V_3 barrier which are quite close to the ones calculated at the B3LYP/6-311++G(d,p) level of theory. These values could be obtained also from ERHAM using its tunneling energy parameters and Meyer's flexible model,^[43] as described previously,^[61] where the tops are treated as independent tops using the *F* parameters to calculate two-top case.

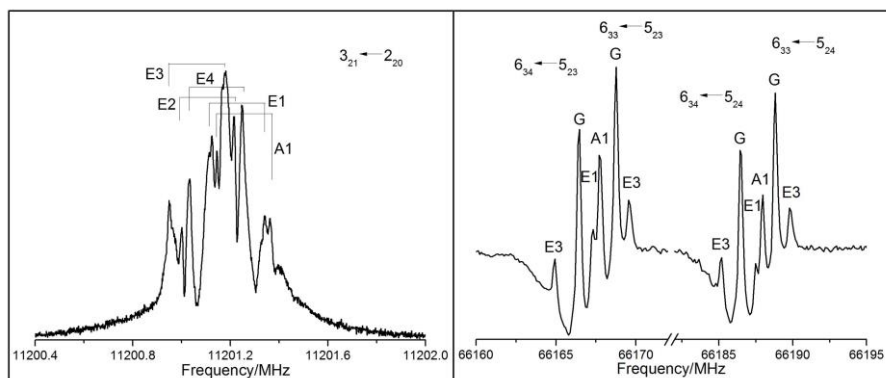


Figure 3.2.3. Portion of the rotational spectra for *TGG'* (left) and *TGT'* (right) conformers, respectively. The left spectrum is measured by PJ-FTMW spectrometer when the right is measured by FJ-MMWA spectrometer. Each transition from PJ-FTMW is split by the instrumental Doppler effect.

Table 3.2.2. Spectroscopic parameters of the two conformers fitted by XIAM and ERHAM program.

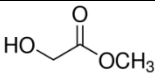
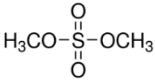
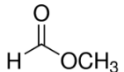
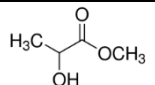
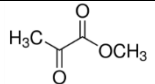
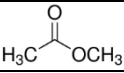
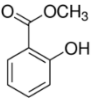
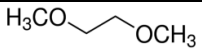
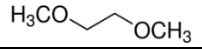
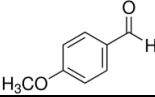
	XIAM			ERHAM		
	<i>TGT</i>	<i>TGG'</i>		<i>TGT</i>	<i>TGG'</i>	
A/MHz	11152.3399(4) ^a	6875.403(1)		11152.3396(8) ^a	6875.403(2)	
B/MHz	1532.5191(2)	2019.9333(3)		1532.4951(3)	2019.9142(5)	
C/MHz	1446.6840(2)	1692.4548(3)		1446.7075(2)	1692.4738(4)	
D _J /kHz	0.494(2)	0.83(3)		0.485(4)	0.84(1)	
D _{JK} /kHz	-16.37(3)	-0.82(3)		-16.53(6)	-0.82(4)	
D _K /kHz	207.49(9)	17.0(3)		208.0(2)	16.8(4)	
d _J /kHz	-0.0918(4)	-0.221(5)		-0.0916(9)	-0.215(4)	
d _K /kHz		-0.020 (2)			-0.0220(9)	
	<i>C₆-top/ C₁-top</i>	<i>C₆-top</i>	<i>C₁-top</i>	<i>C₆-top/ C₁-top</i>	<i>C₆-top</i>	<i>C₁-top</i>
V ₃ /kJ·mol ⁻¹	9.821(9)	6.58(2)	10.10(3)	9.944 ^b	6.79 ^b	9.84 ^b
δ∠(a,i)/°	19.5(5)	84.3(1)	{19.4} ^c	{22.0}	84.3(2) ^b	{19.4}
ε/°	84.3(1)	160.4(9)	{-72.9}			
qq ^d				01 or 10	10	01
ε _{qq} /MHz ^e				-1.64(1)	-21.6(4)	-1.41(5)
ρ				0.0672(5)	{0.0128}	{0.0415}
β/°				{3.0}	71.1(6)	{5.3}
α/°				{-74.5}	-16(1)	{-70.0}
∠(b,i)/°	85.2(1) ^b	160(1) ^b	{84.4}	{84.5}	19(2) ^b	{84.4}
∠(c,i)/°	108.8(5) ^b	109(1) ^b	{108.5}	{111.3}	108(2) ^b	{108.9}
N ^f	108	168		108	168	
σ ^g /kHz	1.9	4.5		1.5	4.4	

^aError in parentheses in units of the last digit. ^bDerived parameters from the fit. ^cValues in brackets fixed to those obtained from *ab-initio* geometry. ^dLabels used to identify the localized state to which a tunneling parameter is related to. ^eEnergy tunnelling parameter. ^fNumber of lines in the fit. ^gRoot-mean-square deviation of the fit.

In Table 3.2.3, we have also reported the experimental values of the V_3 barrier for the internal rotation of methyl group in different molecules investigated by microwave spectroscopy. It is worth noting how the V_3 barrier is much higher for DME rather than for dimethyl sulfate or dimethoxymethane.^[62] For the last two studies, the anomeric effect is reported which could lead to structural effects. Depending on the functional groups in the molecular systems, the V_3 values can be divided in three classes: (i) esters with -OCH₃ V_3 barriers below 6 kJ mol⁻¹; (ii) ethers with -OCH₃ V_3 barrier values between 6 and 11 kJ mol⁻¹; (iii) -OCH₃ functional groups involved in the weak intra-hydrogen bond with V_3 barrier values around 13 kJ mol⁻¹. It is worth noting that in ethers when a hydrogen atom belonging to a methyl group interacts with the oxygen atom, the V_3 barrier decreases from about 10 to 6.5 kJ mol⁻¹. Such effect is well displayed in our system. In fact, in the *TGT* conformer the two equivalent methyl groups present a V_3 barrier around 10 kJ mol⁻¹ belonging to the (ii) category, whilst in the *TGG'* conformer the intra-molecular interaction decreases the second V_3 barrier to 6.58 kJ mol⁻¹. This effect is even amplified when the sulfur atom replaces the oxygen atom. Additionally, by comparing the barrier between *TGG'*-DME and the last class, one can see that the V_3 of the -OCH₃ group involved in the wHB as the proton donor is lower than the V_3 of the -OCH₃ group involved in the wHB as proton acceptor, as shown in the Figure 3.2.4. This is out of our expectation, because the internal rotation of CH₃ which is the proton donor need to

periodically break and rebuild the wHB $\text{CH}\cdots\text{O}$.

Table 3.2.3. Experimental V_3 barrier for methoxy compounds.

			V_3 / kJmol^{-1}	Ref.
Class I	Methyl Glycolate		4.7(1)	24
	Dimethyl Sulfate		4.731(6)	22
	Methyl Formate		4.7738(1)	25
	Methyl Lactate		4.84(2)	26
	Methyl Pyruvate		4.883	27
	Methyl Acetate		1.2171(4); 5.0500(7)	28
	Methyl Salicylate		5.38(2)	29
Class II	Dimethoxymethane	$\text{CH}_3\text{OCH}_2\text{OCH}_3$	6.61(4)	30
	Dimethyl ether	CH_3OCH_3	10.81(8)	31
	<i>TGG'</i> -DME		10.30(3); 6.58(2)	This work
	<i>TGT</i> -DME		9.821(9)	This work
	<i>anti/syn p</i> -anisaldehyde		9.6(8); 9.2 (13)	32
Class III	2-methoxyethanol	$\text{CH}_3\text{OCH}_2\text{CH}_2\text{OH}$	13.0(4)	33
	2-methoxyethylamine	$\text{CH}_3\text{OCH}_2\text{CH}_2\text{NH}_2$	13.2(2)	33

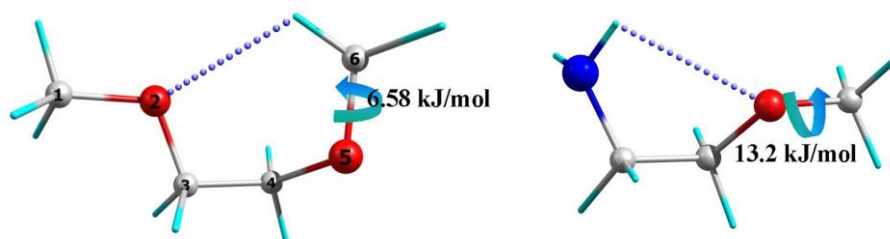


Figure 3.2.4. Comparison of the V_3 barrier to methyl internal rotation when the group is involved in a hydrogen bond or not.

3.2.5. Structure information and relative abundances of conformers

Different procedures have been introduced for deriving structural information from the measured data. A recent review highlights the importance of these treatments.^[63] The conformational assignment of *TGT* and *TGG'* conformers is directly obtainable by comparison of the theoretical rotational constants to the experimental ones. However, to obtain supplemental

structural information we have investigated the microwave spectra of the mono-substituted ^{13}C isotopomers, and the XIAM fitted rotational constants of the isotopomers of the two conformers are listed in Table 3.2.4. From the parameters of the isotopologues it was possible to obtain a complete substitution carbon-framework structures using Kraitchman's equations. These structures, reported in Table 3.2.5 and shown in Figure 3.2.5, clearly confirm both assignments to the *TGT* and *TGG'* conformers and they also agree quite well with the theoretical equilibrium structures. The substitution structure is becoming increasingly important because it doesn't include any a priori assumption while other methods (such as effective structure (r_0)) correct to various degrees for vibrational effects and lead to different conceptions of interatomic distance.

Table 3.2.4. Rotational constants of the measured isotopologues of the two conformers.

	<i>TGT</i>		<i>TGG'</i>			
	C1(C6)	C3(C4)	C1	C3	C4	C6
A/MHz	11108.082(3)	11001.906(2)	6853.20(3)	6800.40(1)	6775.62 (2)	6753.42 (1)
B/MHz	1498.807(2)	1530.005(1)	1970.5370(2)	2016.89314(9)	2013.7369(1)	1994.42192(9)
C/MHz	1415.9658(6)	1442.3287(3)	1656.5932(2)	1.68601364(7)	1683.14377(9)	1667.20194(7)
N^b	24	24	55	55	55	55
σ^c /kHz	4.8	3.0	3.1	1.5	1.8	1.4

^aError in parentheses in units of the last digit. ^bNumber of lines in the fit. ^cRoot-mean-square deviation of the fit.

Table 3.2.5. Substitution coordinates (r_s) of the carbon atoms in the principal axes system.

		$a/\text{\AA}$		$b/\text{\AA}$		$c/\text{\AA}$	
		$ r_s $	$ r_e $	$ r_s $	$ r_e $	$ r_s $	$ r_e $
<i>TGT</i>	C1&C6	2.7314(6) ^a	2.714	0.420(4)	0.436	0.10(1)	0.122
	C3&C4	0.701(2)	0.717	0.755(2)	0.760	0.235(6)	0.237
<i>TGG'</i>	C1	2.5078(6)	2.500	0.474(3)	0.472	0.15(1)	0.166
	C3	0.596(3)	0.612	0.891(2)	0.899	0.16(1)	0.136
	C4	0.819(2)	0.830	0.996(2)	0.998	0.322(5)	0.324
	C6	1.7884(8)	1.788	1.166(1)	1.160	0.05(3)	0.096

^aErrors in parenthesis are expressed in units of the last digit.

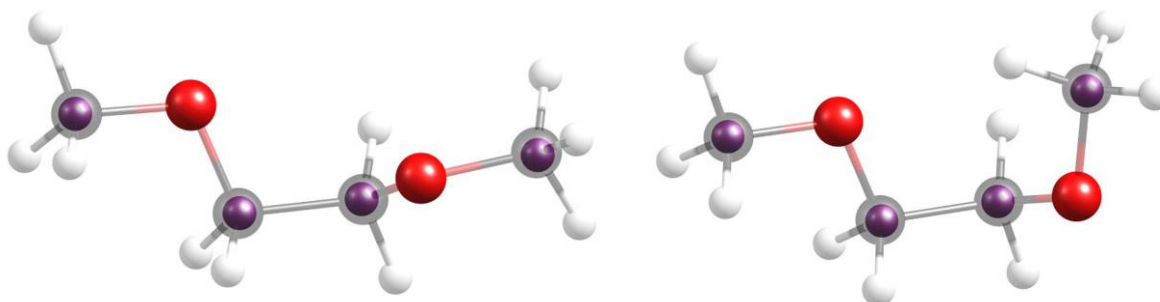


Figure 3.2.5. Sketch of the *TGT* and *TGG'* DME conformers. The r_s substitution positions of the carbon atoms are shown as violet spheres, superimposed to the MP2/6-311++G(d,p) geometries.

By assuming a Boltzmannian distribution, it is possible to evaluate the relative abundance of the two observed conformers from the relative intensity of nearby rotational transitions using the formula:

$$\frac{N_{TGG'}}{N_{TGT}} = \frac{I_{TGG'} \mu_{TGT} \gamma_{TGT} \nu_{TGT}}{I_{TGT} \mu_{TGG'} \gamma_{TGG'} \nu_{TGG'}} = g e^{\frac{-\Delta E}{kT}}$$

where I , μ , γ and ν are the peak intensity, dipole moment component, line strength and frequency of the considered transitions, respectively. The conformation degeneracy of the two conformers, 2:4, has been taken into account. The results $N_{TGG'}/N_{TGT} = 2.1/1$ support the expected value obtained by the *ab initio* calculations (1.8/1), considering the thermodynamic equilibrium. It is worth noting that the most abundant conformer in the jet must be the *TTT* which cannot be revealed by rotational spectroscopy.

3.2.6. Conclusions

In summary, we studied the high resolution spectra of two conformers (*TGT* and *TGG'*) of DME and of all ^{13}C mono-substituted isotopologues. This has allowed the determination of the experimental substitution structures of the heavy atoms skeleton which agree quite well with the theoretical ones. The analysis of the spectra has been done following two different approaches: that of the XIAM and ERHAM programs. Both procedures led to similar spectroscopic and structural values and it was also possible to obtain information on the internal dynamics of the two methyl groups. From the measurements of the intensity of the rotational transitions we have estimated the relative abundances of the two conformers in the jet, which is in agreement with the one predicted by *ab initio* calculation, confirming the values of the calculated relative energies between different conformers. However, the most stable conformer (*TTT*) has not been observed because, due to its symmetry, it has no permanent electric dipole moment.

3.3. 1-Methylcyclohexanol with OH rotation

3.3.1. Introduction

In the alcohol's family of organic compounds when the hydroxyl group is linked to an aliphatic carbon atom, the hydroxyl group can rotate along the C–O bond, connecting energy minima separated by $\sim 120^\circ$. In this way, with the variation of the aliphatic chain, a considerable number of stable conformers can exist. In addition, the internal rotation of the light OH group can generate tunneling splitting which are then reflected in the complicated splitting of the rotational spectra. Rotational spectroscopy is a powerful tool to analyze the potential energy surface related to these motions. However, little is available so far on the conformational studies of alcohols with carbon chains up to four carbon atoms. Methyl alcohol has, of course, only one conformer, but its large permutation inversion group makes the spectrum unbelievably complicated.^[64] The *trans* and *gauche* forms of ethyl alcohol^[65] and of isopropanol^[66] have been rotationally characterized, with the *gauche* forms giving rise to two mirror images undergoing rapid tunneling motions. As to n-propyl alcohol, rotational transitions in all five conformers of the molecule, Gt, Gg, Gg', Tt, and Tg, have been unambiguously assigned.^[67] Butanol consists of four chemical isomers, n-butanol, isobutanol, *sec*-butanol, and *tert*-butanol. The last isomer has only one shape, but due to the three equivalent minima it has a very complex rotational spectrum, the interpretation of which requires a Hamiltonian with 60 parameters.^[68] The microwave (MW) spectra of three conformers of 2-butanol (*sec*-butanol) are known,^[69] while no MW investigations have been reported for isobutanol and *n*-butanol. An infrared investigation in CCl₄ solution reports the observation of the OH *gauche* and *trans* conformers for all isomers.^[70] For pentanol and hexanol, the rotational spectra have characterized 5 and 14 conformers for the chiral chemical isomers n-pentan-2-ol and n-hexan-2-ol, respectively.^[71] These studies have been greatly simplified by the application of the CP-FTMW broad band spectroscopy.^[72] So far little literature has reported on the cyclic alcohols. The rotational spectrum of cyclopropanol displayed only the *gauche* form,^[73] and for cyclobutanol only the *equatorial-trans* species has been observed.^[74] The rotational spectrum of cyclopentanol has not been reported yet, probably due to the complications arising from the ring pseudorotation. Here we report the spectrum of a tertiary cyclic alcohol, 1-methylcyclohexanol (1MCH). 1MCH is an important organic solvent and synthetic intermediate compound, which is widely used in producing of medicine and compound perfume.^[75] The conformational equilibrium of 1MCH has been previously investigated by NMR spectroscopy.^[76] However, because of the low barrier hindering the internal rotation of the hydroxyl group, just two conformers were discussed in which the orientation

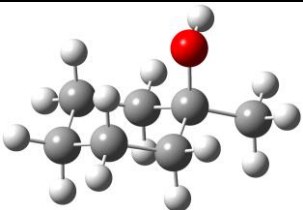
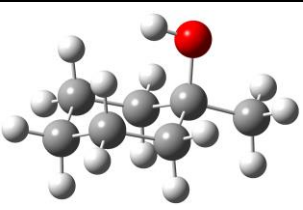
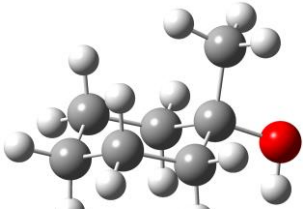
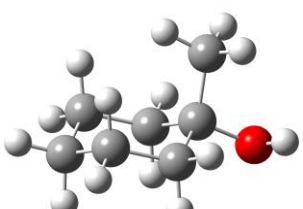
of the hydroxyl group was ignored. Since rotational spectroscopy can easily locate the position of a hydroxyl hydrogen, we decided to investigate the rotational spectra of 1MCH with PJ-FTMW, aiming at giving a detailed description of its conformational variation.

3.3.2. Experimental and computational methods

PJ-FTMW spectrometer was used to measure the spectra. Helium at a stagnation pressure of 0.3 MPa was used as the carrier gas of 1MCH (commercial sample) under room temperature. The deuterated species were obtained by direct proton exchange with D₂O.

The conformational equilibrium of 1MCH is driven by the internal rotation of the hydroxyl group, which can generate *gauche* and *trans* forms of the hydroxyl hydrogen with respect to the methyl group, and by the ring puckering, which can interconvert the *axial* or *equatorial* arrangement of the oxygen atom. These two internal motions generate six energy minima, which correspond to four different conformers, labeled as *At*, *Et*, *Ag*, and *Eg* (*A*, *E*, *t*, and *g* stand for *axial*, *equatorial*, *trans*, and *gauche*, respectively), the last two forms being doubly degenerate. MP2/6-311++G(d,p) calculations supplied the structures and relative energies of the four conformers and the values of the rotational and centrifugal distortion constants and of the electric dipole moment components. Vibrational frequency analysis confirmed that all these conformers are stable energy minima. All theoretical data are summarized in Table 3.3.1.

Table 3.3.1. The structures, energies and spectroscopic parameters of the plausible conformers of 1-Methylcyclohexanol at MP2/6-311++G(d,p) level.

	<i>Ag</i>	<i>At</i>
		
<i>A</i> , <i>B</i> , <i>C</i> /MHz	3119.4,1752.1,1514.7	3128.2,1732.3,1501.6
<i>D</i> _J , <i>D</i> _{JK} , <i>D</i> _K /kHz	0.106,0.135,0.103	0.102,0.129,0.108,
<i>d</i> ₁ , <i>d</i> ₂ /kHz	-0.017,0.003	-0.016,0.003
μ_a, μ_b, μ_c /D	0.4,1.1,-1.0	-1.7,0.0,1.0
$\Delta E, \Delta(E+ZPE)/\text{kJ}\cdot\text{mol}^{-1}$	0.0, ^a 0.0 ^b	3.03,2.52
	<i>Et</i>	<i>Eg</i>
		
<i>A</i> , <i>B</i> , <i>C</i> /MHz	3075.4,1710.2,1498.4	3060.7,1719.3,1504.5
<i>D</i> _J , <i>D</i> _{JK} , <i>D</i> _K /kHz	0.097,0.098,0.117	0.099,0.076,0.149
<i>d</i> ₁ , <i>d</i> ₂ /kHz	-0.013,0.003	-0.013,0.003
μ_a, μ_b, μ_c /D	-1.9,0.0,0.5	0.8,1.1,1.1

$\Delta E, \Delta(E+ZPE)/\text{kJ}\cdot\text{mol}^{-1}$	2.99,3.25	3.35,3.75
---	-----------	-----------

^aAbsolute energy: -349.4558771 E_h; ^bAbsolute energy: -349.251770 E_h.

3.3.3. Rotational Spectra

As shown in table 3.3.1, all the conformers have similar values of the rotational constants, and with non-zero μ_a electronic dipole moment. This implies that the *a*-type transitions of all the conformers are close to each other, especially in lower *J* transition frequency range. Therefore, we started the scan around 9.5 GHz where the *a*-type $J_{\text{upper}} = 3$ for all the conformers were expected and the $K_a = 0$ transitions were identified firstly as shown in Figure 3.3.1.

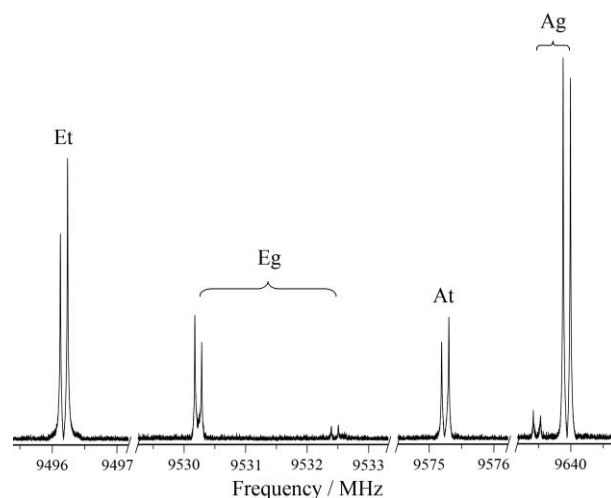


Figure 3.3.1. the $3_{03} \leftarrow 2_{02}$ transition spectra of the four conformers. Each line is doublet due to the Doppler effect, and the transitions of *gauche* geometries are split into two tunneling components.

The measurement of the *a*-type transitions was finally extended to $J = 6$ and $K_a = 4$. Then the *c*-type transitions for all conformers were assigned. The transition intensity ratios of corresponding transitions were satisfactorily in agreement with the *ab initio* prediction. The rotational transitions of Ag and Eg conformers are split into two component lines (0^+ and 0^-) due to the tunneling between two equivalent chiral forms. The complicated split can be taken as an evidence of the assignment. From Figure 3.3.1, one can also see that the 0^- transitions are much weaker than the 0^+ transitions. This indicates a considerably large energy splitting (ΔE_{01}) between 0^+ and 0^- states which causes a huge splitting of the *c*-type inter-transitions. All the transitions were fitted with Watson's Hamiltonian using Pickett's SPFIT program, and with I' representation and S reduction. The fit results are reported in table 3.3.2. The rotational constants agree with the ones calculated for the corresponding conformers very well, which can allow a straightforward assignment. Nevertheless, the value of ΔE_{01} was impossible to determine with the available transitions. Additionally, the difference of the centrifugal distortions between the two sub-states of the *gauche* conformers also implies a big splitting (ΔE_{01}). Due to the lack of the important parameters one can only match the

average values of the centrifugal distortion constants of the *gauche* conformers with the *ab initio* values, while for *trans* configurations they agree with the theoretical value directly.

Table 3.3.2: Experimental spectroscopic constants of 1-Methylcyclohexanol (*S*-reduction, *F* representation).

conformers	Ag		At	Et	Eg	
	0	1			0	1
A/MHz	3107.7518(5) ^a	3107.202(1)	3114.6536(6)	3061.9203(6)	3049.7507(8)	3050.470(1)
B/MHz	1741.9139(4)	1741.9323(5)	1728.1207(3)	1702.6330(4)	1709.8878(4)	1710.2904(5)
C/MHz	1507.4698(4)	1507.3484(5)	1498.0058(5)	1492.2991(5)	1497.3632(4)	1497.7084(6)
D _I /kHz	0.122(9)	0.058(12)	0.098(9)	0.088(8)	0.106(8)	0.06(1)
D _{JK} /kHz	0.44(2)	-0.12(6)	0.14(2)	0.12(3)	0.87(3)	-0.75(5)
D _K /kHz	-0.22(2)	0.44(6)			-0.57(6)	0.98(14)
d _K /kHz					0.0173(3)	
σ ^b /kHz	3.0		3.4	2.9	3.7	2.7
N ^c	50	29	37	34	40	26

^aErrors in parenthesis are expressed in units of the last digit. ^bStandard deviation of the fit. ^cNumber of fitted transitions.

The relatively high intensity of each conformer encouraged us to measure the OD monodeuterated species which is produced by mixing the sample with deuterated water. Due to the quadrupolar effects of the deuterium nucleus ($I = 1$), the transition of *Et* and *At* conformers displayed a hyperfine structure. The *Ag* and *Eg* conformers still showed the tunneling splitting due to the OD internal rotation. However, due to the mass effect, the splittings (ΔE_{01}) are considerably lower than the parent species. This allows a reliable value of the ΔE_{01} value to be deduced from the fit of the rotational transitions. Using Pickett's SPFIT program, all the transitions were fitted with the Hamiltonian:

$$H = \sum_i (H_i^R) + H^{CD} + H^{\text{int}} ; \text{ with } i = 0^+, 0^- \quad (1)$$

where

$$H^{\text{int}} = \Delta E_{01} + F_{bc} \times (P_b P_c + P_c P_b) + F_{ab} \times (P_a P_b + P_b P_a) \quad (2)$$

The fit results for the deuterated species are listed in table 3.3.3, where one can see the good agreement between the centrifugal distortion parameters with the results of the quantum chemical calculations. Especially for the *gauche* conformers they match the prediction results much better than parent species. This can be contributed to the successful fit of the rotation-vibration interaction in the deuterated species.

Table 3.3.3. Experimental spectroscopic constants of deuterated 1-Methylcyclohexanol (*S*-reduction, *F* representation).

conformers	Ag		At	Et	Eg	
	0	1			0	1
ν						
A/MHz	3048.1043(6) ^a	3047.8950(6)	3051.7095(4)	3013.7235(7)	3035.4711(5)	3035.2774(5)
B/MHz	1711.5882(7)	1711.6517(7)	1707.6229(4)	1666.0333(4)	1669.7168(6)	1669.8380(6)
C/MHz	1494.4048(8)	1494.4208(8)	1497.0626(5)	1475.2920(4)	1465.8493(5)	1465.9272(5)

D_J/kHz	0.11(1)	0.098(9)	0.093(8)	0.105(7)
D_{JK}/kHz			0.13(3)	
d_1/kHz	-0.036(9)			-0.035(5)
χ_{aa}/MHz		0.175(9)	-0.140(7)	
χ_{bb}/MHz		-0.18(2)	-0.12(2)	
χ_{cc}/MHz		0.01(2)	0.26(2)	
$\Delta E_{01}/\text{MHz}$	15580.7(54)			18173.4(292)
F_{ab}/MHz	1.0(1)			3.06(3)
F_{bc}/MHz	4.827(8)			1.16(4)
σ^b/kHz	3.2	3.9	2.8	3.3
N^c	40	61	65	56

^aErrors in parenthesis are expressed in units of the last digit. ^bStandard deviation of the fit. ^cNumber of fitted transitions.

3.3.4. Structure information

From the rotational constants of different isotopologues, straightforward information can be obtained, which are the substituted coordinates (r_s).^[77] These can be calculated with Kraitchman's method. We used Costain's uncertainties, without imposing planarity constraints. The r_s values are in agreement with the theoretical results, as shown in table 3.3.4. This can confirm the assignment of the four conformers.

Table 3.3.4. r_s coordinates of the hydrogen atom of hydroxyl group in 1- Methylcyclohexanol.

	Ag			At		
	$a/\text{\AA} (v=0/1)$	$b/\text{\AA} (v=0/1)$	$c/\text{\AA} (v=0/1)$	$a/\text{\AA}$	$b/\text{\AA}$	$c/\text{\AA}$
Exptl.	$\pm 1.550(1)/1.547(1)$	$\pm 0.684(2)/0.669(2)$	$\pm 1.6645(9)/1.6649(9)$	$\pm 0.430(3)^b$	0.0	$\pm 1.8265(8)$
Calc. ^a	1.547	0.688	1.656	0.336	0.0	-1.829
	Et			Eg		
	$a/\text{\AA}$	$b/\text{\AA}$	$c/\text{\AA}$	$a/\text{\AA} (v=0/1)$	$b/\text{\AA} (v=0/1)$	$c/\text{\AA} (v=0/1)$
Exptl.	$\pm 1.9604(8)$	0.0	$\pm 1.6415(9)$	$2.6027(6)/2.6077(6)$	$0.696(2)/0.718(2)$	$0.578(3)/0.595(3)$
Calc.	-1.944	0.0	-1.648	-2.600	0.724	-0.572

^aCalculated at MP2/6-311++G** level; ^bError in parentheses in units of the last digit.

3.3.5. The internal rotation of hydroxyl group

The internal of the hydroxyl group is described by the dihedral angle CC-OH (τ). The potential energy curves along this parameter are shown in Figure 3.3.2 with the red lines.

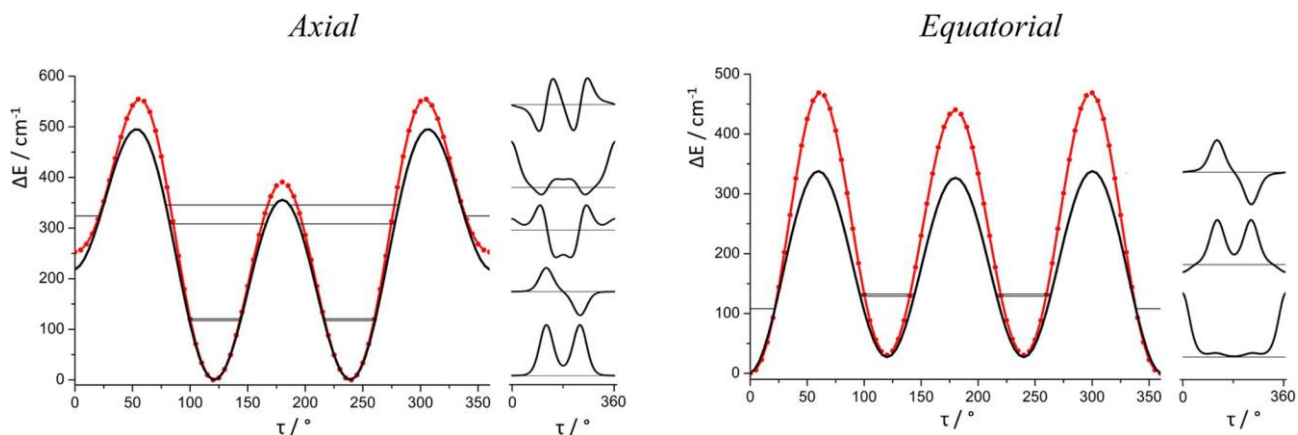


Figure 3.3.2. *Ab initio* (red) and experimental (black) potential energy function of the internal rotation of the OH group for the *axial* and *equatorial* conformers (cm^{-1} vs deg). The wave functions of the lower states are also drawn on the right hand of each panel.

From the precise ΔE_{01} values of the OD species, we can obtain the potential energy function of the internal rotation of hydroxyl group by using Meyer's one-dimensional flexible model. This model allows the numerical calculation of the rotational and vibrational wave functions and eigenvalues with a preconditioned description of the pathway and a potential energy function. So from the MP2/6-311++G(d,p) energy calculation the potential function of the internal rotation of hydroxyl group can be written as:

$$V(\tau) = V_0 + V_1 \cdot (1 - \cos\tau) + V_2 \cdot (1 + \cos 2\tau) + V_3 \cdot (1 + \cos 3\tau) \quad (3)$$

The values of V_i are listed in table 3.3.5. From the calculation optimization, the structure relaxation parameters are taken account according to the equation:

$$S_i(\tau) = S_i^0 + \Delta S_i(\tau) \quad (4)$$

S^0 is the value of S at $\tau = 0$, and ΔS is its variation as the function of τ . Twelve structure relaxations were taken into account of both *equatorial* and *axial* forms models. The detailed information has been reported in appendix III.

Finally, the splittings have been reproduced by multiplying equation 3 by a scale factors 0.90 and 0.72 for the *axial* and *equatorial* species, respectively. The barriers B_2 were estimated to be = 356 cm^{-1} , and 320 cm^{-1} , respectively. All these data are listed in Table 3.3.6. The obtained potential energy functions are shown in Figure 3.3.2 (black lines), where the wave function patterns of the lower energy levels are also presented (five for the *axial* and three for the *equatorial* species, respectively). The value ΔE_{01} of the parent species has been deduced to be 102.5 and 103.0 GHz, respectively. Surprisingly, they are larger than that observed for isopropanol,³ in spite of the fact that the inversion of the OH group takes place in our case in the proximity of a methyl group and for isopropanol in proximity of a aliphatic hydrogen.

The τ coordinate was restricted within the 2π cyclic range and solved into 61 mesh points.²²

Table 3.3.5. MP2/6-311++G(d,p) Values^a of the V_i Coefficients in Equation 3 for Potential Energy Functions of the *Axial* and *Equatorial* Forms

	V_0 , cm^{-1}	V_1 , cm^{-1}	V_2 , cm^{-1}	V_3 , cm^{-1}	B_2 , cm^{-1}	$E_t - E_g$, cm^{-1}	$B_{t \rightarrow g}$, cm^{-1}
<i>axial</i>	-79.0	129.4	30.9	206.3	390.9	252.7	301.7
<i>equatorial</i>	50.0	-8.0	-18.0	219.6	410.0	-30.6	438.2

^aAlso the energy values at the critical points, relative to the *gauche* energy minimum, are given.

Table 3.3.6. Results of the Flexible Model Calculations.

	<i>axial</i>		<i>equatorial</i>	
	obs	calc	obs	calc
ΔE_{01} (OD), GHz	15.6	15.6	18.2	18.2
ΔE_{01} (OH), GHz		102.5		103.0
parameters				
Scale factor f (fitted)	0.90		0.72	
Barrier B_2 (extrapolated), cm^{-1}	356		320	

3.3.6. Conclusion

We reported the rotational spectra of the biggest cyclic alcohol, and four conformers have been assigned, which are Ag, At, Eg, Et, respectively. According to the transition intensities one can see that the *axial* ring form is preferred than *equatorial*, and Ag is more stable than At. But in the *equatorial* ring form the *trans* geometry is more stable than the *gauche*. The tunneling splittings between the two mirror *gauche* forms have been reflected in the rotational spectra. The split transitions allow us to precisely determine the splitting energies (ΔE_{01}) and from them to estimate B_2 inversion barriers.

Chapter IV

Clusters formed by the cooperation of different classes of HBs

Hydrogen Bond (HB) certainly plays a key role in many chemical processes and biologically relevant functions. HB is a form of association between an electronegative atom and a hydrogen atom attached to a second, relatively electronegative atom or group. It is best considered as an electrostatic interaction, heightened by the small size of hydrogen, which permits proximity of the interacting dipoles or charges. Both electronegative atoms are usually (but not necessarily) from the first row of the periodic table, *i.e.* N, O or F. Hydrogen bonds may be either inter-molecular or intra-molecular.^[78] Based on the binding energies or the electronegativity of the atoms of groups linked with H, HB can be classified into different classes, strong, moderate, and weak HB. The hydrogen bond covers a wide range of energies: from 2 kJ/mol (0.5 kcal/mol) to nearly 170 kJ/mol (40 kcal/mol) This means that the weakest hydrogen bonds are close in energy to *van der Waals* interactions and the strongest hydrogen bonds are stronger than some covalent bonds it is therefore very difficult to draw a line that separates weak hydrogen bonds from strong ones. However we can roughly classify them and give an ideal for the interactions as: strong HB (15-40 kcal/mol) with H...X length 1.2-1.5 Å; 2) medium (4-15 kcal/mol) with H...X length 1.5-2.2 Å; 3) weak (< 4 kcal/mol) with H...X length 2-3 Å. Despite a single WHB is characterized by a binding energy remarkably smaller than the one occurring for strong HBs, it has been shown that often a WHB network takes place between two or more molecules, reinforcing the interaction strength through a sort of cooperative effect which can lead to stable oligomers.^[79]

Microwave spectroscopy is endowed with the talent for measuring the structures of isolated molecular systems. The rotational spectroscopy of molecular adducts can supply the information on HB.

In this chapter, I will report the works of the rotational study of the clusters linked by HB and WHB. The study of formic acid clustering with dimethyl ether and cyclobutanone, respectively, indicate that both complexes are formed with one typical O-H...O HB and two C-H...O WHBs. The investigation of the complex of indan and trifluoromethane showed a cage structure based on the cooperative effects of C-H... π and C-H...F WHB interactions. The study of oligomer of (CH₂F₂)_m-W_n, (m,n = 1,2) has broaden our knowledge of the cooperation of different HB in a cluster.

The $(\text{CH}_2\text{F}_2)\text{-W}_2$ displayed a cyclic structure linked with $\text{O-H}\cdots\text{O}$, $\text{C-H}\cdots\text{O}$, and $\text{O-H}\cdots\text{F}$ bonds. The $(\text{CH}_2\text{F}_2)_2\text{-W}$ showed a geometry connected with $\text{O-H}\cdots\text{F}$, $\text{C-H}\cdots\text{O}$, and $\text{C-F}\cdots\text{H-C}$ bonds. In the tetramer $(\text{CH}_2\text{F}_2)_2\text{-W}_2$, the cluster is stable by 7 non-covalent bonds including $\text{O-H}\cdots\text{O}$, $\text{O-H}\cdots\text{F}$, $\text{C-H}\cdots\text{O}$, $\text{C-F}\cdots\text{H-C}$ bonds.

4.1. Formic acid cluster with Dimethyl ether

4.1.1. Introduction

Recently, considerable efforts have been dedicated to the rotational study of molecular adducts involving carboxylic acids. Since the carboxy group can offer either a proton donor or a acceptor site for HB, generally the carboxylic acids prefer to form a homo-dimer forming a eight-member group ring. The interaction in the dimer, where a double HB is present, can be as strong as ~ 60 kJ/mol, which is the strongest non-covalent bond between neutral species. The first observation of this kind of dimers by microwave spectroscopy can be traced back to half a century ago.^[41,80] However, the details of this interaction, such as proton transfer, internal rotation, and Ubbelohde effect were characterized only recently.^[81-95] The hydrated carboxylic acids have been also investigated by rotational spectroscopy.^[96-101] The tunneling splitting were always displayed on the spectra. Jäger et al. hypothesized four different reasons responsible for the splitting in the study of benzoic acid-water, and only the internal rotation of the water along its C_2 symmetric axis is pointed out to be the most promising candidate for the tunneling splitting.^[101] The complexes of formic acid with other partners with various functional groups, like anhydrides,^[102] aldehydes,^[103] amides,^[104] and azines,^[105] have already been characterized by microwave spectroscopy. The study of formic acid with formamide^[104] and pyridine^[105] showed that the dimers are connected forming a seven-member ring involving two HBs and the interactions are as strong as ~ 40 kJ/mol. When it comes to CO_2 ^[102] and CH_2O ^[103], the interaction with formic acid is only ~ 20 kJ/mol. In this work, the interaction between carboxylic acid with the ether family will be discussed for the first time.

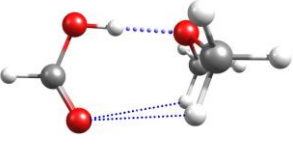
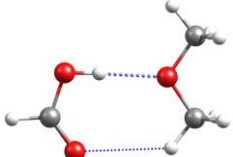
4.1.2. Experimental and computational methods

The PJ-FTMW was used for this experiment. Commercial samples of Formic acid and $(\text{CH}_3)_2\text{O}$ were obtained from Aldrich and used without further purification. A mixture of $(\text{CH}_3)_2\text{O}$ with ca. 1% in Helium at a total pressure of 0.3 MPa was streamed over HCOOH at 273 K.

Two stationary points of $\text{HCOOH}-(\text{CH}_3)_2\text{O}$ were found on the conformational potential energy surface at the MP2/6-311++G(d,p) level. The corresponding shapes, relative energies, rotational constants, and dipole moment components are reported in table 4.1.1. In the most stable isomer (*vertical*), the heavy atom's symmetry planes of the two constituent molecules are orthogonal to each other, while in the second one (*planar*) the symmetry planes are nearly co-planar. The two constituent molecules are held together by one "classical" $\text{O}-\text{H}\cdots\text{O}$ (HB) and a bifurcated $\text{CH}_2\cdots\text{O}$ (WHB) in the *vertical* structure, and again by one $\text{OH}\cdots\text{O}$ interaction but only a simple $\text{C}-$

H...O WHBin the *planar* structure. In order to have a better understanding of the molecular properties, the nature of all stationary points was verified by subsequent harmonic frequency calculation. Estimates of the intermolecular binding energy values for the most stable species were counterpoise corrected for basis set superposition error (BSSE)^[106] also applying the zero-point energies (E_0).

Table 4.1.1. The structure shapes, relative energies, dissociation energies, rotational constants, and dipole moments of two most stable isomers at MP2/6-311++G** level.

	<i>Vertical</i>	<i>Planar</i>
		
$\Delta E, \Delta E_0 / \text{kJ} \cdot \text{mol}^{-1}$	0 ^a , 0 ^b	2.3, 1.4
$E_D, E_{D,0} / \text{kJ} \cdot \text{mol}^{-1}$	47.5, 40.9	
$E_{D,BSSE}, E_{D,0,BSSE} / \text{kJ} \cdot \text{mol}^{-1}$	33.5, 27.0	
$A, B, C / \text{MHz}$	5160, 1858, 1834	5955, 1684, 1341
$D_J, D_{JK}, D_K, d_1, d_2 / \text{kHz}$	1.78, 8.23, -7.16, -0.03, 1.31	
$\mu_a, \mu_b, \mu_c / \text{D}$	1.7, 0.1, 0.0	2.8, 0.5, 0.5

^aAbsolute energy: -344.0043087 Eh. ^bAbsolute energy: -343.8865972 Eh.

4.1.3. Rotational spectra

The calculation results suggest that the *vertical* structure is the energetically preferred geometry, and the strong μ_a (1.7D) dipole moment component facilitates the scan of the *a*-type *R*-band transitions in our spectroscopic range. We firstly assigned the three transitions of this band, $2_{02} \leftarrow 1_{01}$, $2_{12} \leftarrow 1_{11}$ and $2_{11} \leftarrow 1_{10}$. Then totally 22 μ_a -type lines were assigned in the 7-18.5 GHz range. We failed trying to assign the μ_b and μ_c type transitions. This is consistent with the theoretical prediction of the *vertical* structure, which reports the near zero value of μ_b , and zero value of μ_c by symmetry. All the transitions have been fitted within the F' -representation of Watson's S reduction.^[39] The fit results including the rotational constants and four quartic centrifugal parameters are reported in the left column of the table 4.1.2.

Table 4.1.2. Experimental spectroscopic parameters of the isotopologues of HCOOH-(CH₃)₂O. (S -reduction, F' -representation)

	Parent	FA- ¹³ CH ₃ OCH ₃	H ¹³ COOH-(CH ₃) ₂ O	HCOOD-(CH ₃) ₂ O	DCOOH-(CH ₃) ₂ O ^a
A / MHz	5168(8) ^b	5095 ^c	5168 ^c	5126 ^c	5167 ^c
B / MHz	1824.846(2)	1799.4138(6)	1800.2425(6)	1823.1162(5)	1766.2896(6)
C / MHz	1808.391(2)	1790.7518(6)	1784.2554(6)	1801.1519(5)	1750.8267(6)
D_J / kHz	2.08(1)	[2.08] ^d	[2.08]	[2.08]	1.87(1)
D_{JK} / kHz	6.78(4)	[6.78]	[6.78]	[6.78]	[6.78]
d_1 / kHz	-0.05(2)	[-0.05]	[-0.05]	[-0.05]	[-0.05]
d_2 / kHz	0.190(7)	[0.190]	[0.190]	[0.190]	[0.190]
σ^e / kHz	2.2	6.4	8.1	7.1	5.9

N^f	22	10	10	18	36
-------	----	----	----	----	----

^aNuclear quadrupole coupling constant $\chi_{aa} = 0.37(3)$ MHz. ^bError in parentheses in units of the last digit.

^cExtrapolated from the experimental A value of the parent species by applying the *ab initio* predicted difference between isotopologues. ^dValues in brackets fixed to the corresponding values of the parent species. ^eRoot-mean-square deviation of the fit. ^fNumber of lines in the fit.

After the measurements on the parent species we also measured the mono- ^{13}C substituted species in natural abundance. The population of ^{13}C is 1% of the parent in natural abundance. So, the intensities of $\text{FA-}^{13}\text{CH}_3\text{OCH}_3$, and $\text{H}^{13}\text{COOH-(CH}_3)_2\text{O}$ should be 2% (due to the symmetry), and 1% as strong as the parent species, respectively. So, we were only able to see 10 lines for each ^{13}C isotopologues due to the very low intensities. The lines have been fitted with the same Hamiltonian as the normal species while the centrifugal distortion parameters have been fixed to the values of the normal species parameters, and the A rotational constants were derived from the *ab initio* value with a correction of the difference between the experimental and *ab initio* values of the parent species. The results of the fit are listed in the second and third columns in table 4.1.2.

Additionally, we also assigned the deuterated species by substituting HCOOH with DCOOH and HCOOD , in the expansion respectively. The former was purchased from Aldrich while the latter was formed by hydrogen exchange obtained by mixing HCOOH with D_2O . For the $\text{DCOOH-(CH}_3)_2\text{O}$ species we observed the quadruple pattern due to the deuterium nucleus with nuclear spin $I = 1$. The spectrum of the $2_{11} \leftarrow 1_{10}$ transition compared to the spectrum of the parent species is shown in Figure 4.1.1 as an example. The fitted results of hyperfine structures of the deuterated species from Pickett's SPFIT program^[38] are reported in table 4.1.2. Similarly, to the ^{13}C isotopologues the centrifugal distortion parameters are fixed to the parameters obtained for the parent species and the values of constant A are extrapolated from parent species.

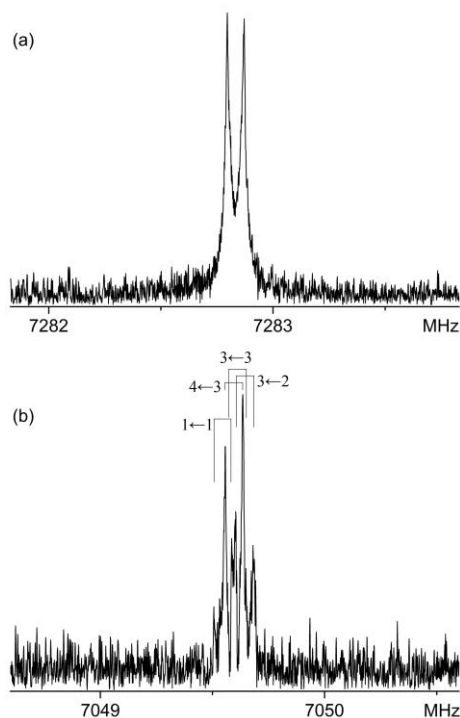


Figure 4.1.1. Transition $2_{11} \leftarrow 1_{10}$ of formic acid and dimethyl ether: (a) $\text{HCOOH}-(\text{CH}_3)_2\text{O}$ parent species (270 FIDs). (b) $\text{DCOOH}-(\text{CH}_3)_2\text{O}$ isotopologue (1000 FIDs). The four D-hfs components $F' \leftarrow F''$ are labeled with the total angular momentum quantum number $F = |J + I|$.

4.1.4. Structure analysis

The observed conformer, shown in Figure 4.1.2 with the principal axes system, has a plane of symmetry, containing atoms 1-6 and the reference point X7 (lying along the bisector of the C8O6C9 angle). $(\text{CH}_3)_2\text{O}$ is linked to HCOOH through a main $\text{O-H}\cdots\text{O}$ HB, and a bifurcated $\text{CH}\cdots\text{O}$ WHB. The structure parameters from the MP2/6-311++G** level are reported in table 4.1.3.

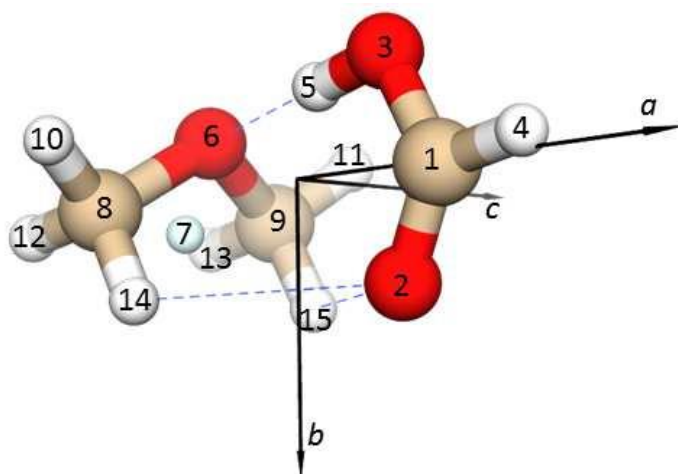


Figure 4.1.2. Sketch, atom numbering, main structural parameters and principal axes of the observed form of $\text{HCOOH}\cdots(\text{CH}_3)_2\text{O}$. Number 7 indicates a dummy atom (0 mass) placed on the bisector of the C8O6C9 angle.

Table 4.1.3. MP2/6-311++G(d,p) geometry of the observed isomer of $\text{HCOOH}\cdots(\text{CH}_3)_2\text{O}$.

Bond lengths/Å	Valence Angles/°	Dihedral angles/°
----------------	------------------	-------------------

O2C1	1.2140				
O3C1	1.3321	O3C1O2	125.7		
H4C1	1.0982	H4C1O2	123.7	H4C1-O2O3	180.0
H5O3	0.9939	H5O3C1	106.9	H5O3-C1O2	0.0
O6H5	1.6692	O6H5O3	179.9	O6H5-O3C1	0.0
X7O6a	1.0000	X7O6H5	128.0	X7O6-H5O3	0.0
C8O6	1.4245	C8O6X7	55.4	C8O6-X7H5	90.0
C9O6	1.4245	C9O6X7	55.4	C9O6-X7H5	-90.0
H10C8	1.0904	H10C8O6	107.0	H10C8-O6C9	180.0
H11C9	1.0904	H11C9O6	107.0	H11C9-O6C8	180.0
H12C8	1.0960	H12C8O6	110.1	H12C8-O6H10	-118.9
H13C9	1.0960	H13C9O6	110.1	H13C9-O6H11	118.9
H14C8	1.0960	H14C8O6	110.4	H14C8-O6H10	119.5
H15C9	1.0960	H15C9O6	110.4	H15C9-O6H11	-119.5

^aX7 indicates a dummy atom (0 mass) placed on the bisector of the C8O6C9 angle.

Since the error on the rotational constant A is relatively large, due to the lack of measured b and c type transitions, the precise values of the substitution coordinates cannot be obtained.^[40] However, the effective (partial r_0) structure are able to be reproduced from the theoretical structure. Taking the *ab initio* geometry as a starting point, and just changing the O6...H5 hydrogen bond length (from 1.669 to 1.673(2) Å), the rotational constants B and C of all isotopologues can be reproduced within deviation of 1-2 MHz, and the rotational constant A within its experimental uncertainty. The hydrogen bond structural parameters obtained with this effective geometry are given in table 4.1.4.

Table 4.1.4. r_0 structural parameters of the hydrogen bonds which link the constituent molecules of HCOOH... $(\text{CH}_3)_2\text{O}$.

O-H...O HB		C-H...O WHB	
$r_{\text{O6H5}}/\text{Å}$	1.673	$r_{\text{O2H14(15)}}/\text{Å}$	2.824
$\angle\text{O6H5O3}/^\circ$	179.9	$\angle\text{C8H14(15)O2}/^\circ$	115.5
$\angle\text{X7O6H5}/^\circ$	128.0	$\angle\text{C1O2H14(15)}/^\circ$	112.5

In table 4.1.5 we compare the experimental and *ab initio* values of the planar moment of inertia P_{cc} . It is defined as $P_{\text{cc}} = 1/2(I_{\text{a}}+I_{\text{b}}-I_{\text{c}})$ and it gives the mass extension along the c -axis, i.e. the mass extension out of the ab -plane. For the *vertical* isomer, it should correspond to the P_{aa} value of isolated $(\text{CH}_3)_2\text{O}$,^[107] which is also reported in table 4.1.5.

Table 4.1.5. Experimental and *ab initio* P_{cc} values of HCOOH... $(\text{CH}_3)_2\text{O}$ are compared to the P_{aa} value of $(\text{CH}_3)_2\text{O}$.

$P_{\text{cc}}(\text{HCOOH-O}(\text{CH}_3)_2)/\text{uÅ}^2$		$P_{\text{aa}}(\text{O}(\text{CH}_3)_2)/\text{uÅ}^2$
Exptl.	<i>ab initio</i>	Exptl.
47.6(2) ^a	47.2	47.0466(1) ^b

^aError in parentheses in units of the last digit. ^bFrom Ref. 107.

Both experimental and *ab initio* P_{cc} values of HCOOH- $\text{O}(\text{CH}_3)_2$ are larger than the P_{aa} value of $(\text{CH}_3)_2\text{O}$. It seems that the COC angle of $(\text{CH}_3)_2\text{O}$ becomes slightly larger upon complexation

with HCOOH.

4.1.5. Dissociation energy

The intermolecular stretching motion which leads to the dissociation is almost parallel to the α -axis of the complex. In this case, a *pseudo*-diatomic approximation can be used to roughly estimate the force constant of the stretching mode leading to the dissociation through the equation:^[108]

$$k_s = 16\pi^4(\mu_D R_{CM})^2 [4B^4 + 4C^4 - (B - C)^4 \times (B + C)^4] / (hD_J) \quad (1)$$

where μ_D is the pseudo diatomic reduced mass, R_{CM} (3.1 Å) is the distance between the centers of the mass of the two subunits, and B , C and D_J are the spectroscopic parameters of table 4.1.2. We obtained $k_s = 21.4$ N/m, corresponding to a harmonic stretch fundamental $\nu = 142$ cm⁻¹. Assuming a Lennard-Jones type potential the zero point dissociation energy of the complex can be estimated to be ~11 kJ/mol by applying the approximate expression:^[109]

$$E_B = k_s R_{CM}^2 / 72 \quad (2)$$

Such a value is considerably lower than the *ab initio* suggestions. We found the *pseudo*- diatomic approximation to work and to give consistent results for several families of related adducts. However, in the present case we are unhappy with the result. Probably, for HCOOHO(CH₃)₂ the detachment motion of the monomers does not take place along the α -axis (for example, the carbonyl group, which is linked to O(CH₃)₂ by a WHB, could move away before of the OH group). Then, the stretching motion could be coupled to bending vibrations making the pseudo diatomic approximation to crude.

4.1.6. Conclusion

We reported the results of the first rotational investigation of a molecular adduct constituted of a carboxylic acid and an ether. We observed the spectrum of the most stable isomer (*vertical*) and described the structural aspects of the non-bonding interactions which link the two subunits, a classical OH...O HB and a bifurcated CH...O WHB. The planar conformation was not observed, probably because undergoing a conformational relaxation upon supersonic expansion. The dissociation energy appears comparable to the values obtained for HCOOH-CH₂O and HCOOH-CO₂, and about half the values reported for the complexes of HCOOH with pyridine and formamide, where a quasi-conjugated ring system is formed.

4.2. The cluster of Formic acid with Cyclobutanone

4.2.1. Introduction

With respect to internal dynamics, due to the tunneling motions connecting equivalent minima, the rotational transitions will be split and reflected in the spectra. From the splitting it is generally possible to determine the potential energy barrier connecting the equivalent minima. Rotational spectroscopy has investigated the splitting derived from the internal motions involving carboxylic acid: (i) double proton transfer in dimers of carboxylic acids with a suitable symmetry;^[83-86,94] (ii) internal rotation of a light symmetric group (*i.e.* a CH₃ group);^[81,84,99] (iii) inversion of an asymmetric group (e.g. a hydroxyl or carboxylic acid) connecting two equivalent minima^[90,91,100] or (iv) internal motion of water in hydrated forms of carboxylic acids.^[96-101,110]

Here we report on a huge spectral splittings observed in the jet-cooled rotational spectrum, which arises from a relative motion of a partner as heavy as cyclobutanone (CBU) with respect to formic acid (FA) in their 1:1 complex (FA-CBU), . The tunneling pathway and the potential energy function of the motion have been derived from the experimental values of the ΔE_{01} splittings.

4.2.2. Experimental and computational results

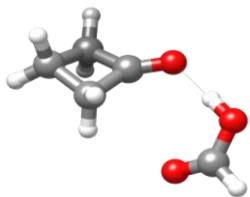
Commercial samples of HCOOH, DCOOH and CBU were obtained from Aldrich and used without further purification. The HCOOD species has been prepared by mixing HCOOH and D₂O in the same ratio. The rotational spectra of FA...CBU isotopologues have been measured in two different laboratories:

a) Bologna. The PJ-FTMW spectrometer was used. Adducts were formed by flowing helium at ~5 atm through two stainless steel reservoirs containing, respectively. CBU was kept at room temperature, and FA (or isotopologues) was at 273 K.

b) Valladolid. The rotational spectrum of the parent species was initially recorded with a broadband chirp-excitation microwave spectrometer in Valladolid covering the frequency range 2-8 GHz, which follows Pate's design.^[111] In this spectrometer a 5s chirp is created by an arbitrary waveform generator, which is amplified to 20 W and radiated perpendicular to the direction of the jet expansion through a horn antenna. A molecular transient emission spanning 40s is finally amplified, recorded with a digital oscilloscope and Fourier-transformed to the frequency domain. Sample preparation was similar to the one in Bologna, with optimal conditions requiring backing pressures of ca. 4 atm and neon as carrier gas. The accuracy of the frequency measurements is better than 15 kHz.

The shapes and relative energies of the plausible isomers of FA-CBU were optimized at the MP2/6-311++G(d,p) and B3LYP-D3/6-311++G(d,p) levels. The two subunits were assumed to be in a nearly co-planar arrangement in the complex. MP2 method suggests that the CBU molecular ring is slightly distorted (up or down) from planarity and located in two located minima, while the B3LYP-D3 calculation predicts a single minimum, with the CBU ring remaining planar in the complex. Actually, the isolated CBU has been proved to be with the distorted structure undergoing the ring puckering motion with a small barrier close to 5 cm^{-1} at the planar ring.^[112] However, an effective planar ring will be adopted in the spectroscopy study, if the ground vibrational state lies above the barrier. It is well-known that MP2 tends to overestimate ring-puckering barriers while B3LYP underestimates them. Additionally, in previous investigations of complexes of CBU with water^[113] and trifluoromethane,^[11] MP2 suggested two conformers differing from the distorted CBU ring, but the experimental results showed only one conformer with effectively planar CBU. Therefore, we assumed the prediction with the B3LYP-D3 method was more precise and initially scanned the rotational spectrum with its guide. The corresponding shapes, relative energies, rotational constants, and dipole moment components are reported in table 4.2.1.

Table 4.2.1. B3LYP-D3/6-311++G(d,p) shape, energy, spectroscopic constants and dipole moment components of the most stable form of FA...CBU.

A/MHz	4120	
B/MHz	993	
C/MHz	843	
$\mu_a, \mu_b, \mu_c/\text{D}$	3.0, 0.7, 0.7	
Absolute energy/Eh	-344.004309	

The rotational spectrum of the parent species was first recorded with the chirped-pulse microwave spectrometer in Valladolid (see Experimental Section) within the frequency range 2-8 GHz. Unfortunately, the spectrum was weak, and considerably perturbed in that frequency region. We could only reliably assign three transitions, $2_{02} \leftarrow 1_{01}$, $3_{03} \leftarrow 2_{02}$, $4_{04} \leftarrow 3_{03}$, and they were split into two component lines. We then recorded the spectrum within the 6-18.5 GHz frequency range using the PJ-FTMW (Chapter II) spectrometer in Bologna.

In this spectrum, we could finally measure 31 μ_a - and 6 μ_b -type transitions, and all the transitions display two tunneling components lines with the split up to 10 MHz. Additionally, we also assigned 6 μ_c -type transitions, with the two component lines evenly spaced by ca. 2245 MHz, i.e. twice the energy separation of the two sublevels of the vibrational ground state. It is worth noting that the μ_c -type transitions are inter-states transition.

All rotational transitions have been satisfactorily fitted using the following coupled

Hamiltonian:

$$H = H_{R0} + H_{R1} + H_{CD} + H_{int} \quad (4.2.1)$$

where H_{R0} and H_{R1} are the rotational terms for the 0 and 1 inversion sub-states, respectively, and H_{CD} represents the centrifugal distortion corrections (assuming the same value for the two inversion sub-states v). The coupling term between the $v = 0$ and $v = 1$ states is expressed as:

$$H_{int} = \Delta E_{01} + F_{bc} \times (P_b P_c + P_c P_b) + F_{ac} \times (P_a P_c + P_c P_a) \quad (4.2.2)$$

where ΔE_{01} is the energy difference between the two sub-states, and F_{bc} and F_{ac} are Coriolis coupling parameters. The $(P_a P_b + P_b P_a)$ Coriolis term was not fitted in the Hamiltonian equation, which is consistent with an inversion motion through the c -axis. Pickett's SPFIT program has been used for this purpose, using the F -representation of Watson's S reduction. The fitted spectroscopic parameters are shown in the left column of table 4.2.2.

Table 4.2.2. Experimental spectroscopic constants of the observed isotopologues of FA...CBU (Watson's S -reduction, F representation)

	HCOOH...CBU	DCOOH...CBU	HCOOD...CBU
A_0/MHz	4151.912(9) ^a	4139.417(9)	4119.26(1)
A_1/MHz	4151.222(9)	4138.707(10)	4118.54(1)
B_0/MHz	988.452(2)	961.557(2)	983.636(2)
B_1/MHz	988.562(2)	961.671(2)	983.745(2)
C_0/MHz	843.447(4)	823.406(5)	838.570(5)
C_1/MHz	843.683(4)	823.627(5)	838.816(5)
D_J/kHz	0.596(1)	0.565(2)	0.586(1)
D_{JK}/kHz	-0.86(4)	-1.04(7)	-0.91(5)
D_K/kHz	11(1)	[11] ^b	11(2)
d_1/kHz	0.039(1)	0.037(2)	0.040(1)
d_2/kHz	-0.016(1)	-0.016(5)	0.014(1)
$\Delta E_{01}/\text{MHz}$	1122.756(3)	1084.538(5)	1180.282(5)
F_{bc}/MHz	5.2261(2)	4.9179(7)	5.2584(2)
F_{ac}/MHz	15.5(5)	16.4(5)	14.0(6)
σ/kHz^c	5.1	5.2	4.5
N^d	84	54	74

^aError in parentheses in units of the last digit. ^bValues in brackets have been held at the values of the parent species. ^cRoot-mean-square deviation of the fit. ^dNumber of lines in the fit.

After the fit of parent species, we also assigned the spectra of the two mono-deuterated species DCOOH...CBU and HCOOD...CBU, by using ca. 99% enriched samples of DCOOH and a 1:1 mixture between HCOOH and D₂O, respectively. The measured transition frequencies were fitted in the same Hamiltonian expression with that of the parent species. The results of the fits are reported in the second and third columns of table 4.2.2. No effects of the hyperfine quadrupole

structure of the D atom ($I = 1$) have been satisfactorily resolved.

All the experimental frequencies are listed in the appendix V.

4.2.3. Structure analysis

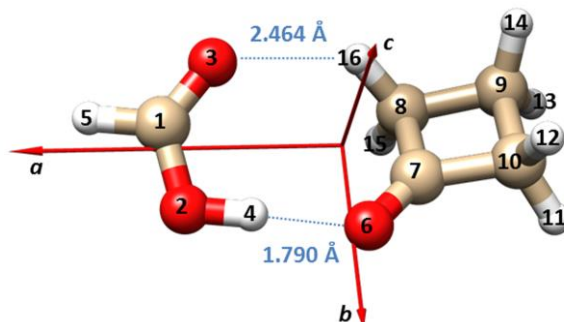


Figure 4.2.1. Principal inertial axes and atom numbering of the observed dimer of FA...CBU. The effective lengths of the non-covalent bonds are shown.

From the rotational constants of the assigned isotopologues, the Kraitchman substitution coordinates of the two hydrogen atoms of the FA unit (H5 and H4) have been calculated as listed in table 4.2.3. The atom numbering and the principal inertial axes system of the complex are in agreement with Figure 4.2.1. As we know the deriving of the Kraitchman's coordinates does not rely on any geometry assumption. However, these Kraitchman's positions are in good agreement with the theoretical values as seen in the table 4.2.3.

Table 4.2.3. Substitution (r_s), equilibrium (r_e , B3LYP-D3/6-311++G(d,p)) and effective (r_0) atomic coordinates of the two substituted hydrogen atoms in the principal axes system of the parent species of FA...CBU.

		r_s	r_e	r_0^a
H5	$ a /\text{\AA}$	3.7785(8) ^b	3.7924	3.7720
	$ b /\text{\AA}$	0.579(6)	0.5712	0.6365
	$ c /\text{\AA}$	0.22(2)	0.0682	0.1247
H4	$ a /\text{\AA}$	1.584(2)	1.4549	1.4991
	$ b /\text{\AA}$	0.989(3)	1.0365	1.0635
	$ c /\text{\AA}$	0.06(5)	0.1812	0.1806

^aCalculated from the partial r_0 structure (see text). ^bError in parenthesis are in units of the last digits.

The B3LYP-D3/6-311++G(d,p) structures of the two equivalent energy minima and of the transition state in the potential energy function connecting the two minima (see Figure 4.2.2) are reported in the appendix IV. By adjusting the theoretical values of the structural parameters r_{O6-O2} , $\angle O6O2C1$ and $\angle O6O2-C1O3$ from 2.7475 Å, 111.0° and -2.2° to 2.7800 Å, 109° and 0.4°, respectively, we were able to reproduce the experimental rotational constants within a few MHz errors. From this structure, the bond lengths of the two hydrogen bonds have been estimated to be:

$r_{O6-H4} = 1.790 \text{ \AA}$ and $r_{O3-H16} = 2.464 \text{ \AA}$, respectively.

4.2.4. Large amplitude motion

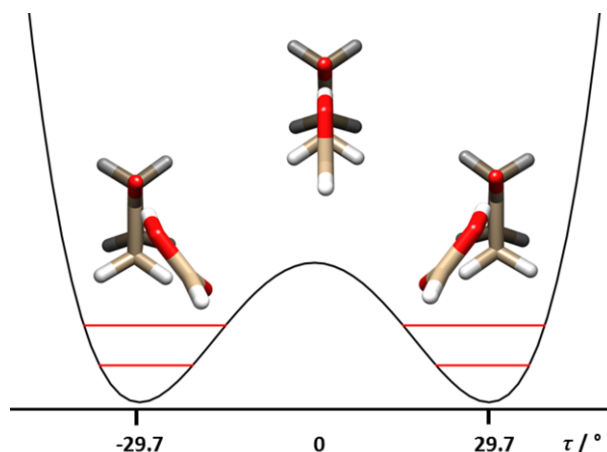


Figure 4.2.2. The tunneling motion in FA-CBU is due to the internal rotation around the C7O6-O2C1 (τ) dihedral angle, accompanied by structural relaxation of some other parameters.

As we know, the energy splitting ΔE_{01} are related the potential barrier connecting the two equivalent minima. Meyer's flexible model is especially suitable to determine potential energy surfaces from the experimental data. The interconversion path is depicted in Figure 4.4.2. As shown in the results of the fit, $\Delta E_{01}(\text{DCOOH}\dots\text{CBU}) = 1084.538 \text{ MHz}$ is smaller than $\Delta E_{01}(\text{HCOOH}\dots\text{CBU}) = 1122.756 \text{ MHz}$, due to the higher reduced mass of the moieties' motion in $\text{DCOOH}\dots\text{CBU}$. However, unexpectedly, $\Delta E_{01}(\text{HCOOD}\dots\text{CBU}) = 1180.282 \text{ MHz}$ is larger than the value of the parent species. This is probably related to the Ubbelohde effect, that is the change of the distance between the two monomers upon H \rightarrow D substitution. For this reason, only the former two ΔE_{01} values were used to model the potential energy surface of the intermolecular motion. According to the symmetry between the two minima, the large amplitude motion should be depicted by variation of the dihedral angle C7O6-O2C1 (τ), and the B_2 barrier is a function of τ . The transition state is consistent with $\tau = 0$ where all the heavy atoms of the framework lie in the same plane. The other structural parameters should change with the variation of τ , which could also affect the reduced mass of the motion. As the depiction of *ab initio* calculation, the double minimum potential can be described by the following function:

$$V(\tau) = B_2 [1 - (\tau/\tau_0)^2]^2 \quad (4.2.3)$$

where the value of barrier B_2 is at $\tau = 0^\circ$ and the equilibrium value is at the inversion angle τ_0 (see Figure 4.2.2). Limited by only two sets of experimental data, τ_0 was fixed at its B3LYP-D3/6-311++G(d,p) value (29.7°). Guided by the theoretical structures, four structural parameters as a

function of the dihedral angle τ have been accounted as listed below (see the labels in Figure 4.2.1):

$$\angle C8C7-O6O2/^{\circ} = 12.0 \cdot (\tau/\tau_0) \quad (4.2.4)$$

$$\angle O6O2-C1O3/^{\circ} = -2.2 \cdot (\tau/\tau_0) \quad (4.2.5)$$

$$\angle C7O6O2/^{\circ} = 126.7 - 3 \cdot (\tau/\tau_0)^2 \quad (4.2.6)$$

The outputs of the flexible model calculations are summarized in table 4.2.4. By modifying the relaxation parameter of the O6O2-C1O3 dihedral angle at τ_0 point from -2.2° to $+10^{\circ}$, both the energy splittings $\Delta E_{01}(\text{DCOOH}\dots\text{CBU})$ and $\Delta E_{01}(\text{HCOOH}\dots\text{CBU})$ can be reproduced within few MHz deviations. The value $(+10^{\circ})$ $\angle O6O2-C1O3$ suggests that the tunneling is due to an asymmetric butterfly motion of the two moieties with respect to each other. In addition, the potential function model with the satisfactorily reproduced energy splittings decided a barrier $B_2 \sim 39.7 \text{ cm}^{-1}$.

Table 4.2.4. Results of the flexible model calculations.

Tunneling splittings		
	Obs.	Calc.
$\Delta E_{01}(\text{HCOOH}\dots\text{CBU})/\text{MHz}$	1122.8	1119.8
$\Delta E_{01}(\text{DCOOH}\dots\text{CBU})/\text{MHz}$	1084.5	1079.6
Potential energy parameters		
$B_2 = 39.7(5) \text{ cm}^{-1}$	$\tau_0 = 29.7^\circ$	
Structural relaxation parameters		
$\angle\text{C8C7-O6O2}/^\circ = 12.0 \cdot (\tau/\tau_0)$		
$\angle\text{O6O2-C1O3}/^\circ = 10(1) \cdot (\tau/\tau_0)$		
$\angle\text{C7O6O2}/^\circ = 126.7 - 3.0 \cdot (\tau/\tau_0)^2$		

In the flexible model calculations, the τ coordinate has been probed within the $\pm 60^{\circ}$ range and solved into 41 mesh points. For the HCOOD...CBU isotopologue, a barrier of $\sim 1 \text{ cm}^{-1}$ lower than parent species can reproduce the ΔE_{01} splitting adhering to the parametrization used for the other two isotopologues.

4.2.5. dissociation energy

The intermolecular stretching motion which leads to the dimer dissociation is almost parallel to the a -axis of the complex. In this case, a pseudo diatomic approximation can be used to roughly estimate the force constant of the stretching mode leading to the dissociation employing the equation:^[108]

$$k_s = 16\pi^4 (\mu_D R_{CM})^2 [4B^4 + 4C^4 - (B-C)^2 \times (B+C)^2] / (hD_I) \quad (4.2.7)$$

where μ_D is the pseudo-diatomic reduced mass, R_{CM} ($= 3.89 \text{ \AA}$) is the distance between the centers of mass of the two subunits, and B , C and D_J are the spectroscopic parameters of table 4.2.2. We obtained $k_s = 7.3 \text{ N m}^{-1}$, corresponding to a harmonic stretch fundamental $\nu = 67 \text{ cm}^{-1}$. Assuming a Lennard-Jones type potential the zero-point dissociation energy of the complex is estimated to be 9.7 kJ/mol by applying the approximate expression:^[109]

$$E_B = k_s R_{CM}^2 / 72 \quad (4.2.8)$$

Such a value should be underestimated, because the butterfly motion implies that the D_J parameter includes the contributions from other vibrational motions besides the co-linear stretching motion with a axis. The theoretical calculations at MP2/6-311++G** and B3LYP/6-311++G**-D3 levels indicate the values to be 40.7 and 47.9 kJ/mol, respectively, which supports our thought.

4.2.6. Conclusion

In conclusion, all the rotational spectra for three isotopologues of FA...CBU display the splitting patterns, which allows to describe the inversion pathway and to determine the potential energy surface along the C7O6-O2C1 dihedral angle variation. This is the first time that the large tunneling splitting in the rotational spectrum of a hetero-dimer involving a relative motion between two large molecules has been quantitatively characterized. The two subunits are linked through a conventional O-H...O hydrogen bond, which acts as a fulcrum for a butterfly-like motion that the O3 oxygen alternately bond with H15 or H16 through the C-H...O weak hydrogen bond, corresponding to the two equivalent minima.

4.3. The dimer of Indan-CHF₃

4.3.1. Introduction

As a proton donor in weak hydrogen bonds (WHBs), the C–H group recently attracted a lot of attentions. X-rays investigations showed its same directional properties as the “classical” hydrogen bond (HB).^[114] Plenty of information on WHBs has been obtained with IR spectroscopy^[115]. In addition, microwave (MW) spectra of complexes in supersonic jets have provided precise information on the energies, structures and dynamics of such kinds of interaction.^[116] Due to the high withdrawing effect of the fluorine atoms on the electronic density, CHF₃ has a quite acidic hydrogen atom and can represent a prototype proton donor to study and characterize WHB in molecular complexes. Indeed, the C-H...O, C-H...F-C, C-H...N, C-H...S and C-H... π linkages of the complexes of CHF₃ with several organic molecules have been characterized by the rotational spectra.^[117–125] More interestingly, the internal rotation of CHF₃ around its C₃ symmetry axis can split each rotational transition into two components. This unique feature of the rotational spectra can provide the information of the internal dynamics. Large splittings have been observed in the case of Ar-CHF₃,^[126] while small splittings have been found for the complexes of HCF₃ with CH₃F,^[120] C₂H₄O,^[121] thiirane^[122] and pyridine.^[123] In complexes of CHF₃ with heavier molecules, such as cyclobutanone^[124] and 1,4-dioxane,^[125] the V_3 barrier was too high to observe the tunneling splittings. In addition, The rotational study of benzene-CHF₃,^[118] CHF₃-NH₃^[117] and quinuclidine-CHF₃^[119] indicated that the dimers are symmetric rotors with the two subunits can freely rotate with respect to each other. In this case, the transition frequencies are a direct function of the rotational constant B , the centrifugal distortion parameters, and the quantum numbers J , K and m (the torsional quantum number). In this work, we are interested to investigate the behaviour of CHF₃ when forming a complex with a molecule in which a cyclopentene ring is condensed to the benzene ring: indan.

4.3.2. Computational and experimental methods

As described in the paragraph on the indan monomer, indan is characterized by several large amplitude motions,^[127] such as the ring puckering of the CH₂ apex opposite to the benzene ring, the butterfly motion of the two rings with respect to each other, and the twisting of the two methylenic groups attached to the benzene ring. The potential energy function of the ring puckering showed two energy minima with the ring puckering angle at $\tau_0 = \pm 35^\circ$. So for the adduct indan-CHF₃, two conformers are expected, which differ from the entgegen (E) or zusammen (Z) position of the CHF₃

subunit with respect to the CH₂ apex, both showing a C_s symmetry (as shown in Figure 4.3.1). The full geometry optimizations were carried out at the MP2/6-311++G** level of theory using the GAUSSIAN 09 suite of programs. All energies have been corrected for basis set superposition error (BSSE) using the counterpoise procedure.^[106] The relative energies and the spectroscopic parameters are listed in table 4.3.1. Conformation Z (left) is more stable probably due to the interactions of the fluorine atoms with hydrogens of the cyclopentene ring.

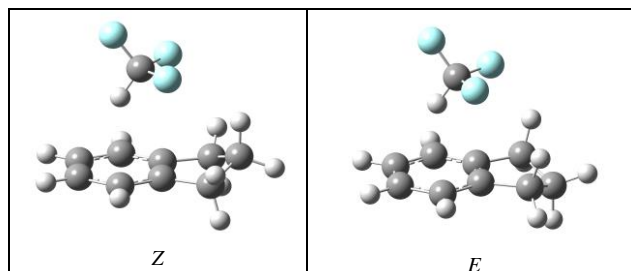


Figure 4.3.1. Z and E conformations of indan-CHF₃.

Table 4.3.1. *Ab initio* (MP2/6-311++G**) spectroscopic parameters for indan-CHF₃

	Z	E
$\Delta E/\text{kJ}\cdot\text{mol}^{-1}$	0 ^[a]	0.99
$\Delta E_{\text{ZPE}}/\text{kJ}\cdot\text{mol}^{-1}$	0 ^[b]	0.94
$\Delta E_{\text{BSSE}}/\text{kJ}\cdot\text{mol}^{-1}$	0 ^[c]	0.24
$E_{\text{D(ZPE+BSSE)}}/\text{kJ}\cdot\text{mol}^{-1}$	11.7 ^[d]	11.4
A/MHz	937.8	964.1
B/MHz	673.9	633.8
C/MHz	545.8	527.0
μ_a/D	2.14	2.06
μ_b/D	0.61	0.79

[a] Absolute energy $E = -685.636923 \text{ E}_h$. [b] Absolute energy $E = -685.445575 \text{ E}_h$. [c] Absolute energy $E = -685.630552 \text{ E}_h$. [d] Dissociation energy, including zero point (ZPE, harmonic approximation) and basis set superposition error (BSSE) corrections.

Commercial samples of Indan, CHF₃ and CDF₃ (Aldrich) have been used without further purification. The rotational spectra in the 6-18.5 GHz frequency region was measured using the PJ-FTMW spectrometer. A gas mixture of ~ 0.5% of CHF₃ in He at a stagnation pressure of ca. 0.2 MPa was flowed over liquid indan at 323 K.

4.3.3. Rotational spectra

Guided by the theoretical prediction of the rotational constants and the large value of the μ_a dipole moment component, the μ_a -type transitions were assigned first. Finally, eight μ_a -type *R* bands with *J* in the range from 5 to 12 and with *K*₋₁ ranging from 0 to 6 have been identified. Then, relatively weaker μ_b -type transitions were measured. Watson's Hamiltonian in the *I'* representation and the *S* reduction have been chosen to fit all the transitions. The fitted spectroscopic parameters

are reported in the left column of table 4.3.2. As an example, a portion of the spectrum with two nearby transitions: $8_{08}-7_{07}$ and $8_{18}-7_{07}$, respectively, is shown in Figure 4.3.2. Their intensity ratio supplies the ratio of the electric dipole moment components $\mu_a/\mu_b \cong 3.8(5)$, which is in good agreement with the theoretical value of *Z* type geometry (3.5) and not with that of the *E* geometry (2.6).

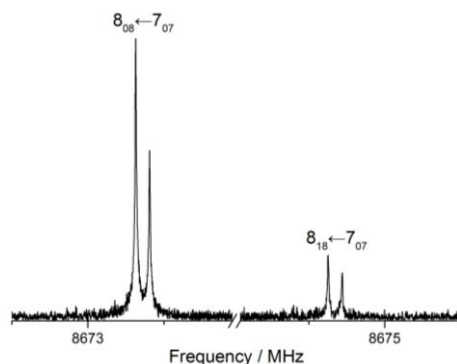


Figure 4.3.2. Nearby μ_a $8_{0,8}-7_{0,7}$ and μ_b $8_{1,8}-7_{0,7}$ transitions of indan-CDF₃, recorded at the $\pi/2$ power conditions. The intensity ratio is in agreement with the μ_a/μ_b ratio of the theoretical values of the electric dipole moment components.

Table 4.3.2. Experimental spectroscopic constants of indan-CHF₃ (*S*-reduction, *F* representation).

	indan-CHF ₃	indan-CDF ₃
<i>A</i> /MHz	940.9516(3) ^[a]	940.0022(8)
<i>B</i> /MHz	648.7726(2)	648.2286(6)
<i>C</i> /MHz	528.7273(1)	528.0866(4)
<i>D_J</i> /kHz	0.1807(6)	0.180(2)
<i>D_{JK}</i> /kHz	0.464(5)	0.450(1)
<i>D_K</i> /kHz	-0.598(6)	-0.579(1)
<i>d₁</i> /kHz	-0.0363(4)	-0.037(2)
<i>d₂</i> /kHz	-0.0046(3)	-0.0044(8)
$\sigma^{[b]}$ /kHz	1.7	1.3
<i>N</i> ^[c]	105	45

[a] Errors in parenthesis are expressed in units of the last digit. [b] Standard deviation of the fit. [c] Number of fitted transitions.

After the assignment of indan-CHF₃, we then measured and identified the rotational spectrum of the indan-CDF₃ isotopologue. The spectroscopic parameters fitted by same Hamiltonian as above are reported in the right column of table 4.3.2. All measured frequencies are listed in appendix VI.

The rotational constants extrapolated from the observed spectrum corresponds to that of conformer *Z*, and appear 3-4% lower than *B* and *C* rotational constants calculated from the *ab initio* applying the experimental-to *ab initio* corrections. Such decrements have already been observed in a similar cage adduct, dioxane-CHF₃.^[125] The results showed ~4% and ~3%, respectively, decrease in going from *ab initio* values (661 and 624 MHz, respectively) to the experimental values of *B* and

C (634.221 and 602.787 MHz, respectively, Ref. [12]). Additionally, there were no splittings due to the internal rotation of the CF₃ group displaying on our spectra, which implies V_3 exceeds 50 cm⁻¹.

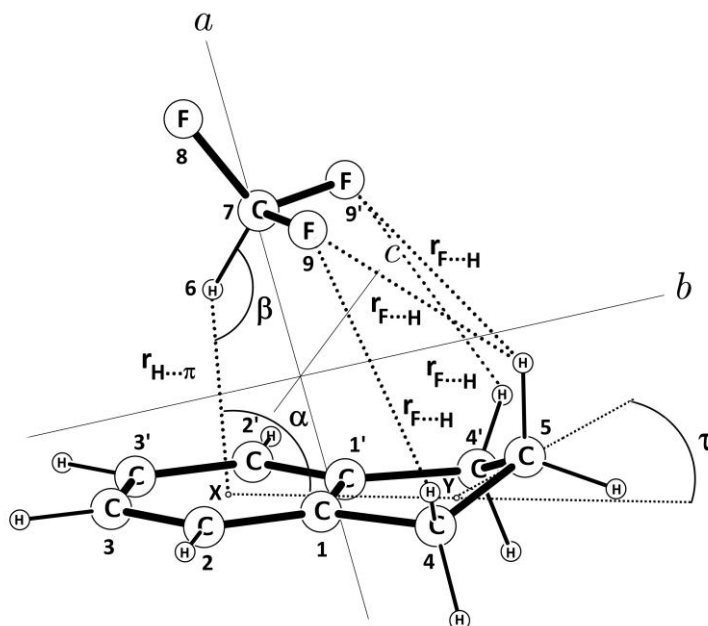


Figure 4.3.3. Configuration, principal axes, main parameters and atom numbering of the most stable conformer of indan-CHF₃

4.3.4. Structure information

The geometry of conformer Z is shown in Figure 4.3.3. The principal axes system, the atom labels and the intermolecular interactions between two monomers have also been marked. In order to easily describe the parameters, we have introduced two points X and Y. There, X and Y are the intermediate points between the carbon atoms C2 and C2', and the carbon atoms C4 and C4', respectively. The geometry parameters of the main framework are listed in table 4.3.3. The experimental rotational constants have been reproduced within 0.5 MHz by slightly increasing XH6 (from 2.317 to 2.39 Å) and α (from 90.8° to 91.8°) of the *ab initio* structure, as shown in table 4.3.3. X is roughly the center of the benzene ring, so the H6...X distance can be regarded as the H... π “bond length”. The complex is bonded by, besides the H... π , another four CF...HC weak HBs. The F...H distances and the C-H...F angles have been derived from the r_0 structure, and their values are given at the bottom of the table 4.3.3.

Table 4.3.3. MP2/6-311++G** geometry of the heavy frame and of the Hbond parameters of indan-CHF₃.

bond lengths/Å		angles/°	
C1C1'	1.406	C1'C1C2	120.5
C1C2	1.399	C1C2C3	119.0
C2C3	1.403	C1'C1C4	110.1
C3C3'	1.401	τ	31.6
C1C4	1.512	α	91.8(6) ^[a]
YC5	0.944	β	146.7

XH6	2.39(1) ^[a]	H6C7F8	110.9
H6C7	1.085	H6C7F9	110.7
C7F8	1.340	XH6C7F8	180.0
C7F9	1.342	H6C7F8F9	120.1
Derived (r_0) WHB parameters			
F9...H _{C4}	3.307	C4HF9	100.3
F9...H _{C5}	3.045	C5HF9	125.7

[a] Error in parentheses in units of the last digit. The *ab initio* values of the two fitted parameters are 2.317 Å and 90.8°, respectively.

Generally, from the rotational constants of isotopologues the substituted coordinates can be obtained. However, in this work, the determined rotational constants of the indan-CDF₃ species are not suitable to indicate the location of the CHF₃ hydrogen atom. As a result of the reverse Ubbelohde effect involved in the C–H... π WHB. The normal Ubbelohde effect is the phenomenon in which the distance between the two constituent subunits increases of a few mÅ upon deuteration. It happens apparently when a double equivalent minima potential is associated with the double proton transfer such as for the carboxylic acid dimer.^[128] However, when it comes to the case of a single HB O–H...O or a single WHB C–H... π between CHF₃ and benzene, the reverse Ubbelohde effect takes place.^[129] This effect evokes a decrease in the distance between the two monomers upon H→D substitution.^[128,129] Such effect can induce quantitatively similar changes in the moments of inertia as those due to the isotopic substitution. Therefore, Kraitchman's substituted coordinates cannot be obtained when the Ubbelohde effect occurs

However, in turn, from the rotational constants of the isotopologues, the Ubbelohde effect can be sized. First of all, to quantify the Ubbelohde effect, P_{aa} planar moments of inertia (defined as $P_{aa} = \sum_i m_i a_i^2$), which means the mass extension along the a -axis are necessary. These values can be easily obtained from the rotational constants through the relation:

$$P_{aa} = h/[(16\pi^2)(-1/A+1/B+1/C)] \quad (4.3.1)$$

The P_{aa} difference (ΔP_{aa}) between experimental and calculated value is 0.636 uÅ² for the parent species while the difference is 1.439 uÅ² for the D6 deuterated species. The calculated values are obtained from the model structure. This discrepancy of the ΔP_{aa} of the two isotopologues is due to the reverse Ubbelohde effect as mentioned above. This discrepancy can be offset by changing the distance between the two centers of mass of the two subunits -2.5 mÅ upon H→D substitution. Such a shrinkage is smaller than that obtained in benzene-CHF₃, which is 4.4 mÅ.^[5] Additionally both of them, involving the C–H... π bond, are smaller than the shrinkage in the OH...O bond, which is observed in dimers of alcohols, and in adducts of alcohols with ethers ($\Delta r = 5$ -7 mÅ).^[129]

In the case of the indan-CHF₃ complex the stretching motion which can induce the complex's

dissociation is almost parallel to the a -axis. This allows us to estimate the stretching force constant (k_s) by using the approximated equation:

$$k_s = 16\pi^4(\mu_A R_{CM})^2 [4B_A^4 + 4C_A^4 - (B_A - C_A)^2(B_A + C_A)^2] / (hD_J) \quad (4.3.2)$$

where the suffix A is for “Adduct” and μ_A , R_{CM} , B/C and D_J are the reduced mass, the distance between the centers of mass, the rotational constants and the first order centrifugal distortion constant, respectively. The value of R_{CM} , calculated from the fitted geometry, is 3.59 Å. Substituting the spectroscopic parameters into Eq. (1), the resolution gives a value $k_s = 9.6 \text{ N}\cdot\text{m}^{-1}$, corresponding to a harmonic stretching frequency of 61 cm^{-1} . The dissociation energy (E_D) has been evaluated to be 11.2 kJ mol^{-1} by assuming a Lennard-Jones potential function, according to $E_D = 1/72 k_s R_{CM}^2$. E_D is in good agreement with the *ab initio* value, once that the BSSE corrections have been introduced (see table 4.3.1). As expected, the dissociation energy is stronger than in benzene-CHF₃, contributed by the adjuvant four C-H...F WHBs.

It is worth noting that conformer *E* is slightly higher in energy than the *Z* one. Its spectrum ought to be observed. However, the barrier of the conformational interconversion (ring-puckering barrier) between *E* and *Z* is smaller than $2kT$, it is plausible that a conformational relaxation to the most stable conformer takes place upon supersonic expansion.

In table 4.3.4, we have compared the interactions in the complexes of CHF₃ with different partners. It appears that among the various kinds of WHB, C-H... π and C-H...N are stronger than C-H...S, C-H...O, and C-H...F. In addition, multiple WHB contacts involving the F atoms of the rotor CHF₃ can raise the barrier of the internal motion.

Table 4.3.4. Experimental values of the dissociation energy (E_D), barrier to internal rotation of the CF₃ group (V_3 or V_6 , depending on the symmetry of the complex) and number of WHBs for the complexes of CHF₃ with several organic molecules.

partner molecule	E_D (kJ/mol)	WHBs	Barrier (kJ/mol)	Ref.
Benzene	8.4	CH... π	$V_6 = 0$	[5]
Quinuclidine	10.2	CH...N	$V_6 = 0$	[6]
CH ₃ F	5.3	3*CH...F	$V_3 = 0.84$	[7]
Oxirane	6.7	CH...O, 2*CH...F	$V_3 = 0.55$	[8]
Thiirane	9.8	CH...S, 2*CH...F	$V_3 = 0.53$	[9]
Pyridine	11.4	CH...N, CH...F	$V_3 = 0.57$	[10]
Cyclobutanone	7.5	CH...O, 2*CH...F	$V_3 > 0.70^{[a]}$	[11]
1,4 dioxane	6.8	CH...O, 2*CH...F	$V_3 > 0.70^{[a]}$	[12]
Indan	11.2	CH... π , 4*CH...F	$V_3 > 0.70^{[a]}$	This work

[a] Splittings due to the internal rotation not resolved.

4.3.5. Conclusion

We assigned the rotational spectra of indan-CHF₃ and indan-CDF₃. The complex presents a

cage structure where the two moieties are held together by one $\text{CH}\cdots\pi$ and four $\text{CH}\cdots\text{F}$. The adjuvant four $\text{C-H}\cdots\text{F}$ WHBs can fix the free rotor CHF_3 on the π cloud, and strengthen the binding energy between the two subunits. As observed in previous work, the reverse Ubbelohde effect takes place upon $\text{H}\rightarrow\text{D}$ substitution in the $\text{CH}\cdots\pi$ bond. However, due to the cooperative effect of the multiple WHB again, this kind effect is much smaller than that in complex Benzene- CHF_3 .

4.4. $[\text{CH}_2\text{F}_2]_n \cdots [\text{H}_2\text{O}]_m$ trimers and tetramers

4.4.1. Introduction

Thanks to the development of the techniques over the decades, nowadays we can spectroscopically characterize the weakly bound complexes such as the oligomers held by WHB. In this work, the complex network held together by different classes of HBs have been investigated using CP-FTMW, revealing for the first time the existence of stable heterotrimers and heterotetramers of difluoromethane (D) with water (W). Besides their importance in critical processes as atmospheric ozone depletion, freons are molecular species of fundamental interest in the context of WHB frameworks. In 1999, Caminati *et al.* firstly investigated the interaction between water with Freon 32 (CH_2F_2) using the Stark and pulse modulated free jet absorption millimeter-wave spectrometer,^[130-132] and observed a set of evenly spaced line, which were finally assigned to the spectrum of CH_2F_2 dimer.^[133] In CH_2F_2 -water dimer the O-H group acts as strong donor and F as weak acceptor while in DFM_2 the C-H and C-F groups can act as weak HB donor and weak acceptors respectively. Since that, a gate has been opened for the rotational study of the Freon clusters. After 8 years the CH_2F_2 trimer was characterized by PJ-FTMW spectrometer,^[134] and another 7 years later the rotational spectra.^[135] of the tetramer was recorded. Now we extend the study to the heterotrimer and heterotetramer of CH_2F_2 with water. Considering the chemical structure of both H_2O and CH_2F_2 molecules, the combination of them can assemble a big family of HBs, ranging from medium ($\text{OH} \cdots \text{O}$) HBs between two water molecules, to WHB's of different types as medium donor – weak acceptor ($\text{O-H} \cdots \text{F}$), weak donor – medium acceptor ($\text{C-H} \cdots \text{O}$) and the most elusive yet efficient, weak donor - weak acceptor ($\text{C-H} \cdots \text{F}$). Such complexes should be characterized by a subtle interplay of all the aforementioned contributions, and could yield a wealth of structural and dynamical information, allowing for a further step in the comprehension of WHBs.

4.4.2. Computational and experimental methods

All calculations were performed with the Gaussian09 software package. A statistical method complemented with density functional theory (DFT) approach has been proposed and successfully applied for the identification of DFM dimer, trimers and tetramers.^[135,136] The results, obtained with the dispersion corrected functional B97D functional,^[137] were found in good agreement with both experimental data and, as far as the dimer and the trimer are concerned, with QM predictions previously^[133,134] obtained with MP2 theory. So DFT optimizations were performed with the B97D dispersion corrected functional,^[137] with both *aug-cc-pvDz* and *aug-pv-ccTz* basis sets. For all

calculations, the binding energies were computed taking care of the basis set superposition error though the standard Counterpoise correction.^[106]

The first step of the present approach concerned finding the most stable conformers for the two possible hetero-trimers and one hetero-tetramer, namely $[\text{CH}_2\text{F}_2]_2\text{H}_2\text{O}$ (D2W), $\text{CH}_2\text{F}_2[\text{H}_2\text{O}]_2$ (DW2), and $[\text{CH}_2\text{F}_2]_2[\text{H}_2\text{O}]_2$ (D2W2), respectively. However, it is well known that the choice of both DFT functional and the dispersion correction scheme is crucial to the accuracy of the results, and may significantly depend on the investigated system, especially when WHBs are involved.^[138] For these reasons, only a first screening was performed at B97D level, and the resulting optimized geometries were then refined at MP2 level with the 6-311++G** basis set. In fact, besides the good agreement found with DFT for the aforementioned DFM clusters, MP2 was successfully applied in several works to describe WHBs,^[79] and in particular the DFM-W interaction.^[130-132] The whole screening protocol, essentially based on a series of QM geometry optimizations, successively performed at different levels of theory, is described in detail in the appendix. The structures optimizations calculation parameters are listed in appendix. VII.

The MW spectra of parent species were performed in Pate's group at the University of Virginia using a CP-FTMW spectrometer^[10] which covers the frequency ranges 2–8 and 6–18 GHz.^[139] The DFM sample was obtained from Sigma Aldrich. The spectrometer has 5-nozzle sample injection system which reduces the measurement time and sample consumption required to reach a given target sensitivity. The chirped pulse is generated by a 24 GHz sample rate arbitrary wave generator (Tektronix AWG 7122B) and amplified by a 300 W peak power pulsed traveling wave tube amplifier (Applied System Engineering 167X/KU). The bandwidth of the wave generator (2–8 GHz) can be extended using a pulse generation circuit to create microwave output in the 6–18 GHz range. The measurements use a 4 μs duration chirped pulse with a linear frequency sweep from 2 to 8 GHz or a 2 μs duration pulse from 6 to 18 GHz. After sample excitation, the coherent broadband emission of the free induction decay (FID) is amplified using a high-gain, low-noise MW amplifier and recorded using a 100 $\text{Gs}\cdot\text{s}^{-1}$ digital oscilloscope (Tektronix DPO 73304D). The FID is collected for 40 μs in the 2–8 GHz range at a sampling rate of 25 GHz or 20 μs for 6–18 GHz at a sampling rate of 50 GHz. A gas sample injection repetition rate of 3.3 Hz is achieved, with 26.4 or 33 Hz FID signal averaging in the 2–8 or 6–18 GHz ranges, respectively. The frequency domain spectrum is obtained from this averaged FID by fast Fourier transformation following the application of a Kaiser-Bessel window function to improve baseline resolution. A gas mixture of 1% CH_2F_2 in Ne at a backing pressure of 350 kPa passed through a container with water and then was expanded into the spectrometer.

CH_2F_2 with deuterated species were measure in Cocinero's group at the University of the

Basque country. The details of the CP-FTMW spectrometer of Cocinero's group was described in Chapter II.^[15] The D₂O was purchased from Sigma Aldrich and DOH was achieved by mixing D₂O and H₂O with 1:1 ratio. A gas mixture of 1% DFM in He with a stagnant pressure 300 kPa was expanded into the cavity after passing over the water reservoir.

4.4.3. Rotational spectra

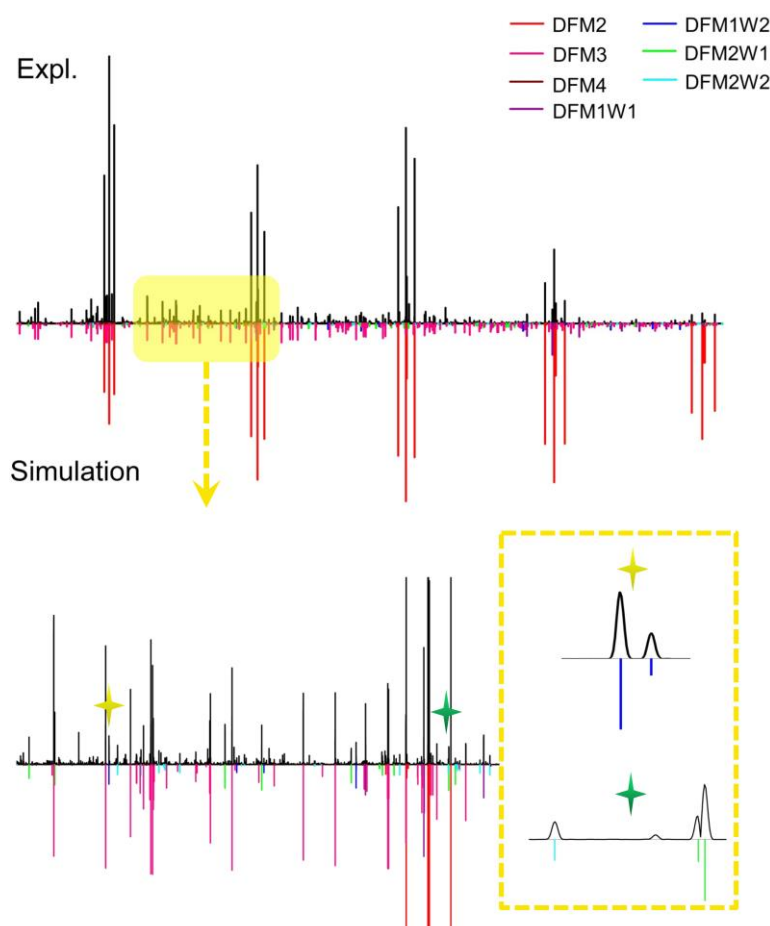


Figure 4.4.1. The black trace shows the CP-FTMW spectrum in the 6-18 GHz frequency region. The colored traces are the simulations of observed clusters.

One portion of the broadband rotational spectrum is shown in Figure 4.4.1. After removing the transition frequencies of (CH₂F₂)₂, (CH₂F₂)₃, (CH₂F₂)₄, and CH₂F₂-W from the whole spectrum, which were already assigned in previous works, one set of transitions for each oligomer, DW2, D2W, and D2W2, respectively, has been successfully assigned based on the corresponding predictions. Among them, 50 spectral lines with splitting pattern were inferred to the μ_a -R type transitions (J_{upper} from 1 to 6) of DW2 with the configuration as shown in Figure 4.4.2. No lines belong to b and c type transition can be found in the spectra. This is in agreement with the conformer we assigned which is with negligible dipole moments of μ_b and μ_c (see in table 4.4.1 and

A7.1). 114 μ_a -R and 16 μ_b -R type transitions with splitting were assigned to D2W complex. In addition, one set of lines with 77 μ_a -R type, 37 μ_b type and 48 μ_c type transitions was assigned for D2W2 cluster. All the rotational frequencies were fitted with Watson's Hamiltonian (I' -representation, S -reduction) using Pickett's SPFIT program and the results of the fits are listed in table 4.4.1 and appendix VII. From the fitted rotational constants and dipole moments patterns one can easily identify the experimental conformers among the stable structures in the theoretical potential surface for DW2 and D2W2. All the possible conformers are shown in the appendix VII and the assigned conformers are listed in Figure 4.4.2. However, it is difficult to try to understand which structure the spectrum originates as from the calculation results on D2W, because two possible conformers with quite close rotational constants are found. One possesses C_s symmetry with moieties CH_2 , CF_2 and whole H_2O on the symmetry plane, while another one belongs to the C_1 symmetry group (as see in appendix VII). Therefore, it is necessary to observe the rotational spectra of isotopologues to discriminate between the two isomers. For this reason, we proceeded to measure the rotational spectra of the previous clusters with deuterated water using the CP-FTMW spectrometer in the 6-18 GHz frequency range. To further confirm our assignment and locate the hydrogen atom of the water, we then performed the experiment by replacing water with a mixture of normal and deuterated water, where H_2O , D_2O and HOD can exist simultaneously in the spectrum. Therefore, there are totally $2n$ (n is the number of the hydrogen atoms of water) isotopologues for each conformer. Finally, we identified all the isotopologues for D2W, 11 isotopologues for DW2 and 7 isotopologues for D2W2. It is acceptable for the missing of some isotopologues due to the relative low population for each isotopologue and the vibrational relaxation from some of them to the others with lower zero-point energy. The latter effect has been found in the microwave investigation of DFM-W dimer, where the DFM-HOD (the primed H participates in the hydrogen bond) was not observed in the microwave spectrum, and this is related to the relaxation to DFM-DOH during the supersonic expansion.^[130,131] It should be noted that in this work some isotopologues with -HOD have been identified.

Table 4.4.1: Binding energies (BE), rotational constants (A, B and C) and electric dipole components (μ_A , μ_B , μ_C), computed for the structures of the $\text{CH}_2\text{F}_2[\text{H}_2\text{O}]_2$ (DW2) and $[\text{CH}_2\text{F}_2]_2\text{H}_2\text{O}$ (D2W) trimers shown in Figure 4.4.2.

	DW2			D2W			D2W2	
	Calc.	Expl.		Calc.	Expl.		Calc.	Expl.
		$\nu=0$	$\nu=1$		$\nu=0$	$\nu=1$		
A/MHz	5560	5249.96(5) ^b		2304	2248.047(7) ^b	2248.194(7)	1774	1759.4167(7)
B/MHz	1736	1729.540(2)	1729.658(2)	1103	1096.505(1)	1096.516(1)	737	763.3094(2)
C/MHz	1339	1316.196(2)	1316.166(2)	874	860.5625(6)	860.5106(7)	700	696.9655(2)
μ_a/D	2.1	Yes		1.6	strong		2.7	Yes

μ_b/D	0.0	No	0.4	weak	0.6	Yes
μ_c/D	0.3	No	0.1	no	1.2	Yes
BE/kJ·mol ⁻¹	-41.7		-28.0		-53.1	

4.4.4. Structure information

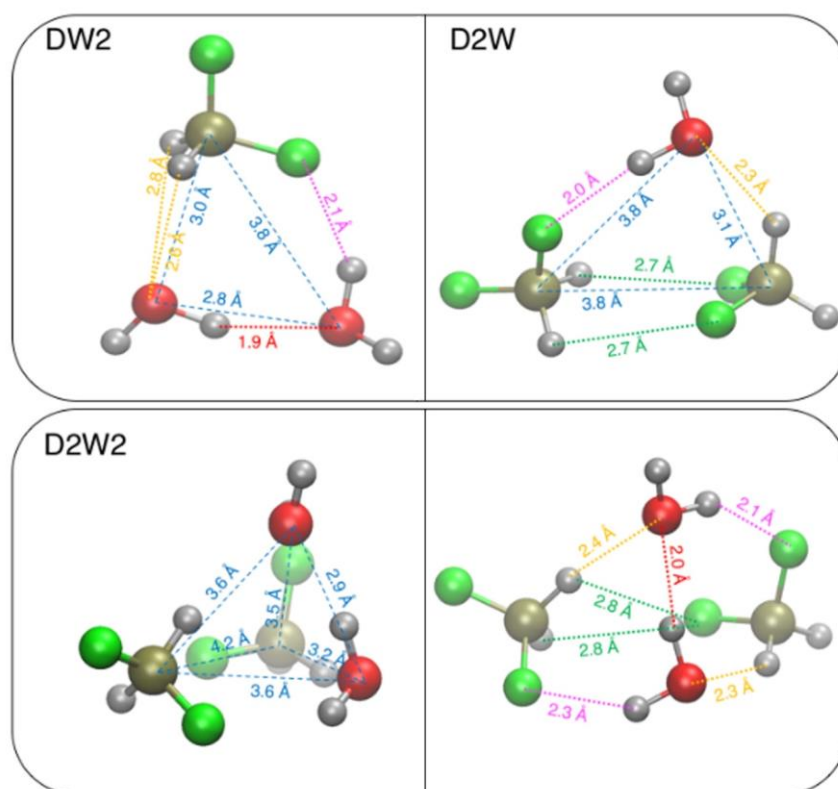


Figure 4.4.2. Upper: Most stable structures for the $\text{CH}_2\text{F}_2 \cdots [\text{H}_2\text{O}]_2$ (DW2, left) and $[\text{CH}_2\text{F}_2]_2 \cdots \text{H}_2\text{O}$ (D2W, right) trimers. Lower: Structures of the $[\text{CH}_2\text{F}_2]_2 \cdots [\text{H}_2\text{O}]_2$ (D2W2) tetramer: side view (left) and top view (right). The $\text{O} \cdots \text{O}$, $\text{C} \cdots \text{O}$ and $\text{C} \cdots \text{C}$ distances that characterize the cluster structure are displayed with blue dashed lines, whereas the different WHB, whose distance is less than 3.0 Å, are evidenced with dotted lines in different colors (OH \cdots O red; O-H \cdots F magenta; C-H \cdots O orange; C-H \cdots F green).

The rotational constants and dipole moments pattern for each complex can provide a strong evidence to discriminate between geometries of the optimized minima and the assigned isomers. Some other methods should be also used to confirm the assignment, especially for D2W, for which is difficult to distinguish between the two conformers C_s and C_1 as shown in Figure A7.4 (Appendix VII) with just rotational constants and dipole moments. There are two evidences for supporting the C_1 structure. The first one is the mass extension along c axis. This information can be obtained from the planar moments of inertia: $P_{cc} = (-I_{cc} + I_{aa} + I_{bb})/2$. For C_s structure the value is 47.88 uÅ², and for C_1 structure it is 49.34 uÅ². The value from the experimental result is 49.2 uÅ² and agrees with the C_1 structure. The second method to identify the geometry is using Kraitchman's equations to calculate the coordinates of the substituted atoms from the isotopic variation of the moments of inertia. The substitution structure, r_s , has an advantage of giving the substituted atom positions in

the principal axes without the information of the assumed structure of the molecular system. But it is worth noting that Kraitchman's method has also some limitations such as bad analysis for the atoms close to principal axes due to the vibrational contribution in the measured rotational constants of the ground state. From the rotational constants of the isotopologues as listed in the appendix VII, Kraitchman's structure related to the hydrogen atoms of the water molecules involved in the oligomers can be obtained, as shown in Figure 4.4.3. One can see that the substituted coordinates match the theoretical structure quite well for DW2. For the other two complexes, the position of one hydrogen was not well located by Kraitchman's coordinates, because, of the limitation of Kraitchman's method related to the internal motion of the water described in the following paragraph. But even the location of only one hydrogen atom by Kraitchman's coordinates for D2W is enough to rule out the C_s conformer. When it comes to D2W2, the substituted positions do not match the configuration with high precision. However, that Kraitchman's position is clear enough to prove that the D2W2 adopts the conformer as we report.

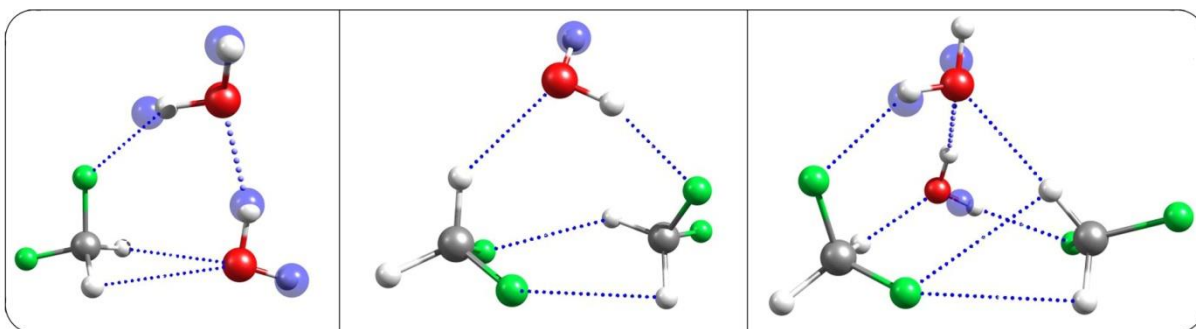


Figure 4.4.3. Determined substitution structures. The full skeletons are from an initio structure, and the blue transparent spheres represent the Kraitchman coordinates.

a) Trimers. From a first visual inspection it is evident that in both trimers a net of four HBs is settled among monomers. In DW2, the strong HB between the two water molecules (1.9 Å, evidenced in red in the left panel of Figure 4.4.2) is the driving force that keeps them at close distance ($R_{O...O} = 2.8$ Å), whereas two WHBs, between two weak C-H donors and a single strong acceptor O (yellow dashed lines), hold the DFM monomer at a rather short distance ($R_{O...C} = 3.0$ Å) with respect to the closest H₂O molecule. Finally, the stability of this cluster is further enforced by a last WHB, which takes place between the strong O-H donor of the second water molecules and the fluorine, as weak acceptor (evidenced with a dashed magenta line in the left panel of Figure 4.4.2). All the HBs make the cluster form a cyclic structure and locate almost all the atoms in one plane except for the two hydrogen atoms of DFM and two free H atoms of the water. The H atoms of DFM are located on two side of the plane symmetrically. The two free hydrogen atoms of water also lie out of the plane with tunneling between both sides.

Previous work on the DFM dimer showed us a C_s symmetric structure which is formed by three $F\cdots H$ non-covalent bonds. When a H_2O molecule is added to the dimer, as in the D2W trimer, it is inserted in the $F\cdots H$ interaction in the C_s symmetric plane. The addition of this water molecule destroys the C_s structure. The assigned and most stable conformer is shown in the right panel of Figure 4.4.2. No strong HB can be formed in this cluster, and the oligomer is mainly kept together by four WHBs. Two of them are of weak-donor/weak-acceptor kind (green lines in Figure 4.4.2) between the two DFM monomers, showing a typical $F\cdots H$ distance of about 2.7 Å. The remaining WHBs involve the $C-H\cdots O$ and $O-H\cdots F$ triads (yellow and magenta lines in right panel of Figure 4.4.2) and result in shorter distances with respect to their DW2 analogues (2.3 Å and 2.0 Å vs. 2.6 Å and 2.1 Å, respectively) indicating that in this case these WHBs are more effective in stabilizing the molecular cluster. It is worth noticing that all HB distances, evidenced with different colors in Figure 4.4.2, agree with previous values found for similar interactions.^[79,130-136]

The binding energy (BE) of both trimers was computed at MP2//6-311++G(d,p) level and reported in table 4.4.1. The comparison between DW2 and D2W BEs reflects the structural parameters commented above: the former trimer is found to be the more stable by almost 14 kJ/mol, due to the settlement of the strong HB between the two H_2O molecules. The computed BEs are consistent with the average values found in literature for each kind of HB involved.^[79,140,141]

b) Tetramer. The computational screening for the most stable $[CH_2F_2]_2[H_2O]_2$ (D2W2) tetramers resulted more difficult, due to the increased complexity of the subtending IPES. Nonetheless, as detailed in the appendix VII, two different quasi degenerate conformers were eventually found, exhibiting rather similar rotational constants but not negligibly different dipole components. Concretely, the first, most stable (BE: ~54 kJ/mol) tetramer showed significant components along both A and B directions (appendix VII), whereas the second D2W2 cluster (reported in table 4.4.1), although slightly less stable (BE: ~53 kJ/mol), is characterized by greater μ_a and μ_c values, in better agreement with the experimental intensities and rotational constants. The structure of this latter tetramer is shown in Figure 4.4.2 in two different views. This cluster is linked together as a cage structure with 7 hydrogen bonds. From the left panel, the tetrahedron-like, 3D structure clearly appears. It is interesting to note as the main distortion with respect to a regular tetrahedron is caused by the short $O\cdots O$ distance (2.9 Å), due to the strong HB between water molecules, and by the elongated $C\cdots C$ distance (4.2 Å) between the two DFM monomers, which still interact through WHB of the $C-H\cdots F$ type (green lines)). As most evident in the left panel, the hard socket is formed by the two strongly bound water molecules which are able to attract the lateral DFMs by means of WHBs, even if a further stability originates from a direct interaction between DFMs. The overall effect of the WHB network, evidenced in the right panel of Figure

4.4.2, is to stabilize the tetrameric structure, favoring it with respect to two separate dimer arrangements. The great stability of the tetramer with respect to fragmentation is confirmed by comparing the total binding energy of 53 kJ/mol, with the result expected for either a water and a DFM dimer or two DFM/W dimers: in the former case the interaction energy by previous findings would be approximatively 33.5 kJ/mol (21 kJ/mol for $[\text{H}_2\text{O}]_2$ + 12.5 kJ/mol for $[\text{CH}_2\text{F}_2]_2$ ^[133,136]), while only 20 kJ/mol (10 kJ/mol for each $\text{CH}_2\text{F}_2 \cdots \text{H}_2\text{O}$ dimer^[130]) should be expected for the latter pair.

Table 4.4.2. The comparison of non-covalent bonds in DFM and water clusters (Å).

	H...F (CH...F)	O...O	C...C	H...F (OH...F)	C...O (CH ₂ ...O)	H...O (CH...O)
D ₂	2.759/2.628 ^{ref133}		3.55			
D ₃	2.476-3.246 ^{ref134}		3.648-3.942			
D ₄	2.541-3.549 ^{ref135}		4.22			
W ₂		2.98(2.92) ^{ref142}				
W ₃		2.88(2.80)				
W ₄		2.81(2.75)				
W ₅		2.76(2.73)				
DW				2.20(1)	2.997/3.040	
DW ₂		2.82		2.07	2.97	
D ₂ W	2.74/2.67		3.81	2.04		2.29
D ₂ W ₂	2.79/2.87	2.88	4.23	2.32/2.08		2.27/2.42

The interactions comparison between different DFM and water clusters is reported in table 4.4.2. One can see that the CH...F bonds in this work are comparable with the bond length of the pure DFM oligomers. The typical hydrogen bond O...O between the water moieties in the hetero-cluster are in agreement with that in the pure water trimer and tetramer. The bond C...C between the DFM units in this work is consistent with that in the pure DFM oligomers, where the bond in D₂W (3.81Å) agrees with the DFM trimer and D₂W₂ (4.23Å) agrees with the DFM tetramer. For the distance of C...O in the interaction of CH₂...O, which is a bifurcated wHB, does not change from DFM-w (3Å) to DFM-W₂ (2.97Å).

4.4.5. Tunneling splitting

As previously reported, the D₂W and DW₂ isomers show splitting for each transition of their spectra. The internal motions which raises these splitting have been interpreted using also the isotopologues spectra.

For D2W isomer, the normal specie shows an intensity ratio of the two component which is about 3:1 and the isotopologues do not show any tunneling splitting. These experimental evidences suggest that splitting originates from the internal motion of water in along its C_2 axis which involves the exchange of two fermion originating a ratio of intensity 3:1.

Instead for DW2 splitting is still present despite the single replacement of hydrogen atoms with deuterium atoms. As highlighted in previous works (water trimer^[143], *tert*-butylalcohol – water^[144]), in this case the splitting is originated from the concerted motion of the hydrogen atoms above and below the plane.

A mathematical model for describing these internal motions is currently in the processing phase. The diagrams showing these two motions are schematically shown in Figure 4.4.4.

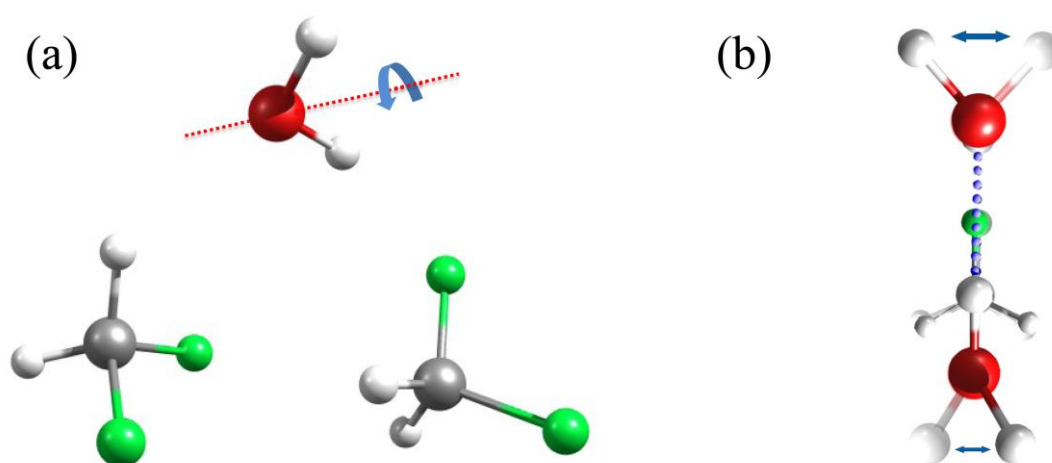


Figure 4.4.4. Internal motions in two trimers: (a) the internal motion of water along its C_2 axis in DFM2W; (b) the hydrogen atoms flipping motion in DFMW2.

4.4.6. Conclusion

In summary, I report the rotational spectra of $(DFM)_m-(W)_n$ clusters ($m, n = 1, 2$) and their isotopologues. The isomers in the supersonic expansion have been assigned by their rotational spectra. This work can broaden our knowledge about the cluster formed by the cooperation of the weak/medium hydrogen bonds.

Chapter V

Pre-reactivity and reactivity between gaseous carboxylic acids and alcohols

In order to understand the nature of the non-covalent interactions and to have information on the internal dynamics and on the conformational equilibria, a lot of molecular complexes involving carboxylic acids^[80-104,145,146] have been investigated by rotational spectroscopy. However, no literature about MW studies of complexes between carboxylic acids and alcohols are reported. As we know, when the carboxylic acid is treated with the alcohol, the ester can be formed. This reaction is called esterification, which is one of the most important reactions in organic synthesis. To produce ester in 100% yield from the condensation between the carboxylic acid and the alcohol is the ultimate goal of the organic and industrial chemist. The rate and the extent of the equilibrium of the esterification are dependent on the structure of the molecules and the types of the functional substituents of the alcohols and acids.^[147] Understanding the esterification mechanism on the molecular level will help the people to reach the ultimate goal. Therefore, I thought to try to investigate the prototype of this kind of complexes between carboxylic acids and alcohols.

I have investigated the rotational spectra of formic acid with a series of primary, secondary and tertiary alcohols. In the experiments all samples were obtained from Aldrich and used without further purification. The rotational spectra in the 6-18.5 GHz frequency region were measured with PJ-FTMW spectrometer (as described in Chapter II). For each measurement, the samples of carboxylic acid and alcohol were filled in separated containers. Helium at a total pressure of 0.3 MPa was streamed over the various samples, in such a way to have ca. 1% concentration of the species of interest in the molecular beam.

In detail, the following systems were studied: $\text{HCOOH-CH}_3\text{OH}$, $\text{HCOOH-C}_2\text{H}_5\text{OH}$, $\text{HCOOH-(CH}_3)_2\text{CHOH}$ and $\text{HCOOH-(CH}_3)_3\text{COH}$. In the experiment of $\text{HCOOH-(CH}_3)_3\text{COH}$, only the spectra of the adducts was observed, while in the other cases only rotational transitions were obtained to belong to the esters. Then I replaced linear alcohols with cyclic alcohols, such as cyclohexanol and 1-methyl-cyclopropanol. The same situations have been found: only the rotational spectrum of the ester was obtained for the secondary alcohol, while for the tertiary alcohol only that of the adduct was obtained. In addition, I performed the experiments by replacing HCOOH with

carboxylic acids with stronger (CF_3COOH) and weaker (pivalic acid) acidity. In the first case I observed only the ester, while in the second case the experiment did not succeed, because pivalic acid was rapidly obstructing the nozzle.

As an analysis example, the case of the mixture of FA with isopropanol is shown in Figure 5.1. In the upper panel, the expected spectrum of the ester is drawn in blue, while the predicted spectrum of the adduct is drawn in red with negative values. From the picture one can see that the transitions for ester and adduct are absolutely separated from each other.

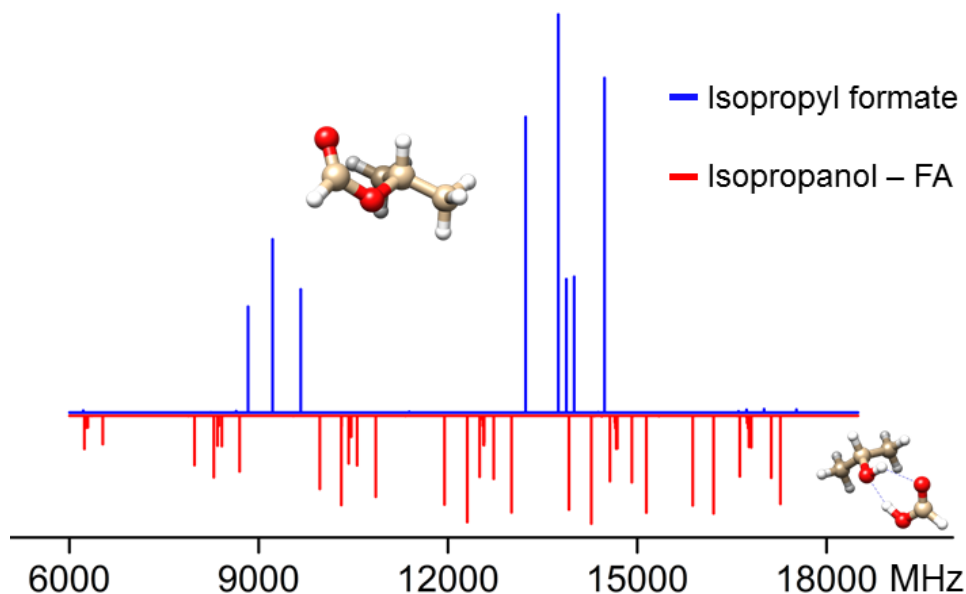


Figure 5.1. Spectra expected for the mixture FA-isopropyl alcohol in the case of esterification (blue, positive values) and of formation of the adduct (red, negative values).

After careful scans, only strong transitions of the ester have been identified in the rotational spectrum, according to the blue spectrum. In the same way, the scans of other alcohols with carboxylic acids were performed. In tables 5.1 and 5.2, the experimental evidences for the observed esters or adducts are summarized, respectively.

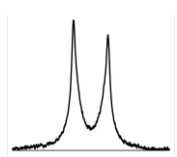
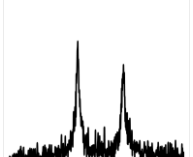
Table 5.1. Details (one transition example) of the spectra of the esters which have been formed in a supersonic expansion of binary mixture of carboxylic acids with primary and secondary alcohols. All spectra cover a range of 0.4 MHz. The central frequency (ν_c) and the number of accumulation cycles (N_c) of each spectrum are given.

$\text{HCOOH} + \text{CH}_3\text{OH} \rightarrow$ Methylformate ^a	$\text{HCOOH} + \text{CH}_3\text{CH}_2\text{OH} \rightarrow$ Ethylformate ^a	$\text{HCOOH} + (\text{CH}_3)_2\text{CHOH} \rightarrow$ Isopropylformate	$\text{HCOOH} + \text{cy-C}_6\text{H}_{11}\text{OH} \rightarrow$ Cyclohexylformate ^e	$\text{CF}_3\text{COOH} + \text{CH}_3\text{OH} \rightarrow$ Trifluoroacetylformate ^e

$4_{13} \leftarrow 4_{14}$ transition of the “E” species. $\nu_c = 16037.30$ MHz; $N_c = 200$.	$2_{02} \leftarrow 1_{01}$ transitions of <i>gauche</i> (upper, ν_c = 14059.25 MHz; $N_c = 1000$) and <i>trans</i> (lower, ν_c = 10962.45 MHz; $N_c = 1000$) conformers	$2_{20} \leftarrow 2_{11}$ transition It is split into two tunneling components. $\nu_c = 11836.55$ MHz; $N_c = 50$.	$7_{07} \leftarrow 6_{06}$ transition. $\nu_c = 12942.45$ MHz; $N_c = 385$.	$5_{05} \leftarrow 4_{04}$ transition. It is split into “A” and “E” component lines due to the internal rotation of the methyl group. $\nu_c = 14036.80$ MHz; $N_c = 50$.
---	---	---	---	---

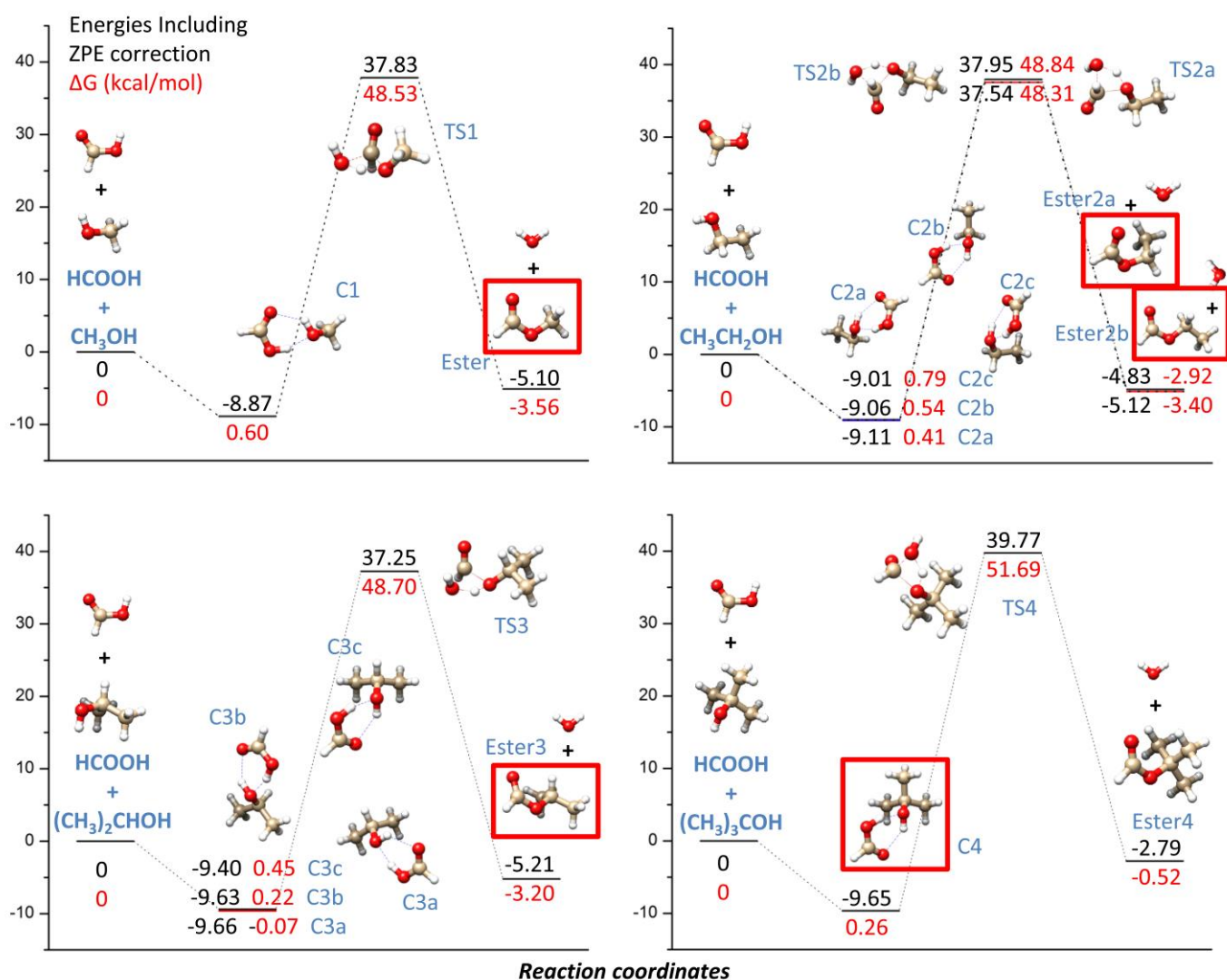
^aThe rotational spectra of methylformate and ethyl formate are available in the literature.^[148,149]

Table 5.2. Details (one transition example) of the spectra of the adducts which have been formed in a supersonic expansion of binary mixture of carboxylic acids with tertiary alcohols. All spectra cover a range of 0.4 MHz. The central frequency (ν_c) and the number of accumulation cycles (N_c) of each spectrum are given.

HCOOH + (CH ₃) ₃ COH → FA-TBA adduct	HCOOH + cy-C ₃ H ₄ CH ₃ OH → adduct
	
$4_{13} \leftarrow 3_{12}$ transition $\nu_c = 7645.00$ MHz; $N_c = 1113$.	$5_{14} \leftarrow 4_{13}$ transition $\nu_c = 8961.95$ MHz; $N_c = 504$.

We tried to interpret the different behavior of tertiary alcohols with chemical dynamics calculations. All calculations have been performed with a locally modified version of the Gaussian suite of programs. The computations were carried out with the double-hybrid B2PLYP functional,^[150-152] where *d*-functions on hydrogens have been removed. Semiempirical dispersion contributions were also included into DFT computations by means of the D3 model of Grimme, leading to B2PLYP-D3 functional.^[153] Full geometry optimizations have been performed for all minima and transition states checking the nature of the obtained structures by diagonalizing their Hessians. In the case of complexes, the basis set superposition error (BSSE) has been corrected using the Counterpoise method.^[152-155]

Energies of complexation and esterification have been obtained for the most significant examples listed above, including zero point corrections and, for the complexes, basis set superposition errors.^[150] In addition, also the free energy changes at 298 K have been evaluated.



Scheme 5.1. Energy profile of the multiple chemical process paths for the FA – methanol, FA – ethanol, FA – isopropanol and FA – *tert*-butyl alcohol mixtures.

The obtained results are shown graphically in Scheme 5.1 for some of the mixtures mentioned above. The starting point, with the acid and alcohol molecules separated from each other, is assumed to be the zero-point energy (of free energy) value. The complete set of data obtained with the above mentioned calculations are reported in appendix VIII.

It seems that the ΔG values are the most significant ones in interpreting the experimental evidences. Their changes in going from the adducts to the ester are close to zero for the tertiary alcohols, but ca. -3 to -5 kcal/mol for the primary and secondary alcohols.

It is worth noting that the formation of the dimer during the supersonic expansion is not a simple and linear process. For example, when more than one conformation can exist in the potential surface, the constituting molecules can reach the thermal quasi-equilibrium as a result of dissociation and reformation of the dimers in the low-temperature molecular beam. Then, the conformational enrichment differs from the thermodynamic equilibrium. The same argumentation is

also suitable for the quasi-equilibrium conditions for the esterification reaction. So, even a small free energy difference between different esterification reactions can turn out in completely different reaction advancements.

Moreover, we have to take into account another factor which generally happens in the gas phase spectroscopic study. The carrier gas (He in our case), is constituting our mixtures, in a concentration of about 99%. In the supersonic expansion process, its function is to convert the internal energy of the molecules into the translational kinetic energy, up to supersonic speed. This effect can cause a conformational relaxation. When the interconversion barrier is smaller than $2kT$, the less stable conformer disappears.^[53] Probably this factor has influenced the esterification processes.

The organic chemists have paid much attentions to the fact that in tertiary alcohols the OH group is more “protected” than in the alcohols of the other classes, which results in a reduced propensity to undergo the esterification reaction. Anyway, the step before the esterification should be the formation of the adduct, as what we detected in the case of tertiary alcohols. This experimental investigation outlines a sharp cut out of the esterification reaction in going from primary and secondary to tertiary alcohols. Theoretical molecular dynamics calculations supply an indication in support of the experimental evidences.

In summary, by mixing primary and secondary alcohols with carboxylic acids just before the supersonic expansion within pulsed Fourier transform microwave experiments, only the rotational spectrum of the ester has been observed. However, when formic acid was mixed with tertiary alcohols, adducts have been formed and their rotational spectra have been easily measured. Molecular dynamics calculations have been performed to interpret the experimental evidences.

Appendices

I. Ring puckering splitting in indan

Table A1.1. Experimental transition frequencies (ν , MHz) and experimental – calculated values ($\Delta\nu$, kHz) of the parent species of indan.

Interstate transition				
$J'(K_a', K_c') \leftarrow J''(K_a'', K_c'')$	$\nu/0 \leftarrow 1$		$\nu/1 \leftarrow 0$	
	ν/MHz	$\Delta\nu/\text{kHz}$	ν/MHz	$\Delta\nu/\text{kHz}$
2(1,1)-1(0,1)	8003.793	-4	8048.536	4
3(1,2)-2(0,2)	11226.988	4	11271.724	-3
2(2,0)-1(1,0)	11711.039	-12	11755.790	7
2(2,1)-1(1,1)	12069.121	-7	12113.875	14
3(2,2)-2(1,2)	15065.870	2	15110.615	4
4(2,2)-3(1,2)	16569.516	16	16614.232	-18
4(2,3)-3(1,3)	18259.194	1	18303.941	-7
Intrastate transition				
	$\nu/0 \leftarrow 0$		$\nu/1 \leftarrow 1$	
3(1,3)-2(1,2)			7086.771	-2
3(0,3)-2(0,2)	7520.955	3	7520.955	-3
3(2,2)-2(2,1)	7743.734	2	7743.734	-3
3(2,1)-2(2,0)	7966.510	-3	7966.524	7
3(1,2)-2(1,1)	8328.251	-4	8328.263	4
4(1,4)-3(1,3)	9392.648	4	9392.648	-4
4(0,4)-3(0,3)	9806.520	4	9806.520	-4
4(2,3)-3(2,2)	10280.095	-2	10280.106	2
4(3,2)-3(3,1)	10426.292	-3	10426.307	5
4(3,1)-3(3,0)	10456.021	3	10456.021	-3
4(2,2)-3(2,1)	10798.189	-2	10798.200	3
4(1,3)-3(1,2)	11024.926	-3	11024.939	4
5(1,5)-4(1,4)	11662.803	5	11662.803	-5
5(0,5)-4(0,4)	11987.456	3	11987.456	-8
5(2,4)-4(2,3)	12778.806	-3	12778.819	1
5(3,3)-4(3,2)	13056.570	-4	13056.585	3
5(3,2)-4(3,1)	13157.742	-6	13157.759	3

5(1,4)-4(1,3)	13639.103	-3	13639.118	5
5(2,3)-4(2,2)	13694.679	-6	13694.698	6
6(1,6)-5(1,5)	13900.512	7	13900.512	-6
6(0,6)-5(0,5)	14118.865	8	14118.865	-5
6(2,5)-5(2,4)	15232.433	0	15232.443	-1
6(4,3)-5(4,2)	15678.728	-5	15678.746	4
6(3,4)-5(3,3)	15683.130	0	15683.144	5
6(4,2)-5(4,1)	15691.498	-4	15691.515	4
6(3,3)-5(3,2)	15938.998	-5	15939.017	6
7(1,7)-6(1,6)	16112.267	8	16112.267	-7
6(1,5)-5(1,4)	16137.398	-2	16137.412	2
7(0,7)-6(0,6)	16243.781	7	16243.781	-8
6(2,4)-5(2,3)	16588.240	-7	16588.262	8
7(2,6)-6(2,5)	17636.059	0	17636.070	-2
8(1,8)-7(1,7)	18305.446	13	18305.446	-5
8(0,8)-7(0,7)	18378.964	13	18378.964	-5
7(1,6)-6(1,5)	18494.004	-4	18494.016	-4

Table A1.2. Experimental transition frequencies (ν , MHz) and experimental – calculated values ($\Delta\nu$, kHz) of the ^{13}C isotopologues of indan.

C(13)-2				
$J'(K_a', K_c') \leftarrow J''(K_a'', K_c'')$	$\nu/0 \leftarrow 0$		$\nu/1 \leftarrow 1$	
	ν/MHz	$\Delta\nu/\text{kHz}$	ν/MHz	$\Delta\nu/\text{kHz}$
3(1,3)-2(1,2)	6988.134	2	6988.134	0
3(0,3)-2(0,2)	7415.595	2	7415.595	-1
3(1,2)-2(1,1)	8192.013	3	8192.014	-2
4(1,4)-3(1,3)	9264.585	2	9264.585	-1
4(0,4)-3(0,3)	9678.243	1	9678.243	-2
4(1,3)-3(1,2)	10849.076	-1	10849.084	-1
5(1,5)-4(1,4)	11507.069	0	11507.069	-2
5(0,5)-4(0,4)	11838.019	2	11838.019	0
5(1,4)-4(1,3)	13430.006	-2	13430.019	2
13C3				
$J'(K_a', K_c') \leftarrow J''(K_a'', K_c'')$	$\nu/0 \leftarrow 0$		$\nu/1 \leftarrow 1$	
	ν/MHz	$\Delta\nu/\text{kHz}$	ν/MHz	$\Delta\nu/\text{kHz}$
3(1,3)-2(1,2)	7027.815	0	7027.815	-3
3(0,3)-2(0,2)	7458.639	3	7458.639	-2

3(1,2)-2(1,1)	8262.903	6	8262.903	-4
4(1,4)-3(1,3)	9314.032	4	9314.032	0
4(0,4)-3(0,3)	9723.632	2	9723.632	-2
4(1,3)-3(1,2)	10937.593	0	10937.605	-1
5(1,5)-4(1,4)	11564.589	1	11564.589	-3
5(0,5)-4(0,4)	11884.816	2	11884.816	-1
5(1,4)-4(1,3)	13529.534	0	13529.549	0
13C4				
J'(Ka', Kc')←J''(Ka'', Kc'')	v/0←0		v/1←1	
	v/MHz	Δv/kHz	v/MHz	Δv/kHz
3(1,3)-2(1,2)	7080.996	1	7080.996	-3
3(0,3)-2(0,2)	7514.945	3	7514.945	-3
3(1,2)-2(1,1)	8325.550	1	8325.563	0
4(1,4)-3(1,3)	9384.458	3	9384.458	-2
4(0,4)-3(0,3)	9796.861	3	9796.861	-2
4(1,3)-3(1,2)	11020.422	-1	11020.440	0
5(1,5)-4(1,4)	11651.973	3	11651.973	-2
5(0,5)-4(0,4)	11974.216	2	11974.216	-2
13C5				
J'(Ka', Kc')←J''(Ka'', Kc'')	v/0←0		v/1←1	
	v/MHz	Δv/kHz	v/MHz	Δv/kHz
3(1,3)-2(1,2)	7048.204	3	7048.204	0
3(0,3)-2(0,2)	7480.472	3	7480.472	-2
3(1,2)-2(1,1)	8296.490	-1	8296.501	-1
4(1,4)-3(1,3)	9339.756	2	9339.756	-2
4(0,4)-3(0,3)	9747.768	3	9747.768	-1
4(1,3)-3(1,2)	10979.832	1	10979.847	1
5(1,5)-4(1,4)	11594.959	1	11594.959	-3
5(0,5)-4(0,4)	11910.963	1	11910.963	-2
5(1,4)-4(1,3)	13577.600	0	13577.614	-1
13C6				
J'(Ka', Kc')←J''(Ka'', Kc'')	v/0←0		v/1←1	
	v/MHz	Δv/kHz	v/MHz	Δv/kHz
3(1,3)-2(1,2)	7000.921	3	7000.921	0
3(0,3)-2(0,2)	7429.751	2	7429.751	-3
3(1,2)-2(1,1)	8215.429	7	8215.429	-4
4(1,4)-3(1,3)	9280.512	1	9280.512	-3
4(0,4)-3(0,3)	9693.193	2	9693.193	-2

4(1,3)-3(1,2)	10878.380	0	10878.393	0
5(1,5)-4(1,4)	11525.584	2	11525.584	-2
5(0,5)-4(0,4)	11853.349	2	11853.349	-1
5(1,4)-4(1,3)	13463.093	-1	13463.109	0

II. The microwave spectroscopy study of 1,2-dimethoxyethane

Table A2.1. Theoretical structures of 1,2-dimethoxyethane at MP2/6-311++G** level of theory.

	TTT			TGT			<i>TGG'</i>		
	<i>a</i> / Å	<i>b</i> / Å	<i>c</i> / Å	<i>a</i> / Å	<i>b</i> / Å	<i>c</i> / Å	<i>a</i> / Å	<i>b</i> / Å	<i>c</i> / Å
C	-2.959	0.180	-0.000	-2.713	-0.435	-0.121	-2.500	-0.472	-0.166
O	-1.722	-0.500	0.000	-1.404	-0.301	0.390	-1.166	-0.334	0.282
C	-0.638	0.407	0.000	-0.716	0.760	-0.237	-0.612	0.899	-0.135
C	0.638	-0.407	-0.000	0.716	0.760	0.236	0.829	0.997	0.324
O	1.722	0.500	-0.000	1.404	-0.301	-0.390	1.718	0.169	-0.399
C	2.959	-0.180	0.000	2.713	-0.435	0.121	1.788	-1.160	0.096
H	-3.745	-0.576	-0.000	-3.189	-1.253	0.421	-2.869	-1.428	0.206
H	-3.065	0.811	0.892	-3.297	0.484	0.027	-3.134	0.336	0.224
H	-3.064	0.811	-0.893	-2.697	-0.674	-1.194	-2.552	-0.464	-1.263
H	-0.668	1.050	0.892	-1.187	1.723	0.017	-1.184	1.737	0.296
H	-0.668	1.050	-0.891	-0.732	0.641	-1.330	-0.646	0.981	-1.232
H	0.668	-1.050	0.891	1.187	1.723	-0.018	1.167	2.026	0.156
H	0.668	-1.050	-0.892	0.732	0.642	1.330	0.885	0.783	1.401
H	3.745	0.576	0.000	3.189	-1.253	-0.420	2.571	-1.660	-0.475
H	3.065	-0.811	0.893	3.297	0.484	-0.028	2.063	-1.162	1.159
H	3.065	-0.811	-0.893	2.698	-0.673	1.194	0.840	-1.690	-0.026

Table A2.1. Experimental transition frequencies of the isomers.

Table A2.1.1. Transitions frequencies measured for the TGT isotopologues.

							Parent species	C1	C2
<i>J</i>	<i>K_a</i>	<i>K_c</i>	<i>J'</i>	<i>K_a'</i>	<i>K_c'</i>				
4	3	2	3	2	1	S1	60218.01		
						S2	60216.44		
						S3	60217.53		
						S4	60214.53		
4	3	1	3	2	2	S1	60220.91		
						S2	60222.03		
						S3	60220.42		
						S4	60223.45		

4	3	1	3	2	1	S2	60218.8		
4	3	2	3	2	2	S2	60219.72		
						S4	60218.8		
5	3	3	4	2	2	S1	63194.71		
						S2	63193.27		
						S3	63194.26		
						S4	63191.69		
5	3	2	4	2	3	S1	63203.36		
						S2	63204.32		
						S3	63202.9		
						S4	63205.46		
5	3	2	4	2	2	S2	63195.6		
						S4	63196.33		
5	3	3	4	2	3	S2	63201.99		
						S4	63200.79		
6	3	4	5	2	3	S1	66167.75		
						S2	66166.44		
						S3	66167.31		
						S4	66164.92		
6	3	3	5	2	4	S1	66187.94		
						S2	66188.84		
						S3	66187.49		
						S4	66189.82		
6	3	3	5	2	3	S2	66168.78		
6	3	3	5	2	3	S4	66169.56		
6	3	4	5	2	4	S2	66186.48		
6	3	4	5	2	4	S4	66185.13		
7	1	6	7	0	7	S1	10919.77		
						S2	10919.72		
						S3	10919.67		
						S4	10919.67		
6	1	5	6	0	6	S1	10595.16		
						S2	10595.12		
						S3	10595.07		
						S4	10595.07		
1	1	1	0	0	0	S1	12598.94	12523.9651	12444.1483
						S2	12598.89	12523.9102	12444.0991
						S3	12598.84	12523.8642	12444.0434

						S4	12598.83	12523.8642	12444.0434
1	1	0	1	0	1	S1	9705.522	9691.9889	9559.4441
						S2	9705.475	9691.9298	9559.3975
						S3	9705.425	9691.8876	9559.3498
						S4	9705.437	9691.8876	9559.3498
2	1	2	1	0	1	S1	15492.41	15355.9959	15328.9030
						S2	15492.36	15355.9394	15328.8577
						S3	15492.31	15355.8885	15328.8058
						S4	15492.31	15355.8885	15328.8058
2	1	1	2	0	2	S1	9791.943	9775.3733	9647.7399
						S2	9791.897	9775.3236	9647.6913
						S3	9791.848	9775.2729	9647.6423
						S4	9791.848	9775.2729	9647.6423
3	1	3	2	0	2	S1	18343.21	18146.8375	18170.0898
						S2	18343.16	18146.7885	18170.0438
						S3	18343.11	18146.7389	18169.9952
						S4	18343.11	18146.7389	18169.9952
3	1	2	3	0	3	S1	9922.64	9901.4532	9781.3089
						S2	9922.593	9901.4053	9781.2659
						S3	9922.547	9901.3609	9781.2223
						S4	9922.547	9901.3609	9781.2223
3	2	2	4	1	3	S1	16641.68		
						S2	16641.33		
						S3	16641.38		
						S4	16640.68		
3	2	1	4	1	4	S1	17502.32		
						S2	17502.38		
						S3	17502.03		
						S4	17502.72		
4	1	3	4	0	4	S1	10098.88		
						S2	10098.84		
						S3	10098.79		
						S4	10098.79		
5	1	4	5	0	5	S1	10322.36		
						S2	10322.31		
						S3	10322.27		
						S4	10322.27		
6	0	6	5	1	5	S1	8819.063		

						S2	8819.111		
						S3	8819.164		
						S4	8819.164		
6	1	5	6	0	6	S1	10595.16		
						S2	10595.12		
						S3	10595.07		
						S4	10595.07		
7	0	7	6	1	6	S1	12027.72		
						S2	12027.77		
						S3	12027.82		
						S4	12027.82		
7	1	6	7	0	7	S1	10919.77		
						S2	10919.72		
						S3	10919.67		
						S4	10919.67		
8	0	8	7	1	7	S1	15266.11		
						S2	15266.16		
						S3	15266.21		
						S4	15266.21		
8	1	7	8	0	8	S1	11299		
						S2	11298.96		
						S3	11298.91		
						S4	11298.91		

Table A2.1.2. Transitions frequencies measured for the *TGG'* isotopologues.

							Parent species	C1	C2	C3	C4
J	K_a	K_c	J'	K_a'	K_c'						
2	0	2	1	0	1	S1	7408.769	7239.6010	7389.2391	7377.1435	7306.9517
						S2	7408.769	7239.6010	7389.2391	7377.1435	7306.9517
						S3	7408.728	7239.5638	7389.1991	7377.0991	7306.9141
						S4	7408.728	7239.5638	7389.1991	7377.0991	7306.9141
						S5	7408.728	7239.5638	7389.1991	7377.0991	7306.9141
2	1	2	1	1	1	S1	7097.33				
						S2	7097.335				
						S3	7097.31				
						S4	7097.31				
						S5	7097.31				
2	1	1	1	1	0	S1	7752.227				

						S2	7752.227					
						S3	7752.167					
						S4	7752.167					
						S5	7752.167					
3	0	3	2	0	2	S1	11073.33	10822.9320	11042.6474	11024.3940	10919.9021	
						S2	11073.33	10822.9320	11042.6474	11024.3940	10919.9021	
						S3	11073.28	10822.8772	11042.5944	11024.3406	10919.8489	
						S4	11073.28	10822.8772	11042.5944	11024.3406	10919.8489	
						S5	11073.28	10822.8772	11042.5944	11024.3406	10919.8489	
3	1	3	2	1	2	S1	10636.19	10401.5314	10602.3060	10584.6308	10484.1134	
						S2	10636.19	10401.5314	10602.3060	10584.6308	10484.1134	
						S3	10636.16	10401.4993	10602.2734	10584.5957	10484.0815	
						S4	10636.16	10401.4993	10602.2734	10584.5957	10484.0815	
						S5	10636.16	10401.4993	10602.2734	10584.5957	10484.0815	
3	1	2	2	1	1	S1	11618.01	11342.8127	11594.3012	11575.7622	11465.1429	
						S2	11618.01	11342.8127	11594.3012	11575.7622	11465.1429	
						S3	11617.93	11342.7313	11594.2153	11575.6775	11465.0596	
						S4	11617.93	11342.7313	11594.2153	11575.6775	11465.0596	
						S5	11617.93	11342.7313	11594.2153	11575.6775	11465.0596	
3	2	2	2	2	1	S1	11137.13					
						S2	11137.15					
						S3	11137.1					
						S4	11137.08					
						S5	11137.13					
3	2	1	2	2	0	S1	11200.91					
						S2	11200.9					
						S3	11200.83					
						S4	11200.84					
						S5	11200.79					
4	0	4	3	0	3	S1	14691.58	14363.7117	14648.1837	14623.6609	14485.7644	
						S2	14691.58	14363.7117	14648.1837	14623.6609	14485.7644	
						S3	14691.51	14363.6499	14648.1191	14623.5970	14485.6988	
						S4	14691.51	14363.6499	14648.1191	14623.5970	14485.6988	
						S5	14691.51	14363.6499	14648.1191	14623.5970	14485.6988	
4	1	4	3	1	3	S1	14163.95	13852.5192	14118.1775	14094.5669	13960.8858	
						S2	14163.95	13852.5192	14118.1775	14094.5669	13960.8858	
						S3	14163.91	13852.4768	14118.1347	14094.5244	13960.8427	
						S4	14163.91	13852.4768	14118.1347	14094.5244	13960.8427	

						S5	14163.91	13852.4768	14118.1347	14094.5244	13960.8427
4	1	3	3	1	2	S1	15470.72	15105.5197	15438.3689	15413.5936	15266.5077
						S2	15470.72	15105.5197	15438.3689	15413.5936	15266.5077
						S3	15470.6	15105.4112	15438.2547	15413.4818	15266.3970
						S4	15470.6	15105.4112	15438.2547	15413.4818	15266.3970
						S5	15470.6	15105.4112	15438.2547	15413.4818	15266.3970
4	2	3	3	2	2	S1	14836.97	14496.9848			
						S2	14836.97	14496.9848			
						S3	14836.88	14496.9128			
						S4	14836.88	14496.9128			
						S5	14836.89	14496.9128			
4	2	2	3	2	1	S1	14994.75	14641.6086			
						S2	14994.75	14641.6086			
						S3	14994.66	14641.5132			
						S4	14994.66	14641.5132			
						S5	14994.65	14641.5132			
5	0	5	4	0	4	S1	18252.42	17851.4515	18194.6243	18163.7188	17993.4341
						S2	18252.42	17851.4515	18194.6243	18163.7188	17993.4341
						S3	18252.35	17851.3829	18194.5554	18163.6478	17993.3671
						S4	18252.35	17851.3829	18194.5554	18163.6478	17993.3671
						S5	18252.35	17851.3829	18194.5554	18163.6478	17993.3671
5	1	5	4	1	4	S1	17678.01	17290.8546	17619.9197	17590.3405	17423.7459
						S2	17678.01	17290.8546	17619.9197	17590.3405	17423.7459
						S3	17677.95	17290.8069	17619.8661	17590.2901	17423.6944
						S4	17677.95	17290.8069	17619.8661	17590.2901	17423.6944
						S5	17677.95	17290.8069	17619.8661	17590.2901	17423.6944
5	2	4	4	2	3	S1	18526.07				
						S2	18526.07				
						S3	18525.97				
						S4	18525.97				
						S5	18525.97				
1	1	0	0	0	0	S1	8895.322				
						S2	8895.302				
						S3	8895.302				
						S4	8895.29				
						S5	8895.29				
2	1	1	1	0	1	S1	12935.15				
						S2	12935.14				

						S3	12935.09				
						S4	12935.08				
						S5	12935.08				
2	2	1	2	1	1	S1	14566.24				
						S2	14566.17				
						S3	14566.25				
						S4	14566.24				
						S5	14566.17				
2	2	0	2	1	2	S1	15564.57				
						S2	15564.56				
						S3	15564.61				
						S4	15564.54				
						S5	15564.61				
3	2	2	3	1	2	S1	14085.37				
						S2	14085.31				
						S3	14085.42				
						S4	14085.38				
						S5	14085.38				
3	2	1	3	1	3	S1	16129.3				
						S2	16129.26				
						S3	16129.27				
						S4	16129.22				
						S5	16129.22				
4	2	3	4	1	3	S1	13451.61				
						S2	13451.56				
						S3	13451.72				
						S4	13451.66				
						S5	13451.66				
4	2	2	4	1	4	S1	16960.11				
						S2	16960.07				
						S3	16960.03				
						S4	16959.98				
						S5	16959.98				
1	1	1	0	0	0	S1	8567.873				
						S2	8567.854				
						S3	8567.863				
						S4	8567.854				
						S5	8567.854				

2	1	2	1	0	1	S1	11952.81				
						S2	11952.79				
						S3	11952.81				
						S4	11952.79				
						S5	11952.79				
3	1	3	2	0	2	S1	15180.24				
						S2	15180.22				
						S3	15180.24				
						S4	15180.22				
						S5	15180.22				
4	1	4	3	0	3	S1	18270.85				
						S2	18270.83				
						S3	18270.87				
						S4	18270.85				
						S5	18270.85				
2	2	1	2	1	2	S1	15548.57				
						S2	15548.51				
						S3	15548.54				
						S4	15548.51				
						S5	15548.47				
2	2	0	2	1	1	S1	14582.24				
						S2	14582.2				
						S3	14582.33				
						S4	14582.24				
						S5	14582.31				
3	2	2	3	1	3	S1	16049.52				
						S2	16049.46				
						S3	16049.47				
						S4	16049.43				
						S5	16049.42				
3	2	1	3	1	2	S1	14165.14				
						S2	14165.1				
						S3	14165.21				
						S4	14165.16				
						S5	14165.17				

III. 1-Methylcyclohexanol

Table A3.1. The labels for the geometry description.

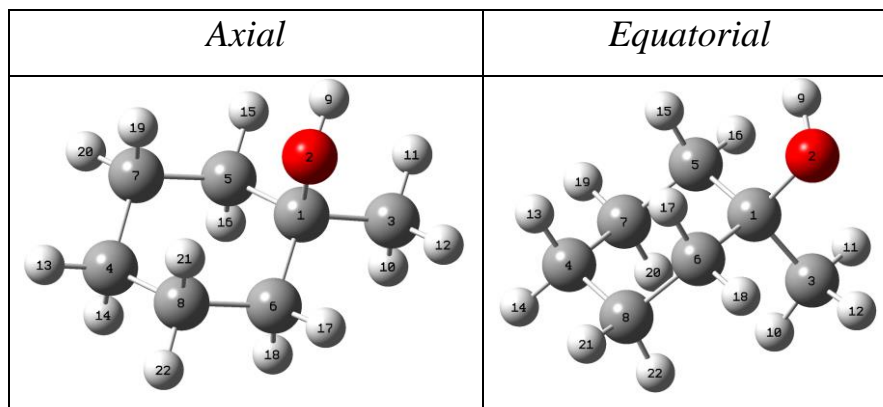


Table A3.2 Geometry of conformer *Ag*.

Bond lengths/Å		Angles/°		Dihedral angle/°	
O2C1	1.4391				
C3C1	1.5252	C3C1O2	109.5		
C4C1	2.9705	C4C1O2	99.8	C4C1O2C3	178.6
C5C1	1.5341	C5C1O2	109.8	C5C1O2C3	-122.0
C6C1	1.5288	C6C1O2	105.1	C6C1O2C3	119.3
C7C5	1.5308	C7C5C1	112.3	C7C5C1O2	-61.3
C8C6	1.5309	C8C6C1	112.2	C8C6C1O2	64.1
H9O2	0.9638	H9O2C1	106.9	H9O2C1C3	59.0
H10C3	1.0950	H10C3C1	110.9	H10C3C1O2	177.7
H11C3	1.0972	H11C3C1	110.5	H11C3C1H10	119.7
H12C3	1.0943	H12C3C1	109.9	H12C3C1H10	-120.6
H13C4	1.0963	H13C4C1	152.2	H13C4C1O2	2.7
H14C4	1.0999	H14C4C1	100.8	H14C4C1O2	-177.2
H15C5	1.0997	H15C5C1	108.9	H15C5C1O2	61.6
H16C5	1.0991	H16C5C1	108.5	H16C5C1O2	177.4
H17C6	1.0966	H17C6C1	108.3	H17C6C1O2	-58.5
H18C6	1.0987	H18C6C1	108.1	H18C6C1O2	-174.9
H19C7	1.0963	H19C7C5	109.3	H19C7C5C1	64.4
H20C7	1.0964	H20C7C5	109.8	H20C7C5C1	-178.1
H21C8	1.0958	H21C8C6	109.1	H21C8C6C1	-64.5
H22C8	1.0964	H22C8C6	109.6	H22C8C6C1	178.1

Table A3.3. Geometry of conformer *At*.

Bond lengths/Å		Angles/°		Dihedral angle/°	
O2C1	1.4384				
C3C1	1.5204	C3C1O2	104.6		
C4C1	2.9833	C4C1O2	105.5	C4C1O2C3	180.0
C5C1	1.5345	C5C1O2	110.1	C5C1O2C3	-119.2
C6C1	1.5345	C6C1O2	110.1	C6C1O2C3	119.2
C7C5	1.5325	C7C5C1	112.7	C7C5C1O2	-68.1
C8C6	1.5325	C8C6C1	112.7	C8C6C1O2	68.1
H9O2	0.9624	H9O2C1	107.7	H9O2C1C3	180.0
H10C3	1.0944	H10C3C1	110.5	H10C3C1O2	180.0
H11C3	1.0943	H11C3C1	109.9	H11C3C1H10	120.3

H12C3	1.0943	H12C3C1	109.9	H12C3C1H10	-120.3
H13C4	1.0962	H13C4C1	152.5	H13C4C1O2	0.0
H14C4	1.0991	H14C4C1	100.4	H14C4C1O2	180.0
H15C5	1.0964	H15C5C1	108.4	H15C5C1O2	54.8
H16C5	1.0989	H16C5C1	108.4	H16C5C1O2	171.3
H17C6	1.0964	H17C6C1	108.4	H17C6C1O2	-54.8
H18C6	1.0989	H18C6C1	108.4	H18C6C1O2	-171.3
H19C7	1.0998	H19C7C5	110.1	H19C7C5C1	65.7
H20C7	1.0959	H20C7C5	109.7	H20C7C5C1	-178.0
H21C8	1.0998	H21C8C6	110.1	H21C8C6C1	-65.7
H22C8	1.0959	H22C8C6	109.7	H22C8C6C1	178.0

Table A3.4. Geometry of conformer *Et*.

Bond lengths/Å		Angles/°		Dihedral angle/°	
O2C1	1.4367				
C3C1	1.5234	C3C1O2	104.1		
C4C1	2.9855	C4C1O2	147.4	C4C1O2C3	180.0
C5C1	1.5331	C5C1O2	109.6	C5C1O2C3	-119.8
C6C1	1.5331	C6C1O2	109.6	C6C1O2C3	119.8
C7C5	1.5331	C7C5C1	112.9	C7C5C1O2	-174.3
C8C6	1.5331	C8C6C1	112.9	C8C6C1O2	174.3
H9O2	0.9638	H9O2C1	107.0	H9O2C1C3	180.0
H10C3	1.0923	H10C3C1	111.9	H10C3C1O2	180.0
H11C3	1.0942	H11C3C1	109.5	H11C3C1H10	120.6
H12C3	1.0942	H12C3C1	109.5	H12C3C1H10	-120.6
H13C4	1.0993	H13C4C1	101.0	H13C4C1O2	0.0
H14C4	1.0962	H14C4C1	152.0	H14C4C1O2	180.0
H15C5	1.1011	H15C5C1	107.9	H15C5C1O2	-54.4
H16C5	1.0965	H16C5C1	108.8	H16C5C1O2	61.4
H17C6	1.1011	H17C6C1	107.9	H17C6C1O2	54.4
H18C6	1.0965	H18C6C1	108.8	H18C6C1O2	-61.4
H19C7	1.0962	H19C7C5	109.6	H19C7C5C1	177.5
H20C7	1.0974	H20C7C5	109.9	H20C7C5C1	-65.8
H21C8	1.0962	H21C8C6	109.6	H21C8C6C1	-177.5
H22C8	1.0974	H22C8C6	109.9	H22C8C6C1	65.8

Table A3.5. Geometry of conformer *Eg*.

Bond lengths/Å		Angles/°		Dihedral angle/°	
O2C1	1.4371				
C3C1	1.5283	C3C1O2	108.8		
C4C1	2.9799	C4C1O2	142.8	C4C1O2C3	175.8
C5C1	1.5331	C5C1O2	109.5	C5C1O2C3	-122.4
C6C1	1.5281	C6C1O2	104.9	C6C1O2C3	119.8
C7C5	1.5328	C7C5C1	112.9	C7C5C1O2	-169.0
C8C6	1.5323	C8C6C1	112.6	C8C6C1O2	171.6
H9O2	0.9641	H9O2C1	107.0	H9O2C1C3	60.2
H10C3	1.0932	H10C3C1	112.3	H10C3C1O2	177.6
H11C3	1.0971	H11C3C1	110.0	H11C3C1H10	120.0
H12C3	1.0942	H12C3C1	109.5	H12C3C1H10	-120.9
H13C4	1.0989	H13C4C1	100.9	H13C4C1O2	4.2
H14C4	1.0963	H14C4C1	152.1	H14C4C1O2	-175.5
H15C5	1.0979	H15C5C1	107.3	H15C5C1O2	-48.5
H16C5	1.0994	H16C5C1	109.2	H16C5C1O2	67.4
H17C6	1.0978	H17C6C1	107.3	H17C6C1O2	51.2

H18C6	1.0965	H18C6C1	108.9	H18C6C1O2	-64.6
H19C7	1.0962	H19C7C5	109.6	H19C7C5C1	177.4
H20C7	1.0975	H20C7C5	110.2	H20C7C5C1	-65.7
H21C8	1.0960	H21C8C6	109.4	H21C8C6C1	-177.5
H22C8	1.0977	H22C8C6	110.2	H22C8C6C1	65.8

Table A.3.6. Experimental transition frequencies (ν , MHz) and observed-calculated values ($\Delta\nu$, kHz) of parent species of 1MCH: parent species, conformer Ag.

$J''_{Ka',Kc} \leftarrow J''_{Ka'',Kc''}$	0^+		0^-	
	ν/MHz	$\Delta\nu/\text{kHz}$	ν/MHz	$\Delta\nu/\text{kHz}$
μ_a -transitions				
2(1,1)-1(1,0)	6733.2074	1.4		
3(0,3)-2(0,2)	9639.9369	0.4	9639.4747	-0.6
3(1,3)-2(1,2)	9380.0903	0.1	9379.5581	-0.7
3(1,2)-2(1,1)	10081.3649	0.9	10081.2458	-1.9
3(2,2)-2(2,1)	9748.1327	6.0		
3(2,1)-2(2,0)	9856.327	-3.2		
4(0,4)-3(0,3)	12741.2906	-0.7	12740.5417	2.0
4(1,4)-3(1,3)	12478.9253	1.2	12478.1808	-0.6
4(1,3)-3(1,2)	13404.4632	0.7	13404.2518	0.4
4(2,3)-3(2,2)	12975.8936	-0.8	12975.4864	-3.1
4(2,2)-3(2,1)	13231.9825	-2.3		
4(3,1)-3(3,0)	13059.39	-6.8		
4(3,2)-3(3,1)	13047.1648	2.0		
5(0,5)-4(0,4)	15781.3355	-0.4	15780.2660	-0.1
5(1,5)-4(1,4)	15559.2211	1.5	15558.2484	1.4
5(1,4)-4(1,3)	16689.4504	1.9	16689.0839	1.5
5(2,3)-4(2,2)	16649.9524	1.5		
5(2,4)-4(2,3)	16185.4266	-0.7	16184.8813	-0.6
5(3,2)-4(3,1)	16364.22	-3.7		
5(3,3)-4(3,2)	16322.2491	-0.3		
5(4,1)-4(4,0)	16309.2044	0.5		
5(4,2)-4(4,1)	16308.194	-1.4		
μ_c -transitions				
2(1,1)-1(0,1)	8333.4877	0.4	8332.9977	-1.2
2(2,0)-1(1,0)	10858.3825	2.1	10856.6570	0.9
2(2,1)-1(1,1)	11065.1585	0.8	11063.5297	-2.5
3(1,2)-2(0,2)	11943.7568	1.5	11943.3986	3.9
3(2,1)-2(1,1)	13981.5057	1.2	13979.7113	-0.4
3(2,2)-2(1,2)	14548.9625	-4.9	14547.3858	-11.3
3(3,0)-2(2,0)	17154.1868	3.5	17151.3841	0.6
3(3,1)-2(2,1)	17179.7969	4.0	17177.0261	-3.3
3(0,3)-2(1,1)	7777.5428	-2.0	7777.3344	6.1
3(3,0)-3(2,2)	7433.7172	-7.0	7431.2596	9.5
3(3,1)-3(2,1)	7295.7943	-0.8	7293.1187	-0.2
4(1,3)-3(0,3)	15708.284	2.3		
4(2,2)-3(1,2)	17132.1255	0.2	17130.3918	2.7
4(2,3)-3(1,3)	18144.7697	-1.9	18143.3328	5.0
4(3,2)-4(2,2)	7110.9735	0.4	7108.0763	0.2
4(4,1)-4(3,1)	10322.6253	-2.0	10319.0064	-3.9
4(0,4)-3(1,2)	10437.4709	-1.2	10436.6183	-2.0
4(3,1)-4(2,3)	7517.2249	-1.7	7514.9096	4.5
4(4,0)-4(3,2)	10337.0418	-4.3		
5(4,2)-5(3,2)	10266.5993	0.3		

5(5,1)-5(4,1)	13289.4622	-0.8		
5(3,2)-5(2,4)	7696.0246	1.6	7694.0100	-2.1
5(4,1)-5(3,3)	10324.0021	1.5		
5(5,0)-5(4,2)	13290.608	1.1		
6(4,3)-6(3,3)	10149.9467	3.8		
6(5,2)-6(4,2)	13261.8342	0.0		
6(4,2)-6(3,4)	10319.627	-1.7		
6(5,1)-6(4,3)	13267.539	1.3		

Table A3.7. Experimental transition frequencies (ν , MHz) and observed-calculated values ($\Delta\nu$, kHz) of parent species of 1MCH: parent species, conformer *At*.

$J'_{Ka',Kc'} \leftarrow J''_{Ka'',Kc''}$	ν/MHz	$\Delta\nu/\text{kHz}$
μ_a -transitions		
3(0,3)-2(0,2)	9575.2478	-1.8
3(1,2)-2(1,1)	10006.0277	-1.5
3(1,3)-2(1,2)	9317.5823	-0.6
3(2,1)-2(2,0)	9781.4832	-1.3
3(2,2)-2(2,1)	9678.3642	-1.2
4(0,4)-3(0,3)	12659.5894	-0.7
4(1,3)-3(1,2)	13305.9712	-3.1
4(1,4)-3(1,3)	12396.8041	-1.9
4(2,2)-3(2,1)	13128.7026	-3.3
4(2,3)-3(2,2)	12883.9280	-0.7
4(3,1)-3(3,0)	12963.2052	-0.5
4(3,2)-3(3,1)	12951.9173	2.7
5(0,5)-4(0,4)	15683.6557	-1.2
5(1,4)-4(1,3)	16569.9267	-8.2
5(1,5)-4(1,4)	15458.1558	1.5
5(2,3)-4(2,2)	16518.1452	-5.4
5(2,4)-4(2,3)	16072.1209	-5.3
5(3,2)-4(3,1)	16241.6678	-0.4
5(3,3)-4(3,2)	16202.8780	-2.5
5(4,1)-4(4,0)	16189.9186	4.1
5(4,2)-4(4,1)	16189.0164	3.8
6(1,6)-5(1,5)	18502.2599	6.5
μ_c -transitions		
2(1,1)-1(0,1)	8299.0116	0.0
2(2,0)-1(1,0)	10868.2935	0.2
2(2,1)-1(1,1)	11072.0750	-0.3
3(1,2)-2(0,2)	11879.1316	7.6
3(2,1)-2(1,1)	13967.4211	7.3
3(2,2)-2(1,2)	14528.3080	1.6
3(3,0)-2(2,0)	17177.4871	0.0
3(3,1)-2(2,1)	17201.9194	-2.3
4(1,3)-3(0,3)	15609.8513	2.6
4(2,2)-3(1,2)	17090.0928	2.3
4(2,3)-3(1,3)	18094.6562	4.0
5(4,1)-5(3,3)	10455.7482	-3.4
5(4,2)-5(3,2)	10402.7563	-2.9
6(4,2)-6(3,4)	10450.1771	0.3
6(4,3)-6(3,3)	10293.3148	0.0

Table A3.8. Experimental transition frequencies (ν , MHz) and observed-calculated values ($\Delta\nu$, kHz) of parent species of 1MCH: parent species, conformer *Et*.

$J'_{Ka',Kc} \leftarrow J''_{Ka'',Kc''}$	ν/MHz	$\Delta\nu/\text{kHz}$
μ_a -transitions		
3(0,3)-2(0,2)	9496.1799	-1.3
3(1,2)-2(1,1)	9885.3397	-0.4
3(1,3)-2(1,2)	9255.8619	-0.8
3(2,1)-2(2,0)	9673.3904	1.2
3(2,2)-2(2,1)	9584.7843	0.5
4(0,4)-3(0,3)	12568.0918	-1.1
4(1,3)-3(1,2)	13150.3699	-4.5
4(1,4)-3(1,3)	12318.1146	-0.2
4(2,2)-3(2,1)	12973.6251	0.3
4(2,3)-3(2,2)	12762.0952	-2.2
4(3,1)-3(3,0)	12829.6958	0.4
4(3,2)-3(3,1)	12820.6265	7.1
5(0,5)-4(0,4)	15585.0230	0.3
5(1,4)-4(1,3)	16385.0558	-5.9
5(1,5)-4(1,4)	15364.6495	1.4
6(0,6)-5(0,5)	18564.8681	1.5
6(1,6)-5(1,5)	18395.7430	3.7
5(2,3)-4(2,2)	16313.4171	-3.3
5(2,4)-4(2,3)	15924.5007	-5.0
5(3,2)-4(3,1)	16068.7244	2.3
5(3,3)-4(3,2)	16037.4702	-0.3
5(4,1)-4(4,0)	16025.3811	-1.6
μ_c -transitions		
2(1,1)-1(0,1)	8169.8206	4.9
2(2,0)-1(1,0)	10700.6237	-1.2
2(2,1)-1(1,1)	10888.3941	5.5
3(1,2)-2(0,2)	11687.8687	4.0
3(2,1)-2(1,1)	13773.8184	-1.0
3(2,2)-2(1,2)	14293.6412	-4.4
3(3,0)-2(2,0)	16899.4232	-1.8
3(3,1)-2(2,1)	16920.4700	-0.9
4(1,3)-3(0,3)	15342.0609	3.0
4(2,2)-3(1,2)	16862.1056	1.5
4(2,3)-3(1,3)	17799.8813	1.0
5(1,4)-4(2,2)	12673.3330	1.0

Table A3.9. Experimental transition frequencies (ν , MHz) and observed-calculated values ($\Delta\nu$, kHz) of parent species of 1MCH: parent species, conformer *Eg*.

$J'_{Ka',Kc} \leftarrow J''_{Ka'',Kc''}$	$\nu/0 \leftarrow 0$		$\nu/1 \leftarrow 1$	
	ν/MHz	$\Delta\nu/\text{kHz}$	ν/MHz	$\Delta\nu/\text{kHz}$
μ_a -transitions				
2(1,1)-1(1,0)	6627.0223	1.71		
3(0,3)-2(0,2)	9530.2200	-8.55	9532.4519	1.94
3(1,2)-2(1,1)	9925.0500	-1.44	9927.3933	3.05
3(1,3)-2(1,2)	9289.0800	-10.15	9291.2558	-0.61
3(2,1)-2(2,0)	9713.2472	10.28	9715.5466	1.68
3(2,2)-2(2,1)	9621.7170	-3.74		
4(0,4)-3(0,3)	12610.8416	1.87	12613.7823	0.37
4(1,3)-3(1,2)	13202.2130	0.6	13205.3263	-2.76
4(1,4)-3(1,3)	12361.7143	1.17	12364.5972	-3.33
4(2,2)-3(2,1)	13028.7987	0.65	13031.9020	2.42
4(2,3)-3(2,2)	12810.7454	-1.05	12813.8022	2.99
4(3,1)-3(3,0)	12880.7225	0.19		

4(3,2)-3(3,1)	12871.1233	-0.22		
5(0,5)-4(0,4)	15635.8115	1.57	15639.4672	1.27
5(1,4)-4(1,3)	16447.8196	-1.17	16451.7116	-3.74
5(1,5)-4(1,4)	15418.2341	4.49	15421.8398	0.84
5(2,3)-4(2,2)	16384.0357	-1.92	16387.9465	1.59
5(2,4)-4(2,3)	15984.3669	-1.04	15988.1901	-2
5(3,2)-4(3,1)	16133.8098	-1.81	16137.7388	-1.53
5(3,3)-4(3,2)	16100.7820	-3.79	16104.7148	2.48
5(4,1)-4(4,0)	16088.5855	-0.68		
6(1,6)-5(1,5)	18459.0285	8.1	18463.3533	-1.25
μ_c -transitions				
2(1,1)-1(0,1)	8179.4048	-0.62	8181.3420	-1.49
2(2,0)-1(1,0)	10669.9303	0.65	10672.4594	2.66
2(2,1)-1(1,1)	10859.1232	0.13	10861.7011	-0.93
3(0,3)-2(1,1)	7741.9941	2.53		
3(1,2)-2(0,2)	11713.2889	0.49	11716.0748	-0.91
3(2,1)-2(1,1)	13756.1479	1.91	13759.4202	-0.85
3(2,2)-2(1,2)	14278.8751	2.43		
3(3,0)-2(2,0)	16844.4718	-1.31	16848.4830	-0.61
3(3,1)-2(2,1)	16866.1943	2.46	16870.2069	-1
4(1,3)-3(0,3)	15385.2738	1.53	15388.9526	-2.22
4(2,2)-3(1,2)	16859.8907	-1.9	16863.9315	1.12
4(2,3)-3(1,3)	17800.5314	2.44	17804.8385	2.55
5(0,5)-4(1,3)	12861.3746	-2.79		
5(4,1)-5(3,3)	10072.8805	-5.36		
5(4,2)-5(3,2)	10027.8144	-6.75		
6(1,5)-5(2,3)	16054.9410	-3.76		
6(4,2)-6(3,4)	10066.2199	1.85		
6(4,3)-6(3,3)	9932.6056	5.49		

Table A3.10. Experimental transition frequencies (ν , MHz) and observed-calculated values ($\Delta\nu$, kHz) of deuterated species of 1- Methylcyclohexanol.

$J'_{Ka',Kc'} \leftarrow J''_{Ka'',Kc''}$	Ag			
	$\nu/0 \leftarrow 0$		$\nu/1 \leftarrow 1$	
	ν /MHz	$\Delta\nu$ /kHz	ν /MHz	$\Delta\nu$ /kHz
μ_a -transitions				
3(0,3)-2(0,2)	9522.3825	0.88	9522.7337	5.72
3(1,2)-2(1,1)	9927.4870	-1.39	9927.9653	-4.04
3(1,3)-2(1,2)	9277.6809	0.62	9278.0285	1.87
3(2,2)-2(2,1)	9617.8459	-3.55	9618.2584	-4.45
4(0,4)-3(0,3)	12596.5509	1.39	12597.1380	-0.24
4(1,3)-3(1,2)	13203.8746	-0.71	13204.7679	-1.14
4(1,4)-3(1,3)	12345.4688	2.14	12346.2284	2.19
4(2,2)-3(2,1)	13032.0613	0.6	13032.1052	-0.38
4(2,3)-3(2,2)	12804.6085	-3.24	12805.0065	-4.16
5(0,5)-4(0,4)	15613.7981	-1.73	15614.7489	4.94
5(1,4)-4(1,3)	16447.0105	6.48	16448.5473	-2.35
5(1,5)-4(1,4)	15396.5483	-1.2	15398.1624	-1.77
5(2,3)-4(2,2)	16390.7703	-0.6	16389.8181	1.75
5(2,4)-4(2,3)	15975.1478	0.02	15975.5101	-2.78
μ_c -transitions				
2(1,1)-1(0,1)	8182.8553	5.65	8182.8553	-3.53
2(2,0)-1(1,0)	10663.0927	0.61	10662.4903	-2.98
2(2,1)-1(1,1)	10855.8768	7.07	10855.3512	6.32
3(1,2)-2(0,2)	11722.7430	-2.99	11723.0575	7.33

3(3,0)-2(2,0)	16835.2209	-1.35	16834.3177	-1.4
3(3,1)-2(2,1)	16857.9108	-2.86	16856.9744	-2.3
At				
$J'_{Ka',Kc} \leftarrow J''_{Ka'',Kc''}$	$F' \leftarrow F''$	ν/MHz	$\Delta\nu/\text{kHz}$	
μ_a -transitions				
3(0,3)-2(0,2)	4-3	9524.3705	-0.43	
3(0,3)-2(0,2)	3-2	9524.3594	-6.4	
3(0,3)-2(0,2)	2-1	9524.3848	1.52	
3(1,2)-2(1,1)	4-3	9914.7413	4.42	
3(1,2)-2(1,1)	3-2	9914.7583	6.41	
3(1,2)-2(1,1)	2-1	9914.7413	-2.27	
3(1,3)-2(1,2)	4-3	9284.6214	2.01	
3(1,3)-2(1,2)	3-2	9284.6317	-0.73	
3(1,3)-2(1,2)	2-1	9284.6214	6.98	
3(2,1)-2(2,0)	4-3	9703.7058	-0.72	
3(2,1)-2(2,0)	3-2	9703.7672	-2.64	
3(2,1)-2(2,0)	2-1	9703.6706	-3.21	
3(2,2)-2(2,1)	4-3	9614.0364	2.87	
3(2,2)-2(2,1)	3-2	9614.0845	-5.14	
3(2,2)-2(2,1)	2-1	9614.0040	1.64	
4(0,4)-3(0,3)	5-4	12604.7519	-3.17	
4(0,4)-3(0,3)	4-3	12604.7519	4.14	
4(0,4)-3(0,3)	3-2	12604.7519	-9.34	
4(1,3)-3(1,2)	5-4	13189.1578	5.2	
4(1,3)-3(1,2)	4-3	13189.1578	0.45	
4(1,3)-3(1,2)	3-2	13189.1578	-0.36	
4(1,4)-3(1,3)	5-4	12356.2086	1.88	
4(1,4)-3(1,3)	4-3	12356.2086	-2.3	
4(1,4)-3(1,3)	3-2	12356.2086	1.93	
4(2,2)-3(2,1)	5-4	13014.7597	2.17	
4(2,2)-3(2,1)	4-3	13014.7900	1.23	
4(2,2)-3(2,1)	3-2	13014.7597	9.09	
4(2,3)-3(2,2)	5-4	12800.8788	-6.48	
4(2,3)-3(2,2)	4-3	12800.9080	0.11	
4(2,3)-3(2,2)	3-2	12800.8788	-0.66	
5(0,5)-4(0,4)	6-5	15630.0539	4.25	
5(0,5)-4(0,4)	5-4	15630.0370	-5	
5(0,5)-4(0,4)	4-3	15630.0539	0.61	
5(1,4)-4(1,3)	6-5	16432.7518	-1.54	
5(1,4)-4(1,3)	5-4	16432.7518	-1.63	
5(1,4)-4(1,3)	4-3	16432.7518	-5.68	
5(1,5)-4(1,4)	6-5	15411.9520	5.33	
5(1,5)-4(1,4)	5-4	15411.9520	4.39	
5(1,5)-4(1,4)	4-3	15411.9520	4.71	
5(2,3)-4(2,2)	6-5	16365.2670	-2.24	
5(2,3)-4(2,2)	5-4	16365.2855	-2.8	
5(2,3)-4(2,2)	4-3	16365.2670	-0.66	
5(2,4)-4(2,3)	6-5	15972.6417	-2.9	
5(2,4)-4(2,3)	5-4	15972.6585	3.34	
5(2,4)-4(2,3)	4-3	15972.6417	-1.96	
μ_c -transitions				
2(2,0)-1(1,0)	3-2	10675.0530	1.09	
2(2,0)-1(1,0)	2-1	10674.9892	-9.51	
2(2,1)-1(1,1)	3-2	10862.7542	2.47	
2(2,1)-1(1,1)	2-1	10862.7542	4.35	
3(3,0)-2(2,0)	4-3	16853.1760	-2.07	

3(3,0)-2(2,0)	3-2	16853.1520	-6.37
3(3,0)-2(2,0)	2-1	16853.1760	1.59
3(3,1)-2(2,1)	4-3	16874.4691	1.02
3(3,1)-2(2,1)	3-2	16874.4549	2.01
3(3,1)-2(2,1)	2-1	16874.4691	7.24
3(1,2)-2(0,2)	4-3	11702.8001	5.41
3(1,2)-2(0,2)	3-2	11702.8113	-5.16
3(1,2)-2(0,2)	2-1	11702.8001	2.47
4(2,2)-3(1,2)	5-4	16858.8694	5.93
4(2,2)-3(1,2)	4-3	16858.8418	8.21
4(2,2)-3(1,2)	3-2	16858.8694	-8.55
<i>Et</i>			
$J'_{Ka',Kc} \leftarrow J''_{Ka'',Kc''}$	$F' \leftarrow F''$	ν/MHz	$\Delta\nu/\text{kHz}$
μ_a -transitions			
3(0,3)-2(0,2)	4-3	9349.7743	1.14
3(0,3)-2(0,2)	3-2	9349.7556	-4.39
3(0,3)-2(0,2)	2-1	9349.7743	7.32
3(1,2)-2(1,1)	4-3	9697.6609	1.92
3(1,2)-2(1,1)	3-2	9697.6461	0.06
3(1,2)-2(1,1)	2-1	9697.6609	-10.22
3(1,3)-2(1,2)	4-3	9126.6107	0.7
3(1,3)-2(1,2)	3-2	9126.5907	-2.31
3(1,3)-2(1,2)	2-1	9126.5907	-8.38
3(2,1)-2(2,0)	4-3	9498.1670	-0.04
3(2,1)-2(2,0)	3-2	9498.1357	2.15
3(2,1)-2(2,0)	2-1	9498.1890	-0.56
3(2,2)-2(2,1)	4-3	9423.9708	-1.89
3(2,2)-2(2,1)	3-2	9423.9348	7.12
3(2,2)-2(2,1)	2-1	9424.0036	5.91
4(0,4)-3(0,3)	5-4	12386.9405	0.29
4(0,4)-3(0,3)	4-3	12386.9189	-6.07
4(0,4)-3(0,3)	3-2	12386.9405	2.47
4(1,3)-3(1,2)	5-4	12905.3491	-0.16
4(1,3)-3(1,2)	4-3	12905.3397	-0.92
4(1,3)-3(1,2)	3-2	12905.3491	-4.62
4(1,4)-3(1,3)	5-4	12149.3667	0.6
4(1,4)-3(1,3)	4-3	12149.3568	0.98
4(1,4)-3(1,3)	3-2	12149.3568	-2.76
4(2,2)-3(2,1)	5-4	12728.8626	0.33
4(2,2)-3(2,1)	4-3	12728.8626	7.12
4(2,2)-3(2,1)	3-2	12728.8626	-3.19
4(2,3)-3(2,2)	5-4	12550.5885	4.21
4(2,3)-3(2,2)	4-3	12550.5627	-0.63
4(2,3)-3(2,2)	3-2	12550.5885	-1.18
4(3,1)-3(3,0)	5-4	12606.6975	8.94
4(3,1)-3(3,0)	4-3	12606.6494	-2.02
4(3,1)-3(3,0)	3-2	12606.6975	-6.27
4(3,2)-3(3,1)	5-4	12599.7169	7.9
4(3,2)-3(3,1)	4-3	12599.6685	-2.18
4(3,2)-3(3,1)	3-2	12599.7169	-7.58
5(0,5)-4(0,4)	6-5	15374.8491	3.25
5(0,5)-4(0,4)	5-4	15374.8277	-2.65
5(0,5)-4(0,4)	4-3	15374.8491	4.42
5(1,4)-4(1,3)	6-5	16088.1973	-0.65
5(1,4)-4(1,3)	5-4	16088.1886	-0.85
5(1,4)-4(1,3)	4-3	16088.1973	-3.21

5(1,5)-4(1,4)	6-5	15158.5932	2.26	
5(1,5)-4(1,4)	5-4	15158.5851	2.08	
5(1,5)-4(1,4)	4-3	15158.5851	-1.59	
5(2,3)-4(2,2)	6-5	15995.9898	4.24	
5(2,3)-4(2,2)	5-4	15995.9898	2.53	
5(2,3)-4(2,2)	4-3	15995.9898	3.93	
5(2,4)-4(2,3)	6-5	15664.7331	2.26	
5(2,4)-4(2,3)	5-4	15664.7169	-0.96	
5(2,4)-4(2,3)	4-3	15664.7331	0.74	
5(3,2)-4(3,1)	6-5	15784.0603	0.21	
5(3,2)-4(3,1)	5-4	15784.0439	0.47	
5(3,2)-4(3,1)	4-3	15784.0603	-4.46	
5(3,3)-4(3,2)	6-5	15759.9657	0.75	
5(3,3)-4(3,2)	5-4	15759.9480	2.25	
5(3,3)-4(3,2)	4-3	15759.9657	-4.35	
μ_c -transitions				
2(1,1)-1(0,1)	3-2	8011.8064	1.84	
2(2,0)-1(1,0)	2-1	10535.2857	4.57	
2(2,0)-1(1,0)	3-2	10535.3076	2.44	
2(2,1)-1(1,1)	3-2	10707.1805	-1.82	
2(2,1)-1(1,1)	2-1	10707.2611	-0.78	
3(3,0)-2(2,0)	4-3	16632.8313	2.67	
3(3,0)-2(2,0)	3-2	16632.8313	-5.77	
3(3,0)-2(2,0)	2-1	16632.8313	-5.18	
E_g				
$J'_{Ka',Kc'} \leftarrow J''_{Ka'',Kc''}$	v/0 \leftarrow 0		v/1 \leftarrow 1	
	v/MHz	Δ v/kHz	v/MHz	Δ v/kHz
μ_a -transitions				
3(0,3)-2(0,2)	9323.5089	-0.65	9324.0654	-0.72
3(1,2)-2(1,1)	9698.4878	-3.29	9699.1617	-2.78
3(1,3)-2(1,2)	9088.2783	0.78	9088.8270	0.81
3(2,2)-2(2,1)	9406.6607	0.67	9407.3284	2.28
4(0,4)-3(0,3)	12343.0562	-1.11	12343.7625	-1.98
4(1,3)-3(1,2)	12903.2311	0.77	12904.1159	-0.43
4(1,4)-3(1,3)	12096.0153	3.61	12096.7429	3.36
4(2,2)-3(2,1)	12724.7986	-2.56	12725.8264	1.6
4(2,3)-3(2,2)	12525.6934	-1.62	12526.6398	-8.3
4(3,1)-3(3,0)	12588.8616	-7.88	12589.9297	2.7
4(3,2)-3(3,1)	12580.6366	0.3	12581.6876	0.17
5(0,5)-4(0,4)	15309.5120	2.09	15310.3712	3.2
5(1,4)-4(1,3)	16079.7426	2.59	16080.8274	4.54
5(1,5)-4(1,4)	15088.8246	1.06	15089.7371	4.03
5(2,3)-4(2,2)	15998.4100	-5.89	15999.7473	1.17
5(2,4)-4(2,3)	15630.7444	3.81	15632.0945	1.68
5(3,2)-4(3,1)	15765.3889	0.38	15766.7150	-6.16
5(3,3)-4(3,2)	15737.0056	-2.68	15738.3203	-1.1
6(1,6)-5(1,5)	18066.8487	-0.07	18067.9481	-4.57
μ_c -transitions				
2(2,0)-1(1,0)	10593.4172	2.33	10592.9365	1.41
2(2,1)-1(1,1)	10776.1186	-1.39	10775.6718	1.28
3(1,2)-2(0,2)	11493.1437	5.22	11493.5954	-8.07
3(2,1)-2(1,1)	13608.2613	0.24	13608.0416	1.88
3(3,0)-2(2,0)	16737.9192	-1.12	16737.0889	0.12
3(3,1)-2(2,1)	16757.6959	-5.04	16756.8779	-2.36
4(1,3)-3(0,3)	15072.8624	3.14	15073.6598	6.12
4(2,2)-3(1,2)	16634.5726	1.47	16634.7002	0.16

4(2,3)-3(1,3)	17552.9444	4.22	17553.1928	-0.47
---------------	------------	------	------------	-------

Table A3.11. Description of the structural relaxations taken into account in the flexible model calculations.

a) *Axial* species

$$\begin{aligned}
vp(10) &= 180. - 2.3 * \sin(xpi) \\
Vt(4) &= 98.4 + 3. * (1. - \cos(xpi)) \\
Vt(5) &= 107.3 + 2.6 * \sin(xpi) \\
Vt(6) &= 107.3 - 2.6 * \sin(xpi) \\
Vp(8) &= 61. + 4. * (1. - \cos(xpi)) \\
Vp(7) &= -61. - 4. * (1. - \cos(xpi)) \\
Vt(3) &= 110.1 - 3. * (1. - \cos(xpi)) \\
Vr(4) &= 2.9673 + 0.008 * (1. - \cos(xpi)) \\
Vp(16) &= 178.1 - 3.5 * (1. - \cos(xpi)) \\
Vp(18) &= -178.1 + 3.5 * (1. - \cos(xpi)) \\
Vp(15) &= 61.4 - 3.5 * (1. - \cos(xpi)) \\
Vp(17) &= -61.4 + 3.5 * (1. - \cos(xpi))
\end{aligned}$$

b) *Equatorial* species

$$\begin{aligned}
Vt(4) &= 141.8 + 2.8 * (1. - \cos(xpi)) \\
Vp(4) &= 180. - 2.5 * \sin(xpi) \\
Vt(5) &= 107.3 + 2.6 * \sin(xpi) \\
Vt(6) &= 107.3 - 2.6 * \sin(xpi) \\
Vp(8) &= 169.0 + 2.6 * (1. - \cos(xpi)) \\
Vp(7) &= -169.0 - 2.6 * (1. - \cos(xpi)) \\
Vt(3) &= 109.6 + -2.3 * (1. - \cos(xpi)) \\
vp(10) &= 180. + 2.3 * \sin(xpi) \\
Vp(16) &= 66.8 - 2.7 * (1. - \cos(xpi)) \\
Vp(18) &= -66.8 + 2.7 * (1. - \cos(xpi)) \\
Vp(15) &= -48.5 - 2.7 * (1. - \cos(xpi)) \\
Vp(17) &= 48.5 + 2.7 * (1. - \cos(xpi))
\end{aligned}$$

IV. Formic Acid-Dimethylether

Table A4.1. Experimental transition frequencies (ν , MHz) and observed – calculated values ($\Delta\nu$, kHz) of HCOOH-O(CH₃)₂ (parent species)

J'	Ka'	Kc'	J''	Ka''	Kc''	ν/MHz	$\Delta\nu/\text{KHz}$
2	1	2	1	1	1	7249.925	-6.2
2	0	2	1	0	1	7266.344	-0.7
2	1	1	1	1	0	7282.836	7.7
3	1	3	2	1	2	10874.73	-4.9
3	0	3	2	0	2	10899.24	-1.1
3	2	2	2	2	1	10899.3	-5.3
3	2	1	2	2	0	10899.59	0.6
3	1	2	2	1	1	10924.08	4.3
4	1	4	3	1	3	14499.34	1
4	0	4	3	0	3	14531.81	-2.1
4	2	3	3	2	2	14532.11	6.9
4	2	2	3	2	1	14532.8	-0.7
4	1	3	3	1	2	14565.14	2.9
5	1	5	4	1	4	18123.7	9
5	0	5	4	0	4	18163.94	-8.6
5	2	4	4	2	3	18164.65	3.2
5	2	3	4	2	2	18166.04	5.7
5	4	2	4	4	1	18164.2	2.5
5	4	1	4	4	0	18164.2	2.5
5	3	3	4	3	2	18164.74	-7.9
5	3	2	4	3	1	18164.74	-12.7
5	1	4	4	1	3	18205.93	-4.3

Table A4.2. Experimental transition frequencies (ν , MHz) and observed – calculated values ($\Delta\nu$, kHz) of HCOOH-¹³CH₃OCH₃.

J'	Ka'	Kc'	J''	Ka''	Kc''	ν/MHz	$\Delta\nu/\text{KHz}$
2	1	2	1	1	1	7171.575	-5.8
2	0	2	1	0	1	7180.245	3.9
2	1	1	1	1	0	7188.889	-0.5
3	1	3	2	1	2	10757.23	-8.4
3	0	3	2	0	2	10770.2	4.3
3	1	2	2	1	1	10783.2	2.4
4	0	4	3	0	3	14359.96	5
5	1	5	4	1	4	17928.03	7.4
5	0	5	4	0	4	17949.44	-8.1
5	1	4	4	1	3	17971.29	-1.3

Table A4.3. Experimental transition frequencies (ν , MHz) and observed – calculated values ($\Delta\nu$, kHz) of H¹³COOH-CH₃OCH₃.

J'	Ka'	Kc'	J''	Ka''	Kc''	ν/MHz	$\Delta\nu/\text{KHz}$
2	1	2	1	1	1	7152.913	-2.4
2	0	2	1	0	1	7168.867	3
2	1	1	1	1	0	7184.883	8.3
3	1	3	2	1	2	10729.21	-8.5
3	0	3	2	0	2	10753.03	-2.3
3	1	2	2	1	1	10777.16	2.7
4	0	4	3	0	3	14336.89	0.3

5	1	5	4	1	4	17881.21	5.9
5	0	5	4	0	4	17920.32	0.1
5	1	4	4	1	3	17961.09	-5.1

Table A4.4. Experimental transition frequencies (ν , MHz) and observed – calculated values ($\Delta\nu$, kHz) of HCOOD-CH₃OCH₃.

J'	Ka'	Kc'	J''	Ka''	Kc''	ν/MHz	$\Delta\nu/\text{KHz}$
2	0	2	1	0	1	7248.354	-6.4
2	1	1	1	1	0	7270.392	-13.5
3	1	3	2	1	2	10839.52	-7.8
3	0	3	2	0	2	10872.14	-5.4
3	1	2	2	1	1	10905.41	-6.6
4	1	4	3	1	3	14452.36	2.1
4	0	4	3	0	3	14495.45	0.1
4	1	3	3	1	2	14540.18	0.1
5	1	5	4	1	4	18064.88	5.5
5	0	5	4	0	4	18118.12	-3.3
5	1	4	4	1	3	18174.64	5.8
3	2	2	2	2	1	10872.4	1.6
3	2	1	2	2	0	10872.86	-8.4
4	2	3	3	2	2	14496.19	-0.6
4	2	2	3	2	1	14497.38	-0.7
5	2	4	4	2	3	18119.7	5
5	2	3	4	2	2	18122.08	15.2

Table A4.5. Experimental transition frequencies (ν , MHz) and observed – calculated values ($\Delta\nu$, kHz) of DCOOH-CH₃OCH₃.

J'	Ka'	Kc'	F'	J''	Ka''	Kc''	F''	ν/MHz	$\Delta\nu/\text{KHz}$
2	0	2	2	1	0	1	1	7034.117	-2.8
2	1	1	1	1	1	0	0	7049.545	1
2	1	1	3	1	1	0	2	7049.61	12.6
2	1	1	2	1	1	0	1	7049.644	-4
2	1	2	3	1	1	1	2	7018.677	2.6
2	1	2	2	1	1	1	1	7018.727	1.5
3	0	3	4	2	0	2	3	10550.94	0.6
3	0	3	3	2	0	2	2	10550.95	14.1
3	0	3	2	2	0	2	1	10550.95	6
3	1	3	4	2	1	2	3	10527.88	-0.3
3	1	3	2	2	1	2	1	10527.88	-1
3	1	3	3	2	1	2	2	10527.9	6.6
3	1	2	4	2	1	1	3	10574.25	-3.2
3	1	2	2	2	1	1	1	10574.25	-3.1
3	1	2	3	2	1	1	2	10574.27	-0.2
3	2	2	4	2	2	1	3	10550.93	-19.4
4	0	4	5	3	0	3	4	14067.46	-1.3
4	0	4	4	3	0	3	3	14067.46	-2.5
4	0	4	3	3	0	3	2	14067.46	-0.2
4	1	3	5	3	1	2	4	14098.74	0.5
4	1	3	3	3	1	2	2	14098.74	6.3
4	1	3	4	3	1	2	3	14098.74	1.8
4	1	4	5	3	1	3	4	14036.92	4
4	1	4	3	3	1	3	2	14036.92	1.6
4	1	4	4	3	1	3	3	14036.92	-2.6
4	2	2	5	3	2	1	4	14068.29	-5.3
4	2	2	4	3	2	1	3	14068.31	-4.7

5	0	5	6	4	0	4	5	17583.6	3.1
5	0	5	5	4	0	4	4	17583.6	2.2
5	0	5	4	4	0	4	3	17583.6	0.3
5	1	4	6	4	1	3	5	17622.98	3.3
5	1	4	5	4	1	3	4	17622.98	-0.2
5	1	5	6	4	1	4	5	17545.72	2.3
5	1	5	4	4	1	4	3	17545.72	0.4
5	1	5	5	4	1	4	4	17545.72	-1.3

V. Formic Acid and Cyclobutanone

Table A5.1. Measured line frequencies (v/MHz) and observed-calculated values (Δv /kHz) of HCOOH-CBU.

N	J'	K_a'	K_c'	v'	J''	K_a''	K_c''	v''	v/MHz	Δv /kHz
1	4	0	4	1	3	0	3	1	7279.7897	-5.3
2	4	0	4	0	3	0	3	0	7278.5599	3.4
3	4	1	4	1	3	1	3	1	7017.0642	1.8
4	4	1	4	0	3	1	3	0	7026.9827	8.0
5	4	1	3	1	3	1	2	1	7608.7788	-1.4
6	4	1	3	0	3	1	2	0	7619.3977	-4.4
7	4	2	2	1	3	2	1	1	7373.0216	-6.4
8	4	2	2	0	3	2	1	0	7371.8964	0.8
9	4	2	3	1	3	2	2	1	7324.9138	-5.5
10	4	2	3	0	3	2	2	0	7323.7302	4.4
11	5	0	5	1	4	0	4	1	9064.1524	-2.4
12	5	0	5	0	4	0	4	0	9062.5619	4.9
13	5	1	5	1	4	1	4	1	8780.1124	-7.4
14	5	1	5	0	4	1	4	0	8775.0086	6.1
15	5	1	4	1	4	1	3	1	9501.0683	-2.7
16	5	1	4	0	4	1	3	0	9496.8392	5.4
17	5	2	4	1	4	2	3	1	9150.1847	-4.8
18	5	2	4	0	4	2	3	0	9148.5579	3.3
19	5	2	3	1	4	2	2	1	9245.4086	-4.0
20	5	2	3	0	4	2	2	0	9243.9018	3.3
21	6	0	6	1	5	0	5	1	10826.8385	-0.4
22	6	0	6	0	5	0	5	0	10824.8584	3.1
23	6	1	6	1	5	1	5	1	10520.7594	-5.4
24	6	1	6	0	5	1	5	0	10517.8301	3.9
25	6	1	5	1	5	1	4	1	11386.1088	-0.6
26	6	1	5	0	5	1	4	0	11384.2211	2.0
27	6	2	5	1	5	2	4	1	10971.7377	-6.1
28	6	2	5	0	5	2	4	0	10969.2396	6.3
29	6	2	4	0	5	2	3	0	11132.9333	0.2
30	6	2	4	1	5	2	3	1	11135.2304	-5.8
31	7	0	7	1	6	0	6	1	12566.5864	2.5
32	7	0	7	0	6	0	6	0	12564.1892	1.0
33	7	1	7	1	6	1	6	1	12257.8812	1.1
34	7	1	7	0	6	1	6	0	12254.9125	2.7
35	7	1	6	1	6	1	5	1	13261.8654	-1.3
36	7	1	6	0	6	1	5	0	13260.1086	-1.5
37	7	2	6	1	6	2	5	1	12789.9384	-2.7
38	7	2	6	0	6	2	5	0	12784.8966	4.4
39	7	2	5	0	6	2	4	0	13038.2176	2.0
40	7	2	5	1	6	2	4	1	13042.9435	0.9
41	8	1	8	1	7	1	7	1	13989.2216	3.7
42	8	1	8	0	7	1	7	0	13985.9480	0.3
43	8	1	7	1	7	1	6	1	15126.0221	2.7
44	8	1	7	0	7	1	6	0	15124.1189	-4.1
45	8	2	6	1	7	2	5	1	14966.6261	0.8
46	8	2	6	0	7	2	5	0	14944.1480	-4.5
47	8	2	7	0	7	2	6	0	14594.7261	2.2
48	8	2	7	1	7	2	6	1	14617.6611	2.3

49	9	0	9	1	8	0	8	1	15983.5382	5.0
50	9	0	9	0	8	0	8	0	15980.2385	-6.1
51	9	1	9	1	8	1	8	1	15714.5178	4.8
52	9	1	9	0	8	1	8	0	15710.8593	-7.5
53	9	1	8	1	8	1	7	1	16975.9494	4.8
54	9	1	8	0	8	1	7	0	16973.8181	-5.7
55	9	2	8	1	8	2	7	1	16350.4797	0.7
56	9	2	8	0	8	2	7	0	16398.0087	-2.4
57	9	2	7	0	8	2	6	0	16950.2037	-1.5
58	9	2	7	1	8	2	6	1	16902.0546	4.9
59	10	0	10	1	9	0	9	1	17668.7085	12.0
60	10	0	10	0	9	0	9	0	17664.9263	-10.7
61	10	1	10	1	9	1	9	1	17433.8730	9.5
62	10	1	10	0	9	1	9	0	17429.7979	-12.0
63	3	1	3	1	2	0	2	1	8302.5384	-10.6
64	3	1	3	0	2	0	2	0	8297.6474	3.7
65	4	1	4	1	3	0	3	1	9842.7974	-3.0
66	4	1	4	0	3	0	3	0	9848.7145	3.5
67	5	1	5	1	4	0	4	1	11343.1152	-9.9
68	5	1	5	0	4	0	4	0	11345.1613	4.3
69	6	1	6	1	5	0	5	1	12799.7275	-7.6
70	6	1	6	0	5	0	5	0	12800.4374	11.1
71	6	0	6	1	5	1	5	1	8547.8685	-0.1
72	6	0	6	0	5	1	5	0	8542.2551	-0.2
73	7	0	7	1	6	1	6	1	10593.6900	2.3
74	7	0	7	0	6	1	6	0	10588.6119	-5.4
75	3	1	2	1	2	0	2	0	10292.3525	-4.3
76	3	1	2	0	2	0	2	1	8041.2570	-0.7
77	4	1	3	1	3	0	3	0	12425.2303	0.8
78	4	1	3	0	3	0	3	1	10183.8584	9.6
79	2	2	1	0	1	1	0	0	13299.2176	3.9
80	2	2	1	1	1	1	0	1	13297.3366	3.2
81	2	2	0	0	1	1	1	0	13449.1731	1.4
82	2	2	0	1	1	1	1	1	13447.1083	4.4
83	2	2	1	0	1	1	1	1	12321.9640	-5.7
84	2	2	0	0	1	1	0	1	12181.8855	-7.2

Table A5.2. Measured line frequencies (ν /MHz) and observed-calculated values ($\Delta\nu$ /kHz) of DCOOH-CBU.

N	J'	K_a'	K_c'	ν'	J''	K_a''	K_c''	ν''	ν /MHz	$\Delta\nu$ /kHz
1	4	0	4	1	3	0	3	1	7096.5666	-3.0
2	4	0	4	0	3	0	3	0	7095.4035	6.0
3	4	1	4	1	3	1	3	1	6844.4701	-1.4
4	4	1	4	0	3	1	3	0	6853.8341	2.8
5	4	1	3	1	3	1	2	1	7408.2407	4.1
6	4	1	3	0	3	1	2	0	7418.2460	-3.4
7	5	0	5	1	4	0	4	1	8838.3997	-2.2
8	5	0	5	0	4	0	4	0	8836.8973	4.9
9	5	1	5	1	4	1	4	1	8564.4200	-7.1
10	5	1	5	0	4	1	4	0	8559.3704	5.2
11	5	1	4	1	4	1	3	1	9251.3639	-1.1
12	5	1	4	0	4	1	3	0	9247.1122	-0.4
13	5	2	4	1	4	2	3	1	8916.3803	-4.9
14	5	2	4	0	4	2	3	0	8914.8548	3.7
15	5	2	3	1	4	2	2	1	9002.7076	-2.9

16	5	2	3	0	4	2	2	0	9001.2854	2.5
17	6	0	6	1	5	0	5	1	10560.3784	-4.1
18	6	0	6	0	5	0	5	0	10558.5161	4.4
19	6	1	6	1	5	1	5	1	10262.9303	-6.2
20	6	1	6	0	5	1	5	0	10260.1505	6.1
21	6	1	5	1	5	1	4	1	11087.9781	1.7
22	6	1	5	0	5	1	4	0	11086.1464	-2.1
23	7	0	7	1	6	0	6	1	12261.1035	0.2
24	7	0	7	0	6	0	6	0	12258.8492	1.6
25	7	1	7	1	6	1	6	1	11958.4514	-7.4
26	7	1	7	0	6	1	6	0	11955.6587	3.9
27	7	1	6	1	6	1	5	1	12916.2732	3.0
28	7	1	6	0	6	1	5	0	12914.5808	-1.8
29	9	0	9	1	8	0	8	1	15603.0404	7.2
30	9	0	9	0	8	0	8	0	15599.9425	-2.3
31	9	1	9	1	8	1	8	1	15333.2655	7.6
32	9	1	9	0	8	1	8	0	15329.8211	-4.8
33	9	1	8	1	8	1	7	1	16539.4154	7.7
34	9	1	8	0	8	1	7	0	16537.3740	-7.8
35	10	0	10	1	9	0	9	1	17250.8947	2.6
36	10	0	10	0	9	0	9	0	17247.3539	-10.1
37	10	1	10	1	9	1	9	1	17012.2929	11.0
38	10	1	10	0	9	1	9	0	17008.4604	-8.4
39	3	1	3	1	2	0	2	1	8192.4925	0.9
40	3	1	3	0	2	0	2	0	8188.1869	-4.3
41	4	1	4	1	3	0	3	1	9699.1692	3.3
42	4	1	4	0	3	0	3	0	9705.0794	-2.3
43	5	1	5	1	4	0	4	1	11167.0127	-10.6
44	5	1	5	0	4	0	4	0	11169.0557	6.3
45	6	1	6	1	5	0	5	1	12591.5526	-5.3
46	6	1	6	0	5	0	5	0	12592.3098	8.4
47	6	0	6	1	5	1	5	1	8231.7545	-6.6
48	6	0	6	0	5	1	5	0	8226.3572	2.5
49	7	0	7	1	6	1	6	1	10229.9241	-3.8
50	7	0	7	0	6	1	6	0	10225.0630	5.0
51	3	1	2	1	2	0	2	0	10103.5147	4.3
52	3	1	2	0	2	0	2	1	7929.4514	-4.3
53	4	1	3	1	3	0	3	0	12174.8025	-3.8
54	4	1	3	0	3	0	3	1	10009.9125	4.7

Table A5.3. Measured line frequencies (v/MHz) and observed-calculated values (Δv /kHz) of HCOOD-CBU.

N	J'	K_a'	K_c'	v'	J''	K_a''	K_c''	v''	v/MHz	Δv /kHz
1	4	0	4	1	3	0	3	1	7240.6720	-6.0
2	4	0	4	0	3	0	3	0	7239.3814	0.7
3	4	1	4	1	3	1	3	1	6977.1175	5.2
4	4	1	4	0	3	1	3	0	6988.0793	6.7
5	4	1	3	1	3	1	2	1	7570.0873	-1.7
6	4	1	3	0	3	1	2	0	7581.7734	-6.6
7	4	2	2	1	3	2	1	1	7334.7673	3.8
8	4	2	2	0	3	2	1	0	7333.5878	10.4
9	4	2	3	1	3	2	2	1	7286.2186	1.3
10	4	2	3	0	3	2	2	0	7284.9803	10.4
11	5	0	5	1	4	0	4	1	9014.9450	-5.2
12	5	0	5	0	4	0	4	0	9013.2831	4.5

13	5	1	5	1	4	1	4	1	8732.8518	-6.6
14	5	1	5	0	4	1	4	0	8726.3019	3.0
15	5	1	4	1	4	1	3	1	9452.6176	2.7
16	5	1	4	0	4	1	3	0	9446.9658	4.1
17	5	2	4	1	4	2	3	1	9101.7470	-9.4
18	5	2	4	0	4	2	3	0	9100.0595	-0.3
19	5	2	3	1	4	2	2	1	9197.8209	-9.6
20	5	2	3	0	4	2	2	0	9196.2569	1.5
21	6	0	6	1	5	0	5	1	10767.3934	-1.0
22	6	0	6	0	5	0	5	0	10765.3254	3.6
23	6	1	6	1	5	1	5	1	10462.4631	-4.3
24	6	1	6	0	5	1	5	0	10459.2894	7.1
25	6	1	5	1	5	1	4	1	11327.8150	1.4
26	6	1	5	0	5	1	4	0	11325.7118	3.3
27	6	2	5	1	5	2	4	1	10913.5231	-5.5
28	6	2	5	0	5	2	4	0	10910.9671	1.4
29	6	2	4	0	5	2	3	0	11076.0979	2.5
30	6	2	4	1	5	2	3	1	11078.4445	-5.3
31	7	0	7	1	6	0	6	1	12496.7878	-0.9
32	7	0	7	0	6	0	6	0	12494.2924	4.1
33	7	1	7	1	6	1	6	1	12189.6260	2.0
34	7	1	7	0	6	1	6	0	12186.4884	0.0
35	7	1	6	1	6	1	5	1	13193.6314	1.0
36	7	1	6	0	6	1	5	0	13191.7407	-4.8
37	7	2	6	1	6	2	5	1	12721.7689	-0.7
38	7	2	6	0	6	2	5	0	12716.8082	-0.4
39	7	2	5	0	6	2	4	0	12972.3787	-2.1
40	7	2	5	1	6	2	4	1	12977.0177	-0.1
41	8	1	8	1	7	1	7	1	13911.0488	4.5
42	8	1	8	0	7	1	7	0	13907.6116	-4.7
43	8	1	7	1	7	1	6	1	15047.7112	0.4
44	8	1	7	0	7	1	6	0	15045.6991	-0.1
45	8	2	6	1	7	2	5	1	14891.5405	-2.9
46	8	2	6	0	7	2	5	0	14872.5905	-4.3
47	8	2	7	0	7	2	6	0	14516.7717	0.4
48	8	2	7	1	7	2	6	1	14536.1917	5.9
49	9	0	9	1	8	0	8	1	15893.0466	7.6
50	9	0	9	0	8	0	8	0	15889.6060	-6.2
51	9	1	9	1	8	1	8	1	15626.4200	7.4
52	9	1	9	0	8	1	8	0	15622.5911	-9.4
53	9	1	8	1	8	1	7	1	16887.4043	6.0
54	9	1	8	0	8	1	7	0	16885.1519	-7.5
55	9	2	8	1	8	2	7	1	16261.7211	2.6
56	9	2	8	0	8	2	7	0	16310.1263	-3.2
57	9	2	7	0	8	2	6	0	16866.7305	2.3
58	9	2	7	1	8	2	6	1	16817.6915	3.8
59	4	1	4	1	3	0	3	1	9774.4162	-4.9
60	4	1	4	0	3	0	3	0	9782.0535	0.5
61	5	1	5	1	4	0	4	1	11266.5972	-4.3
62	5	1	5	0	4	0	4	0	11268.9754	4.2
63	6	1	6	1	5	0	5	1	12714.1154	-3.2
64	6	1	6	0	5	0	5	0	12714.9757	0.8
65	6	0	6	1	5	1	5	1	8515.7388	-4.3
66	6	0	6	0	5	1	5	0	8509.6303	1.0
67	7	0	7	1	6	1	6	1	10550.0638	-0.6
68	7	0	7	0	6	1	6	0	10544.6347	-0.6

69	4	1	3	1	3	0	3	0	12416.6010	1.9
70	4	1	3	0	3	0	3	1	10061.7668	0.8
71	2	2	1	0	1	1	0	0	13196.3426	1.6
72	2	2	1	1	1	1	0	1	13194.4037	1.9
73	2	2	0	0	1	1	1	0	13346.3847	-4.1
74	2	2	0	1	1	1	1	1	13344.2574	0.7

Table A5.4. B3LYP-D3/6-311++G(d,p) cartesian coordinates of the HCOOH-CBU atoms in the principal axes of inertia.

ATOM	$a / \text{\AA}$	$b / \text{\AA}$	$c / \text{\AA}$
C	2.7146	0.3856	-0.0477
O	1.9302	1.2197	-0.4327
O	2.4242	-0.8644	0.2959
O	-0.2479	-1.3883	-0.0700
C	-1.1143	-0.5510	0.0203
C	-2.5820	-0.5312	-0.3943
C	-2.6426	0.9556	0.0830
C	-1.1539	0.8774	0.5468
H	3.7927	0.5710	0.0684
H	1.4554	-1.0366	0.1813
H	-2.7418	-0.7167	-1.4594
H	-3.1933	-1.2379	0.1738
H	-2.8133	1.6685	-0.7230
H	-3.3598	1.1446	0.8810
H	-0.4315	1.5322	0.0557
H	-0.9881	0.9368	1.6265

Table A5.5. B3LYP-D3/6-311++G(d,p) cartesian coordinates of the transition state of the cluster HCOOH-CBU in the principal axes of inertia.

ATOM	$a / \text{\AA}$	$b / \text{\AA}$	$c / \text{\AA}$
C	-2.7529	0.3591	0
O	-2.4575	-0.936	0
O	-1.9581	1.2686	0
H	-1.4748	-1.0601	0
H	-3.8438	0.5014	0
O	0.2567	-1.3701	0
C	1.1238	-0.5285	0
C	1.1311	0.9954	0
C	2.6911	0.9411	0
C	2.6463	-0.6206	0
H	3.1543	1.3733	0.8865
H	3.154	1.3732	-0.8866
H	3.0496	-1.1185	0.8859
H	3.0493	-1.1179	-0.8863
H	0.6467	1.4318	0.8758
H	0.648	1.4302	-0.8773

VI Indan-CHF₃

Table A6.1. Experimental transition frequencies (ν , MHz) and observed-calculated values of ($\Delta\nu$, kHz).

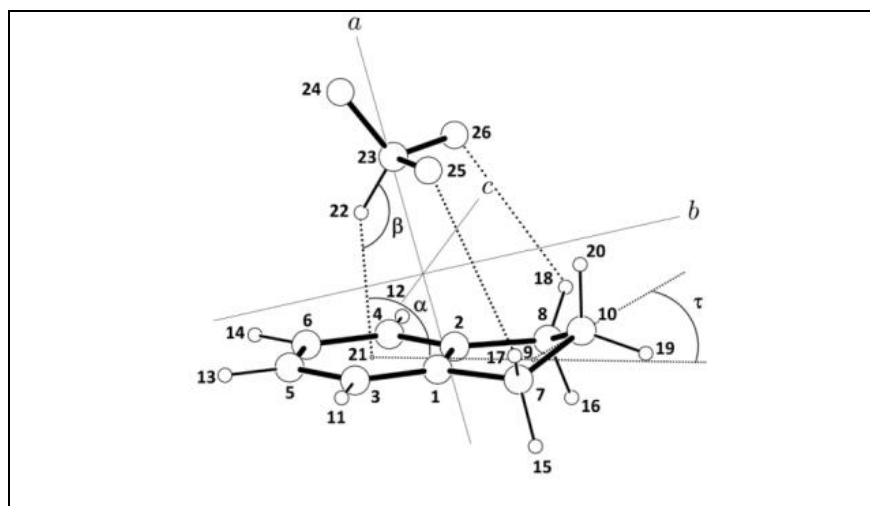
	Indan-CHF ₃		Indan-CDF ₃	
$J''_{Ka'',Kc''} \leftarrow J'_{Ka',Kc'}$ "	ν /MHz	$\Delta\nu$ /kHz z	ν /MHz	$\Delta\nu$ /kHz z
μ_a -transitions				
6(0,6)-5(0,5)	6575.5714	0.2		
6(1,5)-5(1,4)	7085.3504	1.8		
6(2,4)-5(2,3)	7402.7654	-0.5		
6(3,4)-5(3,3)	7131.1717	1.7		
6(3,3)-5(3,2)	7326.5964	0.3		
6(4,3)-5(4,2)	7160.4023	0.4		
6(4,2)-5(4,1)	7182.0688	1.9		
7(0,7)-6(0,6)	7628.3283	0.3	7619.3456	0.3
7(1,7)-6(1,6)	7622.4642	0.1	7613.5173	0.2
7(1,6)-6(1,5)			8118.3492	-2.8
7(2,6)-6(2,5)	8030.0190	0.3	8021.2477	-1.2
7(2,5)-6(2,4)	8578.2707	0.9	8569.8256	0.9
7(3,5)-6(3,4)	8294.4778	-0.2	8286.1206	0.1
7(3,4)-6(3,3)	8625.5992	-0.3	8618.0468	1.5
7(4,4)-6(4,3)	8367.7886	0.7	8359.7457	-0.1
7(4,3)-6(4,2)	8433.3412	-1.6	8425.6651	0.0
7(5,3)-6(5,2)	8350.4115	2.8	8342.4013	1.7
7(5,2)-6(5,1)	8354.5110	2.7	8346.5297	-2.0
8(0,8)-7(0,7)	8683.6112	-0.4	8673.3598	1.0
8(1,8)-7(1,7)	8681.3325	-0.2	8671.0966	-0.1
8(1,7)-7(1,6)	9162.1520	-1.5	9151.7690	0.1
8(2,7)-7(2,6)	9109.3540	0.2	9099.2373	1.4
8(2,6)-7(2,5)	9691.7727	-2.4	9681.6850	-0.5
8(3,6)-7(3,5)	9435.7356	0.3	9426.0206	0.0
8(3,5)-7(3,4)	9899.6445	0.8	9890.7303	0.5
8(4,5)-7(4,4)	9568.9748	-1.6	9559.7156	-2.3
8(4,4)-7(4,3)	9721.8849	-2.7	9713.3684	-1.9
8(5,4)-7(5,3)	9565.2457	-2.2	9556.1335	0.7
8(5,3)-7(5,2)	9580.7158	-3.1	9571.7216	-1.4
8(6,3)-7(6,2)	9536.0009	3.9		
8(6,2)-7(6,1)	9536.6620	-2.0		
9(0,9)-8(0,8)	9740.0619	-0.4	9728.5354	0.6
9(1,9)-8(1,8)	9739.2128	1.4	9727.6918	0.7
9(1,8)-8(1,7)	10203.3359	1.5	10191.7193	-0.6
9(2,8)-8(2,7)	10178.0828	-1.0	10166.6347	0.9
9(2,7)-8(2,6)	10748.0249	-3.4	10736.3199	-0.9
9(3,7)-8(3,6)	10553.8109	-0.3	10542.7021	0.4
9(3,6)-8(3,5)	11123.8820	-0.3	11113.3975	-1.1
9(4,6)-8(4,5)	10756.2154	0.7	10745.6661	3.3
9(4,5)-8(4,4)	11040.1665	-0.9	11030.7105	-0.5
9(5,5)-8(5,4)	10783.4381	1.4	10773.1937	0.1
9(5,4)-8(5,3)	10829.3415	1.3	10819.4340	1.8
10(0,10)-9(0,9)	10796.9930	0.1		
10(1,10)-9(1,9)	10796.6840	-0.3		

10(1,9)-9(1,8)	11251.6951	0.0		
10(2,9)-9(2,8)	11240.5776	5.4		
10(2,8)-9(2,7)	11774.0743	-1.5		
10(3,8)-9(3,7)	11650.8023	-0.7		
10(3,7)-9(3,6)	12283.9047	1.1		
10(4,7)-9(4,6)	11922.9839	0.3		
10(4,6)-9(4,5)	12356.1758	-1.0		
10(5,6)-9(5,5)	11999.6012	-0.8		
10(5,5)-9(5,4)	12111.1448	-1.7		
11(0,11)-10(0,10)	11854.1013	-1.1		
11(1,11)-10(1,10)	11853.9911	-1.8		
11(1,10)-10(1,9)	12304.4788	1.8		
11(2,10)-10(2,9)	12299.8447	-0.8		
11(2,9)-10(2,8)	12798.6586	0.4		
11(3,9)-10(3,8)	12731.1720	-1.5		
11(3,8)-10(3,7)	13374.1759	1.8		
11(4,8)-10(4,7)	13065.5074	0.3		
11(4,7)-10(4,6)	13633.0821	0.5		
11(5,6)-10(5,5)	13431.0043	2.1		
12(0,12)-11(0,11)	12911.2646	-1.4		
12(1,12)-11(1,11)	12911.2290	1.1		
12(1,11)-11(1,10)	13359.4944	-1.0		
12(2,11)-11(2,10)	13357.6458	1.5		
μ_b -transitions				
5(4,2)-4(3,1)	8344.8972	-1.5		
5(4,1)-4(3,2)	8383.4928	0.1		
6(3,4)-5(2,3)	8387.2527	1.7		
6(3,3)-5(2,4)	9426.9536	-0.7		
6(4,3)-5(3,2)	9466.7034	-0.4		
6(4,2)-5(3,3)	9615.4172	-1.6		
6(5,1)-5(4,2)	10251.3022	1.6		
7(0,7)-6(1,6)	7618.8574	-1.1	7609.9419	1.6
7(1,7)-6(0,6)	7631.9334	-0.2	7622.9225	0.4
7(1,6)-6(2,5)	7933.2175	-1.0		
7(2,6)-6(1,5)	8224.2613	1.7		
7(3,5)-6(2,4)	9278.9594	-3.7		
7(4,4)-6(3,3)	10507.8961	0.5		
7(4,3)-6(3,4)	10917.5905	-1.0		
7(5,3)-6(4,2)	11413.0567	2.0		
7(5,2)-6(4,3)	11445.4059	-1.1		
7(6,2)-6(5,1)	12130.1779	-1.6		
7(6,1)-6(5,2)	12131.1495	3.5		
7(7,1)-6(6,0)	12826.0225	2.7	12813.0934	-0.9
7(7,0)-6(6,1)			12813.1058	1.5
8(0,8)-7(1,7)	8680.0090	3.1	8669.7817	-0.4
8(1,8)-7(0,7)	8684.9373	-1.1	8674.6746	1.1
8(1,7)-7(2,6)	9065.3532	0.0		
8(2,7)-7(1,6)	9206.1537	-0.3		
8(4,4)-7(3,5)	12345.0024	1.3		
8(5,4)-7(4,3)	12544.9544	-5.5		
8(5,3)-7(4,4)	12658.3388	0.8		
8(6,3)-7(5,2)	13311.6717	3.5		
8(6,2)-7(5,3)	13317.4012	0.0		
8(8,1)-7(7,0)			14693.0630	0.4
8(8,0)-7(7,1)			14693.0630	-0.7
9(0,9)-8(1,8)	9738.7362	0.7	9727.2170	-3.1

9(1,9)-8(0,8)	9740.5378	-0.4		9729.0058	0.1
9(1,8)-8(2,7)	10159.3337	-0.2			
9(2,8)-8(1,7)	10222.0839	-0.4			
9(2,7)-8(3,6)	10303.3736	-1.2			
9(8,2)-8(7,1)	15894.8426	-3.0			
9(8,1)-8(7,2)	15894.8616	-0.1			
9(9,1)-8(8,0)				16573.0029	-0.1
9(9,0)-8(8,1)				16573.0029	-0.2
10(1,9)-9(2,8)	11232.9457	0.5			
10(2,9)-9(1,8)	11259.3208	-1.3			
11(1,10)-10(2,9)	12296.8511	1.1			
11(2,10)-10(1,9)	12307.4728	0.4			

Table A6.2. MP2/6-311++G** optimized geometry of Indan-CHF3

Bond lengths / Å		Valence angles / °		Dihedral angles / °	
C2C1	1.4056				
C3C1	1.3987	C3C1C2	120.5		
C4C2	1.3987	C4C2C1	120.5	C4C2C1C3	0
C5C1	1.4033	C5C1C1	119.0	C5C3C1C2	-0.4
C6C4	1.4033	C6C4C2	119.0	C6C4C2C1	0.4
C7C1	1.5117	C7C1C2	110.1	C7C1C2C4	179.4
C8C2	1.5117	C8C2C1	110.1	C8C2C1C3	-179.4
X9C7	1.2229	X9C7C1	69.9	X9C7C1C2	0
C10X9	0.9436	C10X9C7	90.0	C10X9C7C1	148.4
H11C3	1.0881	H11C3C1	120.7	H11C3C1C2	-179.8
H12C4	1.0881	H12C4C2	120.7	H12C4C2C1	179.8
H13C5	1.0871	H13C5C3	119.9	H13C5C3C1	-179.5
H14C6	1.0871	H14C6C4	119.9	H14C6C4C2	179.5
H15C7	1.0989	H15C7C1	109.8	H15C7C1C2	-98.5
H16C8	1.0989	H16C8C2	109.8	H16C8C2C1	98.5
H17C7	1.0944	H17C7C1	113.0	H17C7C1C2	141
H18C8	1.0944	H18C8C2	113.0	H18C8C2C1	-141
H19C10	1.0938	H19C10X9	112.9	H19C10X9C7	-153.3
H20C10	1.0948	H20C10X9	109.0	H20C10X9C7	86.3
X21C3	1.4135	X21C3C1	59.5	X21C3C1C2	0
H22X21	2.3166	H22X21C3	90.0	H22X21C3C1	-90.8
C23C22	1.0854	C23C22X21	146.7	C23C22X21C3	90
F24C23	1.3405	F24C23C22	110.9	F24C23C22X21	180
F25C23	1.342	F25C23C22	110.7	F25C23C22X21	-59.9
F26C23	1.342	F26C23C22	110.7	F26C23C22X21	59.9
Hydrogen bond parameters: $r_{H\cdots\pi} = 2.317$ Å; $r_{H17\cdots F25} = 3.204$ Å; $r_{H20\cdots F25} = 2.946$ Å; C7H17F25 = 99.7°; C10H20F25 = 124.9°					



VII. $[\text{CH}_2\text{F}_2]_m \cdots [\text{H}_2\text{O}]_n$ trimers and tetramers

A7.1 Protocol for computational screening.

- For each investigated cluster, a set of plausible configurations was prepared based on symmetry consideration and the possible favorable WHB networks allowed by the different dispositions. All the attempted starting conformation are separately displayed for DW2, D2W and D2W2 clusters in Figures A7.1, 7.3 and 7.5, respectively.
- To reduce the computational burden, a preliminary optimization for each chosen arrangement is carried out at B97D/aug-cc-pvDz level. From the resulting optimized structure, a further energy minimization was done with the larger aug-cc-pvTz basis set. Optimization with both basis sets were performed by minimizing all degrees of freedom without imposing any symmetry constrain.
- The resulting conformers were classified according to their structure (thus rotational constants) and according to their binding energies.
- The structure of the most stable conformers belonging to each class was further refined at MP2/6-311++G** level. It might be important to recall that the B97D functional was validated in previous work against high level CCSD(T) data, but its accuracy was assessed only for CH_2F_2 clusters, while its ability to yield reliable results for complex involving water was not benchmarked. Considering the well-known dependence of DFT results on the adopted functiona, we resorted to the wave-function based MP2 method, which has been successfully adopted in previous studies of WHBs.
- Finally, the MP2 optimized strucutres are collected, and their binding energy and structural data computed, again at MP2/6-311++G** level.

A7.2. Details of DW2 clusters

For the computational screening of DW2 clusters, five starting configurations were considered and subjected to the adopted protocol. All arrangements collapsed into two different classes, namely triangular or linear dispositions. Among these, the three most stable conformers are shown in Figure A7.2, where trimers I and III belong to the former class, while II, less stable, displays a quasi linear geometry. Both MP2 computed binding energies and rotational constants are reported in table A7.1. for all three conformers. It should be noted that cluster I and III have practically the same energy and are characterized by a very similar structure and WHB network. Yet,

they exhibit significantly different rotational constants and dipole moments, confirming the challenges that this kind of computational screening might encounter.

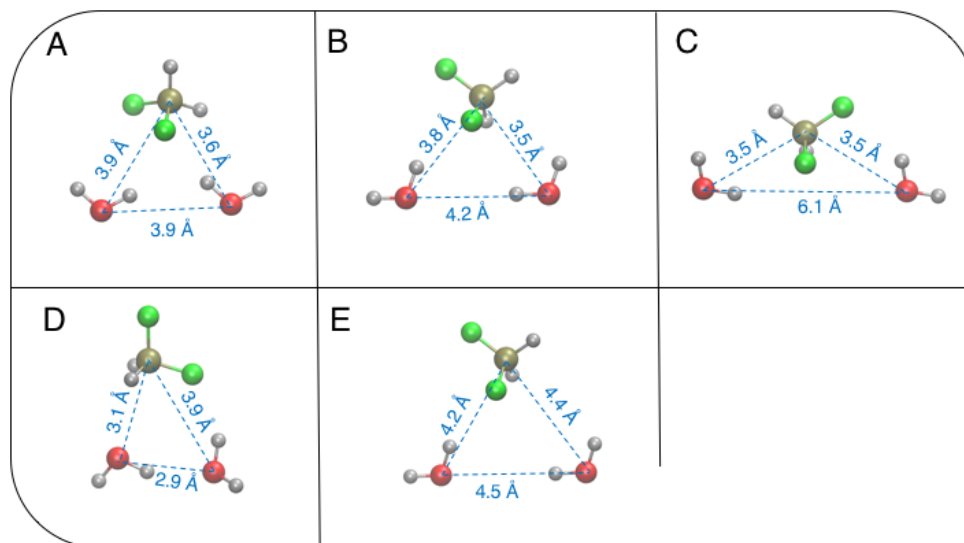


Figure A7.1. Starting structures for the $\text{CH}_2\text{F}_2 \cdots [\text{H}_2\text{O}]_2$ (DW2). The $\text{O} \cdots \text{O}$ and $\text{C} \cdots \text{O}$ distances that characterize the cluster structure are displayed with blue dashed lines.

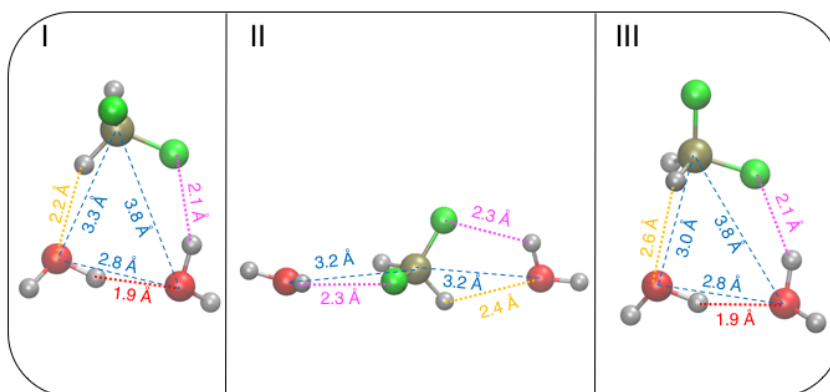


Figure A7.2. Most stable structures for **DW2** trimers. The $\text{O} \cdots \text{O}$ and $\text{C} \cdots \text{O}$ distances that characterize the cluster structure are displayed with blue dashed lines, whereas the different WHB, whose distance is less than 3.0 \AA , are evidenced with dotted lines in different colors (OH \cdots O red; O-H \cdots F magenta; C-H \cdots O orange).

Table A7.1. Relative energies ΔE (with respect to the most stable conformer), binding energies (BE), rotational constants (A, B and C) and electric dipole components (μ_A , μ_B , μ_C), computed for the most stable structures of **DW2** trimers shown in Figure A7.2. The best matching conformer is evidence on bold.

Cluster	ΔE	BE	A	B	C	μ_A	μ_B	μ_C
	kJ/mol	kJ/mol	MHz	MHz	MHz	D	D	D
I	0.0	-41.7	4441	1872	1456	-1.2	0.6	1.2
II	17.1	-25.1	8383	1238	1229	0.0	0.0	0.9
III	0.0	-41.7	5560	1736	1339	2.1	0.0	0.3

A7.3. Details of D2W cluster

For the computational screening of DW2 clusters, six starting configurations, displayed in Figure A7.3, were selected and optimized through the proposed screening protocol, and subjected to the adopted protocol. As for the DW2 trimer, all arrangements collapsed into two either triangular or linear dispositions. As done previously, the three most stable conformers are shown in Figure A7.4, but at difference with DW2, no D2W linear stable cluster was found, resulting instead into three different triangular conformers. MP2 computed binding energies and rotational constants of the three clusters are reported in table A7.2.

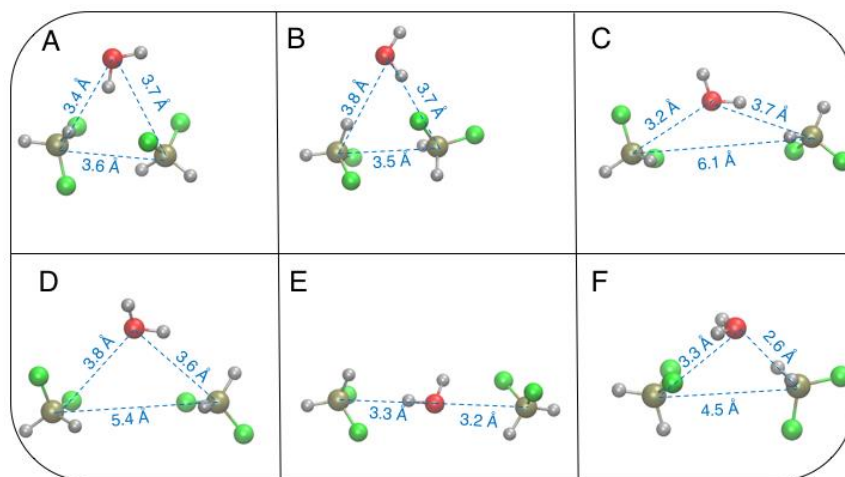
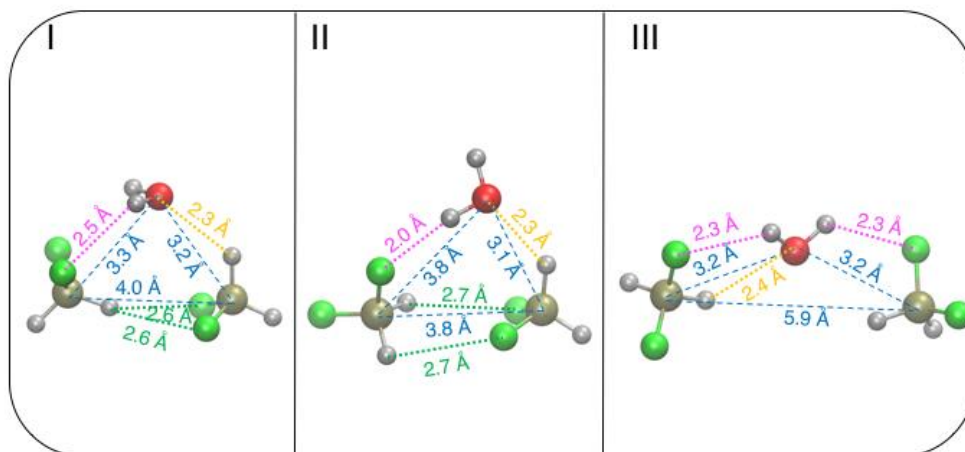


Figure A7.3 Starting structures for the $[\text{CH}_2\text{F}_2]_2 \cdots \text{H}_2\text{O}$ (**D2W**). The $\text{C} \cdots \text{C}$ and $\text{C} \cdots \text{O}$ distances that characterize the cluster structure are displayed with blue dashed lines.



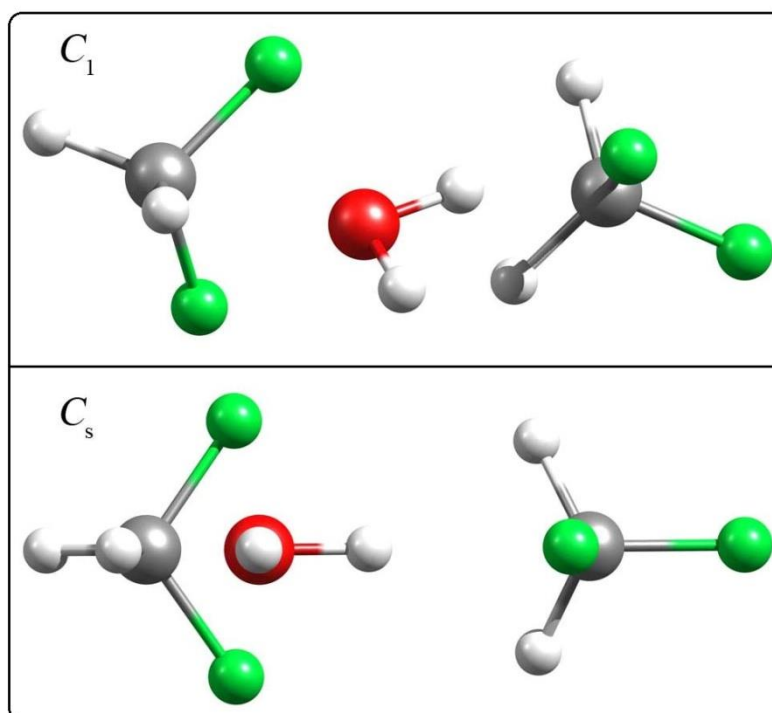


Figure A7.4. Most stable structures for D2W trimers. The C \cdots O and C \cdots C distances that characterize the cluster structure are displayed with blue dashed lines, whereas the different WHB, whose distance is less than 3.0 Å, are evidenced with dotted lines in different colors (O-H \cdots F magenta; C-H \cdots O orange; C-H \cdots F green).

Top views of C_1 and C_s symmetries of conformer II. With the respective energy E ($C_s - C_1$) = 80 cm $^{-1}$ (mp2), and 95 cm $^{-1}$ (b3lyp).

Table A7.2. Relative energies ΔE (with respect to the most stable conformer), binding energies (BE), rotational constants (A, B and C) and electric dipole components (μ_A , μ_B , μ_C), computed for the most stable structures of D2W trimers shown in Figure 7.4. The best matching conformer is evidence on bold.

Cluster		ΔE	BE	A	B	C	μ_A	μ_B	μ_C
		kcal/mol	kcal/mol	MHz	MHz	MHz	D	D	D
I		2.5	-24.7	2585	1056	1037	-0.5	-0.7	0.0
II	C_1	0.0	-28.0	2304	1103	874	1.6	0.4	-0.1
	C_s	0.2		2302	1095	863	1.9	-0.6	0.0
III		4.6	-23.4	4282	478	452	-0.6	0.4	2.2

A7.4. DETAILS ON D2W2 CLUSTERS

Eight different starting clusters were labeled A to H. The resulting optimized conformers were classified according to their structure and energies. It turned out all conformers can be grouped into four different classes, depending on their structure, namely tetrahedral, “bended”, planar and elongated. The two most stable conformer (I and II) belong to the first of the abovementioned classes (tetrahedral), and their structures are displayed in Figure A7.6.

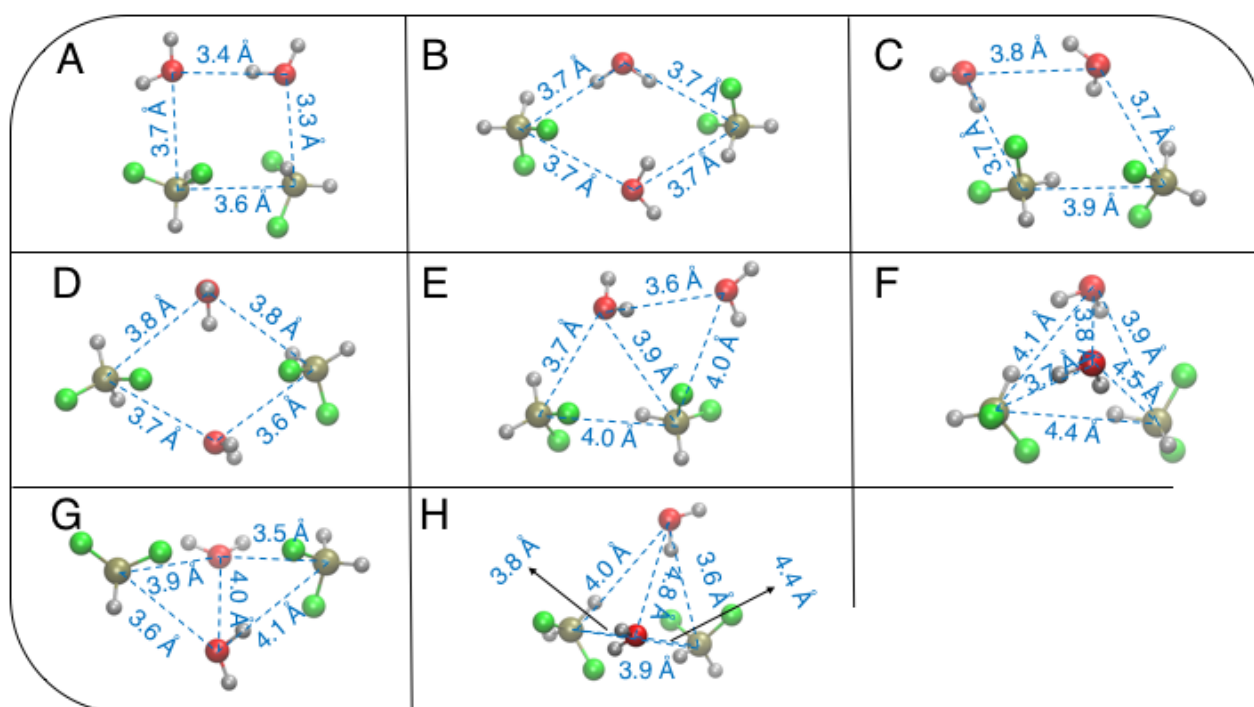


Figure A7.5. Starting structures for the $[\text{CH}_2\text{F}_2]_2 \cdots [\text{H}_2\text{O}]_2$ (**D2W2**). The $\text{O} \cdots \text{O}$, $\text{C} \cdots \text{C}$ and $\text{C} \cdots \text{O}$ distances that characterize the cluster structure are displayed with blue dashed lines.

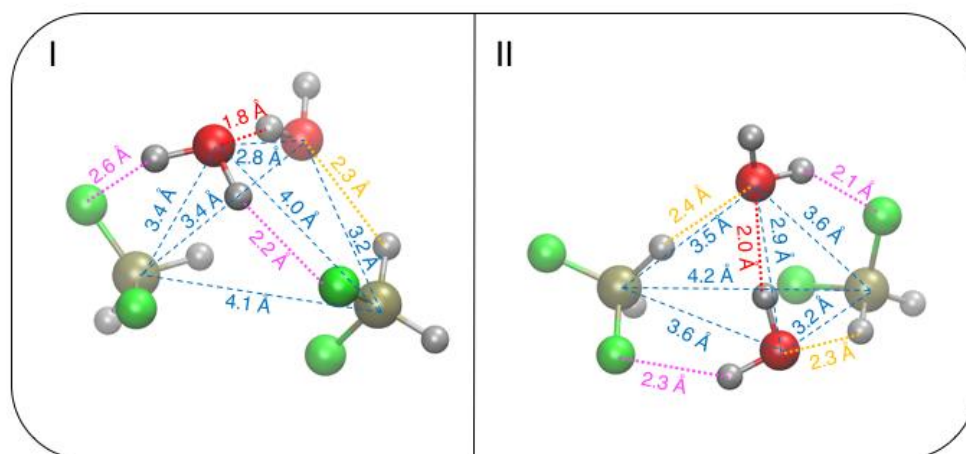


Figure A7.6. Most stable structures for **D2W2** tetramers. The $\text{O} \cdots \text{O}$, $\text{C} \cdots \text{O}$ and $\text{C} \cdots \text{C}$ distances that characterize the cluster structure are displayed with blue dashed lines, whereas the different WHB, whose distance is less than 3.0 \AA , are evidenced with dotted lines in different colors ($\text{OH} \cdots \text{O}$ red; $\text{O-H} \cdots \text{F}$ magenta; $\text{C-H} \cdots \text{O}$ orange; $\text{C-H} \cdots \text{F}$ green).

Table A7.3. Relative energies ΔE (with respect to the most stable conformer), binding energies (BE), rotational constants (A, B and C) and electric dipole components (μ_A , μ_B , μ_C), computed for the most stable structures of **D2W2** tetramers shown in Figure A7.6. The best matching conformer is evidence on bold.

Cluster	ΔE	BE	A	B	C	μ_A	μ_B	μ_C
	kJ/mol	kJ/mol	MHz	MHz	MHz	D	D	D
I	0.0	-54.0	1665	950	834	0.8	1.0	-1.4

II	2.9	-53.0	1774	737	700	2.7	-0.6	1.2
----	-----	-------	------	-----	-----	-----	------	-----

A7.5. Assigned transition frequencies for the isotopologues of each oligomer.

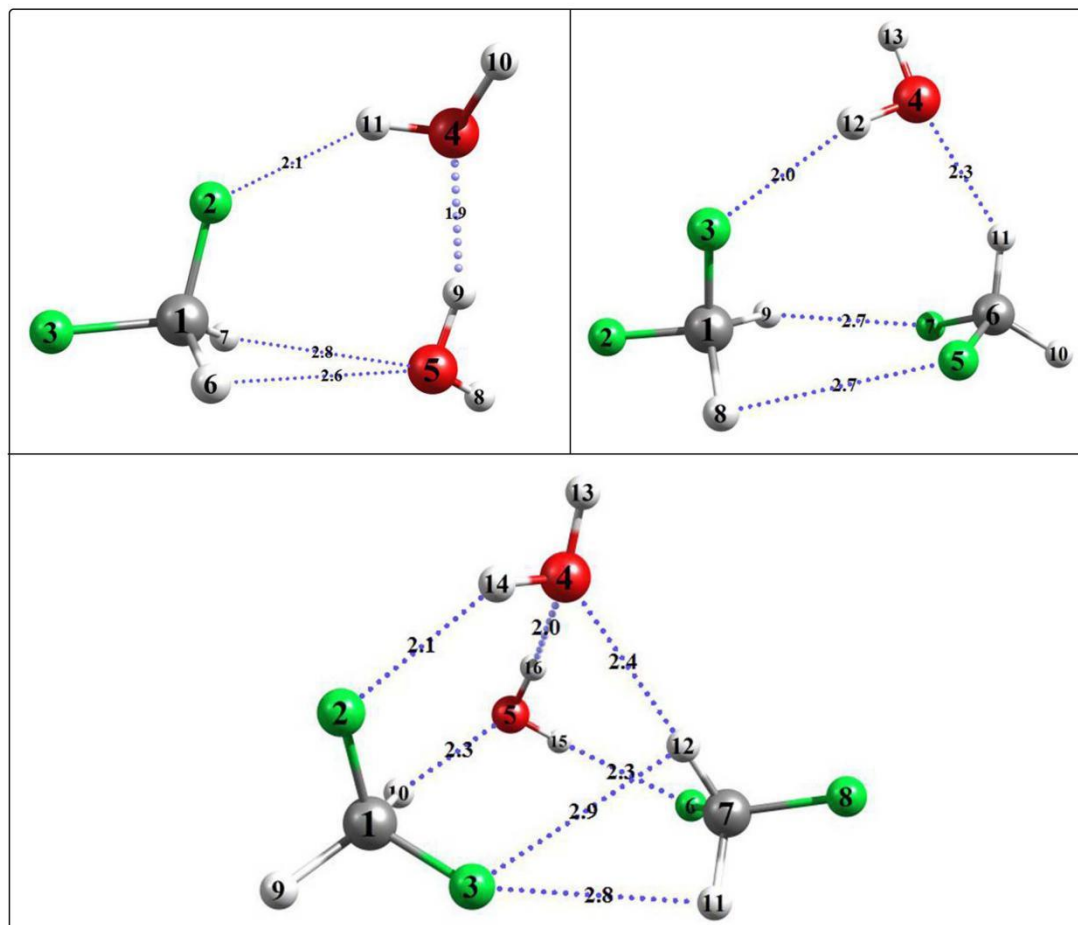


Figure A7.7. Assigned conformers at MP2/6-311++G** level, the atoms labels and (weak) hydrogen bonds are shown. The labels of the hydrogen atoms are used for naming the isotopologues in table A7.4-A7.29.

Table A7.4. Experimental rotational parameters of the parent and deuterated species of DW2.

	Normal		DFM-(D ₂ O) ₂		D8 ^a	
	$\nu=0$	$\nu=1$	$\nu=0$	$\nu=1$	$\nu=0$	$\nu=1$
A/MHz	5249.96(5) ^b		4707.61(4)		4981.9(1)	4985.9(3)
B/MHz	1729.540(2)	1729.658(2)	1628.874(3)	1628.866(3)	1701.276(3)	1702.04(1)
C/MHz	1316.196(2)	1316.166(2)	1225.460(2)	1225.439(2)	1282.948(3)	1282.46(1)
D_J/kHz	1.31(2)	1.26(2)	1.05(2)	1.03(2)	1.12(2)	3.47(9)
D_{JK}/kHz	12.2(1)	12.7(1)	10.6(1)	10.6(1)	13.2(5)	28.(1)
d_1/kHz	-0.41(2)	-0.54(2)	-0.25(3)	-0.35(3)	-0.41(2)	-9.1(2)
d_2/kHz	-0.10(1)	-0.09(2)	-0.03(1)	-0.05(1)	-0.10(2)	-0.5(2)
F_{bc}/MHz	1.2(4)					
$\Delta E/\text{GHz}$	58.8(4)					
σ^c	1.4		1.8		1.7	
N^d	50		40		23	

	D9		D11		D8,9	
	$\nu=0$	$\nu=1$	$\nu=0$	$\nu=1$	$\nu=0$	$\nu=1$
<i>A</i> /MHz	5218.0(1)	5215.0(2)	5140.9(1)		4959.95(6)	
<i>B</i> /MHz	1705.101(2)	1705.225(3)	1721.444(3)	1721.497(7)	1677.409(3)	1677.553(4)
<i>C</i> /MHz	1300.105(2)	1300.098(3)	1304.759(2)	1304.722(5)	1268.016(2)	1267.971(2)
<i>D_J</i> /kHz	1.16(2)	0.46(3)	1.32(2)	1.52(5)	1.16(2)	1.02(3)
<i>D_{JK}</i> /kHz	14.4(4)	21.4(6)	11.3(4)	11(2)	13.4(1)	21.1(4)
<i>d₁</i> /kHz	-0.34(2)	-0.97(4)	-0.40(2)	-1.8(1)	-0.36(3)	-0.84(3)
<i>d₂</i> /kHz	0.07(3)	-0.52(5)	-0.11(2)	-4.5(4)	-0.13(2)	-1.34(2)
σ	1.8		1.8		1.8	
<i>N</i>	28		25		32	
	D8,11		D9,11		D10,11	
	$\nu=0$	$\nu=1$	$\nu=0$	$\nu=1$		
<i>A</i> /MHz	4876.52(5)		5108.50(5)		5001.1(1)	
<i>B</i> /MHz	1694.192(3)	1694.204(3)	1697.582(3)	1697.572(3)	1674.381(4)	
<i>C</i> /MHz	1272.010(2)	1272.020(2)	1288.986(3)	1289.003(3)	1269.670(3)	
<i>D_J</i> /kHz	1.11(2)		1.25(2)	1.11(4)	7.14(4)	
<i>D_{JK}</i> /kHz	11.6(3)		9.9(3)	9.5(4)	14.9(5)	
<i>d₁</i> /kHz	-0.35(2)		-0.42(2)	-0.27(3)	-4.97(4)	
<i>d₂</i> /kHz	-0.12(1)					
σ	1.4		1.2		1.7	
<i>N</i>	30		30		11	
	D8,9,11		D9,10,11			
	$\nu=0$	$\nu=1$	$\nu=0$	$\nu=1$		
<i>A</i> /MHz	4853.69(5)		4960.76(9)			
<i>B</i> /MHz	1670.856(3)	1670.868(3)	1652.551(4)	1652.521(4)		
<i>C</i> /MHz	1257.381(2)	1257.391(2)	1255.188(3)	1255.204(2)		
<i>D_J</i> /kHz	1.08(2)		1.47(3)			
<i>D_{JK}</i> /kHz	11.3(2)		18.4(5)			
<i>d₁</i> /kHz	-0.35(2)		-1.36(3)			
<i>d₂</i> /kHz	-0.10(1)		-2.60(4)			
σ	1.1		1.6			
<i>N</i>	32		19			

^aNamed with the deuterated label.

^bError in parentheses in unit of the last digit.

^cRoot-mean-square deviation of the fit.

^dNumber of the lines in the fit.

Table A7.5. Experimental rotational parameters of the parent and deuterated species of D2W.

	normal		DFM2-D ₂ O	DFM2-DOH ^a	DFM2-HOD
	$\nu=0$	$\nu=1$			
<i>A</i> /MHz	2248.047(7) ^b	2248.194(7)	2124.00(3)	2211.654(3)	2152.61(3)
<i>B</i> /MHz	1096.505(1)	1096.516(1)	1093.182(1)	1096.6134(9)	1093.381(2)
<i>C</i> /MHz	860.5625(6)	860.5106(7)	847.478(1)	857.5869(6)	848.145(1)
<i>D_J</i> /kHz	2.38(6)	2.67(7)	7.44(1)	3.564(4)	4.16(2)
<i>D_{JK}</i> /kHz	36.9(1)	36.0(2)	85.0(1)	51.24(3)	59.5(1)
<i>D_K</i> /kHz	-20(3)	-23(3)	-167(3)	-41.1(2)	-73(5)
<i>d₁</i> /kHz	-0.081(4)	-0.088(4)	-0.139(4)	-0.060(4)	-0.080(7)
<i>d₂</i> /kHz	0.73(4)	0.87(3)	3.803(6)	1.399(2)	1.679(8)
<i>F_{bc}</i> /MHz	4.1(9)				
ΔE /GHz	58.822(8)				
σ^c	1.0		1.9	1.5	1.3
<i>N^d</i>	130		36	59	32

^aThe former hydrogen of the water is involved in HB.

^bError in parentheses in unit of the last digit.

^cRoot-mean-square deviation of the fit.

^dNumber of the lines in the fit.

Table A7.6. Experimental rotational parameters of the parent and deuterated species of D2W2.

	normal	DFM2(D2O)2	D13 ^a	D14
<i>A</i> /MHz	1759.4167(7) ^b	1647.497(5)	1718.01(5)	1740.23(5)
<i>B</i> /MHz	763.3094(2)	749.7241(3)	760.059(2)	759.154(2)
<i>C</i> /MHz	696.9655(2)	684.3165(3)	692.472(2)	693.659(1)
<i>D_J</i> /kHz	0.700(1)	0.597(2)	0.654(6)	0.684(7)
<i>D_{JK}</i> /kHz	-1.89(1)	-1.27(1)	-1.47(7)	-1.55(9)
<i>D_K</i> /kHz	10.66(5)	4.8(9)		
<i>d₁</i> /kHz	-0.1310(9)	-0.106(1)	-0.116(8)	-0.130(7)
<i>d₂</i> /kHz	0.0014(6)	0.0073(8)		
σ^c	0.57874	1.8	0.7	1.4
<i>N</i> ^d	162	78	23	21
	D13,14	D15,16	D13,14,16	
<i>A</i> /MHz	1699.82(7)	1707.6(1)	1665.58(6)	
<i>B</i> /MHz	756.107(1)	758.077(3)	751.785(2)	
<i>C</i> /MHz	689.370(1)	691.145(2)	685.029(2)	
<i>D_J</i> /kHz	0.484(7)	0.07(1)	0.637(6)	
<i>D_{JK}</i> /kHz	-2.0(3)	-22.4(4)	-1.62(9)	
<i>d₁</i> /kHz		-0.18(1)	-0.129(8)	
<i>d₂</i> /kHz		-0.076(8)		
σ	1.7	1.9	0.7	
<i>N</i>	14	15	20	

^aNamed with the deuterated labels.

^bError in parentheses in unit of the last digit.

^cRoot-mean-square deviation of the fit.

^dNumber of the lines in the fit.

Table A7.7. Kraitchman's coordinates (*r_s*) of the hydrogen atoms in the principal axes system, the deuterated labels are same with Figure A7.7.

		<i>a</i> /Å		<i>b</i> /Å		<i>c</i> /Å	
		<i>r_s</i>	<i>r_e</i>	<i>r_s</i>	<i>r_e</i>	<i>r_s</i>	<i>r_e</i>
DW2	D8	2.1703(8) ^a	2.09	2.2997(7)	2.31	0.211(8)	0.35
	D9	2.0456(8)	2.04	0.770(2)	0.84	0.11(1)	0.04
	D10	2.8342(6)	2.88	1.648(1)	1.57	0.396(4)	0.63
	D11	1.158(1)	1.53	1.429(1)	1.34	0.16(1)	0.03
D2W	D13	0.16* <i>i</i> (1)	0.68	2.9238(6)	3.10	1.199(1)	1.00
			0.01 ^b		2.88		1.25
D2W2	D13	0.549(5)	0.52	2.057(1)	2.20	1.645(2)	2.20
	D14	1.394(2)	1.36	1.212(2)	1.10	1.310(2)	1.55
	D15	0.595* <i>i</i> (5)	0.41	1.042(3)	1.51	1.498(2)	1.72

^aErrors in parenthesis are expressed in units of the last digit.

^bThe coordinates are calculated at B3LYP/def2tzvp-D3BJ level.

Table A7.8. Measured rotational transition frequencies (*v_{obs}*) of parent species of DW2 and residual (*v_{obs}*-*v_{calc}*) for the fit of table A7.4. (frequencies in MHz).

<i>J'</i>	<i>K_a'</i>	<i>K_c'</i>	<i>J''</i>	<i>K_a''</i>	<i>K_c''</i>	<i>v</i> =0		<i>v</i> =1	
						<i>v_{obs}</i>	<i>v_{obs}</i> - <i>v_{calc}</i>	<i>v_{obs}</i>	<i>v_{obs}</i> - <i>v_{calc}</i>
1	0	1	0	0	0	3045.7369	0.0061	3045.8221	0.0032
2	1	2	1	1	1	5678.0543	0.0035	5678.1127	0.0305

2	0	2	1	0	1	6057.1325	0.0034	6057.2857	0.0030
2	1	1	1	1	0	6504.7026	-0.0091	6505.0248	-0.0070
3	1	3	2	1	2	8496.4189	0.0128	8496.4189	-0.0327
3	0	3	2	0	2	9001.4137	0.0035	9001.5925	0.0039
3	2	2	2	2	1	9136.7874	0.0043	9137.0471	0.0058
3	2	1	2	2	0	9272.4220	0.0017	9272.7632	-0.0081
3	1	2	2	1	1	9734.5536	-0.0091	9735.0229	-0.0011
4	1	4	3	1	3	11292.3998	0.0294	11292.3998	-0.0321
4	0	4	3	0	3	11852.9800	0.0042	11853.1371	0.0036
4	2	3	3	2	2	12155.5300	0.0121	12155.8615	0.0067
4	3	2	3	3	1	12245.2879	0.0001	12245.6714	0.0125
4	3	1	3	3	0	12255.9457	-0.0057	12256.3420	0.0085
4	2	2	3	2	1	12485.0314	0.0054	12485.5621	-0.0119
4	1	3	3	1	2	12934.8601	-0.0105	12935.4613	0.0118
5	1	5	4	1	4	14062.2463	0.0194	14062.2463	-0.0666
5	0	5	4	0	4	14603.4932	0.0031	14603.5600	-0.0416
5	2	4	4	2	3	15151.4197	0.0094	15151.8027	-0.0194
5	3	3	4	3	2	15327.1889	-0.0032	15327.5549	-0.0255
5	3	2	4	3	1	15364.1501	-0.0060	15364.5945	0.0219
5	2	3	4	2	2	15775.2486	0.0133	15775.9892	-0.0179
5	1	4	4	1	3	16091.5586	-0.0077	16092.2558	0.0251
6	1	6	5	1	5	16804.8633	0.0172	16804.9759	0.0007
6	0	6	5	0	5	17268.5342	-0.0163	17268.6618	0.0299

Table A7.9. Measured rotational transition frequencies (ν_{obs}) of DW2 with full deuterated water and residual ($\nu_{obs}-\nu_{calc}$) for the fit of table A7.4. (frequencies in MHz).

J'	K _a '	K _c '	J''	K _a ''	K _c ''	$\nu=0$		$\nu=1$	
						ν_{obs}	$\nu_{obs}-\nu_{calc}$	ν_{obs}	$\nu_{obs}-\nu_{calc}$
3	1	3	2	1	2	7935.4897	-0.0278	7935.4897	0.0630
3	0	3	2	0	2	8416.5153	-0.0057	8416.4212	-0.0124
3	2	2	2	2	1	8562.6103	-0.0247	8562.6103	0.0561
3	2	1	2	2	0	8708.9955	-0.0016	8708.8897	-0.0267
3	1	2	2	1	1	9143.5598	-0.0048	9143.4890	0.0014
4	1	4	3	1	3	10541.9924	-0.0263	10541.8989	-0.0123
4	0	4	3	0	3	11063.5502	0.0136	11063.3995	-0.0260
4	1	3	3	1	2	12142.7553	-0.0064	12142.6583	0.0076
4	2	3	3	2	2	11387.7885	-0.0260	11387.7885	0.0779
4	2	2	3	2	1	11741.2127	-0.0162	11741.0986	-0.0192
5	1	5	4	1	4	13121.1738	0.0038	13121.0704	0.0109
5	0	5	4	0	4	13608.1835	-0.0094	13608.0792	0.0063
5	2	4	4	2	3	14188.3721	0.0283	14188.2791	0.0565
5	3	3	4	3	2	14376.7221	-0.0039	14376.6062	0.0109
5	3	2	4	3	1	14420.9526	-0.0054	14420.8060	-0.0158
5	2	3	4	2	2	14850.4676	0.0168	14850.3141	0.0156
5	1	4	4	1	3	15093.7536	-0.0048	15093.6111	0.0002
6	1	6	5	1	5	15672.4055	0.0014	15672.3088	-0.0010
6	0	6	5	0	5	16072.8409	0.0056	16072.7356	0.0054
6	2	5	5	2	4	16958.6261	-0.0158	16958.4732	-0.0399

Table A7.10. Measured rotational transition frequencies (ν_{obs}) for the D8 isotopologue of DW2 and residual ($\nu_{obs}-\nu_{calc}$) for the fit of table A7.4 (frequencies in MHz).

J'	K _a '	K _c '	J''	K _a ''	K _c ''	$\nu=0$		$\nu=1$	
						ν_{obs}	$\nu_{obs}-\nu_{calc}$	ν_{obs}	$\nu_{obs}-\nu_{calc}$
2	1	1	1	1	0	6386.7264	0.0527		
3	1	3	2	1	2	8302.5528	0.0062		

3	0	3	2	0	2	8804.4863	-0.0018	8804.66687	0.0
3	2	2	2	2	1	8952.2323	-0.0106	8952.49978	0.0
3	1	2	2	1	1	9555.3005	-0.0308		
4	1	4	3	1	3	11030.8727	0.0041	11030.87268	0.0041
4	0	4	3	0	3	11578.4018	-0.0200	11578.57464	0.0
4	2	3	3	2	2	11906.9512	-0.0306	11907.05050	0.0
4	1	3	3	1	2	12691.3618	-0.0110	12691.95236	0.0
5	1	5	4	1	4	13731.3383	0.0103		
5	0	5	4	0	4	14247.1018	0.0216		
5	2	4	4	2	3	14836.8174	0.0191		
5	2	3	4	2	2	15509.3859	-0.0076		
5	1	4	4	1	3	15778.9612	0.0051	15778.02976	0.0
6	1	6	5	1	5	16403.1757	-0.0141		
4	2	2	3	2	1	12265.0441	0.0237		

Table A7.11. Measured rotational transition frequencies (ν_{obs}) for the D9 isotopologue of DW2 and residual ($\nu_{obs}-\nu_{calc}$) for the fit of table A7.4 (frequencies in MHz).

J'	K _a '	K _c '	J''	K _a ''	K _c ''	$\nu=0$		$\nu=1$	
						ν_{obs}	$\nu_{obs}-\nu_{calc}$	ν_{obs}	$\nu_{obs}-\nu_{calc}$
2	1	1	1	1	0	6415.2987	-0.0024	6415.6309	-0.0115
3	1	3	2	1	2	8388.0802	-0.0006	8388.2886	-0.0202
3	0	3	2	0	2	8884.7806	-0.0068	8885.0202	-0.0245
3	2	2	2	2	1	9015.1854	0.0460	9015.4556	-0.0015
3	2	1	2	2	0	9145.8743	0.0178	9146.2242	-0.0070
3	1	2	2	1	1	9601.2957	-0.0070	9601.7885	-0.0032
4	1	4	3	1	3	11149.2175	-0.0007	11149.6604	0.0385
4	0	4	3	0	3	11702.6156	-0.0191	11702.9272	0.0114
4	2	3	3	2	2	11994.2704	-0.0426	11994.8511	0.0029
5	1	5	4	1	4	13885.1162	0.0204	13885.7544	-0.0152
4	1	3	3	1	2	12758.9165	-0.0037	12759.5765	0.0359
5	0	5	4	0	4	14422.1979	-0.0031		
6	1	6	5	1	5	16594.5330	-0.0032		
5	1	4	4	1	3	15874.7110	0.0250	15875.4189	-0.0187
5	2	3	4	2	2	15554.2028	-0.0132	15555.0881	0.0014

Table A7.12. Measured rotational transition frequencies (ν_{obs}) for the D11 isotopologue of DW2 and residual ($\nu_{obs}-\nu_{calc}$) for the fit of table A7.4 (frequencies in MHz).

J'	K _a '	K _c '	J''	K _a ''	K _c ''	$\nu=0$		$\nu=1$	
						ν_{obs}	$\nu_{obs}-\nu_{calc}$	ν_{obs}	$\nu_{obs}-\nu_{calc}$
2	1	1	1	1	0	6468.9515	-0.0398	6469.0739	0.0121
3	1	3	2	1	2	8431.9309	0.0076	8431.9308	-0.0099
3	0	3	2	0	2	8936.9757	0.0024	8936.9756	-0.0049
3	2	2	2	2	1	9078.2130	0.0067		
3	2	1	2	2	0	9219.6867	0.0078		
3	1	2	2	1	1	9679.9623	0.0016	9679.9624	-0.0297
4	1	4	3	1	3	11204.9426	-0.0048		
4	0	4	3	0	3	11761.3196	0.0013	11761.3196	-0.0239
4	1	3	3	1	2	12859.9866	0.0314	12859.9866	0.0358
5	1	5	4	1	4	13950.9928	-0.0065	13951.1067	0.0082
5	0	5	4	0	4	14482.3538	-0.0092	14482.4673	0.0401
5	2	4	4	2	3	15050.4449	-0.0043		
5	2	3	4	2	2	15697.6400	-0.0066		
5	1	4	4	1	3	15994.0877	-0.0061	15994.2092	-0.0142
6	1	6	5	1	5	16669.1201	0.0088		

6	0	6	5	0	5			17118.2330	-0.0182
---	---	---	---	---	---	--	--	------------	---------

Table A7.13. Measured rotational transition frequencies (ν_{obs}) for the D8,9 isotopologue of DW2 and residual ($\nu_{obs}-\nu_{calc}$) for the fit of table A7.4 (frequencies in MHz).

J'	K _a '	K _c '	J''	K _a ''	K _c ''	$\nu=0$		$\nu=1$	
						ν_{obs}	$\nu_{obs}-\nu_{calc}$	ν_{obs}	$\nu_{obs}-\nu_{calc}$
3	1	3	2	1	2	8200.4489	-0.0070	8200.4489	-0.0202
3	0	3	2	0	2	8694.1581	0.0096	8694.3550	0.0111
3	1	2	2	1	1	9426.5780	0.0027	9427.0562	-0.0060
3	2	1	2	2	0	8977.8286	0.0125		
3	2	2	2	2	1	8835.8355	-0.0035	8836.1260	0.0381
4	1	4	3	1	3	10896.2758	0.0052	10896.2758	-0.0299
4	0	4	3	0	3	11437.4499	0.0039	11437.6379	0.0222
4	1	3	3	1	2	12521.8247	-0.0066	12522.4482	0.0093
4	2	3	3	2	2	11752.9828	-0.0048	11753.4419	-0.0076
4	2	2	3	2	1	12096.7879	-0.0063	12096.8899	-0.0479
5	1	5	4	1	4	13565.1879	-0.0016	13565.2943	0.0482
5	0	5	4	0	4	14078.4399	0.0047	14078.5381	-0.0094
5	1	4	4	1	3	15570.8459	0.0034	15571.5737	-0.0131
5	2	4	4	2	3	14646.2359	0.0032		
5	2	3	4	2	2	15293.4976	-0.0038	15293.6195	0.0274
5	3	3	4	3	2	14829.4266	-0.0088		
5	3	2	4	3	1	14870.3959	0.0113		
6	1	6	5	1	5	16206.3739	-0.0008		
6	0	6	5	0	5			16636.4601	-0.0158

Table A7.14. Measured rotational transition frequencies (ν_{obs}) for the D8,11 isotopologue of DW2 and residual ($\nu_{obs}-\nu_{calc}$) for the fit of table A7.4 (frequencies in MHz).

J'	K _a '	K _c '	J''	K _a ''	K _c ''	$\nu=0$		$\nu=1$	
						ν_{obs}	$\nu_{obs}-\nu_{calc}$	ν_{obs}	$\nu_{obs}-\nu_{calc}$
3	1	3	2	1	2	8241.7102	0.0302	8241.7102	-0.0326
3	0	3	2	0	2	8743.6160	0.0310	8743.6160	-0.0338
3	2	2	2	2	1	8898.2486	0.0282		
3	2	1	2	2	0	9053.1344	0.0352		
3	1	2	2	1	1	9505.8797	0.0267	9505.8797	-0.0443
4	1	4	3	1	3	10948.0638	0.0321	10948.0638	-0.0510
4	0	4	3	0	3	11490.6844	0.0189	11490.6844	-0.0650
4	2	3	3	2	2	11833.5623	-0.0072		
4	2	2	3	2	1	12207.2271	-0.0334		
4	1	3	3	1	2	12622.8939	0.0063	12622.9694	-0.0119
5	1	5	4	1	4	13625.5533	0.0072	13625.6602	0.0112
5	0	5	4	0	4	14130.2701	-0.0009	14130.3829	0.0098
5	2	4	4	2	3	14742.8246	-0.0144	14742.9504	0.0007
5	2	3	4	2	2	15442.0244	-0.0004	15442.1468	0.0013
5	1	4	4	1	3	15688.7753	0.0106	15688.8930	0.0128
6	1	6	5	1	5	16273.7108	0.0081	16273.8220	-0.0033
6	0	6	5	0	5	16686.6745	-0.0050	16686.7948	-0.0049

Table A7.15. Measured rotational transition frequencies (ν_{obs}) for the D9,11 isotopologue of DW2 and residual ($\nu_{obs}-\nu_{calc}$) for the fit of table A7.4 (frequencies in MHz).

J'	K _a '	K _c '	J''	K _a ''	K _c ''	$\nu=0$		$\nu=1$	
						ν_{obs}	$\nu_{obs}-\nu_{calc}$	ν_{obs}	$\nu_{obs}-\nu_{calc}$
2	1	1	1	1	0	6381.6397	0.0008		

3	1	3	2	1	2	8325.9507	0.0408	8325.9507	-0.0249
3	0	3	2	0	2	8823.0113	0.0292	8823.0113	-0.0208
3	2	2	2	2	1	8959.3221	-0.0101		
3	2	1	2	2	0	9095.9203	0.0014		
3	1	2	2	1	1	9549.7791	0.0057	9549.7792	-0.0131
4	1	4	3	1	3	11064.9013	0.0394	11064.9013	-0.0481
4	0	4	3	0	3	11614.4242	0.0226	11614.4242	-0.0625
4	2	3	3	2	2	11918.7105	-0.0074		
4	2	2	3	2	1	12250.2027	0.0151		
4	1	3	3	1	2	12688.0721	-0.0081	12688.1592	0.0189
5	1	5	4	1	4	13777.6889	0.0154	13777.7976	0.0189
5	0	5	4	0	4	14305.1626	-0.0109	14305.2738	-0.0181
5	2	4	4	2	3	14855.1130	0.0136	14855.2317	0.0056
5	2	3	4	2	2	15481.4761	-0.0218	15481.6007	-0.0135
5	1	4	4	1	3	15782.3020	0.0165	15782.4198	0.0075
6	1	6	5	1	5	16463.3194	-0.0041	16463.4361	-0.0014
6	0	6	5	0	5	16911.9762	0.0000		

Table A7.16. Measured rotational transition frequencies (vobs) for the D10,11 isotopologue of DW2 and residual (vobs-vcalc) for the fit of table A7.4 (frequencies in MHz).

J'	K _a '	K _c '	J''	K _a ''	K _c ''	<i>v_{obs}</i>	<i>v_{obs}-v_{calc}</i>
3	1	3	2	1	2	8203.9190	-0.0235
3	0	3	2	0	2	8694.3550	0.0266
3	2	2	2	2	1	8831.0361	0.0114
3	2	1	2	2	0	8968.0681	-0.0108
3	1	2	2	1	1	9415.1225	-0.0126
4	1	4	3	1	3	10902.0834	0.0233
4	0	4	3	0	3	11442.2298	-0.0245
4	1	3	3	1	2	12507.2383	0.0129
5	1	5	4	1	4	13574.0674	-0.0048
5	0	5	4	0	4	14090.1053	0.0039
5	1	4	4	1	3	15554.1418	-0.0032

Table A7.17. Measured rotational transition frequencies (vobs) for the D8,9,11 isotopologue of DW2 and residual (vobs-vcalc) for the fit of table A7.4 (frequencies in MHz).

J'	K _a '	K _c '	J''	K _a ''	K _c ''	ν=0		ν=1	
						<i>v_{obs}</i>	<i>v_{obs}-v_{calc}</i>	<i>v_{obs}</i>	<i>v_{obs}-v_{calc}</i>
3	1	3	2	1	2	8141.7909	0.0310	8141.7909	-0.0310
3	0	3	2	0	2	8635.7818	0.0317	8635.7818	-0.0311
3	2	1	2	2	0	8933.1747	0.0168	8933.1747	-0.0487
3	2	2	2	2	1	8784.3479	0.0156		
3	1	2	2	1	1	9379.9868	0.0346	9379.9868	-0.0312
4	1	4	3	1	3	10816.3752	0.0399	10816.3752	-0.0424
4	0	4	3	0	3	11352.9954	0.0158	11352.9954	-0.0666
4	2	3	3	2	2	11682.9213	-0.0128		
4	3	1	3	3	0	11794.1485	0.0158		
4	2	2	3	2	1	12042.4769	0.0002		
4	1	3	3	1	2	12457.1756	0.0067	12457.2530	-0.0032
5	1	5	4	1	4	13463.0536	0.0144	13463.1521	0.0104
5	0	5	4	0	4	13965.5679	0.0009	13965.6753	0.0070
5	2	4	4	2	3	14556.4659	-0.0131	14556.5809	-0.0042
5	2	3	4	2	2	15230.6369	-0.0090	15230.7506	-0.0069
5	1	4	4	1	3	15485.4763	0.0081	15485.5952	0.0188

6	1	6	5	1	5	16081.2531	0.0090	16081.3663	-0.0002
6	0	6	5	0	5	16495.8021	-0.0122	16495.9285	-0.0062

Table A7.18. Measured rotational transition frequencies (ν_{obs}) for the D9,10,11 isotopologue of DW2 and residual ($\nu_{obs}-\nu_{calc}$) for the fit of table A7.4 (frequencies in MHz).

J'	K _a '	K _c '	J''	K _a ''	K _c ''	$\nu=0$		$\nu=1$	
						ν_{obs}	$\nu_{obs}-\nu_{calc}$	ν_{obs}	$\nu_{obs}-\nu_{calc}$
3	1	3	2	1	2	8106.8365	0.0260	8106.8365	-0.0087
3	0	3	2	0	2	8589.9000	-0.0223	8589.9000	-0.0143
3	1	2	2	1	1	9296.7908	-0.0483	9296.7908	0.0537
4	1	4	3	1	3	10773.7238	0.0359		
4	0	4	3	0	3	11307.4916	0.0081		
4	2	3	3	2	2	11604.3723	-0.0028		
4	2	2	3	2	1	11926.1410	-0.0039		
4	1	3	3	1	2	12351.9058	0.0037	12351.7816	0.0047
5	1	5	4	1	4	13415.0629	-0.0228	13415.1589	-0.0051
5	0	5	4	0	4	13927.0519	-0.0355	13927.1591	0.0068
5	1	4	4	1	3	15364.0329	0.0038	15363.8881	-0.0034
6	0	6	5	0	5	16465.0772	0.0199		

Table A7.19. Measured rotational transition frequencies (ν_{obs}) the parent species of D2W and residual ($\nu_{obs}-\nu_{calc}$) for the fit of table A7.5 (frequencies in MHz).

J'	K _a '	K _c '	J''	K _a ''	K _c ''	ν=0		ν=1	
						<i>V_{obs}</i>	<i>V_{obs}-V_{calc}</i>	<i>V_{obs}</i>	<i>V_{obs}-V_{calc}</i>
μ _a -type transitions									
2	0	2	1	0	1	3881.3803	0.0047	3881.2792	0.0012
2	1	2	1	1	1	3677.9730	0.0037	3677.8236	0.0005
2	1	1	1	1	0	4149.8660	0.0167	4149.8105	-0.0173
3	0	3	2	0	2	5744.1496	0.0037	5743.9693	-0.0008
3	1	3	2	1	2	5497.6330	0.0027	5497.4023	-0.0014
3	1	2	2	1	1	6202.5777	0.0132	6202.5777	0.0547
3	2	2	2	2	1	5869.9782	0.0030	5869.8556	0.0002
3	2	1	2	2	0	5996.9226	0.0043	5996.8433	-0.0011
4	0	4	3	0	3	7532.6041	0.0012	7532.3241	-0.0016
4	1	4	3	1	3	7297.8443	0.0012	7297.5283	-0.0013
4	1	3	3	1	2	8224.5130	-0.0152	8224.5130	0.0588
4	2	3	3	2	2	7800.7214	0.0006	7800.5545	0.0018
4	2	2	3	2	1	8095.9144	-0.0126	8095.9144	0.0546
4	3	2	3	3	1	7882.6141	-0.0034	7882.4862	-0.0033
4	3	1	3	3	0	7899.6609	-0.0001	7899.5226	-0.0177
5	0	5	4	0	4	9261.4269	0.0014	9261.0336	-0.0019
5	1	5	4	1	4	9077.5370	0.0013	9077.1277	-0.0013
5	1	4	4	1	3	10199.1070	-0.0009	10198.9621	-0.0214
5	2	4	4	2	3	9709.6952	-0.0034	9709.4715	-0.0046
5	2	3	4	2	2	10231.4584	-0.0102	10231.4584	0.0483
5	3	3	4	3	2	9866.2383	-0.0090	9866.1000	0.0061
5	3	2	4	3	1	9924.2834	-0.0090	9924.1463	-0.0162
5	4	2	4	4	1	9850.7283	-0.0156	9850.5969	-0.0084
5	4	1	4	4	0	9852.3984	-0.0138	9852.2603	-0.0140
6	0	6	5	0	5	10962.0034	0.0023	10961.4985	-0.0009
6	1	6	5	1	5	10838.5496	-0.0010	10838.0455	-0.0006
6	1	5	5	1	4	12107.0499	-0.0165	12106.8628	-0.0068
6	2	5	5	2	4	11592.5748	-0.0023	11592.2917	-0.0020

6	2	4	5	2	3	12364.7567	-0.0164	12364.7567	0.0459
6	3	3	5	3	2	11994.1768	-0.0217	11994.0654	-0.0096
6	3	4	5	3	3	11847.3436	0.0047	11847.1814	0.0214
6	4	2	5	4	1	11849.5451	-0.0037	11849.3987	-0.0025
6	4	3	5	4	2	11842.1476	0.0025	11842.0108	0.0162
7	0	7	6	0	6	12658.7694	0.0070	12658.1574	0.0026
7	1	7	6	1	6	12584.5718	0.0039	12583.9759	0.0127
7	1	6	6	1	5	13933.5341	-0.0098	13933.2356	-0.0023
7	2	6	6	2	5	13446.4649	-0.0049	13446.1140	-0.0062
7	2	5	6	2	4	14461.7840	-0.0315	14461.7840	0.0530
7	3	5	6	3	4	13818.0151	-0.0005	13817.8148	0.0052
7	3	4	6	3	3	14119.5982	-0.0586	14119.5982	0.0450
7	4	4	6	4	3	13841.8455	0.0056	13841.6884	0.0046
7	4	3	6	4	2	13865.9354	0.0025	13865.7808	-0.0047
8	0	8	7	0	7	14361.1450	0.0013	14360.4366	0.0021
8	1	8	7	1	7	14319.7655	-0.0045	14319.0669	0.0021
8	1	7	7	1	6	15680.4595	-0.0213	15680.0932	-0.0015
8	2	7	7	2	6	15270.5502	-0.0035	15270.1300	-0.0055
8	2	6	7	2	5	16500.2240	-0.0803	16500.2240	0.0439
8	3	6	7	3	5	15770.1286	0.0198	15769.8835	0.0097
8	3	5	7	3	4	16293.6128	-0.0074	16293.5346	-0.0040
8	4	5	7	4	4	15847.1412	0.0169	15846.9713	0.0044
9	0	9	8	0	8	16069.7447	-0.0152	16068.9445	-0.0081
9	1	9	8	1	8	16047.8644	0.0320	16047.0344	0.0065
9	1	8	8	1	7	17372.3637	-0.0014	17371.8769	-0.0146
9	2	8	8	2	7	17066.3674	-0.0033	17065.8940	0.0083
9	3	7	8	3	6	17696.4808	0.0175	17696.2072	0.0077
10	0	10	9	0	9	17782.7005	0.0074	17781.7971	0.0057
10	1	10	9	1	9	17771.4636	-0.0185	17770.5745	-0.0068
μ_b -type transitions									
3	1	3	2	0	2	6445.7093	-0.0032	6445.6041	0.0260
4	1	4	3	0	3	7999.4162	0.0067	7999.1308	-0.0068
5	1	5	4	0	4	9544.3486	0.0063	9543.9424	0.0015
6	1	6	5	0	5	11121.4715	0.0041		
7	1	7	6	0	6	12744.0370	0.0028		
4	0	4	3	1	3	6831.0343	-0.0022	6830.7270	0.0093
5	0	5	4	1	4	8794.6152	-0.0037	8794.2244	0.0008
6	0	6	5	1	5	10679.0758	-0.0085	10678.5909	-0.0030
7	0	7	6	1	6	12499.2955	-0.0007	12498.6977	-0.0049

Table A7.20. Measured rotational transition frequencies (ν_{obs}) for the isotopologue of D2W with full deuterated water and residual ($\nu_{obs}-\nu_{calc}$) for the fit of table A7.5 (frequencies in MHz).

J'	K _a '	K _c '	J''	K _a ''	K _c ''	ν_{obs}	$\nu_{obs}-\nu_{calc}$
4	0	4	3	0	3	7418.7487	-0.0343
4	1	4	3	1	3	7201.3376	-0.0432
4	1	3	3	1	2	8160.6195	0.0016
4	2	2	3	2	1	8070.1305	0.0024
4	2	3	3	2	2	7726.7015	0.0104
4	3	2	3	3	1	7821.9167	0.0041
4	3	1	3	3	0	7845.4183	-0.0035
5	0	5	4	0	4	9108.2720	-0.0104
5	1	4	4	1	3	10099.2206	0.0026
5	1	5	4	1	4	8950.2476	-0.0259

5	2	3	4	2	2	10200.3787	-0.0032
5	2	4	4	2	3	9608.1553	0.0287
5	3	3	4	3	2	9789.3919	-0.0063
5	3	2	4	3	1	9868.7922	-0.0177
6	0	6	5	0	5	10777.1455	0.0257
6	1	5	5	1	4	11955.4435	0.0052
6	1	6	5	1	5	10679.2543	0.0021
6	2	4	5	2	3	12313.0215	-0.0166
6	2	5	5	2	4	11458.1930	0.0416
6	3	4	5	3	3	11750.4012	-0.0052
6	3	3	5	3	2	11947.9361	-0.0063
7	0	7	6	0	6	12447.5271	0.0108
7	1	6	6	1	5	13717.2030	-0.0162
7	1	7	6	1	6	12393.1815	0.0159
7	2	5	6	2	4	14372.5975	0.0093
7	2	6	6	2	5	13274.0392	0.0281
7	3	5	6	3	4	13694.8508	-0.0027
7	3	4	6	3	3	14088.9242	0.0147
8	0	8	7	0	7	14125.0263	0.0285
8	1	8	7	1	7	14096.9106	0.0067
8	2	6	7	2	5	16355.4965	0.0013
8	2	7	7	2	6	15055.8393	-0.0467
8	3	5	7	3	4	16269.8347	-0.0065
8	3	6	7	3	5	15613.0021	0.0121
9	1	9	8	1	8	15794.3254	-0.0231
9	0	9	8	0	8	15808.1781	-0.0044

Table A7.21. Measured rotational transition frequencies (ν_{obs}) for the isotopologue of DFM2-D'OH (primed H involved in HB) and residual ($\nu_{obs}-\nu_{calc}$) for the fit of table A7.5 (frequencies in MHz).

J'	K _a '	K _c '	J''	K _a ''	K _c ''	ν_{obs}	$\nu_{obs}-\nu_{calc}$
4	0	4	3	0	3	7507.0156	0.0071
4	1	3	3	1	2	8214.2826	0.0100
4	1	4	3	1	3	7276.9844	0.0106
4	2	2	3	2	1	8096.2869	0.0130
4	2	3	3	2	2	7786.9691	0.0050
4	3	2	3	3	1	7872.6475	-0.0199
4	3	1	3	3	0	7891.4227	-0.0209
5	0	5	4	0	4	9225.8275	0.0030
5	1	4	4	1	3	10180.7371	0.0055
5	1	5	4	1	4	9049.4887	0.0067
5	2	3	4	2	2	10232.8239	0.0126
5	2	4	4	2	3	9690.0247	0.0272
5	3	3	4	3	2	9853.6896	0.0078
5	3	2	4	3	1	9917.4847	-0.0028
5	4	2	4	4	1	9837.4916	-0.0304
6	0	6	5	0	5	10918.5266	-0.0042
6	1	5	5	1	4	12076.0667	-0.0200
6	1	6	5	1	5	10802.9077	0.0086
6	2	4	5	2	3	12362.8381	-0.0098
6	2	5	5	2	4	11565.4404	-0.0012
6	3	3	5	3	2	11991.8438	-0.0109
6	3	4	5	3	3	11831.1694	0.0140
6	4	2	5	4	1	11835.5988	0.0050

6	4	3	5	4	2	11827.0603	0.0016
7	0	7	6	0	6	12609.1489	0.0071
7	1	6	6	1	5	13885.8502	-0.0503
7	1	7	6	1	6	12541.2188	-0.0237
7	2	5	6	2	4	14451.8035	-0.0054
7	2	6	6	2	5	13410.3876	-0.0314
7	3	5	6	3	4	13796.5885	0.0002
7	3	4	6	3	3	14124.0427	0.0079
7	4	4	6	4	3	13824.8755	0.0212
7	4	3	6	4	2	13852.5670	-0.0161
8	0	8	7	0	7	14305.9465	0.0046
8	1	7	7	1	6	15615.4096	0.0126
8	1	8	7	1	7	14268.9182	0.0038
8	2	6	7	2	5	16477.1816	0.0035
8	2	7	7	2	6	15224.3581	0.0062
8	3	6	7	3	5	15741.3502	0.0060
8	4	5	7	4	4	15827.7031	0.0272
8	4	4	7	4	3	15900.7553	-0.0118
9	0	9	8	0	8	16008.8706	-0.0019
9	1	8	8	1	7	17293.3003	0.0086
9	1	9	8	1	8	15989.6652	-0.0024
4	1	4	3	0	3	7941.5973	0.0027
3	1	3	2	0	2	6393.4258	0.0059
4	0	4	3	1	3	6842.3994	0.0118
2	2	1	1	1	0	7491.8827	-0.0096
2	2	0	1	1	1	7765.4785	0.0212
5	0	5	4	1	4	8791.2525	0.0141
3	2	2	2	1	1	9205.6376	-0.0005
5	1	5	4	0	4	9484.0800	0.0118
6	0	6	5	1	5	10660.2702	-0.0170
4	2	3	3	1	2	10795.5015	-0.0075
6	1	6	5	0	5	11061.1475	0.0047
3	3	1	2	2	0	12019.0151	-0.0140
3	3	0	2	2	1	12056.7600	0.0208
4	3	2	3	2	1	13897.1504	-0.0083
4	3	1	3	2	2	14087.3316	0.0008

Table A7.22. Measured rotational transition frequencies (ν_{obs}) for the isotopologue of DFM2-H'OD (primed H involved in HB) and residual ($\nu_{obs}-\nu_{calc}$) for the fit of table A7.5 (frequencies in MHz).

J'	K _a '	K _c '	J''	K _a ''	K _c ''	ν_{obs}	$\nu_{obs}-\nu_{calc}$
4	0	4	3	0	3	7430.4700	0.0070
4	1	4	3	1	3	7208.2922	-0.0003
4	1	3	3	1	2	8167.1048	-0.0034
4	2	3	3	2	2	7733.1157	-0.0035
4	2	2	3	2	1	8068.2034	0.0071
4	3	2	3	3	1	7826.6063	0.0321
4	3	1	3	3	0	7848.6679	0.0073
5	0	5	4	0	4	9124.1643	0.0101
5	1	5	4	1	4	8960.2080	0.0014
5	1	4	4	1	3	10111.5710	-0.0012
5	2	4	4	2	3	9618.3722	-0.0074
5	2	3	4	2	2	10198.9653	0.0060
5	3	2	4	3	1	9870.7634	0.0078

5	3	3	4	3	2	9796.0341	-0.0113
6	0	6	5	0	5	10795.6402	0.0120
6	1	6	5	1	5	10692.4141	-0.0047
6	1	5	5	1	4	11977.0058	-0.0079
6	2	5	5	2	4	11473.5602	-0.0034
6	2	4	5	2	3	12315.5504	-0.0136
6	3	3	5	3	2	11946.6948	-0.0395
6	3	4	5	3	3	11760.2873	0.0066
7	0	7	6	0	6	12467.7738	-0.0186
7	1	7	6	1	6	12409.5346	-0.0181
7	1	6	6	1	5	13750.5873	-0.0019
7	2	6	6	2	5	13295.9202	0.0036
7	2	5	6	2	4	14382.8115	0.0181
7	3	5	6	3	4	13709.7289	-0.0088
7	3	4	6	3	3	14083.9035	0.0115
8	0	8	7	0	7	14146.9628	0.0162
8	1	8	7	1	7	14116.3750	0.0012
8	1	7	7	1	6	15444.2531	-0.0082
8	2	7	7	2	6	15085.4322	0.0144

Table A7.23. Measured rotational transition frequencies (ν_{obs}) for the parent species of D2W2 and residual ($\nu_{obs}-\nu_{calc}$) for the fit of table A7.6 (frequencies in MHz).

J'	K _a '	K _c '	J''	K _a ''	K _c ''	ν_{obs}	$\nu_{obs}-\nu_{calc}$
2	1	2	1	1	1	2854.1958	0.0004
2	0	2	1	0	1	2917.3231	0.0002
2	1	1	1	1	0	2986.8750	0.0004
3	0	3	2	0	2	4367.9785	-0.0038
3	1	3	2	1	2	4279.3003	-0.0021
3	1	2	2	1	1	4478.2051	-0.0036
3	2	1	2	2	0	4393.5755	0.0139
3	2	2	2	2	1	4380.8131	0.0187
4	0	4	3	0	3	5809.3230	-0.0035
4	1	4	3	1	3	5702.1519	-0.0029
4	1	3	3	1	2	5966.8793	-0.0033
4	2	3	3	2	2	5838.4841	-0.0029
4	2	2	3	2	1	5870.0758	-0.0034
4	3	2	3	3	1	5847.1977	0.0142
4	3	1	3	3	0	5847.7656	0.0018
5	0	5	4	0	4	7239.1106	-0.0019
5	1	5	4	1	4	7122.2159	-0.0008
5	1	4	4	1	3	7451.7770	-0.0040
5	2	3	4	2	2	7355.8730	-0.0032
5	2	4	4	2	3	7293.9802	-0.0020
5	3	2	4	3	1	7313.2438	-0.0007
5	3	3	4	3	2	7311.2204	-0.0003
5	4	1	4	4	0	7308.4621	-0.0022
5	4	2	4	4	1	7308.4578	0.0129
6	0	6	5	0	5	8656.3842	-0.0011
6	1	6	5	1	5	8539.1199	0.0000
6	1	5	5	1	4	8931.5912	-0.0012
6	1	5	5	1	4	8931.5907	-0.0017
6	2	5	5	2	4	8746.7445	-0.0021
6	2	4	5	2	3	8851.3211	-0.0002

6	3	4	5	3	3	8776.2626	0.0006
6	3	3	5	3	2	8781.6244	-0.0010
6	4	3	5	4	2	8772.3034	0.0355
6	4	2	5	4	1	8772.3034	-0.0517
6	5	2	5	5	1	8769.6377	0.0085
6	5	1	5	5	0	8769.6377	0.0080
7	0	7	6	0	6	10061.9376	-0.0012
7	1	7	6	1	6	9952.6755	-0.0034
7	1	6	6	1	5	10404.7758	-0.0022
7	2	6	6	2	5	10196.2694	0.0011
7	2	5	6	2	4	10355.0075	-0.0004
7	3	5	6	3	4	10242.0650	0.0013
7	3	4	6	3	3	10254.0075	-0.0013
7	4	4	6	4	3	10237.2080	-0.0022
7	4	3	6	4	2	10237.5023	0.0027
7	5	3	6	5	2	10233.0036	0.0037
7	5	2	6	5	1	10233.0036	0.0007
8	0	8	7	0	7	11458.2013	0.0038
8	1	8	7	1	7	11362.8963	0.0059
8	1	7	7	1	6	11869.5758	-0.0006
8	2	7	7	2	6	11642.0724	0.0014
8	2	6	7	2	5	11863.8611	0.0081
8	3	6	7	3	5	11708.2025	0.0007
8	3	5	7	3	4	11731.7241	0.0063
8	4	5	7	4	4	11703.4028	0.0065
8	4	4	7	4	3	11704.1971	0.0088
8	5	4	7	5	3	11697.2050	0.0210
8	5	3	7	5	2	11697.2050	0.0089
9	0	9	8	0	8	12848.4249	0.0068
9	1	9	8	1	8	12769.9138	0.0028
9	1	8	8	1	7	13324.0961	0.0072
9	2	8	8	2	7	13083.7241	-0.0081
9	2	7	8	2	6	13373.8696	0.0014
9	3	7	8	3	6	13174.0912	-0.0035
9	3	6	8	3	5	13216.2142	0.0059
9	4	6	8	4	5	13170.8982	0.0006
9	4	5	8	4	4	13172.7824	-0.0020
10	0	10	9	0	9	14235.6606	-0.0038
10	1	10	9	1	9	14174.0173	-0.0040
10	1	9	9	1	8	14766.4882	-0.0053
10	2	9	9	2	8	14520.9042	0.0001
10	2	8	9	2	7	14881.1469	-0.0048
10	3	8	9	3	7	14639.0525	0.0109
10	3	7	9	3	6	14708.8505	-0.0006
11	0	11	10	0	10	15622.1426	-0.0007
11	1	11	10	1	10	15575.5787	-0.0016
11	1	10	10	1	9	16195.4178	-0.0033
3	1	3	2	0	2	5212.2750	-0.0009
4	1	4	3	0	3	6546.4436	-0.0048
5	1	5	4	0	4	7859.3373	-0.0014
6	1	6	5	0	5	9159.3459	-0.0001
7	1	7	6	0	6	10455.6416	0.0019
8	1	8	7	0	7	11756.6001	0.0088
9	1	9	8	0	8	13068.2964	-0.0084

4	0	4	3	1	3	4965.0359	0.0030
5	0	5	4	1	4	6501.9862	-0.0045
6	0	6	5	1	5	8036.1557	-0.0034
7	0	7	6	1	6	9558.9761	-0.0018
8	0	8	7	1	7	11064.4995	0.0029
9	0	9	8	1	8	12550.0412	0.0169
2	2	1	1	1	0	5975.0731	-0.0023
2	2	0	1	1	1	6044.6224	-0.0003
3	2	1	2	1	2	7583.9850	-0.0039
3	2	2	2	1	1	7368.9905	-0.0047
4	2	3	3	1	2	8729.2729	-0.0008
4	2	2	3	1	3	9174.7658	0.0000
5	2	4	4	1	3	10056.3736	0.0004
5	2	3	4	1	4	10828.4840	-0.0032
6	2	5	5	1	4	11351.3367	-0.0022
6	2	4	5	1	5	12557.5956	0.0039
7	2	6	6	1	5	12616.0215	0.0068
8	2	7	7	1	6	13853.3127	0.0050
3	3	0	2	2	1	9528.6671	0.0025
3	3	1	2	2	0	9525.3661	0.0030
4	3	2	3	2	1	10978.9857	0.0007
4	3	1	3	2	2	10995.6394	0.0055
5	3	3	4	2	2	12420.1325	0.0061
5	3	2	4	2	3	12470.3920	0.0007
6	3	4	5	2	3	13840.4976	-0.0146
6	3	3	5	2	4	13958.0345	0.0000
7	3	4	6	2	5	15465.2945	-0.0023
7	3	5	6	2	4	15231.2389	-0.0157
8	3	5	7	2	6	17000.7444	-0.0019
8	3	6	7	2	5	16584.4323	-0.0162
3	1	2	2	0	2	5610.2032	-0.0009
4	1	3	3	0	3	7209.1019	-0.0026
5	1	4	4	0	4	8851.5552	-0.0037
6	1	5	5	0	5	10544.0316	-0.0073
7	1	6	6	0	6	12292.4298	-0.0018
8	1	7	7	0	7	14100.0616	-0.0077
9	1	8	8	0	8	15965.9751	0.0145
2	2	0	1	1	0	5978.2811	0.0012
2	2	1	1	1	1	6041.4176	-0.0006
3	2	1	2	1	1	7384.9667	-0.0002
3	2	2	2	1	2	7568.0259	0.0087
4	2	2	3	1	2	8776.8364	-0.0012
4	2	3	3	1	3	9127.2003	-0.0016
5	2	3	4	1	3	10165.8283	-0.0028
5	2	4	4	1	4	10719.0264	-0.0030
6	2	4	5	1	4	11565.3713	-0.0002
6	2	5	5	1	5	12343.5579	-0.0012
7	2	5	6	1	5	12988.7890	0.0020
7	2	6	6	1	6	14000.7013	-0.0063
8	2	6	7	1	6	14447.8573	-0.0047
9	2	7	8	1	7	15952.1416	-0.0122
3	3	0	2	2	0	9525.4699	0.0100
3	3	1	2	2	1	9528.5710	0.0033
4	3	1	3	2	1	10979.6684	0.0062

4	3	2	3	2	2	10994.9604	0.0036
5	3	2	4	2	2	12422.8352	0.0078
5	3	3	4	2	3	12467.6937	0.0034
6	3	3	5	2	3	13848.5747	-0.0019
6	3	4	5	2	4	13949.9748	0.0047
7	3	4	6	2	4	15251.2579	-0.0062
7	3	5	6	2	5	15445.2838	-0.0035
8	3	5	7	2	5	16627.9706	-0.0035
8	3	6	7	2	6	16957.2127	-0.0081
6	4	2	5	3	2	15964.6684	0.0045
6	4	3	5	3	3	15967.2485	-0.0074
7	4	3	6	3	3	17420.5340	-0.0042
7	4	4	6	3	4	17428.2026	-0.0016
4	3	2	4	2	2	5108.9019	-0.0040
4	3	1	4	2	3	5157.1563	0.0094
5	3	3	5	2	3	5064.2537	0.0035
5	3	2	5	2	4	5176.4172	0.0081
6	3	4	6	2	4	4989.1995	0.0085
6	3	3	6	2	5	5211.2954	0.0074
7	3	5	7	2	5	4876.2507	0.0040
7	3	4	7	2	6	5269.0365	0.0080
5	0	5	4	1	3	5839.3259	-0.0087
6	0	6	5	1	4	7043.9368	-0.0020
7	0	7	6	1	5	8174.2922	0.0071

Table A7.24. Measured rotational transition frequencies (ν_{obs}) for the D2W2 with full deuterated water and residual ($\nu_{obs}-\nu_{calc}$) for the fit of table A7.6 (frequencies in MHz).

J'	K _a '	K _c '	J''	K _a ''	K _c ''	ν_{obs}	$\nu_{obs}-\nu_{calc}$
7	0	7	6	0	6	9869.7600	-0.0103
6	0	6	5	0	5	8492.5247	0.0022
5	0	5	4	0	4	7103.7540	0.0056
8	0	8	7	0	7	11238.4386	-0.0175
9	0	9	8	0	8	12602.1267	0.0099
10	0	10	9	0	9	13963.7965	0.0459
11	0	11	10	0	10	15325.2765	-0.0081
6	1	6	5	1	5	8383.0932	0.0039
5	1	5	4	1	4	6992.5358	0.0046
7	1	7	6	1	6	9770.1913	-0.0056
8	1	8	7	1	7	11153.8822	-0.0222
9	1	9	8	1	8	12534.4374	0.0059
10	1	10	9	1	9	13912.1139	-0.0056
11	1	11	10	1	10	15287.3699	-0.0070
6	1	5	5	1	4	8769.0788	0.0062
5	1	4	4	1	3	7317.1008	0.0091
7	1	6	6	1	5	10213.7899	-0.0072
8	1	7	7	1	6	11649.2845	-0.0321
9	1	8	8	1	7	13073.5851	0.0010
10	1	9	9	1	8	14484.7548	-0.0133
11	1	10	10	1	9	15881.7413	-0.0136
5	2	4	4	2	3	7162.3128	0.0124
5	2	3	4	2	2	7228.4465	0.0079
6	2	5	5	2	4	8588.3282	0.0093
6	2	4	5	2	3	8699.4381	0.0132

7	2	6	6	2	5	10010.8723	-0.0100
7	2	5	6	2	4	10178.2079	-0.0184
8	2	7	7	2	6	11429.4777	-0.0170
8	2	6	7	2	5	11661.1573	-0.0003
9	2	8	8	2	7	12843.7421	0.0152
9	2	7	8	2	6	13143.8679	0.0007
10	2	9	9	2	8	14253.2411	-0.0012
10	2	8	9	2	7	14622.4336	0.0264
11	2	10	10	2	9	15657.8204	-0.0014
5	3	3	4	3	2	7180.7190	0.0138
6	3	4	5	3	3	8619.7802	0.0131
6	3	3	5	3	2	8626.0620	0.0159
7	3	5	6	3	4	10059.5316	-0.0085
7	3	4	6	3	3	10073.5173	0.0182
8	3	6	7	3	5	11499.5397	0.0194
8	3	5	7	3	4	11526.9325	0.0129
9	3	6	8	3	5	12987.8398	-0.0432
9	3	7	8	3	6	12939.0567	0.0193
10	3	8	9	3	7	14377.3141	0.0086
10	3	7	9	3	6	14457.7279	-0.0088
5	4	2	4	4	1	7177.7282	-0.0302
5	4	1	4	4	0	7177.7282	-0.0550
6	4	3	5	4	2	8615.6789	0.0375
6	4	2	5	4	1	8615.6789	-0.0740
7	4	4	6	4	3	10054.7360	-0.0038
7	4	3	6	4	2	10055.1201	0.0102
8	4	5	7	4	4	11495.1832	0.0055
8	4	4	7	4	3	11496.1933	0.0036
9	4	6	8	4	5	12937.0561	0.0430
9	4	5	8	4	4	12939.4670	0.0457
9	5	5	8	5	4	12927.7705	-0.0219
9	5	4	8	5	3	12927.8173	-0.0296
5	1	4	4	0	4	8616.1691	-0.0012
4	1	3	3	0	3	7001.2034	-0.0057
7	1	6	6	0	6	12002.7598	-0.0094
6	1	5	5	0	5	10281.5032	0.0088
3	2	1	2	1	1	7012.4923	-0.0293
3	2	2	2	1	2	7191.5912	0.0163
4	2	2	3	1	2	8381.8159	-0.0003
4	2	3	3	1	3	8723.0876	0.0112
5	2	3	4	1	3	9750.7020	0.0144
5	2	4	4	1	4	10286.6931	-0.0124
6	2	4	5	1	4	11133.0413	0.0206
6	2	5	5	1	5	11882.4908	-0.0023
7	2	5	6	1	5	12542.1557	-0.0188
7	2	5	6	1	5	12542.2024	0.0279
8	2	6	7	1	6	13989.5074	-0.0275
5	1	5	4	0	4	7638.4309	0.0184
7	1	7	6	0	6	10195.4052	-0.0226
8	1	8	7	0	7	11479.5553	-0.0066
6	0	6	5	1	5	7957.8461	-0.0123
7	0	7	6	1	6	9444.5216	-0.0178
8	0	8	7	1	7	10912.8096	0.0110

Table A7.25. Measured rotational transition frequencies (ν_{obs}) for the D13 isotopologue of D2W2 and residual ($\nu_{obs}-\nu_{calc}$) for the fit of table A7.6 (frequencies in MHz).

J'	K _a '	K _c '	J''	K _a ''	K _c ''	ν_{obs}	$\nu_{obs}-\nu_{calc}$
5	0	5	4	0	4	7195.8986	-0.0014
5	1	5	4	1	4	7079.4521	-0.0018
5	1	4	4	1	3	7414.9704	-0.0032
5	2	4	4	2	3	7254.7321	0.0086
5	2	3	4	2	2	7321.1365	0.0071
6	0	6	5	0	5	8602.7202	-0.0020
6	1	6	5	1	5	8487.3233	0.0000
6	1	5	5	1	4	8886.5457	-0.0036
6	2	5	5	2	4	8699.2019	0.0007
6	2	4	5	2	3	8810.9974	0.0008
6	3	4	5	3	3	8730.8070	0.0049
7	0	7	6	0	6	9997.6075	0.0036
7	1	7	6	1	6	9891.6779	-0.0045
7	1	6	6	1	5	10350.8961	-0.0091
7	2	6	6	2	5	10140.1996	-0.0077
7	2	5	6	2	4	10309.0725	-0.0044
7	3	4	6	3	3	10202.7217	-0.0025
7	3	5	6	3	4	10189.1603	0.0058
8	0	8	7	0	7	11383.4011	0.0074
8	1	8	7	1	7	11292.5673	0.0054
8	1	7	7	1	6	11806.1217	0.0132
8	2	7	7	2	6	11577.2151	-0.0236
8	2	6	7	2	5	11811.8111	0.0075

Table A7.26. Measured rotational transition frequencies (ν_{obs}) for the D14 isotopologue of D2W2 and residual ($\nu_{obs}-\nu_{calc}$) for the fit of table A7.6 (frequencies in MHz).

J'	K _a '	K _c '	J''	K _a ''	K _c ''	ν_{obs}	$\nu_{obs}-\nu_{calc}$
5	1	5	4	1	4	7087.1645	-0.0074
5	0	5	4	0	4	7202.4620	-0.0126
5	2	4	4	2	3	7256.7389	-0.0053
5	2	3	4	2	2	7317.9675	-0.0060
6	1	6	5	1	5	8497.1533	0.0022
6	0	6	5	0	5	8612.7585	-0.0046
6	1	5	5	1	4	8884.5792	-0.0044
6	2	4	5	2	3	8805.5544	-0.0112
6	3	3	5	3	2	8736.6167	-0.0054
6	3	4	5	3	3	8731.3160	0.0112
7	1	7	6	1	6	9903.8278	0.0021
7	0	7	6	0	6	10011.4979	0.0165
7	2	6	6	2	5	10144.3152	0.0093
7	2	5	6	2	4	10301.2860	-0.0034
7	1	6	6	1	5	10350.1358	0.0410
8	1	8	7	1	7	11307.1995	0.0060
8	0	8	7	0	7	11401.0326	-0.0051
8	2	6	7	2	5	11802.0770	-0.0079
8	1	7	7	1	6	11807.2921	-0.0121
9	1	9	8	1	8	12707.4329	0.0221
9	0	9	8	0	8	12784.6258	-0.0305

Table A7.27. Measured rotational transition frequencies (ν_{obs}) for the D13,14 isotopologue of

D2W2 and residual ($v_{obs}-v_{calc}$) for the fit of table A7.6 (frequencies in MHz).

J'	K _a '	K _c '	J''	K _a ''	K _c ''	v_{obs}	$v_{obs}-v_{calc}$
7	1	7	6	1	6	9845.7336	-0.0153
6	1	6	5	1	5	8447.8559	0.0018
5	1	5	4	1	4	7046.4866	-0.0006
7	0	7	6	0	6	9950.1493	-0.0067
5	0	5	4	0	4	7161.3982	0.0113
8	0	8	7	0	7	11329.6692	-0.0008
9	0	9	8	0	8	12703.7247	0.0054
6	1	5	5	1	4	8842.1840	-0.0365
5	1	4	4	1	3	7377.9051	0.0185
8	1	8	7	1	7	11240.2319	0.0308
8	1	7	7	1	6	11747.6086	0.0126
9	1	9	8	1	8	12631.3889	-0.0198
5	2	3	4	2	2	7285.3870	0.0113
5	2	4	4	2	3	7219.6284	-0.0100

Table A7.28. Measured rotational transition frequencies (v_{obs}) for the D15,16 isotopologue of D2W2 and residual ($v_{obs}-v_{calc}$) for the fit of table A7.6 (frequencies in MHz).

J'	K _a '	K _c '	J''	K _a ''	K _c ''	v_{obs}	$v_{obs}-v_{calc}$
5	1	5	4	1	4	7065.2094	-0.0234
6	1	6	5	1	5	8470.5356	0.0132
7	1	7	6	1	6	9872.4573	0.0175
8	1	8	7	1	7	11271.0048	-0.0279
5	1	4	4	1	3	7397.4547	-0.0003
6	1	5	5	1	4	8865.8232	0.0008
7	1	6	6	1	5	10327.1548	-0.0131
5	0	5	4	0	4	7180.4399	0.0302
8	1	7	7	1	6	11779.6193	-0.0039
9	0	9	8	0	8	12739.3679	0.0052
5	2	3	4	2	2	7305.0094	0.0117
6	2	5	5	2	4	8681.0678	-0.0347
6	2	4	5	2	3	8791.4616	0.0085
7	2	6	6	2	5	10119.4398	-0.0112
8	2	7	7	2	6	11554.0306	0.0297

Table A7.29. Measured rotational transition frequencies (v_{obs}) for the D13,14,16 isotopologue of D2W2 and residual ($v_{obs}-v_{calc}$) for the fit of table A7.6 (frequencies in MHz).

J'	K _a '	K _c '	J''	K _a ''	K _c ''	v_{obs}	$v_{obs}-v_{calc}$
5	0	5	4	0	4	7116.0757	0.0014
5	1	5	4	1	4	7002.7034	0.0034
5	1	4	4	1	3	7333.9267	0.0040
5	2	3	4	2	2	7243.6306	-0.0081
5	2	4	4	2	3	7175.9756	-0.0120
6	0	6	5	0	5	8506.6051	0.0082
6	1	6	5	1	5	8395.1073	-0.0037
6	2	5	5	2	4	8604.5845	-0.0061
6	2	4	5	2	3	8718.2153	0.0032
6	3	4	5	3	3	8636.7643	-0.0082
6	3	3	5	3	2	8643.2172	0.0073
7	0	7	6	0	6	9885.3580	-0.0031
7	1	7	6	1	6	9783.9989	0.0030

7	1	6	6	1	5	10236.6293	0.0034
7	2	5	6	2	4	10200.7404	0.0004
8	1	8	7	1	7	11169.3998	-0.0082
8	0	8	7	0	7	11255.4119	0.0021
8	1	7	7	1	6	11674.8373	0.0019
9	1	8	8	1	7	13101.5170	-0.0110
8	2	7	7	2	6	11450.7023	0.0198

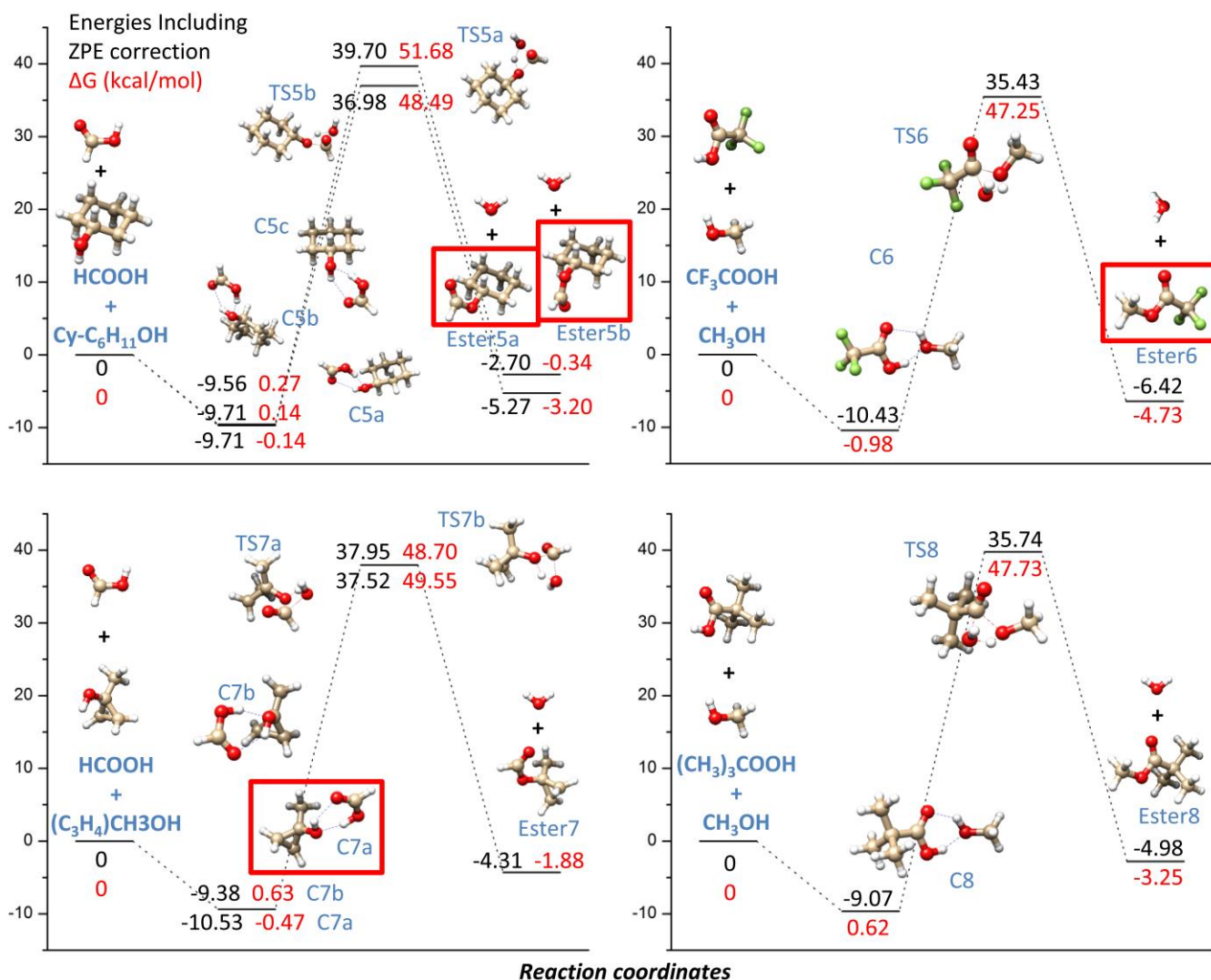
VIII. The Borderline between Reactivity and Pre-reactivity of Binary Mixtures of Gaseous Carboxylic Acids and Alcohols

A8.1. Table of the experimental Signal/Noise ratio.

Table A8.1. Theoretical main dipole moment component (b2plypd3/ mAug-cc-pVTZ) and experimental S/N ratio observed for the strongest transitions of the species listed in table A8.1 and 8.2.

	<i>Main dipole moment component (D)</i>	<i>S/N</i>
HCOOH - CH₃OH (C1)	$\mu_a = 1.2$	Not observed
Methylformate	$\mu_a = 1.6$	>200
HCOOH - CH₃CH₂OH (C2a)	$\mu_a = 1.3$	Not observed
Ethylformate	$\mu_a = 1.8$	>400
HCOOH - (CH₃)₂CHOH (C3a)	$\mu_a = 1.7$	Not observed
Isopropylformate	$\mu_a = 1.8$	>350
HCOOH - cy-C₆H₁₁OH (C5a)	$\mu_a = 2.0$	Not observed
Cyclo-hexylformate	$\mu_a = 1.9$	>100
CF₃COOH - CH₃OH (C6)	$\mu_a = 4.3$	Not observed
Methyl-Trifluoroacetate	$\mu_b = 2.9$	>250
HCOOH - (CH₃)₃COH (C4)	$\mu_a = 1.9$	>30
<i>tert</i>-butylformate	$\mu_a = 2.1$	Not observed
HCOOH - cy-C₃H₄CH₃OH (C7a)	$\mu_a = 1.4$	>45
1-methyl-cyclopropylformate	$\mu_a = 1.6$	Not observed

A8.2. Schemes of theoretical reaction profiles for 4 additional cases: $\text{HCOOH} + \text{C}_6\text{H}_{11}\text{OH}$, $\text{CF}_3\text{COOH} + \text{CH}_3\text{OH}$, $\text{HCOOH} + \text{C}_3\text{H}_4\text{CH}_3\text{OH}$, and $(\text{CH}_3)_3\text{CCOOH} + \text{CH}_3\text{OH}$.



A8.3. Energy values for all reactions.

Table A8.2. Absolute (A.E.E.), relative electronic (R.E.E.), zero-point corrections (ZPE), absolute (A.E.E. + ZPE) and relative (R.E.E. + ZPE) zero-point corrected energies for the $\text{HCOOH} + \text{CH}_3\text{OH}$ reaction, calculated at B2PLYP-D3/mAug-cc-pVTZ level. The A.E.E. for the C1 species is BSSE corrected.

HCOOH + CH ₃ OH					
	A.E.E. (hartrees)	R.E.E. (kcal/mol)	ZPE (hartrees)	A.E.E.+ ZPE (hartrees)	R.E.E.+ ZPE (kcal/mol)
HCOOH	-189.715146		0.033806	-189.681340	
CH ₃ OH	-115.679504		0.051574	-115.627930	
HCOOH+CH ₃ OH	-305.394650	0.00		-305.309270	0.00

C1	-305.411785	-10.75	0.088386	-305.323398	-8.87
TS1	-305.332050	39.28	0.083063	-305.248987	37.83
Ester	-228.990075		0.062313	-228.927762	
H₂O	-76.411052		0.021409	-76.389643	
Ester + H₂O	-305.401127	-4.06		-305.317405	-5.10

Table A8.3. Absolute (A.E.E.), relative electronic (R.E.E.), zero-point corrections (ZPE), absolute (A.E.E.+ ZPE) and relative (R.E.E. + ZPE) zero-point corrected energies for the HCOOH + CH₃CH₂OH reaction, calculated at B2PLYP-D3/mAug-cc-pVTZ level. The A.E.E. for the C2a, C2b and C2c species are BSSE corrected.

HCOOH + CH₃CH₂OH					
	A.E.E. (hartrees)	R.E.E. (kcal/m ol)	ZPE (hartrees)	A.E.E.+ ZPE (hartrees)	R.E.E.+ ZPE (kcal/mol)
HCOOH	-189.7151455		0.03380552	-189.68134	
CH₃CH₂OH	-154.9731447		0.08031574	-154.892829	
HCOOH+CH₃CH₂OH	-344.6882903	0.00		-344.574169	0.00
C2a	-344.7056158	-10.87	0.11692183	-344.588694	-9.11
C2b	-344.7055911	-10.86	0.11698516	-344.588606	-9.06
C2c	-344.7055575	-10.84	0.11703560	-344.588522	-9.01
TS2a	-344.6253015	39.53	0.11160852	-344.513693	37.95
TS2b	-344.6260849	39.03	0.11174494	-344.51434	37.54
Ester2a	-268.2835070		0.09081401	-268.192693	
Ester2b	-268.2832671		0.09104015	-268.192227	
H₂O	-76.4110522		0.02140921	-76.389643	
Ester2a + H₂O	-344.6945592	-3.93		-344.582336	-5.12
Ester2b + H₂O	-344.6943194	-3.78		-344.58187	-4.83

Table A8.4. Absolute (A.E.E.), relative electronic (R.E.E.), zero-point corrections (ZPE), absolute (A.E.E.+ ZPE) and relative (R.E.E. + ZPE) zero-point corrected energies for the HCOOH + (CH₃)₂CHOH reaction, calculated at B2PLYP-D3/mAug-cc-pVTZ level. The A.E.E. for the C3a, C3b and C3c species are BSSE corrected.

HCOOH + (CH₃)₂CHOH					
	A.E.E. (hartrees)	R.E.E. (kcal/mol)	ZPE (hartrees)	A.E.E.+ ZPE (hartrees)	R.E.E.+ ZPE (kcal/mol)
HCOOH	-189.715146		0.03380552	-189.68134	
(CH₃)₂CHOH	-194.267201		0.10839289	-194.158808	
HCOOH+(CH₃)₂CHO H	-383.982346	0.00		-383.840148	0.00
C3a	-384.000408	-11.33	0.14487245	-383.855535	-9.66
C3b	-384.000436	-11.35	0.14493615	-383.855499	-9.63
C3c	-384.000058	-11.11	0.14493024	-383.855128	-9.40
TS3	-383.920441	38.85	0.13965866	-383.780782	37.25
Ester3	-307.577696		0.11888678	-307.458809	
H₂O	-76.4110522		0.02140921	-76.389643	
Ester3 + H₂O	-383.988748	-4.02		-383.848452	-5.21

Table A8.5. Absolute (A.E.E.), relative electronic (R.E.E.), zero-point corrections (ZPE), absolute (A.E.E.+ ZPE) and relative (R.E.E. + ZPE) zero-point corrected energies for the HCOOH + (CH₃)₃COH reaction, calculated at B2PLYP-D3/mAug-cc-pVTZ level. The A.E.E. for the C4 species are BSSE corrected.

HCOOH + (CH₃)₃COH					
	A.E.E. (hartrees)	R.E.E. (kcal/mol)	ZPE (hartrees)	A.E.E.+ ZPE (hartrees)	R.E.E.+ ZPE (kcal/mol)
HCOOH	-189.7151455		0.03380552	-189.68134	
(CH₃)₃COH	-233.56172		0.13608798	-233.425632	
HCOOH+(CH₃)₃COH	-423.2768655	0.00		-423.106972	0.00
C4	-423.2948832	-11.31	0.17252976	-423.122353	-9.65
TS4	-423.2108745	41.41	0.16728246	-423.043592	39.77
Ester4	-346.8682852		0.1465032	-346.721782	
H₂O	-76.41105221		0.02140921	-76.389643	
Ester4+H₂O	-423.2793374	-1.55		-423.111425	-2.79

Table A8.6. Absolute (A.E.E.), relative electronic (R.E.E.), zero-point corrections (ZPE), absolute (A.E.E.+ ZPE) and relative (R.E.E. + ZPE) zero-point corrected energies for the $\text{HCOOH} + \text{C}_6\text{H}_{11}\text{OH}$ reaction, calculated at B2PLYP-D3/mAug-cc-pVTZ level. The A.E.E. for the C5a, C5b and C5c species are BSSE corrected.

HCOOH + C₆H₁₁OH					
	A.E.E. (hartrees)	R.E.E. (kcal/mol)	ZPE (hartrees)	A.E.E.+ ZPE (hartrees)	R.E.E.+ ZPE (kcal/mol)
HCOOH	-189.7151455		0.03380552	-189.681340	
C₆H₁₁OH	-310.9380168		0.17531683	-310.762700	
HCOOH+C₆H₁₁OH	-500.6531623	0.00		-500.444040	0.00
C5a	-500.6712728	-11.36	0.21175883	-500.459514	-9.71
C5b	-500.6712985	-11.38	0.21178752	-500.459511	-9.71
C5c	-500.6711065	-11.26	0.21182545	-500.459281	-9.56
TS5a	-500.5915765	38.65	0.20647152	-500.385105	36.98
TS5b	-500.5873070	41.32	0.20653897	-500.380768	39.70
Ester5a	-424.2485699		0.18577194	-424.062798	
Ester5b	-424.2446278		0.18592078	-424.058707	
H₂O	-76.41105221		0.02140921	-76.3896430	
Ester5a+H₂O	-500.6596222	-4.05		-500.452441	-5.27
Ester5b+H₂O	-500.6556800	-1.58		-500.448350	-2.70

Table A8.7. Absolute (A.E.E.), relative electronic (R.E.E.), zero-point corrections (ZPE), absolute (A.E.E.+ ZPE) and relative (R.E.E. + ZPE) zero-point corrected energies for the $\text{CF}_3\text{COOH} + \text{CH}_3\text{OH}$ reaction, calculated at B2PLYP-D3/mAug-cc-pVTZ level. The A.E.E. for the C6 species are BSSE corrected.

CF₃COOH + CH₃OH					
	A.E.E. (hartrees)	R.E.E. (kcal/mol)	ZPE (hartrees)	A.E.E.+ ZPE (hartrees)	R.E.E.+ ZPE (kcal/mol)
CF₃COOH	-526.709072		0.03897128	-526.670101	
CH₃OH	-115.679504		0.05157436	-115.62793	
CF₃COOH+CH₃OH	-642.388577	0.00		-642.298031	0.00
C6	-642.407629	-11.96	0.09297904	-642.31465	-10.43
TS6	-642.329688	36.95	0.08811055	-642.241577	35.43
Ester6	-565.985824		0.06720917	-565.918615	
H₂O	-76.4110522		0.02140921	-76.389643	
Ester6+H₂O	-642.396876	-5.21		-642.308258	-6.42

Table A8.8. Absolute (A.E.E.), relative electronic (R.E.E.), zero-point corrections (ZPE), absolute (A.E.E. + ZPE) and relative (R.E.E. + ZPE) zero-point corrected energies for the HCOOH + (C₃H₄)CH₃OH reaction, calculated at B2PLYP-D3/mAug-cc-pVTZ level. The A.E.E. for the C7a and C7b species are BSSE corrected.

HCOOH + (C₃H₄)CH₃OH					
	A.E.E. (hartrees)	R.E.E. (kcal/mol)	ZPE (hartrees)	A.E.E. + ZPE (hartrees)	R.E.E. + ZPE (kcal/mol)
HCOOH	-189.715146		0.03380552	-189.68134	
(C₃H₄)CH₃OH	-232.315919		0.1135023	-232.202417	
HCOOH+(C₃H₄)CH₃O H	-422.031065	0.00		-421.883757	0.00
C7a	-422.050937	-12.47	0.15040515	-421.900532	-10.53
C7b	-422.048991	-11.25	0.1502905	-421.898701	-9.38
TS7a	-421.968962	38.97	0.14498931	-421.823973	37.52
TS7b	-421.968154	39.48	0.1448784	-421.823276	37.95
Ester7	-345.625223		0.12423743	-345.500986	
H₂O	-76.4110522		0.02140921	-76.389643	
Ester7+H₂O	-422.036276	-3.27		-421.890629	-4.31

Table A8.9. Absolute (A.E.E.), relative electronic (R.E.E.), zero-point corrections (ZPE), absolute (A.E.E. + ZPE) and relative (R.E.E. + ZPE) zero-point corrected energies for the (CH₃)₃CCOOH + CH₃OH reaction, calculated at B2PLYP-D3/mAug-cc-pVTZ level. The A.E.E. for the C8 species are BSSE corrected.

(CH₃)₃CCOOH + CH₃OH					
	A.E.E. (hartrees)	R.E.E. (kcal/mol)	ZPE (hartrees)	A.E.E. + ZPE (hartrees)	R.E.E. + ZPE (kcal/mol)
(CH₃)₃COOH	-346.885268		0.14705398	-346.738214	
CH₃OH	-115.6795044		0.05157436	-115.62793	
(CH₃)₃COOH+CH₃O H	-462.5647723	0.00		-462.366144	0.00
C8	-462.5819252	-10.76	0.20133147	-462.380594	-9.07
TS8	-462.5049136	37.56	0.19571965	-462.309194	35.74
Ester8	-386.159575		0.17514297	-385.984432	
H₂O	-76.41105221		0.02140921	-76.389643	
Ester8+H₂O	-462.5706272	-3.67		-462.374075	-4.98

A8.3. Tables of free energies.

Table A8.10. Absolute and relative ΔG values for the $\text{HCOOH} + \text{CH}_3\text{OH}$ reaction, calculated at B2PLYP- D3/mAug-cc-pVTZ level. The absolute G value for the C1 species is BSSE corrected.

HCOOH + CH₃OH		
	ΔG	
	<i>Absolute</i> (hartrees)	<i>Relative</i> (kcal/mol)
HCOOH	-189.705421	
CH₃OH	-115.650714	
HCOOH+CH₃OH	-305.356135	0.00
C1	-305.355181	0.60
TS1	-305.278792	48.53
Ester	-228.954528	
H₂O	-76.407283	
Ester + H₂O	-305.361811	-3.56

Table A8.11. Absolute and relative ΔG values for the $\text{HCOOH} + \text{CH}_3\text{CH}_2\text{OH}$ reaction, calculated at B2PLYP-D3/mAug-cc-pVTZ level. The absolute G values for the C2a, C2b and C2c species are BSSE corrected.

HCOOH + CH₃CH₂OH		
	ΔG	
	<i>Absolute</i> (hartrees)	<i>Relative</i> (kcal/mol)
HCOOH	-189.705421	
CH₃CH₂OH	-154.918269	
HCOOH+CH₃CH₂OH	-344.62369	0.00
C2a	-344.622434	0.79
C2b	-344.623039	0.41
C2c	-344.622837	0.54
TSa	-344.54671	48.31
TSb	-344.545855	48.84
Ester2a	-268.221822	
Ester2b	-268.221065	
H₂O	-76.407283	
Ester2a + H₂O	-344.629105	-3.40

Ester2b + H₂O	-344.628348	-2.92
---------------------------------	-------------	-------

Table A8.12. Absolute and relative ΔG values for the $\text{HCOOH} + (\text{CH}_3)_2\text{CHOH}$ reaction, calculated at B2PLYP-D3/mAug-cc-pVTZ level. The absolute G values for the C3a, C3b and C3c species are BSSE corrected.

HCOOH + (CH₃)₂CHOH		
	ΔG	
	<i>Absolute</i> (hartrees)	<i>Relative</i> (kcal/mol)
HCOOH	-189.705421	
(CH₃)₂CHOH	-194.186244	
HCOOH+(CH₃)₂CHOH	-383.891665	0.00
C3a	-383.891781	-0.07
C3b	-383.890940	0.45
C3c	-383.891310	0.22
TS3	-383.814055	48.70
Ester3	-307.489485	
H₂O	-76.407283	
Ester3 + H₂O	-383.896768	-3.20

Table A8.13. Absolute and relative ΔG values for the $\text{HCOOH} + (\text{CH}_3)_3\text{COH}$ reaction, calculated at B2PLYP-D3/mAug-cc-pVTZ level. The absolute G value for the C4 species is BSSE corrected.

HCOOH + (CH₃)₃COH		
	ΔG	
	<i>Absolute</i> (hartrees)	<i>Relative</i> (kcal/mol)
HCOOH	-189.705421	
(CH₃)₃COH	-233.454623	
HCOOH+(CH₃)₃COH	-423.160044	0.00
C4	-423.159625	0.26
TS4	-423.077670	51.69
Ester4	-346.753582	
H₂O	-76.407283	
Ester4+H₂O	-423.160865	-0.52

Table A8.14. Absolute and relative ΔG values for the $\text{HCOOH} + \text{C}_6\text{H}_{11}\text{OH}$ reaction, calculated at B2PLYP- D3/mAug-cc-pVTZ level. The absolute G value for the C5a, C5b and C5c species are BSSE corrected.

HCOOH+C₆H₁₁H		
	ΔG	
	<i>Absolute</i> (hartrees)	<i>Relative</i> (kcal/mol)
HCOOH	-189.705421	
C₆H₁₁OH	-310.79311	
HCOOH+C₆H₁₁OH	-500.498531	0.00
C5a	-500.498762	-0.14
C5b	-500.498314	0.14
C5c	-500.498104	0.27
TS5a	-500.421262	48.49
TS5b	-500.416177	51.68
Ester5a	-424.096355	
Ester5b	-424.091788	
H₂O	-76.407283	
Ester5a+H₂O	-500.503638	-3.20
Ester5b+H₂O	-500.499071	-0.34

Table A8.15. Absolute and relative ΔG values for the $\text{CF}_3\text{COOH} + \text{CH}_3\text{OH}$ reaction, calculated at B2PLYP- D3/mAug-cc-pVTZ level. The absolute G value for the C6 species is BSSE corrected.

CF₃COOH + CH₃OH		
	ΔG	
	<i>Absolute</i> (hartrees)	<i>Relative</i> (kcal/mol)
CF₃COOH	-526.701462	
CH₃OH	-115.650714	
CF₃COOH+CH₃OH	-642.352176	0.00
C6	-642.353741	-0.98
TS6	-642.276874	47.25
Ester6	-565.952437	
H₂O	-76.407283	
Ester6+H₂O	-642.359720	-4.73

Table A8.16. Absolute and relative ΔG values for the $\text{HCOOH} + (\text{C}_3\text{H}_4)\text{CH}_3\text{OH}$ reaction, calculated at B2PLYP-D3/mAug-cc-pVTZ level. The absolute G value for the C7a and C7b species are BSSE corrected.

HCOOH + (C₃H₄)CH₃OH		
	ΔG	
	<i>Absolute</i> (hartrees)	<i>Relative</i> (kcal/mol)
HCOOH	-189.705421	
(C₃H₄)CH₃OH	-232.230902	
HCOOH+(C₃H₄)CH₃O H	-421.936323	0.00
C7a	-421.937074	-0.47
C7b	-421.935326	0.63
TS7a	-421.857359	49.55
TS7b	-421.856789	49.91
Ester7a	-345.532034	
Ester7b	-345.532034	
H₂O	-76.407283	
Ester7a+H₂O	-421.939317	-1.88
Ester7b+H₂O	-421.939317	-1.88

Table A8.17. Absolute and relative ΔG values for the $(\text{CH}_3)_3\text{COOH} + \text{CH}_3\text{OH}$ reaction, calculated at B2PLYP-D3/mAug-cc-pVTZ level. The absolute G value for the C8 species is BSSE corrected.

(CH₃)₃COOH + CH₃OH		
	ΔG	
	<i>Absolute</i> (hartrees)	<i>Relative</i> (kcal/mol)
(CH₃)₃COOH	-526.701462	
CH₃OH	-115.650714	
(CH₃)₃COOH+CH₃OH	-642.352176	0.00
C8	-642.353741	0.62
TS8	-642.276874	47.73
Ester8	-565.952437	
H₂O	-76.407283	
Ester8+H₂O	-642.359720	-3.25

References

- [1] W. Gordy, R. L. Cook, *Microwave Molecular Spectra*, 3rd ed., Wiley, New York, **1984**.
- [2] H. W. Kroto, *Molecular Rotation Spectra*, John Wiley & Sons, London, **1975**.
- [3] J. E. Wollrab, E. M. Loebl, *Rotational spectra and Molecular Structure*, 1st Edition, **1967**.
- [4] W. Caminati, J.-U. Grabow, *Microwave Spectroscopy in Molecular Systems in Frontiers of Molecular Spectroscopy* (Ed.: J. Laane), Elsevier, **2009**.
- [5] W. Caminati, J.-U. Grabow, *Frontiers and Advances in Molecular Spectroscopy* (Ed.: J. Laane), Elsevier, **2018**.
- [6] C.E. Cleeton, N.H. Williams, *Physical Review*. **1934**, 45, 234–237.
- [7] R. H. Hughes and E. B. Wilson, Jr., *Phys. Rev.* **1947**, 71, 562.
- [8] T.J. Balle, W.H. Flygare, *Rev. Sci. Instrum.* **1981**, 52, 33-45.
- [9] G. G. Brown, B. C. Dian, K. O. Douglass, S.M. Geyer, S.T. Shipman, B.H. Pate, *Rev. Sci. Instrum.* **2008**, 79, 053103.
- [10] D. Patterson¹, M. Schnell, J. M. Doyle¹, *Nature*, **2013**, 497, 475-478.
- [11] S. Melandri, W. Caminati, L.B. Favero, A. Millemaggi, P.G. Favero, *J. Mol. Struct.* **1994**, 352/352, 253-258.
- [12] R.D. Brown, J.G. Crofts, P.D. Godfrey, D. McNaughton, A.P. Pierlot, *J. Mol. Struct.*, **1988**, 190, 185.
- [13] C. Calabrese, A. Vigorito, A. Maris, S. Mariotti, P. Fathi, W. D. Geppert, S. Melandri, *J Phys Chem A*. **2015**, 119, 11674-82.
- [14] W. Caminati, A. Millemaggi, J.L. Alonso, A. Lesarri, J.C. López, S. Mata, *Chem. Phys. Lett.* **2004**, 392, 1-6.
- [15] a) I. Uriarte, P. Ecija, L. Spada, E. Zabalza, A. Lesarri, F. J. Basterretxea, J. A. Fernandez, W. Caminati, E. J. Cocinero, *Phys Chem Chem Phys*, **2016**, 18, 3966-74. b) I. Uriarte, C. Perez, E.C. Mancebo, F. J. Basterretxea, A. Lesarri, J. A. Fernandez, E. J. Cocinero, *Chem. Eur.J.* **2017**, 23, 7238–7244.
- [16] T.L. Smithson, J.A. Duckett, H. Wieser, *J. Phys. Chem.* **1984**, 88, 1102.
- [17] K.H. Hassan, J.M. Hollas, *J. Mol. Spectrosc.* **1991**, 147, 100.
- [18] W. Caminati, D. Damiani, G. Corbelli, L.B. Favero, *Mol. Phys.* **1992**, 75, 857.
- [19] W. Caminati, B.L. Favero, B. Velino, F. Zerbetto, *Mol. Phys.* **1993**, 78, 1561.
- [20] K.H. Hassan, J.M. Hollas, *Chem. Phys. Lett.* **1990**, 169, 17.

- [21] W. Caminati, D. Damiani, L.B. Favero, *Mol. Phys.* **1993**, 79, 699.
- [22] S. Sakurai, N. Meinander, J. Laane, *J. Chem. Phys.* **1998**, 108, 3537.
- [23] J.A. Duckett, T.C. Smithson, H. Wieser, *Chem. Phys. Lett.* **1979**, 64, 261.
- [24] K.H. Hassan, J.M. Hollas, *Chem. Phys. Lett.* **1989**, 157, 183.
- [25] W. Caminati, S. Melandri, G. Corbelli, B.L. Favero, R. Meyer, *Mol. Phys.* **1993**, 80, 1297.
- [26] S. Sakurai, N. Meinander, K. Morris, J. Laane, *J. Am. Chem. Soc.* **1999**, 121, 5056.
- [27] J. Laane, E. Bondoc, S. Sakurai, K. Morris, N. Meinander, J. Choo, *J. Am. Chem. Soc.* **2000**, 122, 2628.
- [28] G. Pietraperzia, A. Zoppi, M. Becucci, E. Droghetti, E. Castellucci, *Chem. Phys. Lett.* **2004** 385, 304.
- [29] Z. Kisiel, L.Pszczókowski, G. Pietraperzia, M. Becucci, W. Caminati, R. Meyer, *Phys Chem Chem Phys.* **2004**, 6, 5469.
- [30] P. Ottaviani, W. Caminati, *Chem. Phys. Lett.* **2005**, 405, 68.
- [31] J.A. Yang, K. Okuyama, K. Morris, J. Laane, *J. Phys. Chem. A*, **2005**, 109, 8290.
- [32] E. Bondoc, T. Klots, J. Laane, *J. Phys. Chem. A*, **2000**, 104, 275.
- [33] Z. Arp, N. Meinander, J. Choo, and J. Laane, *J. Chem. Phys.* **2002**, 116, 6648.
- [34] A. Das, K. K. Mahato, S. S. Panja, T. Chakraborty, *J. Chem. Phys.*, **2003**, 119, 2523.
- [35] Y. He and W. Kong, *J. Chem. Phys.* **2005**, 122, 244302.
- [36] T. J. Balle, W. H. Flygare, *Rev. Sci. Instrum.* **1981**, 52, 33-45.
- [37] J.-U. Grabow, W. Stahl, H. Dreizler, *Rev. Sci. Instrum.* **1996**, 67, 4072-4084.
- [38] H. M. Pickett, *J. Mol. Spectrosc.* **1991**, 148, 371-377.
- [39] J.K.G. Watson, in: J.R. Durig (Ed.), *Vibrational Spectra and Structure*, 6, Elsevier, New York/Amsterdam, **1977**, 6, 1-89.
- [40] J. Kraitchman, *Am. J. Phys.* **1953**, 21, 17-25.
- [41] C. C. Costain, G. P. Srivastava, *J. Chem. Phys.* **1961**, 35, 1903-1904.
- [42] Gaussian 09, Revision D.01, M. J. Frisch, G. W. Trucks, H. B. Schlegel, G. E. Scuseria, M. A. Robb, J. R. Cheeseman, G. Scalmani, V. Barone, B. Mennucci, G. A. Petersson, H. Nakatsuji, M. Caricato, X. Li, H. P. Hratchian, A. F. Izmaylov, J. Bloino, G. Zheng, J. L. Sonnenberg, M. Hada, M. Ehara, K. Toyota, R. Fukuda, J. Hasegawa, M. Ishida, T. Nakajima, Y. Honda, O. Kitao, H. Nakai, T. Vreven, J. A. Montgomery, Jr., J. E. Peralta, F. Ogliaro, M. Bearpark, J. J. Heyd, E. Brothers, K. N. Kudin, V. N. Staroverov, T. Keith, R. Kobayashi, J. Normand, K. Raghavachari, A. Rendell, J. C. Burant, S. S. Iyengar, J. Tomasi, M. Cossi, N. Rega, J. M. Millam, M. Klene, J. E. Knox, J. B. Cross, V. Bakken, C. Adamo, J. Jaramillo, R. Gomperts, R. E. Stratmann, O. Yazyev, A. J. Austin, R. Cammi, C. Pomelli, J. W. Ochterski, R. L. Martin, K.

Morokuma, V. G. Zakrzewski, G. A. Voth, P. Salvador, J. J. Dannenberg, S. Dapprich, A. D. Daniels, O. Farkas, J. B. Foresman, J. V. Ortiz, J. Cioslowski, and D. J. Fox, Gaussian, Inc., Wallingford CT, 2013.

- [43] R. Meyer, *J. Mol. Spectrosc.* **1979**, 76, 266–300.
- [44] R.L. Jaffe, G.D. Smith, D.Y. Yoon, *J. Phys. Chem.* **1993**, 97, 12745.
- [45] Y.-K. Han, K.H. Kim, S.-K. Son, Y.S. Lee, *Bull. Korean Chem. Soc.* **2002**, 23, 1267.
- [46] N. Goutev, K. Ohno, H. Matsuura, *J. Phys. Chem. A*, **2000**, 104, 9226.
- [47] K. Inomata, A. Abe, *J. Phys. Chem.* **1992**, 96, 7934.
- [48] H. Liu, F. Muller-Plathe, W.F. van Gunsteren *J. Chem. Phys.* **1995**, 22, 1722.
- [49] D.J. Williams, K.B. Hall, *J. Phys. Chem.* **1996**, 100, 8224.
- [50] P.M. Anderson, M.R. Wilson, *Mol. Phys.* **2005**, 103, 89.
- [51] W. Caminati, L. Evangelisti, G. Feng, B.M. Giuliano, Q. Gou, S. Melandri, J.-U. Grabow *Phys. Chem. Chem. Phys.* **2016**, 18, 17851.
- [52] C. Calabrese, A. Maris, L. Evangelisti, L.B. Favero, S. Melandri, W. Caminati *J. Phys. Chem. A* **2013**, 117, 13712.
- [53] R.S. Ruoff, T.D. Klots, T. Emilson, H.S. Gutowski, *J. Chem. Phys.* **1990**, 93, 3142-3150.
- [54] H. Hartwig, H. Dreizler, *Z. Naturforsch.* **1996**, 51a, 923-932.
- [55] P.J. Groner, *Chem. Phys.* **1997**, 107, 4483.
- [56] I. Kleiner, *J. Mol. Spectrosc.* **2010**, 260, 1.
- [57] L. Evangelisti, L.B. Favero, A. Maris, S. Melandri, A. Vega-Toribio. A. Lesarri., W. Caminati *J. Mol. Spectrosc.* **2010**, 259, 65.
- [58] D. Gerhard, A. Hellweg, I. Merke, W. Stahl, M. Baudelet, D. Petitprez, G. Wlodarczak, *J. Mol. Spectrosc.* **2003**, 220, 234.
- [59] Z. Kisiel, L. Pszczolkowski, E. Bialkowaska-Jaworska, S.B. Charnley, *J. Mol. Spectrosc.* **2007**, 241, 220.
- [60] L.B. Favero, L. Evangelisti, G. Feng, L. Spada, W. Caminati, *Chem. Phys. Lett.* **2011**, 517, 139.
- [61] L.B. Favero, W. Caminati, B. Velino *Phys. Chem. Chem. Phys.* **2003**, 5, 4776.
- [62] L.B. Favero, L. Evangelisti, B. Velino, W. Caminati, *J. Phys. Chem. A* **2014**, 118, 4243–4248
- [63] W.F. van Gunsteren, J.R. Allison, X. Daura, J. Dolenc, N. Hansen, A.E. Mark, C. Oostenbrink, H. Rusu, L.J. Smith *Angew. Chem. Int. Ed.* **2016**, 55, 15990.
- [64] O. I. Baskakov, M.A.O. Pashaev, *J. Mol. Spectrosc.* **1992**, 151, 282–291.
- [65] J.C. Pearson, K.V.L.N. Sastry, E. Herbst, F.C. De Lucia, *J. Mol. Spectrosc.* **1996**, 175, 246–261.
- [66] E. Hirota,; Y. Kawashima, *J. Mol. Spectrosc.* **2001**, 207, 243–253.
- [67] Z. Kisiel, O. Dorosh, A. Maeda, I. R. Medvedev, F. C. De Lucia, E. Herbst, B. J. Drouin, J. C.

- Pearson, S. T. Shipman, *Phys. Chem. Chem. Phys.* **2010**, *12*, 8329–8339.
- [68] E. A. Cohen, B. J. Drouin, E. A. Valenzuela, R. C. Woods, W. Caminati, A. Maris, S. Melandri, *J. Mol. Spectrosc.* **2010**, *260*, 77–83.
- [69] A. K. King, B. J. Howard, *J. Mol. Spectrosc.* **2001**, *205*, 38–42.
- [70] M. A. Czarnecki, D. Wojtko^ó, K. Haufa, *Chem. Phys. Lett.* **2006**, *431*, 294–299.
- [71] M. J. Tubergen, A.R. Conrad, R. E. Chavez III, I. Hwang, R. D. Suenram, J. J. Pajski, B. H. Pate, *J. Mol. Spectrosc.* **2008**, *251*, 330–338.
- [72] G. G. Brown, B. C. Dian, K. O. Douglass, S. M. Geyer, S. T. Shipman, B. H. Pate, *Rev. Sci. Instrum.* **2008**, *79*, 053103.
- [73] J. N. Macdonald, D. Norbury, J. Sheridan, *J. Chem. Soc., Faraday Trans. 2* **1978**, *74*, 1365–1375.
- [74] W. Lin, A. Ganguly, A. J. Minei, G. L. Lindeke, W. C. Pringle, S. E. Novick, J. R. Durig, *J. Mol. Struct.* **2009**, *922*, 83–87.
- [75] E. J. Campbell, H. Zhou, S. T. Nguyen, *Org. Lett.* **2001**, *3*, 2391–2393.
- [76] J. J. Uebel, H. W. Goodwin, *J. Org. Chem.* **1968**, *33*, 3317–3319.
- [77] C.C. Costain, *Trans. Am. Cryst. Assoc.* **1966**, *2*, 157–164.
- [78] IUPAC. Compendium of Chemical Terminology, 2nd ed. (the "Gold Book"). Compiled by A. D. McNaught and A. Wilkinson. Blackwell Scientific Publications, Oxford (1997).
- [79] S. Melandri, *Phys. Chem. Chem. Phys.*, **2011**, *13*, 13901–13911.
- [80] E. M. Jr. Bellott, E. B. Wilson, *Tetrahedron* **1975**, *31*, 2896–2898.
- [81] L. Martinache, W. Kresa, M. Wegener, U. Vonmont, A. Bauder, *Chem. Phys.* **1990**, *148*, 129–140.
- [82] S. Antolinez, H. Dreizler, V. Storm, D. H. Sutter, J. L. Alonso, *Z. Naturforsch.* **1997**, *52a*, 803–806.
- [83] A. M. Daly, K. O. Douglass, L. C. Sarkozy, J. L. Neill, M. T. Muckle, D. P. Zaleski, B. H. Pate, S. G. Kukolich, *J. Chem. Phys.* **2011**, *135*, 154304, 1–12.
- [84] M. C. D. Tayler, B. Ouyang, B. J. Howard, *J. Chem. Phys.* **2011**, *134*, 054316, 1–9.
- [85] G. Feng, L. B. Favero, A. Maris, A. Vigorito, W. Caminati, R. Meyer, *J. Am. Chem. Soc.* **2012**, *134*, 19281–19286.
- [86] L. Evangelisti, P. Eci^o, E. J. Cocinero, F. Castano, A. Lesarri, W. Caminati, R. Meyer, *J. Phys. Chem. Lett.* **2012**, *3*, 3770–3775.
- [87] G. Feng, Q. Gou, L. Evangelisti, Z. Xia, W. Caminati, *Phys. Chem. Chem. Phys.* **2013**, *15*, 2917–2922.
- [88] Q. Gou, G. Feng, L. Evangelisti, W. Caminati, *J. Phys. Chem. Lett.* **2013**, *4*, 2838–2842.

- [89] Q. Gou, G. Feng, L. Evangelisti, W. Caminati, *J. Phys. Chem. A* **2013**, *117*, 13500–13503.
- [90] Q. Gou, G. Feng, L. Evangelisti, W. Caminati, *Chem. Phys. Lett.* **2014**, *591*, 301–305.
- [91] G. Feng, Q. Gou, L. Evangelisti, W. Caminati, *Angew. Chem. Int. Ed.* **2014**, *53*, 530–534.
- [92] L. Evangelisti, G. Feng, Q. Gou, W. Caminati, *J. Mol. Spectrosc.* **2014**, *299*, 1-5.
- [93] Q. Gou, G. Feng, L. Evangelisti, W. Caminati, *ChemPhysChem* **2014**, *15*, 2977–2984.
- [94] I. Kalkman, C. Vu, M. Schmitt, W. L. Meerts, *ChemPhysChem* **2008**, *9*, 1788–1797.
- [95] O. Birer, M. Havenith, *Annu. Rev. Phys. Chem.* **2009**, *60*, 263–75, and ref.s therein.
- [96] D. Priem, T.-K. Ha, A. Bauder, *J. Chem. Phys.* **2000**, *113*, 169-175.
- [97] B. Ouyang, T. G. Starkey, B. J. Howard, *J. Phys. Chem. A* **2007**, *111*, 6165-6175
- [98] B. Ouyang, B. J. Howard, *J. Phys. Chem. A* **2008**, *112*, 8208-8214.
- [99] B. Ouyang, B. J. Howard, *Phys. Chem. Chem. Phys.* **2009**, *11*, 366-373.
- [100] B. Ouyang, B. J. Howard, *J. Phys. Chem. A* **2010**, *114*, 4109–4117
- [101] E. G. Schnitzler, W. Jager, *Phys. Chem. Chem. Phys.* **2014**, *16*, 2305-2314.
- [102] A. Vigorito, Q. Gou, C. Calabrese, S. Melandri, A. Maris, W. Caminati, *ChemPhysChem* **2015**, *16*, 2961–2967.
- [103] Q. Gou, L. B. Favero, S. S. Bahamyirou, Z. Xia, W. Caminati, *J. Phys. Chem. A* **2014**, *118*, 10738–10741.
- [104] A. M. Daly, B. A. Sargus, S. G. Kukolich, *J. Chem. Phys.* **2010**, *133*, 174304.
- [105] L. Spada, Q. Gou, B. M. Giuliano, W. Caminati, *J. Phys. Chem. A* **2016**, *120*, 5094–5098.
- [106] S. F. Boys, F. Bernardi, *Mol. Phys.* **1970**, *19*, 553-566.
- [107] Y. Niidea, M. Hayashi, *J. Mol. Spectrosc.* **2003**, *220*, 65–79.
- [108] D. J. Millen, *Can. J. Chem.* **1985**, *63*, 1477-1479.
- [109] S. E. Novick, S. J. Harris, K. C. Janda, W. Klemperer, *Can. J. Phys.* **1975**, *53*, 2007-2015.
- [110] G. Feng, Q. Gou, L. Evangelisti, L. Spada, S. Blanco, W. Caminati, *Phys. Chem. Chem. Phys.* **2016**, *18*, 23651-23656.
- [111] J. L. Neill, S. T. Shipman, L. Alvarez-Valtierra, A. Lesarri, Z. Kisiel, B. H. Pate, *J. Mol. Spectrosc.* **2011**, *269*, 21-29
- [112] J. L. Alonso, R. Spielh, A. Guarnieri, J. C. Lo'pez and A. Lesarri, *J. Mol. Spectrosc.*, **1992**, *156*, 341–359.
- [113] S. Melandri, A. Maris, B. M. Giuliano, W. Caminati, *J. Chem. Phys.* **2005**, *123*, 164304, 1-6.
- [114] G. R. Desiraju, T. Steiner, *The Weak Hydrogen Bond*, Oxford University Press, Oxford, **1999**.
- [115] S. N. Delanoye, W. A. Herrebout, B. J. Van der Veken, *J. Am. Chem. Soc.* **2002**, *124*, 11854.

- [116] W. Caminati, J.-U. Grabow, Microwave spectroscopy: Molecular systems in *Frontiers of molecular spectroscopy*, (Ed: J. Laane), *Elsevier, Amsterdam*, **2008**, 455-552.
- [117] G.T. Fraser, F.J. Lovas, R.D. Suenram, D.D. Nelson Jr., W. Klemperer, *J. Chem. Phys.* **1986**, *84*, 5983.
- [118] J. C. López, J. L. Alonso, W. Caminati, *Ang. Chem. Int. Ed.* **2006**, *45*, 290; Q. Gou, G. Feng, L. Evangelisti, D. Loru, J. L. Alonso, J. C. López, W. Caminati, *J. Phys. Chem. A* **2013**, *117*, 13531.
- [119] Q. Gou, G. Feng, L. Evangelisti, W. Caminati, *J. Phys. Chem. A* **2014**, *118*, 737.
- [120] W. Caminati, J. C. López, J. L. Alonso, J.-U. Grabow, *Angew. Chem.* **2005**, *117*, 3908; *Angew. Chem. Int. Ed.* **2005**, *44*, 3840.
- [121] J. L. Alonso, S. Antolinez, S. Blanco, A. Lesarri, J. C. López, W. Caminati, *J. Am. Chem. Soc.* **2004**, *126*, 3244.
- [122] E. J. Cocinero, R. Sanchez, S. Blanco, A. Lesarri, J. C. López, J. L. Alonso, *Chem. Phys. Lett.* **2005**, *402*, 4.
- [123] L. B. Favero, B. M. Giuliano, A. Maris, S. Melandri, P. Ottaviani, B. Velino, W. Caminati, *Chem. Eur. J.* **2010**, *16*, 1761.
- [124] P. Ottaviani, W. Caminati, L. B. Favero, S. Blanco, J. C. López, J. L. Alonso, *Chem. Eur. J.* **2006**, *12*, 915-920.
- [125] L. B. Favero, B. M. Giuliano, S. Melandri, A. Maris, P. Ottaviani, B. Velino, W. Caminati, *J. Phys. Chem. A* **2005**, *109*, 7402.
- [126] L. H. Coudert, W. Caminati, A. Maris, P. Ottaviani, *J. Mol. Spectrosc.* **2010**, *261*, 18.
- [127] L. B. Favero, W. Li, G. Spadini, W. Caminati, *J. Mol. Spectrosc.*, **2015**, *316*, 45-48; T. L. Smithson, J. A. Duckett, H. Wieser, *J. Phys. Chem.* **1984**, *88*, 1102; K. H. Hassan, J. M. Hollas, *J. Mol. Spectrosc.* **1991**, *147*, 100; W. Caminati, D. Damiani, G. Corbelli, L. B. Favero, *Mol. Phys.* **1992**, *75*, 857.; Z. Arp, N. Meinander, J. Choo, J. Laane, *J. Chem. Phys.* **2002**, *116*, 6648; A. Das, K. K. Mahato, S. S. Panja, T. Chakraborty, *J. Chem. Phys.* **2003**, *119*, 2523; Y. He and W. Kong, *J. Chem. Phys.* **2005**, *122*, 244302.
- [128] A. R. Ubbelohde, K. J. Gallagher, *Acta Crystallogr.* **1955**, *8*, 71; G. Feng, Q. Gou, L. Evangelisti, W. Caminati, *Phys. Chem. Chem. Phys.* **2013**, *15*, 2917–2922.
- [129] S. Tang, I. Majerz, W. Caminati, *Phys. Chem. Chem. Phys.* **2011**, *13*, 9137; M. S. Snow, B. J. Howard, L. Evangelisti, W. Caminati, *J. Phys. Chem. A* **2011**, *115*, 47; L. Evangelisti, G. Feng, R. Rizzato, W. Caminati, *ChemPhysChem* **2011**, *12*, 1916; L. Evangelisti, F. Pesci, W.

- Caminati, *J. Phys. Chem. A* **2011**, *115*, 9510; L. Evangelisti, W. Caminati, *Chem. Phys. Lett.* **2011**, *514*, 244; L. Evangelisti, W. Caminati, *J. Mol. Spectrosc.* **2011**, *270*, 120.
- [133] W. Caminati, S. Melandri, P. Moreschini, P. G. Favero, *Angew. Chem., Int. Ed.* **1999**, *38*, 2924-2925.
- [130] W. Caminati, S. Melandri, I. Rossi, P. G. Favero, *J. Am. Chem. Soc.*, **1999**, *121*, 10098–10101.
- [131] W. Caminati, S. Melandri, M. Schnell, D. Banser, J. U. Grabow, J. L. Alonso, *J. Mol. Struct.* **2005**, *742*, 87-90.
- [132] W. Caminati, S. Melandri, A. Maris, P. Ottaviani, *Angew. Chem., Int. Ed.* **2006**, *45*, 2438-2442.
- [134] S. Blanco, S. Melandri, P. Ottaviani, W. Caminati, *J. Am. Chem. Soc.* **2007**, *129*, 2700-2703.
- [135] G. Feng, L. Evangelisti, I. Cacelli, L. Carbonaro, G. Prampolini, W. Caminati, *Chem. Commun.* **2014**, *50*, 171-173.
- [136] G. Prampolini, L. Carbonaro, G. Feng, L. Evangelisti, W. Caminati, I. Cacelli, *J. Chem Theory Comput.* **2014**, *10*, 2204-2211.
- [137] S. Grimme, *J. Comput. Chem.* **2004**, *25*, 1463.
- [138] W. Hujo, S. Grimme, M. Malagoli, M. S. Marshall, C. D. Sherrill, J. Olsen, A. K. Wilson, *Phys. Chem. Chem. Phys.* **2011**, *13*, 13942-13942.
- [139] C. Pérez, S. Lobsiger, N. A. Seifert, D. P. Zaleski, B. Temelso, G. C. Shields, Z. Kisiel, and B. H. Pate, *Chem. Phys. Lett.* **2013**, *571*, 1.
- [140] G. R. Desiraju, T. Steiner, *The weak hydrogen bond in structural chemistry and biology. IUCr Monographs on crystallography*. Oxford University Press: Oxford, **2001**; Vol. IX.
- [141] G. R. Desiraju, *Angew. Chem., Int. Ed.* **2011**, *50*, 52-59.
- [142] K. Liu, J.D. Cruzan, R.J. Saykally, *Science*. **1996**, *271*, 929-933.
- [143] N. Pugliano, R. J. Saykally, *Science*, **1992**, *257*, 1937-1940.
- [144] L. Evangelista, W. Caminati, *Phys. Chem. Chem. Phys.*, **2010**, *12*, 14433-14441.
- [145] L. Evangelisti, L. Spada, W. Li, A. Ciurlini, J.-U. Grabow, W. Caminati, *J. Phys. Chem. A*, **2016**, *120*, 2863–2867.
- [146] L. Spada, Q. Gou, B. M. Giuliano, W. Caminati, *J. Phys. Chem. A* **2016**, *120*, 5094–5098.
- [147] Esterification. Van Nostrand's Scientific Encyclopedia. **2006**.
- [148] C. Duan, M. Carvajal, S. Yu, J. C. Pearson, B. J. Drouin, I. Kleiner, *A&A* **2015**, *576*, A39.
- [149] I. R. Medvedev, F. C. De Lucia, Eric Herbst, *Astrophys. J. Suppl. Series* **2009**, *181*, 433.
- [150] S. Grimme, *J. Chem. Phys.* **2006**, *124*, 34108.
- [151] E. Papajak, H. R. Leverentz, J. Zheng, D. G. Truhlar, *J. Chem. Theory Comput.* **2009**, *5*,

1197–1202.

- [152] T. H. Dunning, *J. Chem. Phys.* **1989**, *90*, 1007.
- [153] L. Goerigk, S. Grimme, *J. Chem. Theory Comput.* **2011**, *7*, 291–309.
- [154] S. Grimme, S. Ehrlich, L. Goerigk, *J. Comput. Chem.* **2011**, *32*, 1456–1465.
- [155] S. Simon, M. Duran, J. J. Dannenberg, *J. Chem. Phys.* **1996**, *105*, 11024–11031.

Acknowledgements

I would like to express my sincere gratitude to my supervisor Prof. Sonia Melandri, for her patience, and immense knowledge, for her guidance helped me in all the time writing of this thesis, for the continuous support of my Ph. D study. I appreciate all her contribution of time and idea.

I want to give the deepest gratitude to Prof. Walther Caminati. It is my honor to be his last Ph. D student. He has taught me how a good research is done. He has also shown me how a nice person should be. I am also thankful his family, especially grateful for Caterina. They make me to live in a foreign country much easier and bring me a lot good memory.

I would like to thank all the group members, Dr. Assimo Maris, Dr. Laura B. Favero, Dr. Luca Evangelisti, Dr. Lorenzo Spada, Dr. Camilla Calabrese, Dr. Annalisa Vigorito, Dr. Qian Gou, for their help and contribution on my personal and professional time. I am especially grateful to Dr. Luca Evangelisti and Dr. Lorenzo Spada. They help me a lot on the research and daily life in Italy.

I would like to thank all the other colleagues in Unibo. They have been the source of friendship as well as happiness.

I also thank the group in Bilbao, Dr. Emilio J. Cocinero, Ms. Iciar Uriarte, Dr. Montserrat Vallejo-López, Mr. Mikel Astorkiza, and all the other members in this group. They are very kind, and I spent a lot good time in Bilbao. Especially I want thank Ms. Iciar Uriarte who is a very good friend to me. We worked together several months in Bologna and Bilbao.

I gratefully acknowledge China scholarship council (CSC) funding me for the Ph. D research.

Lastly, I would like to thank my family for all their love and encouragement. Thank you, my parents, my sisters, my nieces, and my nephews, I love you.